Geochimica et Cosmochimica Acta

JOURNAL OF THE GEOCHEMICAL SOCIETY

Executive Editors

C. W. CORRENS, *Göttingen.* E. INGERSON, *Texas* L. R. WAGER, *Oxford.*

Editors

L. H. AHRENS, *Capetown.* S. R. NOCKOLDS, *Cambridge.* H. C. UREY, *La Jolla, Calif.*
JOHN VERHOOGEN, *Berkeley, Calif.* A. P. VINOGRADOV, *Moscow.*
F. E. WICKMAN, *Stockholm.*

UNIVERSITY OF HAWAII LIBRARY FEB 5 '59

CONTENTS VOLUME 15, NOS. 1/2 NOVEMBER 1958

HITOSHI SAKAI and KAZUO SATŌ: Isotopic composition of the common lead of Japan 1

P. W. RICHARDSON and H. E. HAWKES: Adsorption of copper on quartz 6

R. COULOMB, M. GOLDSZTEIN and M. LE MERCIER: L'uranium dans quelques granites français 10

A. E. RINGWOOD: The constitution of the mantle—II. Further data on the olivine-spinel transition . . 18

MARJORIE HOOKER: Data of rock analyses—IV. Icelandic periodical and serial literature. Bibliography of rock analyses 30

H. SAKAI and H. NAGASAWA: Fractionation of sulphur isotopes in volcanic gases 32

R. W. STOENNER and J. ZÄHRINGER: Potassium-argon age of iron meteorites 40

H. F. PHILLIPS and I. A. BREGER: Isolation and identification of an ester from a crude oil 51

R. F. CONLEY and W. M. BUNDY: Mechanism of gypsification 57

G. KULLERUD and G. DONNAY: Natural and synthetic ferroselite. A roentgenographic mimesis of rammelsbergite 73

A. P. VINOGRADOV: The isotopic composition of rocks of the earth and of meteorites 80

HELMUT G. F. WINKLER und HILMAR VON PLATEN: Experimentelle Gesteinsmetamorphose—II. Bildung von anatektischen granitischen Schmelzen bei der Metamorphose von NaCl-führenden kalkfreien Tonen . . 91

R. M. GARRELS and C. R. NAESER: Equilibrium distribution of dissolved sulphur species in water at 25°C and 1 atm total pressure 113

H. T. EVANS, JR. and R. M. GARRELS: Thermodynamic equilibria of vanadium in aqueous systems as applied to the interpretation of the Colorado Plateau ore deposits 131

Geochemical Note
R. K. WEBSTER, J. W. MORGAN and A. A. SMALES: Caesium in chondrites. 150

Letters to the Editors:
ERIK ERIKSSON: On the isotopic composition of the ammonia and the nitrate ion in rain 153

T. C. HOERING: A reply to the preceding note by E. Eriksson 154

R. EULER and E. HELLNER: Hydrothermale und röntgenographische Untersuchungen an gesteinsbildenden Mineralen—V. Uber hydrothermal hergestellen Osumilith 156

G. J. WASSERBERG and R. BIERI: The A^{38} content of two potassium minerals 157

D. M. SHAW: A vanadium-calcium spectral line coincidence at 3185 Å and its effect on vanadium abundance data 159

Book Review:
"The Threshold of Space: The Proceedings of the Conference on Chemical Aironomy" Edited by M. ZELIKOFF (reviewed by G. F. SCHILLING) 162

Papers to be published in future issues 163

PERGAMON PRESS LONDON • NEW YORK • PARIS • LOS ANGELES

GEOCHIMICA ET COSMOCHIMICA ACTA

EXECUTIVE EDITORS

PROF. C. W. CORRENS *Sedimentpetrographisches Institut der Universität, Lotzestr.* 13, *Göttingen, Germany*
PROF. E. INGERSON *Department of Geology, University of Texas, Austin* 12, *Texas, U.S.A.*
PROF. L. R. WAGER, F.R.S. *Department of Geology and Mineralogy, The University, Oxford, England*

EDITORS

PROF. L. H. AHRENS *Department of Chemistry, University of Capetown, Rondebosch, Cape Province, South Africa*
DR. S. R. NOCKOLDS *Department of Mineralogy and Petrology, The University, Cambridge, England*
PROF. H. C. UREY, FOR. MEM. R. S. *University of California, La Jolla, California, U.S.A.*
DR. JOHN VERHOOGEN, *Department of Geology, University of California, Berkeley, California, U.S.A.*
PROF. A. P. VINOGRADOV *Vernadsky Institute, Moscow, U.S.S.R.*
PROF. F. E. WICKMAN *Naturhistoriska Riksmuseets, Mineralogiska Avdelning, Stockholm* 50, *Sweden*

EDITORIAL ADVISORY BOARD

EUROPE

T. BARTH, *Oslo*
L. CAPDECOMME, *Toulouse*
E. J. CONWAY, *Dublin*
P. ESKOLA, *Helsinki*
P. GALLITELLI, *Modena*
A. HADDING, *Lund*
O. HAHN, *Göttingen*
H. W. HARVEY, *Plymouth*
F. HEIDE, *Jena*
A. HOLMES, *Edinburgh*
W. Q. KENNEDY, *Leeds*
PH. H. KUENEN, *Gröningen*
S. LANDERGREN, *Stockholm*
F. MACHATSCHKI, *Vienna*
A. MUIR, *Harpenden*
J. ORCEL, *Paris*
E. RAGUIN, *Paris*
K. RANKAMA, *Helsinki*
E. REINHARD, *Basle*
TH. G. SAHAMA, *Helsinki*
C. E. TILLEY, *Cambridge*
T. VOGT, *Trondheim*
W. WAHL, *Helsinki*

AMERICAN CONTINENT

A. F. BUDDINGTON, *Princeton*
D. GUIMÃRAES, *Belo Horizonte*
G. E. HUTCHINSON, *New Haven*
B. H. MASON, *New York*
F. WHIPPLE, *Cambridge*
R. WILDT, *New Haven*

FAR EAST

T. WATANABE, *Tokyo*

Publishing Offices: Pergamon Press Ltd., 4 & 5 Fitzroy Square, London W.1 (EUSton 4455)

Four issues per volume, three volumes per year

Subscription *per annum* (including postage) (A) £16. 10s. (U.S.A. $46.50); (B) For individual subscribers who certify that the Journal is for their private use, £10. 10s. (U.S.A. $30.00). Members of the Geochemical Society, or non-members who occasionally publish papers in the Journal, £3. 10s. (U.S.A. $10.00) *per annum*.

Payment must be made in advance

Back numbers, £7 (U.S.A. $19.60) per volume

Copyright © 1958 Pergamon Press Ltd.

PERGAMON PRESS LTD.

4 & 5 FITZROY SQUARE, LONDON W.1 122 EAST 55TH STREET, NEW YORK 22, N.Y.

PRINTED AT THE UNIVERSITIES PRESS, BELFAST, NORTHERN IRELAND

667371

Geochimica et Cosmochimica Acta, 1958, Vol. 15, pp. 1 to 5. Pergamon Press Ltd., London

QE351
5856-29 G42
V.1

Isotopic composition of the common lead of Japan

HITOSHI SAKAI and KAZUO SATŌ
Department of Chemistry, Faculty of Science, The University of Tokyo, Hongo, Tokyo, Japan

(*Received* 1 *August* 1957)

Abstract—Lead tetramethyl was synthesized from lead iodide isolated from 14 galenas, 2 anglesites and 6 pyromorphites of Japan. The mass spectrometric analysis was carried out for the peaks of lead and lead hydride ions. The isotopic compositions of leads from these minerals lie within a narrow range. The average values for galenas are 18·51 ± 0·05 for $^{206}Pb/^{204}Pb$, 15·60 ± 0·05 for $^{207}Pb/^{204}Pb$ and 38·76 ± 0·15 for $^{208}Pb/^{204}Pb$. For lead of secondary minerals they are 18·52 ± 0·05, 15·62 ± 0·05 and 38·78 ± 0·15, respectively. No detectable difference was observed between the isotopic compositions of primary and secondary lead ores.

The ratios, $^{238}U/^{204}Pb$ and $^{232}Th/^{238}U$, in the source magma are estimated from the lead abundances. They are 9·10 ~10·0 and 3·81 ~4·00, respectively.

INTRODUCTION

IN the previous paper (SAKAI, HONDA and MINAMI, 1955) it was reported that the isotopic compositions of Japanese common leads fell within a narrow range and were very close to the average composition of lead of present time. It was also pointed out that Japanese secondary lead ores might have relatively high content of thorium lead. Since then, more determinations were performed on typical Japanese lead ores including several secondary ores. In this paper these new data are presented together with the previous ones and their average values are calculated.

EXPERIMENTAL

After lead tetramethyl was synthesized from lead iodide separated from lead ores, it was introduced into the mass spectrometer, Model 21-103A of the Consolidated Electrodynamics Corporation. When a considerable amount of lead was available, the synthesis of lead tetramethyl was done through the standard process of Grignard reactions. With a lead sample weighing less than 20 mg, lead tetramethyl was synthesized in a vacuum system, as shown in Fig. 1. Before the sample and reagents were introduced, the system was evacuated and the stopcock (1) was closed. One of the side tubes, *A*, of the reaction vessel was opened to air. Then a small portion of methyl magnesium iodide in ethyl ether solution and of methyl phenyl ether was introduced as quickly as possible into the bottom of the vessel. Then *A* was sealed off. The system was again evacuated to expel the excess of ethyl ether and methyl iodide in the Grignard reagents. After the stopcock (1) was closed, the other side tube, *B*, was opened and approximately 10 mg of lead iodide was placed in a bulge of the tube. Then *B* was sealed off. After the vessel was thoroughly evacuated, it was separated from the main system by sealing *C*. Lead iodide and reagents were mixed. Lead tetramethyl, thus formed in the reaction vessel, was introduced into the mass spectrometer through a breakable joint.

By this procedure, most of the ethyl ether and of the methyl iodide, which is unfavourable to the mass spectrometric analysis of a small amount of lead, were removed from the product. The volatile component remaining in the vessel was mainly methyl phenyl ether. But small amounts of lead tetramethyl, ethyl ether

and methyl iodide are also present in the vessel. In this system the partial pressure of lead tetramethyl is much higher than in the case where ethyl ether is used as a solvent. This method is, therefore, effective for the isotopic analysis of a small amount of lead. The use of 5 mg of lead iodide is sufficient for the determination of the isotopic abundances.

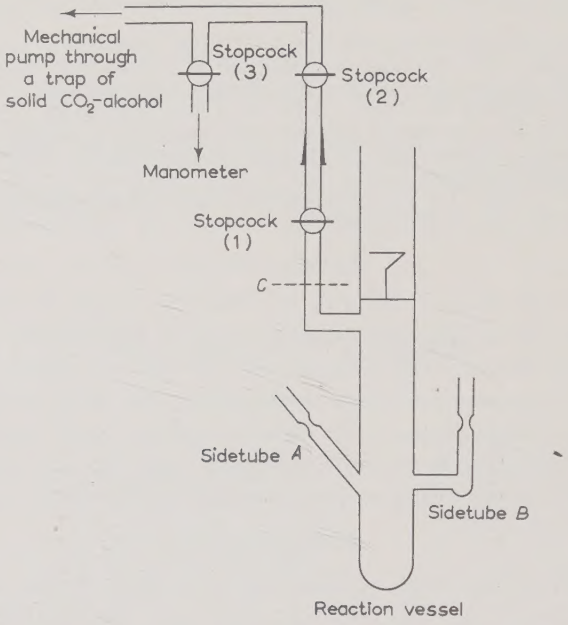

Fig. 1. The reaction vessel for the synthesis of tetramethyl lead.

The mass spectra of lead tetramethyl consist of five main ion groups. They are $Pb^+ + PbH^+$, $Pb(CH_3)^+$, $Pb(CH_3)_2^+$, $Pb(CH_3)_3^+$ and $Pb(CH_3)_4^+$. In this research, the isotopic composition of lead was calculated by analysing the first group, because it gives the simplest spectra.

The abundance of lead isotopes can be calculated from the following equations, where p_m stands for the apparent peak height of ions of mass number $m(m/e)$; i_m and j_m stand, respectively, for a true intensity of an isotope of lead and mercury having a mass number m; and α stands for the PbH^+/Pb^+ ratio in the mono-isotopic spectra,

$$
\begin{aligned}
p_{202} &= j_{202} \\
p_{204} &= i_{204} + j_{604} \\
p_{205} &= \alpha i_{204} \\
p_{206} &= i_{206} \\
p_{207} &= i_{207} + \alpha i_{206} \\
p_{208} &= i_{208} + \alpha i_{207} \\
p_{209} &= \alpha i_{208}
\end{aligned}
$$

In these equations, lead deuteride was not taken into account, because of its negligible abundance.

During the analysis of samples, mercury vapour is always introduced into the mass spectrometer from the inlet and pumping system.

The superposition of ^{204}Hg to ^{204}Pb was corrected by the measured ratio of ^{204}Hg to ^{202}Hg and the intensity of ^{202}Hg. This ratio was $0{\cdot}231 \pm 0{\cdot}001$ for the same mercury as used in the pumping system of the instrument (SAKAI, HONDA and MINAMI, 1955). The PbH^+/Pb^+ ratio was found to vary from 0·085 to 0·088, depending on the ionizing potential (70–90 V), but was fairly constant at a given potential. The standard errors of the calculated values were $\pm 0{\cdot}05$ for both $^{206}Pb/^{204}Pb$ and $^{207}Pb/^{204}Pb$, and $\pm 0{\cdot}15$ for $^{208}Pb/^{204}Pb$.

A calibration sample sent by Drs. J. T. WILSON and R. D. RUSSELL of Toronto University in Canada was analysed in our laboratory. Their results and ours are compared in Table 1.

RESULTS

The isotopic compositions of Japanese common leads are summarized in Table 2. These lead ores are hydrothermal vein-type or replacement-type deposits. With a few exceptions described just below, they are associated with Tertiary igneous rocks or shales. Galenas from the Taishyū mine and the Kamioka mine

Table 1. The isotopic composition of the standard sample of lead (No. 774)

Analyst	Mass spectrometer	^{204}Pb	^{206}Pb	^{207}Pb	^{208}Pb
R. D. RUSSELL*	Metropolitan Vickers MS. 11	1·399 ±0·009	24·52 ±0·06	21·77 ±0·05	52·28 ±0·08
SAKAI and SATO	CEC–21–103A	1·391 ±0·009	24·54 ±0·07	21·75 ±0·07	52·33 ±0·18

* Private communication.

are probably Cretaceous. As seen from the Table, the isotopic compositions of typical Japanese leads remain constant and coincide very closely with the average composition of the ordinary leads of the present time from other parts of the world. For comparison, the isotopic compositions of the present-time lead estimated by COLLINS *et al.* (1953) are also shown in Table 2.

The constancy in the isotopic compositions indicates that uranium, thorium and lead in the source magma have been uniformly distributed throughout their evolution. The ratios, $^{232}Th/^{238}U$ and $^{238}U/^{204}Pb$, in the source magma can be estimated if the appropriate values are assumed for the primeval lead abundances in it and for the age of the earth's crust (the age of Tertiary leads is assumed to be equal to that of the earth's crust). At present, there are two approaches to the estimation of these values. One is based on the isotopic compositions of lead in iron meteorites and the other comes from the lead abundances versus age relation of common leads. In Table 3, two types of estimations for these ratios are presented, together with the figures used in the calculations.

Table 2. Isotopic composition of common lead in Japan ($^{204}Pb = 1.000$)

No.	Locality	Type of deposits	^{206}Pb ± 0.05	^{207}Pb ± 0.05	^{208}Pb ± 0.15	Geologic age
		Galena				
1	Kamioka mine, Gifu Pref.	Pyrometasomatic deposits	18.20	15.55	38.71	Cretaceous
2	Daira mine Miyagi Pref.	Epithermal vein type deposits	18.32	15.43	38.45	Tertiary
3	Hanaoka mine, Akita Pref.	Epithermal vein type deposits	18.55	15.57	38.61	Tertiary
4	Arakawa mine, Akita Pref.	Epithermal deposits	18.44	15.57	38.74	Tertiary
5	Hosokura mine, Akita Pref.	Epithermal vein type deposits	18.59	15.59	38.73	Tertiary
6	Osarusawa mine, Akita Pref.	Epithermal vein type deposits	18.54	15.58	38.82	Tertiary
7	Taishyu mine, Nagasaki Pref.	Mesothermal deposits	18.47	15.59	39.02	Cretaceous
8	Budō mine, Niigata Pref.	Contact vein type deposits	18.42	15.50	38.60	Tertiary
9	Mikawa mine, Niigata Pref.	Epithermal vein type deposits	18.58	15.66	39.00	Tertiary
10	Chichibu mine, Saitama Pref.	Pyrometasomatic deposits	18.71	15.83	39.20	Tertiary
11	Shioya mine, Ibaragi Pref.	Epithermal deposits	18.36	15.53	38.59	Tertiary
12	Tōya mine, Hokkaido	Epithermal replacement deposits	18.52	15.56	38.68	Tertiary
13	Ohara-mura, Miyagi Pref.	Epithermal deposits	18.72	15.73	38.75	Tertiary
14	Nakamaru mine, Gumma Pref.	Epithermal deposits	18.57	15.65	38.59	Tertiary
		Anglesite				
15	Mikawa mine, Niigata Pref.	Epithermal vein type deposits	18.35	15.46	38.60	Tertiary
16	Nakamaru mine, Gumma Pref.	Epithermal deposits	18.50	15.63	38.61	Tertiary
		Pyromorphite				
17	Ogoya mine, Ishikawa Pref.	Epithermal deposits	18.82	15.67	39.32	Tertiary
18	Mikawa mine, Niigata Pref.	Epithermal vein type deposits	18.31	15.50	38.46	Tertiary
19	Chien mine, Miyagi Pref.	Epithermal deposits	18.80	15.79	38.92	Tertiary
20	Nishisuzu-yama mine, Kagoshima Pref. (1)	Mesothermal deposits	18.37	15.53	38.80	Tertiary
21	Nishisuzu-yama mine, (2)	Mesothermal deposits	18.59	15.72	39.02	Tertiary
22	Mikura mine, Shizuoka Pref.	Epithermal deposits	18.39	15.64	38.52	Tertiary
		Hokutolite				
23	Tamagawa Hot Springs, Akita Pref.	Radioactive sinter deposits	18.63	15.61	39.04	Present
	Average of galena		18.51	15.60	38.76	
	Average of secondary ores		18.52	15.62	38.78	
	Lead of present time (COLLINS *et al.*, 1953)		18.45	15.61	38.40	

No detectable fractionation of lead isotopes was observed between the primary and secondary lead ores. The relative mass differences among the lead isotopes are so small that no isotopic effect is expected.

BEGEMANN *et al.* (1954) found a slightly higher content of uranium leads in the radioactive cotunnite from the Volcano Vesuvius. It was attributed to the

Table 3. $^{238}U/^{204}Pb$ and $^{232}Th/^{238}U$ in the source magma estimated from the measured lead abundances

Method based on	Primeval lead		Age of the crust	$^{238}U/^{204}Pb$	$^{232}Th/^{238}U$
	$^{206}Pb/^{204}Pb$	$^{208}Pb/^{204}Pb$	(10^9 years)		
Meteoritic lead*	9·41	29·16	4·5	9·10	3·81
Common lead†	11·35	31·1	3·5	10·0	4·00

* Based on the data given by PATTERSON *et al.* (1955)
† Based on the data given by COLLINS *et al.* (1953)

recent contamination of the source magma of the volcano by uranium leads. Hokutolite from Tamagawa Hot Springs is a radioactive sinter deposit composed of barium and lead sulphate with a trace amount of radium and its decay products. The lead from this mineral shows no detectable difference from other common leads with respect to its isotopic composition.

Acknowledgements—The authors wish to express their sincere thanks to Professors N. SAITŌ and E. MINAMI of the University of Tokyo for their kind guidance throughout this research. The authors are very grateful to Professors T. WATANABE and K. IMAI, and Mr. T. SASAKI of this University; to Dr. K. SAKURAI of Yokohama National University; to Dr. T. ISHIMORI and Messrs. K. MUTA and H. WAKI of Kyushyu University; and to Mr. R. SUGISAKI of Nagoya University. They kindly provided us with a variety of mineral samples. Professor S. ARAKI and his associates were so kind as to give us the useful advice on the operation of the mass spectrometer. Professors J. T. WILSON and R. D. RUSSELL of Toronto University in Canada, to whom the authors' heartful thanks are due, sent us a calibration sample of lead.

A part of the cost of this research was defrayed from the Scientific Research Encouragement Grant from the Ministry of Education of Japan.

LITERATURE

BEGEMANN F., GEISS J. and HOUTERMANS F. G. (1954) Isotopenzusammensetzung und radioaktivität von rezentem vesuvblei. *Nuovo Cim.* **11,** 663–73.

COLLINS C. G., RUSSELL R. D. and FARQUHAR R. M. (1953) The maximum age of the elements and the age of the earth's crust. *Canad. J. Phys.* **31,** 402–18.

PATTERSON C., TILTON G. and INGHRAM M. (1955) Age of the Earth. *Science* **121,** 69–75.

SAKAI H., HONDA M. and MINAMI E. (1955) Isotopic composition of the common lead in Japan. *Bull. Chem. Soc. Japan* **28,** 533–4.

Geochimica et Cosmochimica Acta, 1958, Vol. 15, pp. 6 to 9. Pergamon Press Ltd., London

Adsorption of copper on quartz

P. W. Richardson* and H. E. Hawkes†

(*Received* 27 *September* 1957)

Abstract—Quantitative, colorimetric determinations were made of the amount of copper adsorbed to the surface of fine-grained quartz particles from dilute, aqueous, copper solutions of varying concentration and pH. It was found that the amount of adsorption varies roughly as the square root of the concentration of copper ions in solution, within the pH range where copper does not precipitate as hydroxide and where the adsorbing surface of the quartz has a net negative charge.

Introduction

The adsorption of cations to the surface of mineral grains has long been recognized as an important factor in the cycle of weathering and transportation of weathering products at the surface of the earth. In particular, soil scientists, who are concerned with availability of mineral nutrients to plants, commonly determine the content of readily soluble, or adsorbed potassium, calcium, magnesium, zinc and copper as a measure of the fertility of the soil. More recently, semiquantitative determination of adsorbed metal ions in modern stream sediments has been found to be an effective method of mineral exploration, where traces of the metals weathered from ore deposits in the upstream drainage basin move downstream in the water and are temporarily held as exchangeable ions in the stream sediments (Hawkes and Bloom, 1956).

Most of these observations are of an empirical nature and deal with complex systems in which the mineralogy of the solid phase and the composition of the aqueous phase are only very incompletely known. Very little work has been done on the adsorption of cations on minerals under controlled laboratory conditions.

This paper describes the results of experiments on the adsorption of copper on finely ground quartz from copper sulphate solutions of known composition in which the copper content approximates that in nature. Originally, it was hoped to equate the amounts of copper in the original solutions to the copper found on the quartz and the copper remaining in the supernatant liquid. The percentage of copper withdrawn from the copper solutions during the adsorption experiments varied from 0 to 10 per cent with the change during most of the runs being less than 1 per cent. A method of measuring down to 0·002 p.p.m. copper in water was developed, but the precision was low and was insufficient to measure the change in metal content undergone by the solutions during the experiments. Consequently the experiments dealt solely with the direct determination of copper adsorbed on quartz.

Similar studies have been carried out in the Department of Metallurgy at M.I.T. on the adsorption of sodium on quartz (Bell, 1953; Laxen, 1951) and on the adsorption of barium on quartz (Chang, 1951). In these studies, radioactive tracers were used as a means of measuring the adsorbed material. The present work was based on the use of the colorimetric reagent, dithizone, for determination of copper (Sandell, 1950).

* Dome Exploration (Canada) Ltd., 904–50 King Street W., Toronto 1, Ontario.
† Department of Mineral Technology, University of California, Berkeley 4, California.

Experimental Method

Samples of quartz particles with a surface area of 900 cm^2/g (krypton adsorption determination) were agitated for 30 min in water of varying copper concentration and pH. After agitation, the pH of the solution was measured and the liquid was decanted. The moist quartz was transferred from the shaking bottles to gooch crucibles with glass frits. The crucibles were placed in centrifuge tubes and centrifuged to reduce the water content of the samples without evaporating the water. The samples were transferred to tared weighing bottles and weighed. The weighing bottles were heated to 120°C to evaporate the remaining water and then weighed again. From these weights the amount of water was found and thus the amount of copper deposited on the quartz by the evaporation of water. This would be the total amount of copper on the quartz if there were no adsorption.

The quartz was transferred to ground glass stoppered test tubes to which sodium citrate dissolved in water and dithizone dissolved in toluene were added. The tubes were shaken. The citrate released the copper from the quartz and the dithizone reacted with the copper causing a colour change in the organic (toluene) phase. This colour change may be measured quantitatively with a colorimeter. The colorimeter reading was compared with a previously prepared standard curve to obtain the amount of copper than was on each quartz sample. From this experimentally determined amount of copper on the quartz samples was subtracted the amount of copper precipitated on the quartz by evaporation of the water not removed by centrifuging. The difference was the amount of copper absorbed by the quartz sample. The total amount of copper absorbed by each quartz sample was divided by the weight of the sample to obtain the amount of adsorption of copper per gramme of quartz. The amounts may then be calculated to moles of copper adsorbed per square centimeter of quartz or any other convenient units.

An independent check of the order of magnitude of the copper on the quartz was made using the optical spectrograph (Benson, 1955).

Experimental Results

The experimental determinations are tabulated in Table 1. Fig. 1 shows the amount of adsorption of copper (in $\mu g/g$ of quartz particles with a surface area of 900 cm^2/g). The ordinate shows the concentration of copper in the solutions and the abscissa shows the final pH of the experimental solutions. The copper concentration is plotted on log scale because of the extreme variation of concentrations used.

The area investigated is limited on the right by a line representing the solubility boundary of copper in water. The solubility product of $Cu(OH)_2$ is 6×10^{-20} (Pauling, 1953, p. 468). The left boundary of the investigated area is the isoelectric line for quartz in aqueous solution. To the left of the isoelectric line the surface charge on the quartz is positive and anions rather than cations are attracted to the surface. At copper concentrations greater than 5 p.p.m. the isoelectric line departs from the pH of 3·7. It may be seen in Fig. 1 that the deviation takes place where the concentration of the copper ion approaches that of the hydrogen ion. The upper concentration boundary of the area is 100 p.p.m. copper. This is much higher than copper anomalies found in nature and about 20,000 times normal background in natural stream waters. The lower limit of investigation is 0·1 p.p.m. This

Table 1. Experimental determinations of copper adsorbed on quartz

No.	Copper conc. (p.p.m.)	Copper conc. (moles)	Initial pH	Final pH	Adsorption (μg Cu/g quartz)	Adsorption (moles Cu/cm^2 quartz surface)
1	10	$1{\cdot}57 \times 10^{-4}$	3·80	3·80	−0·01	$-0{\cdot}18 \times 10^{-12}$
2	10	$1{\cdot}57 \times 10^{-4}$	4·50	4·40	0·17	$2{\cdot}9 \times 10^{-12}$
3	10	$1{\cdot}57 \times 10^{-4}$	6·08	5·79	0·32	$5{\cdot}5 \times 10^{-12}$
4	1	$1{\cdot}57 \times 10^{-5}$	3·98	3·92	0·04	$0{\cdot}67 \times 10^{-12}$
5	1	$1{\cdot}57 \times 10^{-5}$	4·95	4·92	0·18	$3{\cdot}1 \times 10^{-12}$
6	1	$1{\cdot}57 \times 10^{-5}$	6·07	5·82	0·26	$4{\cdot}5 \times 10^{-12}$
7	10	$1{\cdot}57 \times 10^{-4}$	5·38	5·29	0·24	$4{\cdot}2 \times 10^{-12}$
8	50	$7{\cdot}85 \times 10^{-4}$	5·32	5·30	0·52	$9{\cdot}1 \times 10^{-12}$
9	100	$1{\cdot}57 \times 10^{-3}$	5·37	5·24	0·59	$10{\cdot}3 \times 10^{-12}$
10	100	$1{\cdot}57 \times 10^{-3}$	4·55	4·50	0·03	$0{\cdot}50 \times 10^{-12}$
11	100	$1{\cdot}57 \times 10^{-3}$	5·66	5·61	0·96	$16{\cdot}7 \times 10^{-12}$
12	100	$1{\cdot}57 \times 10^{-3}$	3·98	3·90	−0·31	$-5{\cdot}4 \times 10^{-12}$
13	100	$1{\cdot}57 \times 10^{-3}$	4·94	4·86	0·36	$6{\cdot}3 \times 10^{-12}$
14	50	$7{\cdot}85 \times 10^{-4}$	5·85	5·70	0·65	$11{\cdot}3 \times 10^{-12}$
15	0	0	5·69	5·43	0·00	0·0
16	0·1	$1{\cdot}57 \times 10^{-6}$	5·50	5·38	0·08	$1{\cdot}4 \times 10^{-12}$

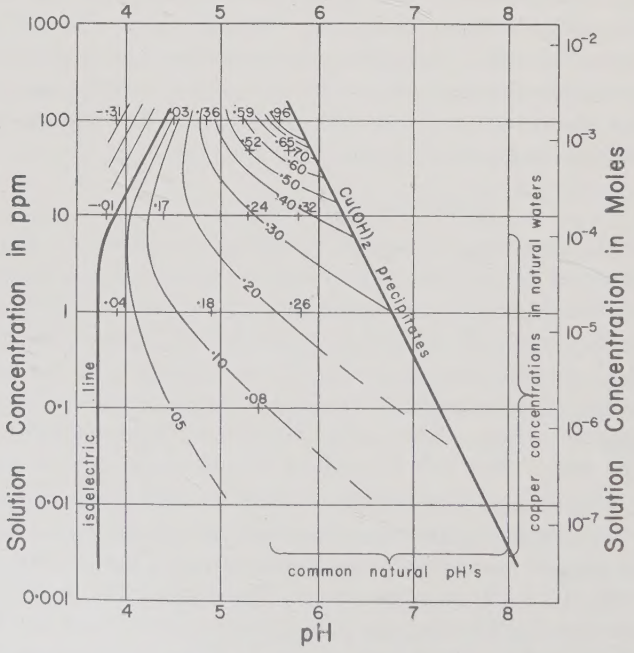

Fig. 1. Amount of copper adsorbed on quartz expressed in μg of copper per g of quartz.

concentration is between 10 and 20 times normal background found in nature.

At the appropriate concentration and pH coordinates the measured amounts of adsorbed copper are plotted. Each of these values is the average of four determinations. The contoured values show an increasing amount of adsorption with increasing copper concentration of the solution and with increasing pH. The amount of copper adsorbed from solutions of concentration and pH which might be encountered in nature varies from 0·1 to 0·3 μg/g of quartz of this particle size. This is equivalent to $1{\cdot}7 \times 10^{-12}$ to $5{\cdot}6 \times 10^{-12}$ moles of copper/cm^2 of quartz.

It was found that the average amount of water remaining after centrifuging was 4 per cent. If the area of the quartz was 900 cm^2/g, the average thickness of the water was $4{\cdot}4 \times 10^{-5}$ cm or 4400 Å.

Conclusions

The amount of copper adsorbed on quartz is measurable but very small. The amount of adsorption increases roughly as the square root of the increase of concentration. For solutions of constant pH and varying concentration, this relationship is modified by the presence and shape of the isoelectric line. The field where copper can exist in ionic solution is very limited in solutions of high pH because of the very low solubility of $Cu(OH)_2$.

As a result of the formation of $Cu(OH)_2$ at high pH, very little copper is carried in true solution in streams with a pH above 7. Of course, copper can be transported as $Cu(OH)_2$ in suspension or on suspended particles. From a consideration of the solubilities of the other heavy metals it appears that they can be transported at normal stream pH in ionic solutions.

In a stream containing 0·01 p.p.m. copper and with a pH of 6, quartz particles 41 μ in size adsorb only 0·1 μg of copper/g of quartz. In the usual geochemical prospecting field test using a 0·1 g sample (Bloom, 1955) this concentration of copper would be undetectable.

Acknowledgements—This paper is a condensation of a thesis entitled "Adsorption of copper on quartz," submitted in 1955 by the senior author to the Department of Geology and Geophysics at M.I.T.

R. Charles, D. W. Furstenau, S. Mitchell, and J. Brown of the M.I.T. Metallurgy Department contributed assistance and advice both during the experimental work and in the interpretation of the results.

References

Bell G. M. (1953) *Adsorption of Sodium and Chloride Ions on Quartz.* Doctoral Thesis, Department of Metallurgy, Massachusetts Institute of Technology.

Bloom H. (1955) A field method for the determination of ammonium citrate soluble heavy metals in soils and alluvium. *Econ. Geol.* **50,** 533–541.

Chang Chen-Siang (1951) *Adsorption of Barium and Laurate Ions on Quartz.* Doctoral Thesis, Department of Metallurgy, Massachusetts Institute of Technology.

Hawkes H. E. and Bloom, H. (1956) Heavy metals in stream sediment used as exploration guides. *Min. Engng., N.Y.* **8,** 1121–1127.

Laxen P. A. (1951) *Concerning the Adsorption of Sodium onto Quartz.* Master's Thesis, Department of Metallurgy, Massachusetts Institute of Technology.

Pauling L. (1953) *General Chemistry.* W. H. Freeman, San Francisco.

Sandell E. B. (1950) *Colorimetric Determination of Traces of Metals.* Interscience, New York.

Geochimica et Cosmochimica Acta, 1958, Vol. 15, pp. 10 to 17. Pergamon Press Ltd., London

L'uranium dans quelques granites français

R. Coulomb, M. Goldsztein et M. Le Mercier
Service de Minéralogie du Commissariat à l'Energie Atomique,
Fontenay-aux-Roses (Seine)

(*Received* 2 *January* 1958)

Résume—Le travail que nous présentons donne les lois de répartition statistique de l'uranium et du potassium dans un important massif granitique français. Des analyses sytématiques nous permettent de répartir géographiquement ces deux éléments et d'établir l'existence de corrélations entre les caractéristiques pétrographiques et les teneurs en uranium.

Nous étudions les variations statistiques et géographiques de teneur en uranium, d'une part en fonction des teneurs en potassium des granites, d'autre part en fonction de la présence de gisements uranifères.

Les travaux de géochimie ont pris au Commissariat à l'Energie Atomique une importance considérable. Le caractère essentiellement expérimental de ces travaux est le reflet des préoccupations d'un organisme minier industriel orienté avant tout vers la prospection et l'exploitation de gisements économiques. Les géochimistes ont pris leur place dans les grandes équipes de recherche de l'uranium; leur rôle n'est pas d'amener de grandes théories, mais de présenter des résultats géochimiques synthétiques sur les zones prospectées.

Ceci ne signifie en aucun cas que la géochimie reste bornée à un aspect étroitement appliqué, bien au contraire: l'expérience des dernières années a prouvé que la connaissance des mécanismes géochimiques fondamentaux était déterminante dans la rentabilité des méthodes de prospection géochimique.

Nous voudrions montrer ici, sur un exemple concret, que la géochimie expérimentale, menée sur un style industriel, peut amener des résultats précieux, non seulement à la géologie de terrain, mais également à la géochimie théorique.

Nous nous attachons depuis quelques années à établir les lois de distribution de divers éléments, dont en particulier les alcalins et l'uranium, dans les massifs granitiques de France et d'Outre-Mer. Nous avons montré au Congrès de Mexico comment on pouvait définir des paramètres caractéristiques de chaque région, paramètres ayant un sens géochimique et statistique précis et comparables de région à région.

Depuis lors, le nombre de nos prélèvements et les zones étudiées se sont considérablement accrus, permettant des analyses statistiques plus détaillées et plus poussées.

Nous présenterons ici une étude portant sur quelques granites de Bretagne.

(I) *La zone étudiée* s'étend d'E. en O. de Pontivy à Quimper, du N. au S. de Rostrenen à Quistinic, soit environ 1500 km^2.

Si l'on se reporte aux études de C. Barrois et de Mme. Jeremine, les grandes lignes géologiques sont les suivantes: du nord au sud, l'on distingue:

(a) Le granite porphyroïde de Rostrenen, à contour nettement circonscrit sur la bordure N; le granite à grain fin de Plélauff.

(b) La granulite de Pontivy, subdivisée en trois massifs par deux bandes sédimentaires, dont la trainée sud, la plus importante, s'allonge jusqu'à Locronan dans le Finistère.

(II) *Les prélèvements:* 215 échantillons ont été effectués à une maille aussi régulière que possible (tous les 2,5 km environ), en affleurements ou en carrières, dans les parties les plus fraîches des roches. On s'est préoccupé de prélever des échantillons suffisamment gros pour éliminer les erreurs statistiques d'échantillonnages dues aux différentes grosseurs des grains des roches: les prises ont varié de 500 g à quelques kilos. Ces échantillons ont été concassés, broyés, quartés avec le plus grand soin dans une installation réservée à cet usage. Le taux et la nature des impuretés introduites par les appareils de broyage ont été évalués. Un témoin pétrographique est gardé pour chaque échantillon, afin de faire des lames minces.

(III) *Les analyses:* Les échantillons sont déterminés pétrographiquement au microscope.

Tous sont dosés: en K_2O, Na_2O, par spectromètrie de flamme,
en uranium, par fluorimètrie.
Tous sont passés: au comptage α par scintillation,
aux comptages β et γ.
Un nombre plus réduit est dosé en SiO_2, CaO, MgO.

Enfin, quelques échantillons font l'objet d'une analyse complète de roche par les méthodes classiques.

(IV) *L'exploitation des résultats:* Ceci nous met en possession d'une masse considérable de résultats, qu'il faut pouvoir classer sous une forme synthétique. Les méthodes statistiques se révèlent indispensables.

Pour simplifier cet exposé, nous ne suivrons l'histoire géochimique que de deux éléments:

(a) un élément majeur de la roche: le potassium;

(b) l'élément trace qui nous intéresse évidemment le plus: l'uranium.

Nous dressons donc pour ces éléments un histogramme de répartition des teneurs. Il est un fait très général que les histogrammes de répartition s'ajustent correctement à des lois logarithme-normales. Ahrens (1954) croit même pouvoir généraliser en une loi de géochimie fondamentale. Nous avons longuement donné au Congrès de Mexico notre point de vue sur la lognormalité et les raisons thermodynamiques qui l'expliquent. Disons simplement que, pour l'uranium, l'ajustement lognormal se confirme comme étant satisfaisant, et que chaque fois qu'une distribution s'écarte grossièrement de la lognormalité, c'est que nous avons à faire à des populations de prélèvements hétérogènes.

Nous avons donc pris l'habitude de représenter systématiquement nos histogrammes avec des abscisses logarithmiques, ce qui nous donne des répartitions en courbes de Gauss faciles à manipuler et à construire. La Fig. 1 donne les répartitions ainsi obtenues. Nous voyons donc les éléments suivis dans une région donnée symbolisés par une courbe de répartition et définis par un petit nombre de paramètres dont il faut saisir le sens géochimique:

(1) *La moyenne géométrique* (*gm*) représente *la valeur la plus fréquente.*

(2) *La moyenne arithmétique* (*am*) représente *l'abondance.* Il est une chose peu connue lorsque l'on parle d'abondance, que cette abondance peut être très différente

de la valeur la plus fréquente. Dans l'exemple que nous présentons, la valeur la plus fréquente est 3 p.p.m., alors que l'abondance est de 5 p.p.m.

(3) *L'écart type logarithmique* (σ) est également pour nous une valeur ayant un sens géochimique très important: il traduit le degré d'homogénéité géochimique des échantillons. C'est en quelque sorte l'indice "figé" de l'histoire géochimique de l'élément étudié.

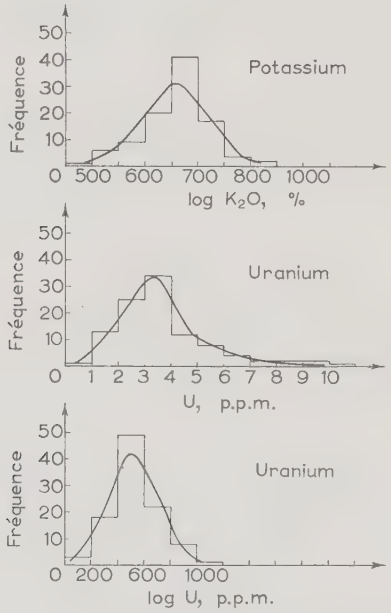

Fig. 1. Représentation statistique globale.

Nous voyons donc que nous sommes armés pour comparer objectivement différents massifs sous l'angle à la fois des valeurs moyennes et des fluctuations autour de ces moyennes.

Il parait immédiatement que ces indices globaux, pour précieux qu'ils soient, méritent d'être dépouillés en indices particuliers de phénomènes géologiques plus élémentaires.

(V) *Exploitation détaillée:* L'expérience montre qu'il est en général difficile de donner une représentation géographique directe (c'est-à-dire par un report sur la carte) des valeurs déterminées par les analyses. Le tracé des courbes ou de région d'isoteneur est trop souvent subjectif. Ces difficultés viennent du fait qu'un échantillon isolé n'a de valeur que si on l'intègre dans une distribution statistique. Si plusieurs distributions se recouvent partiellement, on ne sait plus à laquelle attribuer certains échantillons.

Nous avons donc découpé le massif en panneaux contenant suffisamment d'échantillons pour faire des calculs statistiques et de taille suffisamment réduite pour espérer isoler un phénomène géologique simple. Les panneaux sont reproduits sur la carte (Fig. 2). Les résultats des répartitions sont donnés sur la Fig. 3 pour le potassium et la Fig. 4 pour l'uranium.

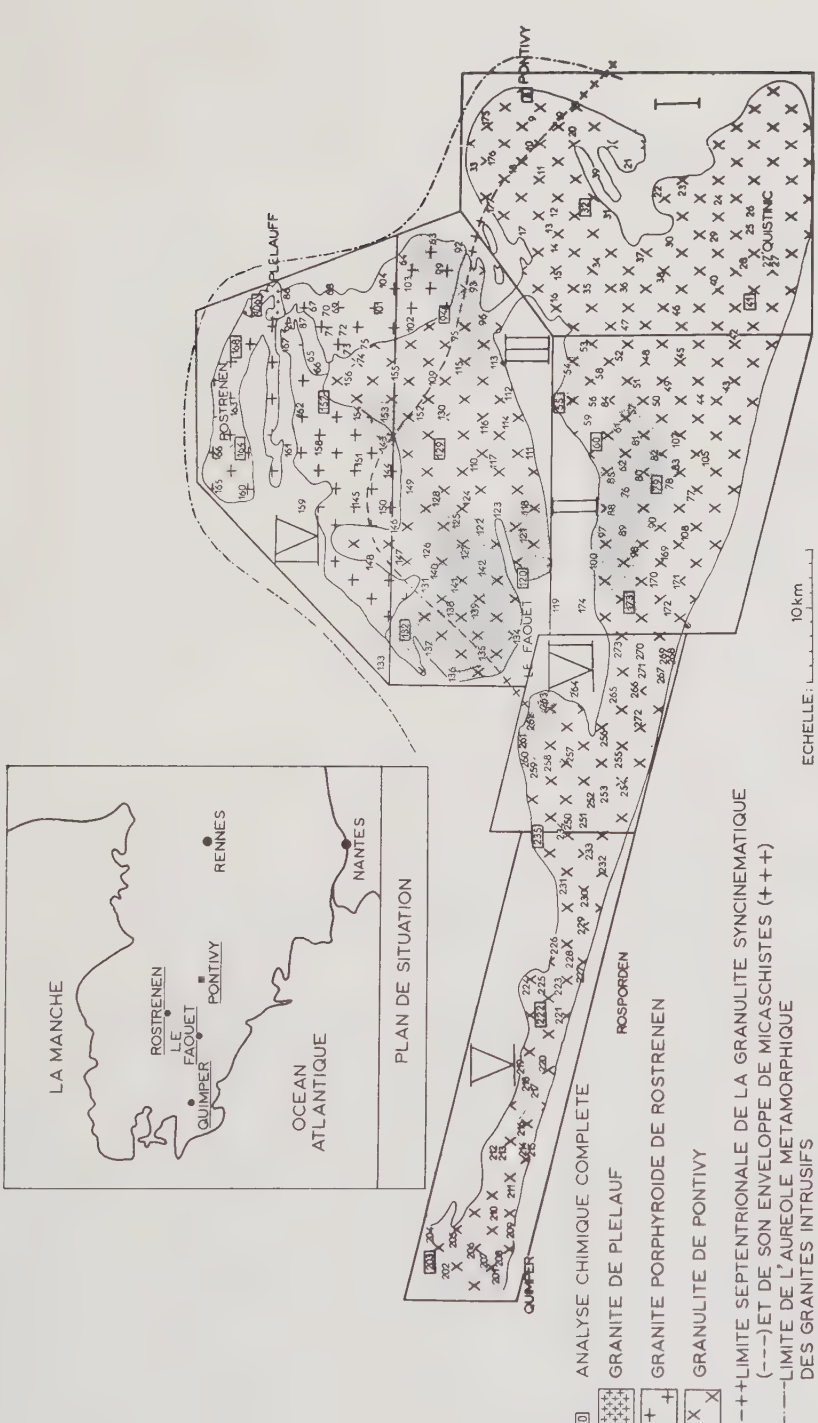

Fig. 2. Carte des prélèvements.

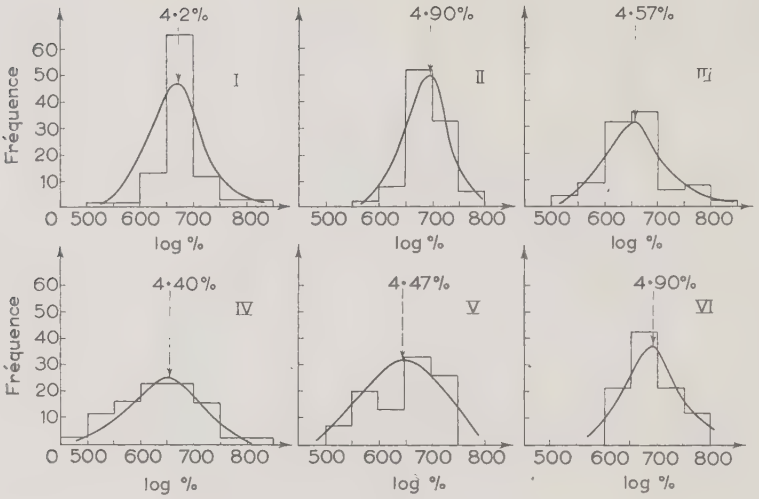

Fig. 3. Distribution du potassium.

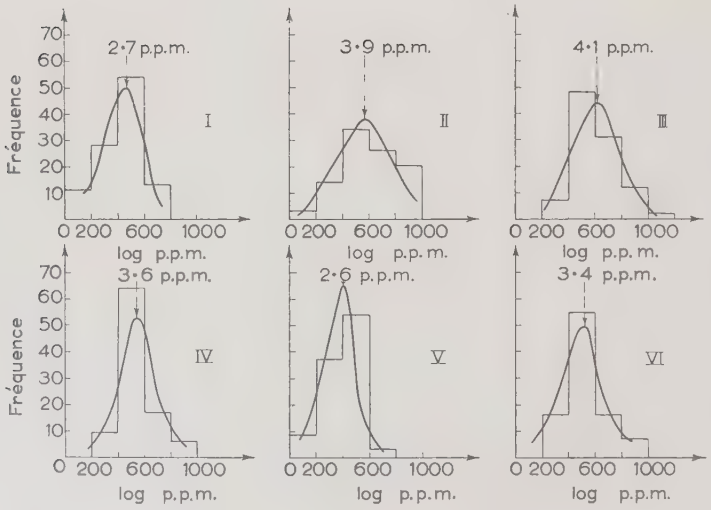

Fig. 4. Distribution de l'uranium.

Le tableau 1 résume les différentes valeurs remarquables ainsi déterminées.

La traduction géochimique de ces résultats est la suivante:

Pour K_2O. Les panneaux I, II, VI représentent des roches très homogènes dont les fluctuations sont peu dispersées autour des valeurs centrales. Le panneau V est "pollué" par quelques échantillons aberrants dus à l'étroitesse de la bande

Tableau 1

Distribution de l'uranium				Distribution du potassium			
Panneaux	*gm* (p.p.m.)	*am* (p.p.m.)	(σ)	Panneaux	*gm* (%)	*am* (%)	(σ)
I	2·7	3	0·160	I	4·72	4·76	0·048
II	3·9	4·4	0·210	II	4·90	4·95	0·040
III	4·1	5·2	0·180	III	4·57	4·65	0·063
IV	3·6	4·2	0·150	IV	4·40	4·46	0·075
V	2·6	2·7	0·120	V	4·47	4·56	0·053
VI	3·4	3·8	0·160	VI	4·90	4·95	0·060
Total	3·4	4·9	0·190	Total	4·55	4·59	0·065

de granulite à cet endroit, mais une distribution semblable à celle du panneau I reste visible sur l'histogramme. Les panneaux II et VI montrent un enrichissement de la roche en potassium.

Le panneau III présente une distribution plus étalée: c'est un début de transition entre la granulite des panneaux précédents et une roche nouvelle moins potassique qui se développe dans le panneau IV.

Le panneau IV reste au contraire pollué par des échantillons potassiques dus à la granulite.

Ces représentations traduisent donc clairement le degré d'homogénéité et les caractéristiques pétrochimiques de chaque panneau. Lorsque la distribution se resserre, on peut penser que le panneau contient une roche homogène. Lorsque la distribution s'étale, on peut avoir affaire soit à des échantillons grossièrement aberrants (altérés ou ne faisant pas partie de la population), soit à un phénomène géologique complexe qui n'a pas été suffisamment décortiqué et qui nécessite un découpage mieux fait.

Au point de vue de l'uranium. Nous voyons que dans les panneaux I, II, III, V, VI, qui présentent, comme nous venons de le voir, une bonne homogénéité pétrochimique, l'uranium est fortement localisé dans deux panneaux seulement: le I et le III, où à la fois les indices de dispersion et les moyennes sont particulièrement élevés.

Dans le panneau IV, au contraire, qui représente autre chose du point de vue pétrographique, nous trouvons des valeurs moyennes relativement fortes (4,2 p.p.m.) mais un indice de dispersion assez bas (0,150).

Si encore plus précisément l'on reporte sur la carte toutes les teneurs supérieures à la moyenne arithmétique de la totalité des échantillons, tous les points "forts" se localisent dans un petit nombre de plages tranchant sur l'ensemble.

On peut noter la continuité de certaines plages de part et d'autre des bandes de sédimentaire, ce qui semblerait confirmer les relations génétiques des différents massifs de granulite.

Conclusion

Nous voyons que cette étude:

(1) Nous permet de donner une image pétrochimique de la région. Cette image doit évidemment être intégrée aux données des études de pétrographie détaillées: mais il est certain que, même limités à l'analyse d'un seul élément majeur de la roche, les renseignements fournis sont très supérieurs à ceux donnés traditionnellement par quelques analyses classiques de roche.

(2) Nous donne l'abondance et les lois de répartition de l'uranium dans les différentes zones.

(3) Nous permet de vérifier une fois de plus la lognormalité des répartitions.

(4) Nous donne les localisations de plages où les valeurs trouvées pour l'uranium sont statistiquement "fortes"; ces zones ne sont pas, comme il est souvent admis, dans les bordures des massifs intrusifs.

Le potassium et l'uranium ne sont pas statistiquement en corrélation: si dans la plage II les teneurs en uranium et en potassium sont simultanément fortes, ceci ne peut être généralisé. Il ne semble donc pas qu'il existe un processus général qui fasse de l'uranium un accompagnateur systématique du potassium, au cours de la formation des roches.

On peut noter que la plupart des points minéralisés actuellement sont situés sur la plage à la fois la plus potassique et la plus uranifère.

Un certain nombre de questions restent posées:

(1) Les plages "fortes" ont-elles un rapport quelconque avec l'existence de gisements?

(2) L'uranium présent dans ces plages appartient-il au granite proprement dit, ou y a-t-il eu un apport ultérieur au cours d'une venue métallogénique, formant ainsi un halo de dispersion primaire?

(3) Sous quelles formes se trouve l'uranium présent dans les différentes zones?

C'est à ce genre de questions que nos travaux actuels tendent à répondre. D'une part, nous multiplions les études comparatives en utilisant les méthodes que nous venons d'exposer, d'autre part, nous continuons à perfectionner nos techniques analytiques, afin d'introduire dans nos représentations statistiques le nombre le plus élevé possible d'éléments.

Si notre objectif principal reste d'aider le géologue dans la découverte et l'exploitation des gisements, nous pensons que l'accumulation de milliers de résultats contribue également à faire progresser la géochimie théorique du cycle de l'uranium.

Bibliographie

Ahrens L. H. (1954) The lognormal distribution of the elements. *Geochim. et Cosmochim. Acta* **6,** 2–3, 121–131.

Aubrey K. V. (1955) Frequency distributions of elements in igneous rocks. *Geochim. et Cosmochim. Acta* **8**, 83–89.

Coulomb R., Goldsztein M. and Le Mercier M. (1956) Etude de la répartition statistique de l'uranium dans les granites. Contribution à la prospection géochimique des grands massifs. *Congrès international de géologie, Mexico.* En cours de publication.

Larsen E. S., Jr., Phair G., Gottfreed D. and Smith W. L. (1955) L'uranium dans la différenciation magmatique. *Actes de la Conference Internationale pour l'application Pacifique de l'Energie Atomique, Genève* Vol. 6, p. 275.

Mabile J. (1956) *Notion de calcul de probabilités et de statistiques de gisements.* Note C.E.A. No. 170.

Matheron G. (1955) Application des méthodes statistiques à l'évaluation des gisements. *Ann. Min.* 50–73.

Neuerburg G. J. (1955) L'uranium dans les roches ignées des Etats-Unis d'Amérique. *Actes de la Conférence Internationale pour l'application Pacifique de l'Energie Atomique, Genève* Vol. 6. p. 264.

Geochimica et Cosmochimica Acta, 1958, Vol. 15, pp. 18 to 29. Pergamon Press Ltd., London

The constitution of the mantle—II

Further data on the olivine–spinel transition*

A. E. Ringwood

(*Received* 7 *November* 1957)

Abstract—Subsolidus phase equilibria were studied in the system Mg_2SiO_4–Mg_2GeO_4 at 660°C and 30,000 bars in a squeezer apparatus. From the compositions of co-existing phases, the free energy of transition of forsterite from the olivine to the spinel structure is calculated. This enables the total pressure needed to cause this transition in forsterite to be determined. It is found to be about 90,000 bars at 660°C. This result, combined with analogous data obtained in Part I makes it possible to construct a P–T curve defining the olivine–spinel transition in forsterite.

A similar study was made in the system Fe_2GeO_4–Fe_2SiO_4 at 700°C and 25,000 bars and it was predicted that a spinel polymorph of fayalite should become stable around 50,000 bars at 700°C. The predicted polymorph was subsequently synthesized and its transition pressure determined as 38,000 bars at 600°C. The spinel has a lattice constant of 8·235 Å and is 12 per cent denser than fayalite.

A thermodynamic study of the stability of $MgSiO_3$ pyroxene in the mantle is made. It is concluded that it will break down into Mg_2SiO_4 spinel and coesite at a maximum pressure not much greater than that required to produce the olivine–spinel transition in forsterite.

The pressures and temperatures required to cause the olivine–spinel transition indicate that the transition will occur in the upper 1000 km of the mantle. Because of solid solution effects, the transition will occur over an appreciable depth range.

1. Introduction

In Part I of this series (Ringwood, 1957) a method of estimating the pressure required to invert forsterite from an olivine to a spinel structure was described. The transition pressure found was 175,000 ± 55,000 bars at 1500°C. This result indicated that the transition should occur in the upper mantle and might be related to the 20° discontinuity (Jeffreys, 1952) and the inhomogeneous region inferred by Birch (1952) between 300 and 900 km.

Further study of these questions indicated the desirability of determining the pressure needed to cause the transition in forsterite at a substantially lower temperature than 1500°C. Such data would give the slope (dP/dT) of the transition and also the heat of transition. The author had previously tried to obtain this datum by an investigation of the system Mg_2SiO_4–Mg_2GeO_4 (Ringwood, 1956). This was unsuccessful since it was found that equilibrium could not be reached under the dry-way conditions used. Subsequently it was learned that Dachille and Roy (1956) had been independently studying the same system using hydrothermal and "squeezer" techniques and had been successful in working out some of the phase relationships under equilibrium conditions. Accordingly, when the necessary equipment became available, it was decided to make some runs across the subsolidus field of the system Mg_2SiO_4–Mg_2GeO_4 at a fixed temperature and pressure in order to determine the desired solid solution relationships.

Mg_2GeO_4 has a spinel structure below about 800°C. Above that temperature it inverts to an olivine structure (Dachille and Roy, 1956). The object of this

* Paper No. 162 published under the auspices of the Committee on Experimental Geology and Geophysics and the Division of Geological Sciences at Harvard University.

study was to determine the amount of Mg_2SiO_4 which would enter into solid solution in the spinel form of Mg_2GeO_4 under appropriate P–T conditions, and also to determine the composition of the olivine solid solution in equilibrium with the spinel. Using these data it is possible to calculate the free energy of transition of Mg_2SiO_4 from the olivine to the spinel structure, and the pressure needed to cause this transition (Part I).

2. The System Mg_2GeO_4–Mg_2SiO_4

The object of studying this system was not to furnish complete phase equilibria. This project has been undertaken by Dachille and Roy (1956) with valuable results. The data required by the author were obtained by studying various compositions in the system at 660°C in a squeezer-type apparatus (Griggs and Kennedy, 1956) under a pressure of 30,000 bars.

Experimental

A series of intimate mixtures of GeO_2 and SiO_2 was made up using a method suggested by Roy (personal communication); $SiCl_4$ and $GeCl_4$ were thoroughly mixed in the required amounts and hydrolysed with ammonium hydroxide. A hydrated, intimately mixed precipitate of SiO_2 and GeO_2 separates. This is quickly filtered, washed and ignited. Samples were made up across the composition range $(SiO_2)_{100}$–$(GeO_2)_{100}$ at intervals of 10 mole per cent. These were thoroughly mixed by grinding under acetone with calcined magnesium oxide in the appropriate ratios to form compounds of $Mg_2(Ge_xSi_{1-x})O_4$ composition.

Charges thus prepared were placed between the pistons of a squeezer apparatus and a small drop of water added to facilitate reaction. A pressure of 30,000 bars was then applied and kept constant whilst the temperature was raised to 660°C for 1 hr. Temperature and pressure were then swiftly lowered and the charge was removed. The olivine–spinel inversion in this system is known to be extremely sluggish (Ringwood, 1956) and this procedure furnishes a satisfactory quench. Descriptions of the squeezer apparatus and its operation have not been supplied since these have already been published in detail by other workers (Griggs and Kennedy, 1956; MacDonald, 1956), and standard procedure was followed. Charges thus treated were examined by X-ray and optical methods.

Results of this investigation are set out in Table 1.

For the purposes of calculation it is necessary to know the compositions of co-existing olivine and spinel solid solutions in equilibrium under the stated conditions. From Table 1 the composition of olivine Mg_2SiO_4 saturated with Mg_2GeO_4 is seen to be MS_{85} MG_{15} with an uncertainty of 5 mole per cent (higher accuracy is not required since the calculation is not sensitive to this value). The composition of the saturated spinel solid solution cannot be found from Table 1 since only a small amount of Mg_2SiO_4 has been dissolved. However, it may be obtained in an indirect manner.

The increase in density when Mg_2SiO_4 inverts from the olivine to the spinel structure is approximately 11 per cent (Part I). The volume of the unit cell of forsterite (containing four molecules) is 291 Å^3 (Swanson and Tatge, 1953) or 582 Å^3 for eight molecules. The volume of the unit cell of Mg_2SiO_4 spinel (eight

molecules) would therefore be 524 Å^3, giving it a lattice constant of 8·06 Å. The average lattice constant of the saturated spinel solid solutions is 8·240 Å. According to Vegard's law, the spinel having this value must lie on a straight line joining the

Table 1. Phases present in system Mg_2SiO_4–Mg_2GeO_4 at 660°C and 30,000 bars

Composition (mole %) MS = Mg_2SiO_4 MG = Mg_2GeO_4	Optical examination	X-ray	Lattice constant of spinel phase (Å)
MG_{100}	Homogeneous spinel	Spinel	8·248
MG_{90} MS_{10}	2-phase	Spinel + olivine	8·242
MG_{80} MS_{20}	2-phase	Spinel + olivine	8·241
MG_{70} MS_{30}	2-phase	Spinel + olivine	8·239
MG_{60} MS_{40}	2-phase	Spinel + olivine	8·238
MG_{50} MS_{50}	2-phase	Spinel + olivine	8·240
MG_{40} MS_{60}	2-phase	Spinel + olivine	
MG_{30} MS_{70}	2-phase	Spinel + olivine	
MG_{20} MS_{80}	2-phase	Spinel + olivine	
MG_{10} MS_{90}	Olivine	Olivine	
MS_{100}	Olivine	Olivine	

lattice constant of Mg_2GeO_4 (8·248 Å) to that of Mg_2SiO_4 spinel (determined above). This allows determination of the composition of the spinel solid solution. It is found to be MG_{96} MS_4.

Discussion

In Part I of this series the free energy of transition of forsterite from the olivine to the spinel structure was derived from the compositions of coexisting olivine and spinel solid solutions in which Mg_2SiO_4 was a component. It was found that

$$\Delta F = RT \ln \frac{a_2}{a_1}$$

where ΔF is the molar free energy difference between the olivine and spinel forms of Mg_2SiO_4, T is the absolute temperature, R is the gas constant, a_1 is the activity of Mg_2SiO_4 in the spinel solid solution and a_2 is the activity of Mg_2SiO_4 in the olivine solid solution with which it is in equilibrium at a temperature T. For further details of this derivation, the reader is referred to the previous paper.

In Part I, the system studied was Ni_2GeO_4 Mg_2SiO_4 but similar principles hold in this case. The solid solutions are assumed to be ideal and consequently the activity of an ion becomes equal to its ionic fraction defined as the ratio of the number of specified ions (n) to the total number of lattice sites available to it. Since the ions which display mutual replacement in this case are Si^4 and Ge^4, the activity of the component Mg_2SiO_4 is given by $(n_{Si})/(n_{Si} + n_{Ge})$, or [Si], which is equal to the mole fraction of the component Mg_2SiO_4. In the general case, as exemplified in Part I, where there is more than one independently replacing pair

of ions (Ni–Mg and Ge–Si) this simple expression does not hold, and the activity of Mg_2SiO_4 is given by the TEMPKIN (1945) expression $[Mg]^2[Si]$.

In the case under consideration, a_1 is equal to $(0{\cdot}04 \pm 0{\cdot}01)$ and a_2 to $(0{\cdot}85 \pm 0{\cdot}05)$. From these values ΔF is calculated according to the above expression:

$$\Delta F_p = 23{,}600 \text{ J/mole}$$

It should be remembered that ΔF_p is the difference in free energy under the experimental conditions employed, $p = 30{,}000$ bars and $T = 660°C$.

The total pressure P required to produce equilibrium between the polymorphs at the given temperature is:

$$P\Delta v_1 = \Delta F_p + p\Delta v_2$$

where Δv_1 is the difference in molar volume of the two phases at a pressure P and Δv_2 is the difference in molar volume at a pressure (p) of 30,000 bars. Because of the relative incompressibility of olivine and spinel, Δv_1 may be put equal to Δv_2 with negligible sacrifice of accuracy. Therefore

$$(P - p)\Delta v = 23{,}600$$

where $p = 30{,}000$ bars. Δv for the transition in forsterite was determined in Part I as $4{\cdot}4 \pm 1{\cdot}0$ cm^3/mole. When an allowance for the effect of compression at the approximate transition pressure is made. Δv becomes equal to $4{\cdot}1 \pm 1{\cdot}0$ cm^3/mole.

Consequently for equilibrium at 660°C between the olivine and spinel modifications of forsterite:

$$4{\cdot}1(P - p) \text{ (bars)} = 23{,}600 \quad \text{(J)}$$

thus

$$P = 88{,}000 \text{ bars}$$

When allowance for uncertainty of data is taken into account, a maximum pressure of 116,000 bars and a minimum of 72,000 bars are found. The range of possible error is asymmetrically distributed around the most probable value of 88,000 bars because of the form of the equation for equilibrium.

In Part I, the transition pressure was calculated to be 175,000 bars at 1500°C. These two determinations allow an approximate P–T curve to be constructed for the transition (Fig. 1). The transition curve is found to have a slope of about 100 bars/°C. The range of uncertainty is considerable, and is controlled principally by uncertainty in the value of Δv. Since this affects both calculations in the same direction, a change in Δv tends to cause a parallel displacement of the transition curve without a large change of slope. However, other sources of error are capable of affecting the slope and this must be regarded as tentative. Data on other polymorphic transitions suggest it is more likely to be decreased than increased.

Once again it should be emphasized that all calculations are based upon the assumption of ideal behaviour of the solid solutions. For further discussion of this point, the reader is referred to Part I, where it is concluded that ideality is probably realized.

From the slope of the transition curve and the volume change, it is possible to calculate the entropy change for the transition (ΔS) using the Clapeyron–Clausius equation. The entropy change, ΔS, is found to be approximately 10 cal/°C per mole.

It is believed that the above data on the olivine–spinel transition in forsterite are of considerable significance in understanding the constitution of the mantle. Detailed discussion of this aspect will be taken up in Part III.

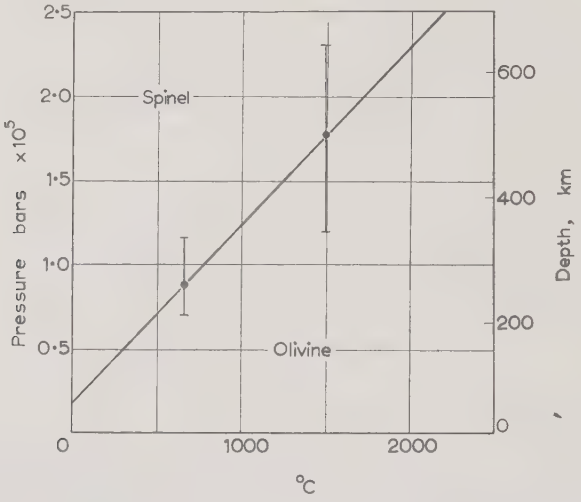

Fig. 1. Calculated equilibrium curve for the olivine–spinel transition in Mg_2SiO_4. Vertical lines indicate ranges of possible error due to experimental uncertainty.

3. The Olivine–Spinel Transition in Fayalite

Common olivine contains about 10 per cent of fayalite in solid solution. Consequently it is desirable to obtain data on the olivine–spinel transition in fayalite as well as forsterite. The first method used was analogous to that employed in the case of forsterite. Subsolidus phase equilibria in the system Fe_2GeO_4–Fe_2SiO_4 were used to obtain the free energy of transition, which was then equated to a $P\Delta V$ term.

Charges were prepared by weighing out Fe_2O_3, metallic iron powder, and the required mixed GeO_2–SiO_2 oxide in the proportions required to make an $Fe_2(Ge_xSi_{1-x})O_4$ solid solution of the desired composition. A slight excess of metallic iron was included. The components were then intimately mixed under acetone. The charges thus prepared covered the composition range at intervals of 10 mol per cent. They were placed in the squeezer and subjected to a temperature of 700°C and a pressure of 25,000 bars for 3 hr. After completion of the run, charges were removed, ground, and examined by X-ray methods.

Phases present were spinel, olivine, and usually residual metallic iron. The Fe_2GeO_4 spinel end member had a lattice constant of 8·401 Å. In bulk the crystals were opaque but when observed singly under magnification were found to be transparent with a greenish brown colour. Compositions of coexisting spinel and

olivine solid solutions in equilibrium under the conditions specified were found by determining limits of phase homogeneity from powder photographs.

Spinel	$Fe_2(Ge_{0\cdot75}\ Si_{0\cdot25})O_4$
Olivine	$Fe_2(Ge_{0\cdot05}\ Si_{0\cdot95})O_4$

The uncertainty was estimated as ± 5 per cent Fe_2SiO_4.

Using this data, and assuming the difference in density between the olivine and spinel polymorphs as 11 per cent, the pressure required to invert fayalite from the olivine to the spinel structure at 700°C may be calculated. The procedure is completely analogous to that used in the previous section for Mg_2SiO_4–Mg_2GeO_4 solid solutions. The inversion pressure thus found is approximately 50,000 bars.

Subsequently the author has realized that the experimental data above are capable of more than one interpretation due to the possibility of various oxidation-reduction equilibria involving Fe^2, Fe^3 and Ge^2, Ge^4. It was assumed that the spinel produced was $Fe_2{}^2\,Ge^4O_4$. It is conceivable however, that some Ge^2 was formed by the reaction $2Fe^2 + Ge^4 = 2Fe^3 + Ge^2$ and that the spinel actually observed was $(GeFe)^2Fe_2{}^3O_4$. There is some reasonably strong evidence that the original assumption was justified, but the situation is by no means clear, and further data are required.

Accordingly it must be emphasized that the previous calculations are based upon the assumption that the system is binary and that the spinel was $Fe_2{}^2Ge^4O_4$. If this assumption is incorrect, the calculation becomes meaningless.

The previous estimate, that a pressure around 50,000 bars at 700°C should suffice to invert fayalite from the olivine to the spinel structure, suggested that the transition might be within the range of capabilities of the squeezer. It was decided to explore for the transition around 400°C. MacDonald (1956) had previously squeezed fayalite at 56,000 bars and 480°C without effect. It appears that reaction rates in crystallized silicates may be too low at these temperatures to allow equilibrium to be reached. It seemed that a more promising approach would be to synthesize fayalite from its components in the squeezer under high pressure.

Ferric oxide, metallic iron powder and Mallinckrodt silicic acid were thoroughly mixed in the proportions required to give fayalite plus a 10 per cent excess of metallic iron. The purpose of the excess iron was to maintain the oxidized iron in the divalent state. The samples were held in the squeezer at 400°C at pressures of 20, 30, 38, 50 and 60 kilobars for periods varying between 4 and 16 hr. The resultant products were then examined by X-ray and optical methods.

The runs at 20, 30 and 38 kilobars consisted substantially of fayalite, together with indeterminate fine grained material and metallic iron. The runs at 50 and 60 kilobars produced considerable amounts of green, transparent, isotropic crystals. Because of their small size and the presence of metallic iron and fine unidentified material, the refractive index was difficult to determine accurately. A value of $1\cdot955 \pm 0\cdot020$ was found.

Additional runs showed that the degree of crystallization was improved by using higher temperatures and leaving a longer time for reaction. A run of 450°C and 55,000 bars resulted in about 80 per cent conversion to the new phase. X-ray

powder patterns showed that the crystals possessed a spinel structure with a lattice constant of 8·235 Å. d spacings and approximate visual intensities are listed in Table 2.

Table 2. Approximate visual intensities and interplanar spacings of fayalite spinel

I	d (Å)	Plane
4	4·7542	111
2	2·9057	220
10	2·4804	311
<1	2·3711	222
5	2·0542	400
2	1·8877	331
4	1·5832	333 / 511
7	1·4540	440
2	1·2548	533
1	1·2414	622
1	1·1896	444
<1	1·1001	642
4	1·0721	553 / 731
1	1·0292	800

$a = 8{\cdot}235$ Å

The calculated density is 4·85 g/cm^3, 12 per cent higher than that of fayalite. This is in agreement with the increase in density derived by applying the Gladstone–Dale law, relating density and elasticity of the two polymorphs.

Further runs have been carried out at 600°C and the position of the transition located around 38,000 bars. It appears that the formation of fayalite at 38,000 bars and 400°C in the first set of runs was due to metastability, since later work has shown that spinel is stable under these conditions. A run at 70,000 bars and 600°C using moistened Rockport fayalite as starting material resulted in complete conversion to the spinel. It seems clear that the new phase is the predicted spinel polymorph of fayalite.

4. P–T Conditions Governing the Stability of Pyroxenes

Since pyroxenes may be important constituents of the mantle it seems desirable to investigate their stability at elevated temperatures and pressures. It is known that protoenstatite melts incongruently to forsterite plus liquid at 1557°C, whilst the pyroxene $FeSiO_3$ does not even occur at liquidus temperatures in the system FeO–SiO_2. Fayalite crystallizes instead. This suggests that Mg–Fe pyroxenes may not be very stable relative to olivines, and that under the high temperatures and

pressures occurring in the mantle, the reaction $2(MgFe)SiO_3 \rightarrow (MgFe)_2SiO_4 + SiO_2$ a possibility. The olivine might crystallize as such, or if the breakdown occurs under sufficient pressure, it might crystallize as the spinel modification. Fortunately, sufficient thermochemical data exist to study this reaction.

The change in free energy with temperature for the reaction:

$$Mg_2SiO_4 + SiO_2 \rightarrow 2MgSiO_3$$

has been computed (Table 4). The data used were from the collection by MacDonald (1954). For convenience, the form of silica occurring in the reaction has

Table 3. Free energies for the reaction $Mg_2SiO_4 + SiO_2 \rightarrow 2MgSiO_3$

T (°K)	ΔG (cal)
298	−2208
1000	−1523
1500	−183
2000	2046
2500	5277

Table 4. Effect of pressure on solubility of Mg_2SiO_4 in Ni_2GeO_4 around 600°C

No.	Composition of charge (mol. %)	Temp. (°C)	Pressure (bars)	Phases present*	Lattice constant of spinel solid solution (Å)	Estimated mol. per cent of Mg_2SiO_4 in spinel
1	NG_{100}				8·221	0
2	$NG_{90}MS_{10}$	600	10,000	spinel	8·220	<1
3	$NG_{90}MS_{10}$	800	10,000	spinel	8·217	3
4	$NG_{45}MS_{55}$	650	20,000	spinel, olivine	8·202	13
5	$NG_{45}MS_{55}$	650	30,000	spinel, olivine	8·197	16
6	$NG_{45}MS_{55}$	660	40,000	spinel, olivine	8·167	36
7	$NG_{45}MS_{55}$	650	50,000	spinel, olivine	8·172	32
8	$NG_{45}MS_{55}$	560	55,000	spinel	8·157	42
9	$NG_{45}MS_{55}$	580	70,000	spinel	8·137	55
10	$NG_{25}MS_{75}$	580	70,000	spinel, hydrous phase	8·137	55
11	$NG_{25}MS_{75}$	580	90,000	spinel, hydrous phase	8·117	68

* Identified from powder photograph. In runs 1, 2 and 8 a small amount of olivine was observed in product by microscopic examination.

been taken to be α quartz. This introduces some uncertainty into the results, but this is unlikely to affect the general conclusions.

Table 3 shows that clinoenstatite (as indicated by the small free energies of formation) is only slightly more stable than a mixture of forsterite and quartz at

temperatures less than 1500°K. At temperatures much above 1500°K, clinoenstatite becomes unstable and breaks down to forsterite and quartz. This is in agreement with the phase equilibrium data.

Because of the low thermal stability of $MgSiO_3$ at atmospheric pressure, it seems that the direction of the reaction considered will be largely controlled by pressure. The following reactions may possibly be of geologic significance:

(1) Mg_2SiO_4 (olivine) + SiO_2 (quartz) → 2Mg SiO_3, $\Delta v = -3{\cdot}44$ cm³.

(2) Mg_2SiO_4 (olivine) + SiO_2 (coesite) → 2Mg SiO_3, $\Delta v = -0{\cdot}73$ cm³.

(3) Mg_2SiO_4 (spinel) + SiO_2 (coesite) → 2Mg SiO_3, $\Delta v = \quad 3{\cdot}3$ cm³.

Reaction (1) shows that pressure will increase the stability of clinoenstatite substantially (by about −80 cal/kbar). Therefore clinoenstatite is stable under conditions existing in the crust and upper mantle.

At shallow depths in the mantle, it is probable that the quartz form of SiO_2 would be replaced by a denser polymorph such as coesite. MacDonald's (1956) results show that at 1500°C, coesite would be stable at a pressure equivalent to that at a depth of approximately 120 km in the mantle. With smaller temperatures, coesite would be stable at lesser depths. Under these conditions reaction (2) becomes applicable. However the Δv for this reaction is small and negative showing that pressure will tend to favour the stability of pyroxene (at temperatures below about 2000°K).

Reaction (3) is of greatest significance. The combination Mg_2SiO_4 (spinel) + coesite has a total molar volume which is 3·3 cm³ smaller than that of the equivalent $MgSiO_3$. It is therefore apparent that high pressures will favour the formation of Mg_2SiO_4 spinel and coesite at the expense of pyroxene. Since increasing temperature also has this effect, it is apparent that (MgFe) pyroxene can possess only a very limited stability range in the mantle.

The total change of free energy when pyroxene breaks down to spinel plus coesite is $\Delta G_{P\rightarrow S+C}$, where

$$\Delta G_{P\rightarrow S+C} = \Delta G_{P\rightarrow F+Q} + \Delta G_{F\rightarrow S} + \Delta G_{Q\rightarrow C}$$

$$\left\{\begin{array}{l} P = \text{pyroxene} \\ S = \text{spinel} \\ F = \text{forsterite} \\ Q = \text{quartz} \\ C = \text{coesite} \end{array}\right.$$

The ΔG terms apply to the reactions indicated by the subscripts, $\Delta G_{P\rightarrow F+Q}$ as tabulated in Table 3. $\Delta G_{F\rightarrow S}$ has been determined earlier, whilst $\Delta G_{Q\rightarrow C}$ may be estimated from MacDonald's (1956) paper.

By far the largest term is $\Delta G_{F\rightarrow S}$. Previous data in this paper show that this is about 12,000 cal/mole at 1000°C and 30,000 cal/mole at 3000°C. $\Delta G_{Q\rightarrow C}$ is only about one-sixth of $\Delta G_{F\rightarrow S}$ at the same temperature. $\Delta G_{P\rightarrow Q+F}$ was found (Table 4) to be insignificant at 1500°C and becoming strongly positive (i.e. favouring pyroxene breakdown) at temperatures greater than this. Thus for the transition:

$$2MgSiO_3 \rightarrow Mg_2SiO_4 \text{ (spinel)} + SiO_2 \text{ (coesite)}$$

the total free energy at zero pressure will be only slightly greater than that for the

fundamental olivine–spinel transition (by about one-sixth) and the Δv change is about three-quarters as great. It is clear then that pyroxene will decompose as indicated in the spinel field in the mantle. The pressure required for this decomposition will be about one-third greater than that required for the olivine–spinel transition at 1500°C. This is a maximum difference, however, since increasing the temperature above 1500°C decreases pyroxene stability and decreases the amount of excess pressure (above that for the olivine–spinel transition) required to cause decomposition. It is clear that the breakdown of pyroxene to spinel plus coesite is dominated by the conditions causing the olivine–spinel transition. The stability of natural pyroxenes will probably be further decreased according to the amount of Fe^2 occurring in solid solution.

5. Transition Phenomena in the Mantle

For an olivine–spinel transition in natural olivine, the transition line for forsterite (Fig. 1) will become broadened into a band, characterized by coexistence of olivine and spinel. This is caused by the presence of fayalite in solid solution. The data in this paper show that at similar temperatures, fayalite requires a much smaller pressure to invert to spinel than forsterite. Accordingly the low-pressure spinels will be rich in fayalite, which is in equilibrium with magnesian olivine. As pressure rises transition occurs continuously over a defined range. It was shown also that MgFe pyroxenes may invert to Mg_2SiO_4 spinel, liberating coesite. The maximum pressures required for this inversion may be somewhat greater than those required for the olivine–spinel transition. The effect of $FeSiO_3$ in solid solution is analogous to the olivine. A transition band is formed which will probably overlap the olivine–spinel transition band.

From an inspection of Fig. 1 it is apparent that these transitions will probably occur in the mantle at depths less than 1000 km if the temperature at this depth is less than 3000°C. Most estimates of temperatures in the mantle (Verhoogen, 1956) imply that the temperature at 1000 km is less than 3000°C. If this is correct, then the phase transition phenomena studied in this paper should occur at depths shallower than 1000 km, covering an appreciable zone. The implications of this conclusion will be considered in detail in Part III.

Appendix—The Effect of Pressure on the Solubility of Mg_2SiO_4 in Ni_2GeO_4

A supplementary series of experiments has recently given strong support to previous conclusions regarding the stability of Mg_2SiO_4 spinel. The experiments are of a reconnaissance nature and a considerable amount of further work will be necessary before the behaviour of the system under high pressures is accurately determined. Nevertheless the general outline seems clear.

It was shown in Part I that Ni_2GeO_4, which has a spinel structure, will dissolve about 9 per cent of Mg_2SiO_4 at 1500°C. At 600°C the solubility appears to be small, probably less than 3 per cent. However at that temperature, solubility is found to increase very substantially with increasing pressure. An analogous effect has been observed in the system Mg_2GeO_4–Mg_2SiO_4 (Dachille and Roy, 1956).

Reactive charges were prepared by mixing co-precipitated magnesium and nickel hydroxides dried at 110°C with co-precipitated hydrous silica and germania, in the ratios required to form $(NiMg)_2(GeSi)O_4$ compounds of desired composition. Chemical analyses of the silica–germania co-precipitates were kindly carried out by Mr. Jun Ito of the Department of Geology, Harvard University. The charges used had compositions $NG_{90}MS_{10}$, $NG_{45}MS_{55}$ and $NG_{25}MS_{75}$ (molecular ratios). Numerous other charges were prepared in different ways, but did not prove sufficiently reactive in the squeezer.

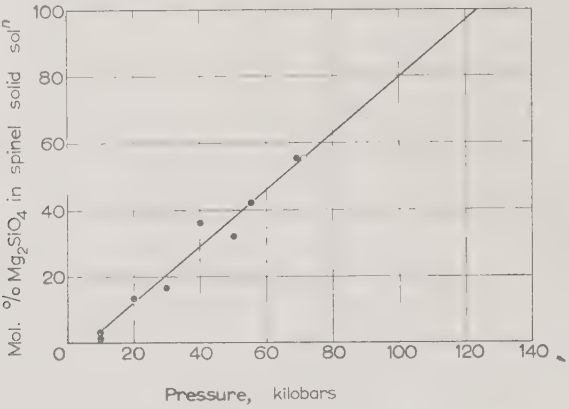

Fig. 2. Effect of pressure on solubility of Mg_2SiO_4 in Ni_2GeO_4 around 600°C.
● Spinel in equilibrium with olivine
○ Spinel in equilibrium with hydrous phase
Pressure at which pure Mg_2SiO_4 spinel should become stable around 600°C (extrapolated)—125,000 bars

Samples were placed in the squeezer and subjected to different pressures at temperatures between 560 and 660°C. Variation of temperature between these limits was aimed at establishing optimum conditions for reaction of charges and obtaining maximum pressure from the squeezer. Runs up to 55,000 bars were made using pistons with faces $\frac{1}{4}$ in. in diameter. For higher pressures pistons with $\frac{3}{16}$ in. faces were used. Results are set out in Table 4.

In run No. 9 a sample of $NG_{45}MS_{55}$ was found by X-ray and optical examination to form a homogeneous spinel at 70,000 bars and 580°C. The lattice constant was 8·137 Å. The lattice constant of pure Ni_2GeO_4 is 8·221 Å. Extrapolation, using Vegard's Law allows determination of the lattice constant of Mg_2SiO_4 spinel, which is found to be 8·07 Å, giving a theoretical density of 3·55 g/cm^3. This is 11 per cent higher than that of forsterite, and thus confirms the value derived in Part I.

Knowledge of the relationship between lattice parameter and composition allows estimation of the composition of the other spinels formed. (Table 4.) Apart from the normal experimental uncertainties, the estimates are subject to the assumption that the behaviour of the system is binary. This subject was fully discussed in Part I where a reasonably close approach was demonstrated. Checks of refractive indices have shown that this is maintained in the system under the present P T conditions. Equality of spinel compositions in runs 9 and 10 support

this. Since in most cases there is only a relatively small amount of olivine present in equilibrium with the spinel, it would need a large deviation from binary behaviour to affect the result significantly.

With the composition $NG_{25}MS_{75}$, at pressures of 70,000 and 90,000 bars, the spinel is no longer in equilibrium with olivine, but with a phase having a 9·9 Å spacing. This is probably a hydrous phase which has become stable relative to olivine at the extreme pressure.

Spinel compositions have been plotted against pressure in Fig. 2. The results are not strictly comparable because of variation of temperature between 560 and 660°C. It does not appear however that this variation is sufficient to significantly change the equilibria. A linear extrapolation indicates that Mg_2SiO_4 spinel should be stable around 600°C at 125,000 bars. This is probably a maximum since the higher experimental pressures may have been somewhat overestimated in the squeezer due to piston distortion. This result thus confirms in essentials, the previous calculations.

Acknowledgements—The project described in this paper was carried out at the Dunbar Laboratory, Harvard University whilst the author was the recipient of a research fellowship provided by the Committee on Experimental Geology and Geophysics, and a travelling scholarship from Melbourne University.

References

Birch F. (1952) Elasticity and constitution of the earth's interior *J. Geophys. Res.* **57,** 227.

Dachille F and Roy R. (1956) System Mg_2SiO_4–Mg_2GeO_4 at 10,000, 60,000 and about 300,000 psi. *Bull. Geol. Soc. Amer.* **67,** 1682.

Griggs D. T. and Kennedy G. C. (1956) A simple apparatus for high pressures and temperatures. *Amer. J. Sci.* **254,** 722.

Jeffreys H. (1952) *The Earth* (3rd Ed.). Cambridge University Press.

MacDonald G. D. F. (1954) *A Critical Review of Geologically Important Thermochemical Data.* Ph. D. Thesis, Harvard Univ.

MacDonald G. D. F. (1956) Quartz coesite stability relations at high temperatures and pressures. *Amer. J. Sci.* **254,** 713.

Ringwood A. E. (1956) The system Mg_2SiO_4–Mg_2GeO_4. *Amer. J. Sci.* **254,** 707.

Ringwood A. E. (1957) The constitution of the mantle—I. Thermodynamics of the olivine spinel transition. *Geochim. et Cosmochim. Acta.* **13,** 303

Romeijn F. C. (1953) Physical and crystallographical properties of some spinels. *Philips Res. Rep.* **8,** 304.

Swanson H. E. and Tatge E. (1953) Standard X-ray diffraction powder patterns *Nat. Bur. Stand. Circ.* No. 539, 1, 83.

Tempkin M. (1945) Mixtures of fused salts as ionic solutions. *Acta. Phys.-chim. URSS.* **20,** 411.

Verhoogen J. (1956) Temperature within the earth. *Physics and Chemistry of the Earth* Vol. 1, Chap. 2. McGraw-Hill, New York.

Geochimica et Cosmochimica Acta, 1958, Vol. 15, pp. 30 to 31. Pergamon Press Ltd., London

Data of rock analyses—IV

Icelandic periodical and serial literature

Bibliography of rock analyses*

MARJORIE HOOKER
U.S. Geological Survey, Washington, D.C.

(*Received* 19 *March* 1958)

. . . and petrographically speaking, the island is now an oceanic rock province.
T. F. W. BARTH, 1950.

THE first chemical analyses of Icelandic rocks to appear in print were undoubtedly those in R. Bunsen's paper *Über die Prozesse der vulkanischen Gesteinsbildungen Islands* published in Poggendorff's *Annalen der Physik und Chemie*, Vol. 83, pp. 197–272, 1851, too early even to be counted among those compiled by H. S. WASHINGTON. From the literature for the years 1884–1913, WASHINGTON lists sixteen analyses in U.S. Geological Survey Prof. Paper 99 (1917), taken from five articles in German, Swedish and American journals. In the 40 years since the publication of WASHINGTON's work, more than one hundred analyses of Icelandic rocks have appeared in books and journal articles, accompanying the reports of geologists who have undertaken field work there. These have been published for the most part in Denmark, Norway, Sweden, Germany, Scotland, and the United States, and will be compiled as the literature of each of these areas is studied.

With the growth of scientific literature in Iceland since 1920, and the more frequent publication therein of geologic papers, it seems advisable to place certain information on rock analysis data on record at this time. Since the first publication of a rock analysis in an Icelandic journal in 1931, a total of twenty-three original analyses (that is, not published elsewhere previously) have appeared. Following the procedure established in the preceding parts of this series, we list first the periodical and serial publications that have been examined, and secondly the references containing analyses, with notes on the rock types, number of analyses, and areas. We have extended the 40 year period, 1914–1953, to include two references published in 1954 and 1955. As one might expect, the literature is regional, containing only analyses of rocks in Iceland, and this fact, together with the small number of references, makes either a rock-name or regional index unnecessary.

I am indebted to T. F. W. BARTH and G. T. FAUST for a critical scanning and review of this work.

* Publication authorized by the Director, U.S. Geological Survey.

Periodicals and Serial Literature

Acta Naturalia Islandica (1946–).
Greinar (Vísindafélag Íslendinga; Societas Scientiarum Islandica) (1935–).
Jökull (Jöklarannsóknafélag Islands) (1951–).
Náttúrufræðingurinn (1931–).
Náttúrugripasafnid (Museum of Natural History, Miscellaneous Papers). Reprints from other periodicals, with one exception.
The Eruption of Hekla, 1947–1948 (Vísindafélag Íslendinga; Societas Scientiarum Islandica) (1949–).
Vísindafélag Íslendinga (Societas Scientiarum Islandica), Rit (1923–).

Bibliography

Áskelsson, Jóhannes (1936) On the last eruptions in Vatnajökull: Vísindafélag Íslendinga (Societas Scientiarum Islandica) Rit 18, 55 pp. *Grímsvötn, Meðalland, and Seyðisfjörður, in Vatnajökull area:* 5; basaltic ash and pumice.

Áskelsson, Jóhannes (1946) A contribution to the geology of the Kerlingarfjöll: Acta Naturalia Islandica **1,** No. 2, 15 pp. *Loðmundur, in Kerlingarfjöll area:* 3; rhyolite and rhyolitic pumice.

Einarsson, Trausti (1950) The eruption of Hekla, 1947–1948. IV. **4,** Chemical analyses and differentiation of Hekla's magma: 34 pp. Vísindafélag Íslendinga (Societas Scientiarum Islandica) *Hekla area:* 8; ash, pumice, lava, bomb, and palagonite tuff.

Emilsson, Steinn (1931) Lössbildung auf Island: Vísindafélag Íslendinga (Societas Scientiarum Islandica) Rit 11, 19 pp. *Ingolfsfjall; Grundarfjörður:* 2; palagonite.

Tryggvason, Tómas (1955) On the stratigraphy of the Sog Valley in SW Iceland: *Acta Naturalia Islandica* **1,** No. 10, 35 pp. *Sog Valley:* 2; basalt.

Þórarinsson, Sigurður (1952) Hverfjall I: Náttúrufraeðingurinn **22,** No. 3, 113–129. *Hverfjall volcano, Mývatn area*: 1; pumice.

Þórarinsson, Sigurður (1954) The eruption of Hekla, 1947–1948. II. **3,** The tephra-fall from Hekla on March 29th, 1947 68 pp. Vísindafélag Íslendinga (Societas Scientiarum Islandica) *Hekla area:* 2; tephra and pumice.

Previously Published Parts of the Series

Hooker M. (1956) I: African periodical and serial literature. *Geochim. et Cosmochim. Acta* **9,** Nos. 1–2, 90–97.

Hooker M. (1956-7) II: Bibliography and index of rock analyses in the African periodical and serial literature. *Geochim. et Cosmochim. Acta* **9,** No. 4, 190–213; Supp. **11,** Nos. 1–2, 138.

Hooker M. (1957) III: New Zealand periodical and serial literature. Bibliography and index of rock analyses. *Geochim. et Cosmochim. Acta* **11,** Nos. 1–2, 130–137.

Geochimica et Cosmochimica Acta, 1958, Vol. 15, pp. 32 to 39. Pergamon Press Ltd., London

Fractionation of sulphur isotopes in volcanic gases

H. Sakai and H. Nagasawa
Department of Chemistry, Faculty of Science, The University of Tokyo, Hongo, Tokyo, Japan

(*Received* 2 *January* 1958)

Abstract—The $^{34}S/^{32}S$-ratios in several samples of SO_2 and H_2S from the fumaroles of Volcano Showashinzan, Japan, were measured. The outlet temperature of the fumaroles from which the samples were collected ranged from 100 to 661°C. It was observed that the lower the outlet temperature of the fumarole, the higher the content of the heavy isotope in the SO_2. The isotopic ratio of H_2S was found, on the other hand, to be almost constant throughout the range of temperature given above. This isotopic fractionation between SO_2 and H_2S was ascribed to the reaction:

$$H_2S + 2H_2O \rightleftharpoons SO_2 + 3H_2$$

The temperatures estimated from the observed fractionation factors and the theoretical ones were in fairly good agreement with the observed outlet temperatures.

The isotopic ratio of both compounds can be reasonably explained by a simplified system containing only H_2S, H_2O, SO_2 and H_2. But, some difficulty arises when the chemical compositions of the actual fumaroles are taken into consideration.

Introduction

In the previous paper (Sakai, 1957), one of the authors reported that the sulphur dioxide from the low-temperature fumaroles in Volcano Shirane, Japan, was enriched in ^{34}S by some 3 per cent as compared with the sulphur dioxide from the high-temperature fumaroles of Volcano Showashinzan, Japan. The fractionation factor between sulphur dioxide and hydrogen sulphide in the former fumarole was $1{\cdot}02_7$, while in the latter nearly no fractionation was observed. It was thought that such fractionation was due to the isotopic exchange of sulphur in the following reaction occurring in the fumaroles:

$$H_2S + 2H_2O \rightleftharpoons SO_2 + 3H_2 \qquad (1)$$

The main purpose of this research is to present further proof for the occurrence of the proposed isotopic exchange reaction. Sulphur dioxide and hydrogen sulphide samples from fumaroles of different temperature in Volcano Showashinzan were subjected to the isotopic analysis of sulphur. An attempt was also made in this paper to explain the observed isotopic ratio from the chemical composition of the fumarolic gases.

Volcano Showashinzan and Its Volcanic Gases

Showashinzan (or spelled as Showa-Shinzan or as Syowa-Shinzan) is a newly formed parasitic volcano of Usu Volcano at the south side of Lake Toya in the southern part of Hokkaido, Japan. This volcanic area has been famous for its activity throughout historic time. The most recent activity started on 28 December 1943 and ended in September 1945, with the formation of the new volcano. This new volcano is composed of Roof Mountain and a dome. Roof Mountain is a platform-shaped mountain of the height of about 250 m above sea level. The dome is situated a little westward from the centre of Roof Mountain and its height is now 405 m above sea level. It is composed chiefly of new lava, a hypersthene dacite. The surface of the dome is, however, largely covered with thick layers of clayey materials, which are commonly burnt into reddish-brown brick-like substance by the heat from the new lava.*

* This brief description of Showashinzan is taken from the paper by K. Yagi (1953).

A number of fumaroles are still spurting on the slopes of the dome. The outlet temperatures of the fumaroles at the upper part of the dome are, on the average, higher than those at the lower part. Outlet temperatures ranging from about 100 to 900°C were found in these fumaroles. S. Oana and his associates have shown that the main components of the volcanic gases are water vapour, carbon dioxide, hydrogen, hydrogen sulphide, sulphur dioxide and nitrogen. Of these, water vapour was always found to be more than about 99 per cent of the total volume.

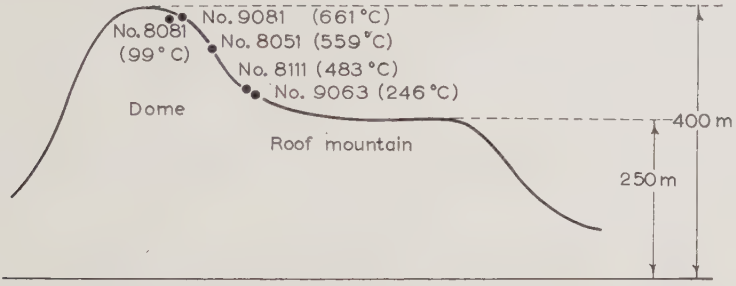

Fig. 1. Approximate position of the fumaroles at Volcano Showashinzan.

Assuming that the chemical equilibrium was attained among some of these components, they calculated the apparent equilibrium temperature at the interior of the fumaroles. They concluded that the minimum temperature of the source of these gases might have been about 1060°C (Oana and Matsuo, 1955; Nemoto *et al.*, 1957). The measurement of the terrestrial magnetism as well as the velocity of seismic waves for this area has been also carried out by other workers (Nemoto *et al.*, 1957). Their results also supported the assumption of the existence of a high-temperature mass in the interior of the dome, which was thought to be a magma reservoir.

Fig. 1 shows the approximate position of the fumaroles, from which we collected the samples of sulphur compounds used in this research. The chemical composition of these gases was analysed, at the same time, by Oana's group. Their results (1957, private communication) are shown in Table 1.

Table 1. Chemical composition of the fumarolic gases of Volcano Showashinzan*

Fumarole	no. 8081	no. 9063	no. 8111	no. 8051	no. 9081
Outlet temp. (°C)	99	246	483	559	661
H_2O (l./1000 l.)	992·8	996·7	995·0	995·4	994·0
SO_2	0·28	0·092	0·095	0·19	0·20
H_2S	0·46	0·068	0·017	0·019	0·0045
CO_2	1·73	2·27	2·75	2·86	3·70
CO	0·0	0·0	0·023	0·0	0·081
O_2	0·57	0·0	0·095	0·0	0·0
NO_2	0·0	0·0	0·0	0·0	0·0
other gases†	4·16	0·87	1·85	1·53	2·02
$\frac{SO_2 + H_2S}{H_2O + 2SO_2 + 2CO_2} \times 10^4$	7·4	1·6	2·8	2·1	2·0
SO_2/H_2S	0·61	1·35	15·3	10·0	44·4

* These samples were collected and measured in August 1957, by S. Oana and his associates (unpublished).

† These include hydrogen, nitrogen, and rare gases and their composition is now being analysed by Oana's group.

Experimental

Fumarolic gases were drawn into an injector through a silica tube plunged into the fumaroles and then bubbled into a KI–I_2 solution slightly acidified with hydrochloric acid. By this process, sulphur dioxide and hydrogen sulphide were oxidized into sulphate ions and free sulphur, respectively. When the colour of iodine almost disappeared, the free sulphur was filtered off and the sulphate was precipitated as barium sulphate from the filtrate. The barium sulphate precipitate was reduced to sulphide by ignition with excess iron powder under a nitrogen stream. The sulphide thus formed, was then treated with hydrochloric acid, and hydrogen sulphide evolved was again precipitated as a sulphide. From these free sulphur and sulphide precipitates, sulphur dioxide was prepared for the mass spectrometric analysis by the same procedure as described by Thode *et al.* (1953).

The isotopic analysis of sulphur dioxide was performed by a CEC Model 21-103A mass spectrometer. The details of the calculation of the isotopic ratio were given in the previous paper. The final expression for the percentage difference between the $^{34}S/^{32}S$-ratio in an unknown sample and that in the standard is as follows:

$$\frac{(p_{66}/p_{64})_{unknown} - (p_{66}/p_{64})_{stand.}}{(p_{66}/p_{64})_{stand.}} \times 1{\cdot}092 \times 100 \quad (2)$$

where p_{66} and p_{64} are the peak height of the mass-66 and -64 ions, respectively. As shown in the previous paper, the isotopic ratio, $^{34}S/^{32}S$, of the troilite sulphur in Tanogami meteorite was assumed to be 0·04500 (or 22·22 in $^{32}S/^{34}S$). As a secondary standard, a galena sample from the Hosokura mine, Japan, was selected and its isotopic ratio was determined to be 0·04493 in comparison with the troilite sulphur. Dr. E. Ingerson of the U.S. Geological Survey kindly sent us three reference samples of sulphur (SO_2, galena, and free sulphur) distributed by the U.S. National Bureau of Standards. The results of our analysis are shown in Table 2. The isotopic ratio of our secondary standard sulphur measured at the same time was 0·04498 ± 0·00009, which is very close to the value previously determined from comparison with the troilite sulphur. In the present paper, however, the old value for the secondary standard sulphur was used in the calculation of the isotopic ratio of the measured samples.

Table 2. The isotopic ratio of National Bureau of Standards reference sulphur*

Species	$^{34}S/^{32}S$	$^{32}S/^{34}S$
Native sulphur no. 120	$0{\cdot}449_4 \pm 0{\cdot}0000_9$†	$22{\cdot}2_5 \pm 0{\cdot}0_4$
Sulphur dioxide no. 120a	$0{\cdot}0449_2 \pm 0{\cdot}0000_9$	$22{\cdot}2_6 \pm 0{\cdot}0_4$
Galena no. 200	$0{\cdot}0449_3 \pm 0{\cdot}0000_9$	$22{\cdot}2_6 \pm 0{\cdot}0_4$

* $2.{}^{18}O/{}^{16}O = 0{\cdot}00409$ (Thode H. G. and Smith S. R. (1944). *Nat. Res. Council Canad., A.E.P. Rep.* MC-57).

† Errors include uncertainties in the calibration of two galvanometers used in the measurement.

Results

In Table 3 are summarized the isotopic ratios of the sulphur dioxide and hydrogen sulphide samples from the seven fumaroles of Volcano Showashinzan as well as from a fumarole of Volcano Shirane. The fractionation factors between the sulphur dioxide and the hydrogen sulphide from three fumaroles are also shown in Table 4. Of these, the data on the samples nos. 52, 69 and 70 were already published in the previous paper. Unfortunately, the amounts of the sulphur dioxide sample from the lowest-temperature fumarole no. 8081 and of the hydrogen

Table 3. The isotopic ratio of sulphur in volcanic sulphur dioxide and hydrogen sulphide

No.	Species	Fumarole no.	Outlet temp. (°C)	δ(%)	$^{34}S/^{32}S$
		Showashinzan			
69*	SO_2	9101 and 9081	ca. 800	$-0{\cdot}3_3 \pm 0{\cdot}1$	$0{\cdot}0447_8 \pm 0{\cdot}1$ %
93	SO_2	9081	661	$-0{\cdot}0_2$	$0{\cdot}0449_2$
94	SO_2	8051	559	$+0{\cdot}1_9$	$0{\cdot}0450_2$
95a	SO_2	8111	483	$-0{\cdot}0_2$	$0{\cdot}0449_4$
95b	H_2S	8111	483	$-0{\cdot}6_1$	$0{\cdot}0446_6$
96a	SO_2	9063	246	$+1{\cdot}0_6$	$0{\cdot}0454_1$
96b	H_2S	9063	246	$-0{\cdot}0_8$	$0{\cdot}0448_9$
97	H_2S	8081	99	$-0{\cdot}1_4$	$0{\cdot}0448_7$
		Shirane†			
70*	SO_2	6	100	$+2{\cdot}0_6$	$0{\cdot}0458_6$
52*	H_2S	6	100	$-0{\cdot}6_2$	$0{\cdot}0446_5$

* These data were already published in the previous paper (SAKAI, 1957). Sample no. 69 was collected on September 1954, by S. OANA and his associates. This is a mixed sample of the two fumarolic gases. Nos. 70 and 52 were collected on August 1956, by H. SAKAI and K. MIZUMACHI, and the other samples collected on August 1957, by the present authors.

† Volcano Shirane is situated in Gumma Prefecture, Japan. The fumarole, no. 6, is violently spurting on the crater rim.

sulphide samples from the fumaroles of nos. 8051 and 9081 were not large enough for isotopic analysis. However, the general trend can be seen from these data: the lower the temperature of the fumarole, the larger the isotopic ratio in sulphur dioxide (see also Fig. 2), that is, the heavy isotope is enriched in the sulphur dioxide from low-temperature fumaroles. The isotopic ratio in hydrogen sulphide, on the other hand, is apparently independent of the outlet temperature of the fumeroles.

Table 4. The equilibrium temperature of the volcanic gases estimated from the isotopic ratio and the theoretical fractionation factor

Fumarole no.	Outlet temp. observed (°C)	Fractionation factor observed	Temp. estimated (°C)
8111	483	$1{\cdot}00_6 \pm 0{\cdot}00_2$	500 ± 100*
9063	246	$1{\cdot}01_2 \pm 0{\cdot}00_2$	320 ± 20
6	100	$1{\cdot}02_7 \pm 0{\cdot}00_2$†	100 ± 20†

* These uncertainties were assigned from the theoretical variation curve of the fractionation factor given in the previous paper and did not include the uncertainties in the calculation of the curve.

† For these values, 1·023 and 140 were erroneously presented in the previous paper (SAKAI, 1957).

If the chemical equilibrium is established for the reaction (1) in the volcanic gases, the following isotopic reactions should also be in an equilibrium state:

$$H_2{}^{32}S + 2H_2O \rightleftharpoons {}^{32}SO_2 + 3H_2 \quad (3)$$

$$H_2{}^{34}S + 2H_2O \rightleftharpoons {}^{34}SO_2 + 3H_2 \quad (4)$$

The free energy change in these reactions is slightly different from each other and hence the isotopic fractionation can occur between sulphur dioxide and hydrogen sulphide. The fractionation factor, k, is expressed as the ratio of the two equilibrium constants, k_3 and k_4, of the reactions (3) and (4), respectively:

$$k = k_4/k_3 = ({}^{34}S/{}^{32}S) \text{ in } SO_2/({}^{34}S/{}^{32}S) \text{ in } H_2S$$

Sakai (1957) calculated the theoretical fractionation factor between sulphur dioxide and hydrogen sulphide at various temperatures. The equilibrium temperature for the fumaroles no. 8111, no. 9063 and no. 6 was estimated from the observed and calculated fractionation factors. As shown in Table 4, the estimated temperatures are in fairly good agreement with the observed values, although the former is always slightly higher than the latter.

Based on the observed chemical equilibrium constant for the reaction (1) in the volcanic gases in this area, Oana and Matsuo (1955*) also calculated the apparent equilibrium temperatures somewhat higher than those measured at the outlet of the fumaroles. These higher values for the estimated temperature can easily be understood because the chemical and isotopic equilibrium could not be reached so fast as to follow the change of the temperature in the passage of the gases through a vent. The lowest temperature at which the isotopic fractionation can attain its equilibrium may depend on the time of passage of the gases through a vent. In Showashinzan, this temperature may be lower than about 320°C, while in Shirane, it is as low as 100°C.

At a higher temperature than 900°C, the fractionation factor between sulphur dioxide and hydrogen sulphide is too small to be measured with good accuracy. As to the temperature of the magma reservoir of Volcano Showashinzan, the authors can only say that it should be higher than about 900°C.

Discussion

If a temperature is given, the fractionation factor between sulphur dioxide and hydrogen sulphide can be uniquely determined. The isotopic ratio depends, however, not only on the temperature, but also on the molecular ratio of sulphur dioxide to hydrogen sulphide.

Sulphur dioxide and hydrogen sulphide from a fumarole are believed to come from a common source of sulphur. Furthermore, the isotopic ratio of the common sulphur can be reasonably assumed to be constant throughout a volcano. When the isotopic ratio in the original sulphur is R_0, the isotopic ratio, R_s, in sulphur dioxide at a given temperature can be expressed as follows:

$$R_s/R_0 = (1 + f)/(1/k + f) \quad (5)$$

* A part of their work was published in the paper by Nemoto *et al.* (1957).

where f stands for the molecular ratio of sulphur dioxide to hydrogen sulphide and k for the isotopic fractionation factor. The isotopic ratio, R_h, in hydrogen sulphide at the temperature can be similarly expressed as shown below:

$$R_h/R_0 = (1 + f)/(1 + kf) \tag{6}$$

If the chemical equilibrium constant K_p and the ratio of the total sulphur to the total oxygen are given for a system containing only H_2S, SO_2, H_2O and H_2, the molecular ratio, f, can be determined at a given temperature and pressure. K_p for the system was experimentally determined by Randall and Bichowsky (1918). In this paper their results were applied to the calculation of the ratio, f,

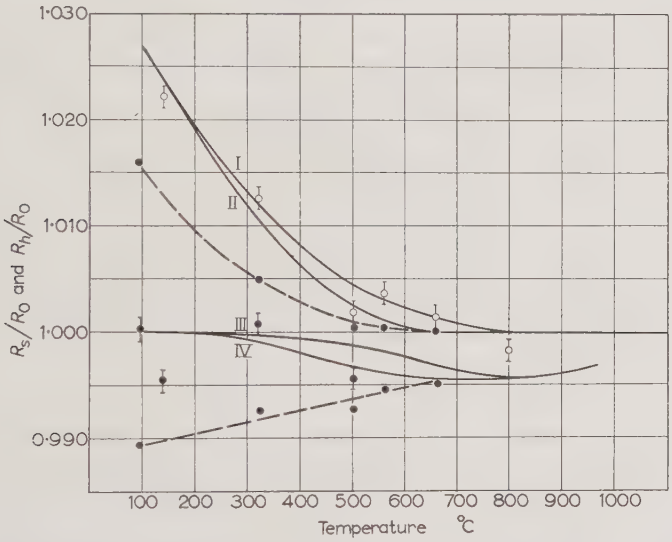

Fig. 2. The observed and theoretical variation of the isotopic ratios in the volcanic SO_2 and H_2S. Solid lines: I and III theoretical variation of the isotopic ratio in $SO_2(R_s/R_0)$ and $H_2S(R_h/R_0)$, respectively, in the simple system of the atomic ratio, S/O, $= 1 \times 10^{-3}$, II and IV theoretical variation of the isotopic ratio in SO_2 and H_2S, respectively, in the system of S/O $= 1 \times 10^{-4}$. Dotted lines: variation of the isotopic ratio in SO_2 (above) and H_2S (below) from the observed ratio: SO_2/H_2S in each fumarole. ○: observed isotopic ratio of SO_2 expressed as the ratio to $R_0(0{\cdot}04486)$ ●: observed isotopic ratio of H_2S expressed as the ratio of R_o.

at temperatures ranging from 100 to 1100°C. The dissociation of the hydrogen sulphide was not taken into consideration, because the temperature of the system was rather low. In the calculation, two values, 1×10^{-3} and 1×10^{-4}, were assumed for the atomic ratio of the total sulphur to the total oxygen, while, in the actual fumaroles, the ratios are found to be of the order of 10^{-4} as shown in Table 1. It was also assumed that the system is under unit atmospheric pressure. This may not be the case in an actual fumarole. The ratio, f, decreases with the increase in pressure.

At a low temperature, R_s/R_0 and R_h/R_0 become equal to k and unity, respectively, because the ratio, f, becomes much smaller than unity as shown in Table 5. At a high temperature, where f is very large, both ratios approach unity. At an intermediate temperature, hydrogen sulphide has a minimum value in the isotopic

ratio. Therefore, the isotopic ratio of the original sulphur, R_0, can be estimated by taking an average of the isotopic ratios of sulphur from the lowest-temperature fumarole no. 8081 and the highest-temperature ones, no. 9081 and no. 9101 + 9081. This gives the isotopic ratio, 0·04486. The theoretical and observed variation in the isotopic ratio in sulphur dioxide and hydrogen sulphide with temperature is shown in Fig. 2, where the observed isotopic ratios are expressed as the ratios to R_0 estimated above. The observed isotopic ratios are very close to the theoretical curves. The isotopic ratio of sulphur from Shirane is also seen to be in good agreement with the curve. This is not surprising because the isotopic ratio of sulphur in igneous rocks should be fairly constant.

Table 5. The calculated molecular ratio, SO_2/H_2S ($=f$) in the system: $H_2S + 2H_2O \rightleftharpoons SO_2 + 3H_2$

Temp. (°C)	SO_2/H_2S	
	Atom. ratio S/O $= 1 \times 10^{-3}$	S/O ... 1×10^{-4}
100	10^{-4}	$.10^{-4}$
300	0·01	0·03
500	0·25	1·30
700	5·10	332
900	249	5000
1100	$>10^3$	$>10^4$

At a given temperature, f depends both on the pressure and on the atomic ratio of sulphur to oxygen as shown above. In addition, the increase in the content of hydrogen would diminish the ratio, f, to a considerable extent. The reaction, $H_2O + CO \rightleftharpoons CO_2 + H_2$, causes the increase in the content of hydrogen at a lower temperature. Further, the net content of hydrogen would vary from one fumarole to another. Therefore, a slight variation in the isotopic ratio can be observed in both sulphur compounds from the different fumaroles, even if they were formed at the same temperature and driven from a common source of sulphur. This may be one of the mechanisms by which sulphur of volcanic origin comes to show some range of variation in its isotopic ratio within each group. The equation (6) indicates that the isotopic ratio in volcanic hydrogen sulphides cannot be larger than that in the original sulphur, because k is always larger than unity. Here, it is of some interest to note that volcanic hydrogen sulphides measured up to date had the isotopic ratio slightly lower than that of the meteoritic sulphur (Sakai, 1957). If their original sulphur or sulphur in igneous rocks has nearly the same isotopic ratio as the meteoritic sulphur, this fact may be partly understood by the above consideration. This cannot, however, explain the fact that igneous sulphides tends to be enriched in ^{34}S compared with volcanic hydrogen sulphides and even with the meteoritic sulphur (Macnamara *et al.*, 1952; Sakai, 1957; and Vinogradov *et al.*, 1957). The original sulphur in Volcano Showashinzan seems to be slightly depleted in the heavy isotope as compared with the meteoritic

sulphur. Its isotopic ratio estimated above coincides rather closely with the range of the isotopic ratio of the volcanic hydrogen sulphide and native sulphur* given in the previous paper. But, here, any significant discussion cannot be made on this matter, when we consider the uncertainties in the estimation (for example, if we take the sulphur dioxide sample of no. 94 in place of no. 69 in the calculation, the estimated value becomes to be 0·04494).

If we use the observed ratio, f, in each fumarole shown in Table 2, instead of the calculated one, the variation curves (the dotted lines in Fig. 2) deviate significantly from the observed isotopic ratios. This discrepancy is partly ascribed to the fact that, in the actual fumaroles of low temperatures, the ratio, f, is much larger than that in the simple system considered above. At low temperatures, the reaction (1), proceeds only slowly if at all, and at a certain temperature the reaction would stop. At Volcano Showashinzan, such a temperature may be lower than 320°C. But even in this fumarole, no. 9063, the discrepancy is too large to be neglected. Randall and Bichowsky's measurements of K_p for the reaction were carried out only at temperatures higher than 1160°K. Their results may not be reasonably applied to the case of such low temperature as considered above. Further, in volcanic gases, sulphur can also exist in the forms other than sulphur dioxide and hydrogen sulphide. A large amount of native sulphur deposits can be always observed at the outlet of the low-temperature fumaroles in this area. The formation of these sulphur compounds would disturb the isotopic equilibrium between sulphur dioxide and hydrogen sulphide. It is also desirable to improve the analytical method for the gaseous composition in the fumaroles, especially for sulphur compounds.

Acknowledgement—The authors are greatly indebted to Professor N. Saito of this laboratory for his kind advice and encouragement throughout the research. The authors are also much obliged to Professor S. Oana and his associates of Nagoya University, Japan, for their kind help in the field work at Volcano Showashinzan. Some of their unpublished data on the chemical composition of the fumarolic gases were presented here with their kind permission.

References

Macnamara J., Fleming W., Szabo A. and Thode H. G. (1952) *Canad. J. Chem.* **30,** 173.
Nemoto T., Hayakawa M., Takahashi K. and Oana S. (1957) *Report on the Geological, Geophysical and Geochemical Studies of Usu Volcano (Showa-Shinzan).* Report of Geological Survey of Japan, No. 170.
Oana S. and Matsuo S. (1955) *Symposium on Geochemistry held at Tokyo.*
Randall M. and Bichowsky F. R. (1918) *J. Amer. Chem. Soc.* **40,** 368.
Sakai H. (1957) *Geochim. et Cosmochim. Acta* **12,** 150.
Thode H. C., Macnamara J. and Fleming W. H. (1953) *Geochim. et Cosmochim. Acta* **3,** 235.
Vinogradov A. P., Chupkhin M. S. and Grinenko V. A. (1957) *Geokhimia* **3,** 183.
Yagi K. (1953) *Trans. Amer. Geophys. Un.* **34,** 449.

Geochimica et Cosmochimica Acta, 1958, Vol. 15, pp. 40 to 50. Pergamon Press Ltd., London

Potassium–argon age of iron meteorites*

R. W. Stoenner and J. Zähringer†
Brookhaven National Laboratory, Upton, L.I., N.Y.

(*Received* 12 *February* 1958)

Abstract—The K^{41} and A^{40} have been determined in seven specimens of five falls of iron meteorites. The measured A^{40} content was found to be principally radiogenic in origin, and associated with the potassium. Under the usual assumptions accepted for this method, ages have been calculated and found to be close to 10×10^9 years, which is about twice the reported age of stone meteorites, and also higher than the supposed age of the universe.

Introduction

The only previous attempt to determine the geological age of an iron meteorite was that by Paneth and co-workers using the helium method (Chackett, Golden, Mercer, Paneth and Reasbeck, 1950; Chackett, Reasbeck and Wilson, 1953). Although measurable amounts of uranium and helium have been reported, more recent investigations have shown that an appreciable amount of the helium consists of He^3 (Paneth, Reasbeck and Mayne, 1952; Paneth, Reasbeck and Mayne, 1953) which is primarily due to cosmic ray effects in outer space, and the uranium content of iron meteorites has been shown to be less than 10^{-10} g U/g iron (Reed and Turkevich, 1955). As a consequence, it would seem that an age determination based on the decay of uranium is not feasible.

Since stone meteorites have far larger concentrations of those elements which are useful for age determinations, investigations on this material have not encountered the same difficulties inherent in the dating of iron meteorites. The ages of stone meteorites have been measured by several methods. The most extensive data have been obtained by the potassium–argon method, with resulting ages ranging from 0·6 to $4{\cdot}5 \times 10^9$ years (Gerling and Levskii, 1956; Wasserburg and Hayden, 1955; Thompson and Mayne, 1955; Reynolds and Lipson, 1957; Begemann, Geiss and Hess, 1957). The lead–lead method applied to two stone meteorites gave an age of $4{\cdot}55 \times 10^9$ years (Patterson, 1956). On one of these meteorites, an age determination with the Rb–Sr method has been done, and this age is not in disagreement with the lead–lead age (Schumacher, 1956). In a recent publication, Reed and Turkevich (1957) have calculated ages from U–He data; some of these ages are somewhat lower than K–A ages, but seem to be generally in agreement with the above results. The maximum age of stone meteorites is therefore believed to be $4{\cdot}5 \times 10^9$ years.

Neutron fluxes currently available give the activation analysis method such a high sensitivity that it seemed possible to attempt the determination of K and A

* Research performed under the auspices of the U.S. Atomic Energy Commission.
† Supported by the Deutsche Forschungsgemeinschaft. Present address: Physikalisches Institut, Freiburg i.B. (Germany).

in iron meteorites. Further, this method is relatively free from any danger of contamination by reagents used in the analysis. According to natural abundances, potassium was expected to be present in higher concentration than uranium. However, the difficulty may arise that argon may not only be due to decay of K^{40}, but may also be produced as the residual nuclei of cosmic ray reactions on the matrix. The amount of argon so produced may be estimated from the amount of He^3 in the meteorite. The ratio of $He^3 : A^{36} : A^{38}$ has been measured in meteorites with large variations in He^3 content, and was found to be practically constant (Genter and Zähringer, 1957). Also, measurements of cross-sections for production of T and A^{37} with protons with cosmic ray energies in iron targets at various depths support this result (Fireman and Zähringer, 1957). Therefore, the amount of He^3 was determined in meteorites, and those specimens with low He^3 content were selected for this investigation in order to keep this correction small.

Experimental

The method of activation analysis was first proposed by Hevesy and Levi (1936). The thermal neutron flux available in a nuclear reactor has made the method extremely useful for the determination of trace constituents in a large variety of materials. The application of neutron activation analysis to iron–nickel meteorites has been made by Goldberg and Brown who determined gallium and palladium (1949) and also gold and rhenium (1950). Since that time there have been numerous other applications of the method to materials of geochemical interest (Berl, 1956).

The general procedure consists of irradiating a sample of the meteorite with neutrons in a nuclear reactor for an appropriate length of time, after which the element to be determined is isolated from the sample and its radioactivity is measured by suitable means. Usually the amount of the element being determined is very small so that its isolation is facilitated by the addition of a convenient, known quantity of the element in the ordinary inactive state to serve as a "carrier".

Preliminary experiments in this study indicated that the distribution of potassium and argon in iron–nickel meteorites is extremely inhomogeneous. In a single specimen, replicate determinations showed a variation of 10^2 in argon content and a variation of 10^3 in potassium content, hence it became imperative to develop a procedure in which potassium and argon were determined in the same sample. Such a procedure was developed and was used for all subsequent determinations.

The procedure finally adopted was as follows: The sample of 1–10 g was first cleaned of surface contamination by etching with three portions of a 1 : 1 mixture of 6N HCl and 6N HNO_3. Heat was used to initiate a vigorous reaction. After the acid etching, the sample was washed three times each with water, acetone and diethylether in that order, and finally was wrapped in aluminium foil for irradiation. All the samples were irradiated for 3 hr in pneumatic tube No. 3 of the Brookhaven Reactor. For purposes of flux calibration, 10–20 mg of potassium acid phthalate was weighed, wrapped in aluminium foil, and irradiated with each sample. After irradiation the meteorite sample was again etched with acid to remove any surface contamination which may have occurred after the initial treatment. The sample was then weighed and placed in the argon extraction furnace.

For the determination of A^{40}, the reaction A^{40} (n, γ) A^{41} was used. The argon was extracted by melting the sample in a graphite crucible with an induction heater. The vacuum system used in the determination of argon was similar to that used by Fireman and Schwarzer (1957) with the addition of calcium and copper oxide furnaces to remove all volatile components other than the noble gases, and a cooled charcoal trap to absorb the argon.

Argon was isolated and determined as follows: the furnace was connected to the vacuum system, and the graphite crucible was degassed by heating before the sample was transferred into the crucible with the aid of a magnet. As an additional precaution against any argon contamination not removed by the etching treatments, the sample was heated in vacuum at 500°C for 10 min. Approximately 0·25 cm^3 of dead carrier argon was admitted to the furnace. The sample was then heated to 1600°C for 20 min. To isolate the argon, the evolved gases were passed over the calcium furnace at a temperature of 600°C, over the copper oxide furnace at a temperature of 400°C, after which the argon was absorbed on charcoal at liquid nitrogen temperature. With a Toepler pump the argon was transferred to a Geiger counter. The counter filling consisted of a 10 : 1 mixture of argon and ethyl acetate. The radiochemical purity of the argon was affirmed by following the decay of A^{41}. The interval between the end of an irradiation and the time when the A^{41} was ready to be counted was usually about 2 hr.

The counting rate of A^{41} was related to the absolute amount of A^{40} by irradiating, under the same conditions prevailing during a sample irradiation, a measured amount of A^{40} together with a weighed quantity of potassium acid phthalate. The potassium was precipitated and counted as described below. The argon was purified as described above and filled in the same gas counter. The specific activity of A^{41} resulting from a standard irradiation is thus compared to the specific activity of K^{42} resulting from the same irradiation. On the basis of the specific activities of the potassium standards irradiated with each meteorite sample, the neutron flux in all experiments was observed to be constant to within 10 per cent. Since both nuclear reactions employed for the determination of A^{40} and K^{41} involve thermal neutrons, possible small self-shadowing effects within the meteorite sample are cancelled out if the A^{40}/K^{41} ratio in the sample is compared to the counting ratio of A^{40} and K^{41} in the standards. Under the conditions of these experiments, 1 count/min was equivalent to 6×10^{-10} cm^3 of A^{40}. The background of the counter was about 30 counts/min.

To be certain that the extracted A^{41} was due only to the reaction, $A^{40}(n, \gamma)A^{41}$, a series of tests was necessary. A^{41} can be produced with fast neutrons by the reaction $K^{41}(n, p)A^{41}$. Therefore, samples of KCl were irradiated under the standard conditions, and it was found that 1×10^{-7} g of potassium gave 1 d/min of A^{41}. Fast neutrons on Ca^{44} can result in A^{41} by means of a (n, α) reaction. Irradiation of $CaCO_3$ gave, however, only an overwhelming A^{37} activity resulting from a $(n.\alpha)$ reaction on Ca^{40}. In the determination of A^{41} in meteorite samples, no significant amounts of any longer lived activity were observed. Hence it was concluded that the reaction $Ca^{44}(n,\alpha)$ could not have contributed to the observed A^{41} activity. To rule out all possible fast neutron reactions, several samples of meteorites were irradiated with Cd cover. No appreciable amounts of A^{41} were

detected. As a further test of the effect of side reactions of neutrons with trace elements, two samples of the stone meteorite, Forest City, were analysed for A^{40} by the method described. In this case, A^{37} activity resulting from the Ca^{40} in the sample gave a high background. The A^{40} is, however, in agreement within 10% with data obtained by mass spectrometry (Wasserburg and Hayden, 1955).

It is believed that the etching of the meteorite samples after irradiation followed by heating and evacuation should remove all absorbed atmospheric argon, but to test further whether this treatment might have been insufficient, several samples were heated overnight in vacuum at 600°C, sealed off in quartz, and irradiated in the pile in the usual fashion. No change in the A/K ratio was observed. Further evidence that precautions taken to avoid atmospheric argon contamination were sufficient is given by the experiments on two samples of Cape York, and one sample of Brenham Township where no A^{41} could be detected.

The He^3 content used to estimate the A^{40} produced by spallation was determined by the activation analysis method of Fireman and Schwarzer (1957). He^3 was activated by a (n, p) reaction to tritium which was counted in a gas counter. By irradiating the sample in a region of the reactor where the fast neutron flux is relatively low, the detection limit has been decreased down to 10^{-9} cm^3 He^3/g iron.

In addition, with the co-operation of Schaeffer of this laboratory, the He^3 content as well as neon and argon isotopes of all these meteorites have been determined with a highly sensitive mass spectrometer. The He^3 content was found to be in agreement with that found by activation analysis, and the amount of neon and argon spallation isotopes were found to be about proportional to the He^3 content. Detailed results of this investigation are to be published in a separate paper.

For the determination of potassium, the reaction K^{41} (n, γ) K^{42} was used. It was of interest to ascertain whether the potassium in the sample was volatile under the conditions of the argon extraction, so the furnace walls and cold trap were analysed separately from the graphite crucible and meteoritic metal, which were treated together as the second part of the sample. In almost every case over 99 per cent of the potassium found in the sample was on the furnace walls and the cold trap. In one experiment the cold trap was examined separately and no potassium was detected.

Potassium was washed from the furnace and cold trap with a boiling mixture of 6N HNO_3 and HF. The metal phase was dissolved in a mixture of 6N HNO_3, 6N HCl, and conc. HF. Potassium was first separated from the matrix material by a cobaltinitrite precipitation; this was followed by decontamination steps of basic carbonate precipitations, acid sulphide precipitations, basic sulphide precipitations, and an anion exchange step from 9N HCl on Dowex 1. Potassium was then precipitated as the perchlorate, once more with cobaltinitrite and finally again as the perchlorate in which form it was counted.

The samples were counted with a standard end-window beta proportional counter, and their counting rates were compared directly with the counting rate of the standard. Samples were generally ready for counting about 24 hr after the end of the irradiation. Under these conditions 1 count/min is equivalent to about 2×10^{-10} g of potassium. After the radiochemical purity of the K^{42} had been

verified by following its decay, the sample and standard were redissolved in water, and the amounts of added potassium carriers recovered were determined flame photometrically. Counting rates were corrected accordingly.

Confirmation of the validity of the potassium measurements is a troublesome matter in that it is difficult to find a homogeneous material of meteorite-like composition which has a very small and known potassium content. To ascertain the practical sensitivity and reproducibility of the method, a series of ten samples of high purity terrestrial iron, with sample weights varying from 0·1 to 1 g, was carried through the entire method, except that the argon extraction procedure was omitted. Seven of the samples showed a potassium content of 4·1 parts per billion (p.p.b.) with an average deviation of 0·3 p.p.b., while the other three samples gave values of 6·6, 7·5, and 19·5 p.p.b. respectively. Since in iron meteorites, the potassium might occur as some form of a silicate, samples of a Bureau of Standards feldspar were taken through the procedure, and the results agreed within 10 per cent with the certificate value. A synthetic sample of 10 p.p.m. potassium in iron was prepared by mixing in powdered iron an appropriate quantity of feldspar. Samples of this mixture weighing from 0·3 to 4 g were analysed. Some of these were melted in the furnace as if argon were being extracted, while some were analysed directly omitting the argon procedure. In all cases the results agreed to within 10 per cent of each other, and the mean agreed to within 10 per cent with the potassium added. As a final check, a sample of the stony meteorite, Forest City, was obtained. Wasserburg and Hayden (1955) by isotope dilution have obtained values of 0·0827 per cent and 0·0835 per cent for the potassium content of this meteorite. Edwards and Urey (1955) measured potassium in this meteorite by flame photometry following a distillation process and found a mean of 0·0842 per cent. The present method was applied to two samples of this meteorite and values of 0·081 per cent and 0·083 per cent were found. From the results of these experiments it was concluded that:

(1) The present method for potassium is reliable to within 10 per cent.
(2) Problems of sample contamination are not prohibitive even at the p.p.b. level.
(3) Self-shadowing effects are negligible for all sample sizes employed.

Discussion of Results

In Table 1 are contained the results of experiments with meteorites having a high He^3 content. It was initially thought that these specimens should give a ratio of He^3 to A^{40} which would be useful in evaluating a correction for spallation A^{40} in other meteorites. However, the potassium contents were so large that most of the observed A^{40} could have resulted from the decay of K^{40} rather than from spallation. Accordingly another approach to evaluate this correction was necessary. It can be estimated from recent measurements of spallation cross-sections of T, He^3 and argon isotopes in iron targets which have been bombarded by high-energy protons (Schaeffer and Zähringer, 1958). Assuming a mean cosmic ray energy of 3 BeV, the T cross-section is 100 mb and the He^3 cross-section is 240 mb. A reasonable estimate for the A^{40} cross-section as derived from these measurements would be about 2 mb. The ratio of He^3 to A^{40} in meteorites, therefore, was taken to be 170, and the appropriate A^{40} correction was applied to all meteorites.

Table 1. Results of three meteorites with high He^3 contents

Meteorite	Sample weight (g)	He^3 (10^{-7} cm^3/g)	A^{40}_{total} (10^{-7} cm^3/g)	$A^{40}_{spall.}$ (10^{-7} cm^3/g)	$A^{40}_{rad.}$ (10^{-7} cm^3/g)	K (10^{-6} g/g)	cm^3 A^{40}/g K	Age ($\times 10^9$ yr)
Mt. Ayliff American Museum of Natural History Catalogue No. 2228	1·8	65	1·20	0·38	0·82	0·29	0·28	6·9
Arispe	3·15	25	0·48	0·15	0·33	0·13	0·25	6·8
H. H. Ninninger Collection	2·5		0·41		0·26	0·092	0·28	6·9
Carbo Harvard Geological Museum	1·8	25	0·35	0·15	0·20	0·031	0·65	8·4

In Table 2 are listed the results of experiments on two different specimens of two separate falls. These meteorites have low He^3 content so no significant correction for spallation A^{40} was necessary. For those experiments in which the potassium and argon were determined on the same sample, an A/K ratio and a

Table 2. Results of four specimens from two falls with low He^3 contents

Meteorite	Sample Weight (g)	$A^{40}_{rad.}$ (10^{-7} cm^3/g)	K (10^{-6} g/g)	cm^3 A^{40}/g K	Age ($\times 10^9$ yr)
Canon Diablo I	6·1	0·18	0·027	0·67	8·5
0·4 $\times$ 10^{-7} cm^3 He^3/g	3·5	0·44	0·16	0·27	6·9
Freiburg	3·3	3·7	1·6	0·23	6·6
	4·3	0·81	0·75	0·11	5·3
	3·2	0·18			
	1·93		0·19		
	2·40		0·41		
	3·0		0·074		
	3·34		0·043		
	2·78		0·064		
	2·97		0·0036		
Canon Diablo II	8·8	0·32	0·004	8·00	13
0·2 $\times$ 10^{-7} cm^3 He^3/g	5·8	0·35	0·011	3·20	11
American Museum of	9·9	0·76	0·040	1·90	10·5
Natural History,	6·7	0·31	0·007	4·40	12
uncatalogued					
Toluca I	5·8	0·81	0·54	0·15	5·9
0·83 $\times$ 10^{-7} cm^3 He^3/g	3·8	0·72	0·24	0·30	7·1
American Museum of	3·5	0·77			
Natural History,	2·0	1·9			
Catalogue No. 730	6·9	2·2			
	3·0	0·8			
	3·0		1·36		
	2·6		0·58		
	2·1		0·11		
	1·9		0·079		
	2·66		0·28		
	3·8		0·24		
	3·95		0·66		
Toluca II	3·9	0·09	0·0062	1·45	10·0
9·3 $\times$ 10^{-7} cm^3 He^3/g	4·4	50·	2·16	2·30	10·8
American Museum of	3·9	0·23	0·029	0·79	8·8
Natural History,	4·1	0·30			
Catalogue No. 729					

calculated age are given. In addition, Table 2 contains the results of those experiments where potassium and argon were determined independently on separate samples. Tabulated directly under the name of the fall, is the He^3 content of that specimen as measured by the methods described above.

It may be noted that the fluctuation in K and A contents is very large within the same specimen. Potassium was found to vary from a few p.p.b. to a few p.p.m. This indicates that the potassium is not homogeneously distributed, but is concentrated in very small spots. It was observed that samples containing troilite inclusions showed a relatively higher potassium content. The argon content fluctuates similarly, and in general follows the variations in potassium content, but these fluctuations are somewhat smaller, indicating that the argon is more evenly distributed in the sample, but is still, however, located in near proximity to the spots containing potassium. It is reasonable to expect that during the course of time, the difference in chemical behaviour of potassium and argon would have promoted a separation of these two elements. An instructive example of such a phenomenon is the formation of Widmannstätten figures. A qualitative picture of the manner in which this separation of potassium and argon took place may be as follows. If at the time of solidification, the potassium was already concentrated in small spots of favourable chemical environment, the argon may have diffused into the surrounding volume while the potassium remained chemically bound to its original position. If at the time of solidification, the potassium was homogeneously distributed throughout the meteorite, and if the potassium concentration process took place over an extended period of time, the A^{40} resulting from the decay of K^{40} during this time would be more evenly distributed.

As a consequence of the observed inhomogeneity of the meteorites, an accurate age determination would require a very large sample. The sample size is limited by considerations of experimental techniques, activity levels at the end of the irradiation, and self-shadowing effects. In order to circumvent these difficulties, numerous measurements were made on smaller samples.

The A/K ratios of these measurements are listed in column 5 of Table 2. It is of interest to note that within one specimen of a meteorite, Toluca II for example, though the potassium content may vary by a factor of 300, the A/K ratio remains constant to within a factor of 2.

It may be seen that the means of the A/K ratios of different specimens of the same meteorite fall, vary quite significantly. For both Canon Diablo and Toluca, this variation between specimens I and II is about a factor of 10. It does not seem reasonable that two specimens from the same fall should have different ages, nor is there any evidence that this variation is due to experimental techniques in that the same experimental conditions obtained for all samples listed in Table 2; further there was complete randomness about the order in which they were run. For both meteorites, specimen I differed qualitatively in appearance from specimen II by having more cracks and irregular features where deterioration of the sample might have occurred. Initial experiments were conducted with specimens designated I, and argon and potassium were determined on separate samples. The widely varying results (see Table 2) were believed at that time to be due to defects in the sample mentioned above. As a consequence, samples as free as possible from these defects,

and taken from the centre of a larger body, were chosen and are designated II. Dr. Brian Mason kindly allowed the authors to cut centre sections from larger specimens of Toluca and Canon Diablo. The analysis of these specimens, however, showed again approximately the same wide fluctuations in argon and potassium contents, but the A/K ratio was higher by a factor of 10. Whether or not the A/K ratio can be correlated with the surface appearance of the specimen may be open to question, but it is believed that the higher A/K ratio must be a criterion for selecting the sample. Mass spectrometric data obtained during the course of this investigation support this contention. Toluca I and Canon Diablo I show anomalous He^3 : neon : argon spallation ratios which could be explained by postulating a loss of He^3, and would indicate that these two specimens have a different history.

Finally, in the last columns of Tables 1 and 2 are given the calculated ages. For this calculation, the following assumptions have been made:

(1) The decay constant of K^{40}, λ is $0{\cdot}53 \times 10^{-9}\ y^{-1}$ and the branching ratio, λ_K/λ_β is 0·12.

(2) The isotopic abundance of K^{40} is the same in iron meteorites as on the surface of the earth.

(3) Natural K^{40} is the only source of A^{40} with the exception of that produced by cosmic ray effects, for which a correction may be applied. This implies, as well, that there was no primordial A^{40} at the time of solidification ($t = 0$).

(4) Leakage of A^{40} has been negligible.

Ages calculated under these assumptions range from 5 to 13 $\times$ 10^9 years. In accordance with the discussion above, the ages calculated from those samples having higher potassium and A^{40} contents are considered to be most nearly correct. It is notable that Canon Diablo II and Toluca II give ages (11 $\times$ 10^9 years) which are in agreement within the variation evident in these investigations. If the above assumptions are valid, the authors believe that the age of these iron meteorites is 10 $\times$ 10^9 years.

The decay constant and the branching ratio of K^{40} have been measured by several methods, and the agreement is such that these are believed to be known to better than 10 per cent.

Isotopic abundances in meteorites have so far never been observed to be significantly different from terrestrial isotopic abundances except for those isotopes whose abundance might be altered by cosmic ray effects. As pointed out, the necessary correction has been applied. A high neutron flux might have produced a considerable amount of A^{40} from K^{39}, however little is known concerning the isotopic composition of trace elements in meteorites. Hamaguchi, Reed and Turkevich (1957) have found in stone meteorites that uranium, whose isotopic abundance would have been changed by neutron irradiation, is not different from terrestrial uranium. From the He^3 content of iron meteorites, Fireman and Schwarzer (1957) have also concluded that the neutron flux out in space is less than 1 n/cm^2 per sec.

The fact that in a single specimen of a meteorite, the potassium content in several samples may vary by a factor of several hundred while the A/K ratios remain fairly constant, would seem to render unlikely the possibility of any significant quantities of primordial A^{40}.

The assumption, however, that there was no leakage of argon from these samples might not be valid. The ages contained in Tables 1 and 2 are therefore believed to be minimum values.

The difference between these results and the accepted age of stone meteorites is remarkable. This is contrary to the general opinion that stone and iron meteorites have the same age. The lower ages of stone meteorites as determined by the K–A method and the He method may possibly be due to diffusion loss. There exists a number of papers on K–A ages indicating there is appreciable loss of argon. Gentner, Goebel and Präg (1954) found in 23 $\times$ 10^6 year old Buggingen sylvenite, that dependent on crystal size, there is an argon deficiency of up to 20 per cent. From these measurements was calculated a diffusion constant of $1{\cdot}5 \times 10^{-19}$ cm^2/sec. Reynolds (1957) has recently determined the diffusion constant of argon in feldspar by measuring the argon released at higher temperatures (400–900°C). Upon extrapolation to room temperature, he arrives at a value in agreement with that of Gentner and co-workers. He concludes that when dating feldspar-containing rocks older than 10^9 years, serious argon losses must be considered.

A more complete theoretical treatment of the diffusion problem has been given by Oser (1954), who calculated for different ages (t), the dependence of A/K ratios on the diffusion constant (D) and crystal size (d). He derives for various values of D/d^2 the maximum determinable age, which is defined as that time elapsed after which the rate of argon loss by diffusion is equal to the rate of argon production by decay of K^{40}. For example, if $D = 1{\cdot}5 \times 10^{-19}$ cm^2/sec, and $d = 1$ mm, the maximum determinable age is about 100 million years; during this time the diffusion loss already amounts to 60 per cent. The crystal size in our specimen of Forest City certainly does not exceed 1 mm. Little is known, however, of the diffusion constant in stone meteorites and factors such as thermal history which affect it. Even if we assume that $D = 10^{-29}$ cm^2/sec, the A/K ratio, given essentially by the diffusion factor $D(\mathrm{T})/d^2\lambda$, cannot exceed a value corresponding to an age of 10^9 years. Assuming that all stone meteorites were created at the same time, differing $D(\mathrm{T})/d^2\lambda$ could account for the variations by a factor of 10 in the reported K–A ages. The fact that He ages in several cases are much lower than K–A ages favours this explanation as well.

Diffusion loss of argon in iron meteorites is difficult to estimate. Paneth and co-workers (1953) have measured the He release in iron and stone meteorites as a function of temperature. At 1000°C for 3 hr, the helium loss in iron meteorites was only 5 per cent. However, the helium is produced primarily by cosmic rays, and is therefore homogeneously distributed. If all the argon were contained in the metal phase, the diffusion loss would be expected to be lower in iron meteorites than in stone meteorites. Argon is believed to be primarily concentrated with potassium in troilite or along grain boundaries, consequently A^{40} loss might be higher than helium loss, and could account for the observed variations of the iron meteorites in this investigation.

The lead–lead method is not affected by diffusion losses of gases, and yet gives an age for three stone meteorites of $4{\cdot}5 \times 10^9$ years. It must be pointed out that there is a discrepancy between the lead measurements of Patterson (1956) and the recent uranium determinations of Hamaguchi, Reed and Turkevich (1957),

but even if one assumes a contamination error in the lead measurements, the resulting ages are not as high as those observed in this investigation. Therefore one is led to assume that stone and iron meteorites had a different time of solidification. This would be consistent with theories that the parent body of meteorites was composed of a silicate phase and an iron phase with the radioactivities concentrated in the silicate phase causing it to have a different thermal history than the iron phase.

Acknowledgements—We are indebted to Dr. E. L. Fireman of the Smithsonian Institution Astrophysical Observatory who suggested this work, and contributed many stimulating discussions during the early stages of this investigation. We also want to thank Dr. Fireman for his help in obtaining many of the samples. We would like to thank Professor Brian Mason of the American Museum of Natural History who provided us with the following samples: Toluca I, Toluca II, Canon Diablo II, Cape York, Brenham Township, Arispe, and Mt. Ayliff. We wish to thank Professor Genter for the sample of Canon Diablo I, as well as for his continued interest. Professor Frondel of the Harvard Geological Museum is to be thanked for furnishing specimens of Forest City and Carbo. Dr. O. A. Schaeffer is to be thanked for his co-operation in obtaining the mass spectrometric data presented herein. We would acknowledge many helpful discussions on various phases of this study with Dr. Raymond Davis Jr.

References

Begemann F., Geiss J. and Hess D. C. (1957) *Phys. Rev.* **107,** 540.
Berl W. G. (1956) *Physical Methods in Chemical Analysis* Vol. III, pp. 580–95. Academic Press, New York.
Chackett K. F., Golden J., Mercer E. R., Paneth F. A. and Reasbeck P. (1950) *Geochim. et Cosmochim. Acta* **1,** 3.
Chackett K. F., Reasbeck P. and Wilson E. J. (1953) *Geochim. et Cosmochim. Acta* **3,** 261.
Edwards G. and Urey H. C. (1955) *Geochim. et Cosmochim. Acta* **7,** 154.
Fireman E. L. and Schwarzer D. (1957) *Geochim. et Cosmochim. Acta* **11,** 252.
Fireman E. L. and Zähringer J. (1957) *Phys. Rev.* **107,** 1695.
Gentner W., Goebel K. and Präg R. (1954) *Geochim. et Cosmochim. Acta* **5,** 124.
Gentner W. and Zähringer J. (1957) *Geochim. et Cosmochim. Acta* **11,** 60.
Gerling E. K. and Levskii L. K. (1956) *Dokl. Akad. Nauk SSSR* **110,** 5, 750.
Goldberg E. D. and Brown H. S. (1949) *Science* **109,** 347; (1950) *Analyt. Chem.* **22,** 308.
Hamaguchi H., Reed G. W. and Turkevich A. (1957) *Geochim. et Cosmochim. Acta* **12,** 337.
Hevesy G. and Levi H. (1936) *K. Danske Vidensk. Selsk. Math. fys. Medd.* **14,** 5.
Oser H. (1954) *Diplomarbeit, Freiburg e.B.* Unpublished.
Paneth F. A. (1953) *Geochim. et Cosmochim. Acta* **3,** 257.
Paneth F. A., Reasbeck P. and Mayne K. I. (1952) *Geochim. et Cosmochim. Acta* **2,** 300; (1953) *Nature, Lond.* **172,** 200.
Patterson C. C. (1956) *Geochim. et Cosmochim. Acta* **10,** 230.
Reed G. W. and Turkevich A. (1955) *Nature, Lond.* **176,** 794.
Reed G. W. and Turkevich A. (1957) *Nature, Lond.* **180,** 594.
Reynolds J. H. (1957) *Geochim. et Cosmochim. Acta* **12,** 177.
Reynolds J. and Lipson J. I. (1957) *Geochim. et Cosmochim. Acta* **12,** 330.
Schaeffer O. A. and Zähringer J. (1958) Abstract of Meeting of American Physical Society, January, 1958.
Schumacher E. (1956) *Z. Naturf.* **11a,** 206.
Thompson S. J. and Mayne K. I. (1955) *Geochim. et Cosmochim. Acta* **7,** 169.
Wasserburg G. J. and Hayden R. J. (1955) *Geochim. et Cosmochim. Acta* **7,** 51.
Wasserburg G. J. and Hayden R. J. (1955) *Phys. Rev.* **97,** 86.

Geochimica et Cosmochimica Acta, 1958, Vol. 15, pp. 51 to 56. Pergamon Press Ltd., London

Isolation and identification of an ester from a crude oil*

H. F. Phillips and I. A. Breger
U.S. Geological Survey, Washington 25, D.C.

(*Received* 4 *March* 1958)

Abstract—A dioctylphthalate has been isolated from a crude oil by means of adsorption column chromatography. The ester was identified by means of elemental analysis, refractive index, and its infra-red absorption spectrum. Saponification of the isolate and examination of the resultant alcohol by means of infrared absorption spectra led to the conclusion that the ester is a branched chain dioctylphthalate. This is the first reported occurrence of an ester in crude petroleum.

Introduction

During a search for the occurrence of pigments in crude oil, an investigation was carried out on a sample from Flat Mesa, Duchesne County, Utah. This oil, light yellow in colour, is very waxy and semisolid at room temperature. It is not known whether the oil was formed in the non-marine Eocene Green River formation or in lower marine strata of Paleozoic age. Hunt, Stewart, and Dickey (1954) have discussed the general geology of the area from which the oil was collected as well as the relationship of the other naturally occurring carbonaceous substances of the region to the various stratigraphic units present. Chromatographic separations followed by purification of the final isolate have led to the identification of a component of the oil as a dioctylphthalate. This is the first reported occurrence of an ester in crude petroleum.

Experimental

Sample preparation. The sample of oil (400 g) was dissolved in about 800 ml of warm *cyclo*hexane. The solution was allowed to cool overnight during which time a white wax precipitated. Centrifugation yielded a clear orange solution which was used for the chromatographic separations described below.

Chromatographic columns. Each column was constructed of Pyrex tubing to the top of which was sealed a sample reservoir. A Pyrex stopcock at the lower end of the tube was used to control the flow rate through the column. Adsorbent was retained by a small wad of glass wool above the stopcock. As shown in Table 1, relatively large columns were used in initial separations in order to permit a large sample charge. Later columns, in which only the concentrates were adsorbed, were usually smaller.

Adsorbents. All adsorbents were thoroughly mixed in a shell blender with equal parts by weight of Celite 545 as a filtering aid. Activated aluminium oxide; ignited aluminium oxide; Florisil, a synthetic magnesium silicate; and silica gel were used in the course of the separations. Each adsorbent–Celite mixture was dried at 110°C for 2–3 hr before use.

*Solvents. cyclo*Hexane, which was found to be excellent for the separation of the wax from the original oil, was also used in initial experiments. Normal

* Publication authorized by the Director, U.S. Geological Survey.

heptane was subsequently used in an attempt to improve the resolution of material on the column.

Chromatographic procedure. The adsorbent was introduced into a column as a thick slurry in the appropriate solvent after which solvent was eluted by applying pressure (4–5 lb/in^2) to the top of the column from a cylinder of nitrogen. The sample was adsorbed on the column and developed using first pure solvent and then solvent containing 1–5 per cent methanol. Adsorption of the sample resulted in the formation of a diffuse dark brown-orange band at the top of the column. Development was continued until a yellow band separated from this dark brown-orange area and moved down the column. The yellow band was recovered by extrusion or by cutting the column. As concentration increased with successive columns the recovered band of material darkened and became red in colour. Adsorbent was stripped using a 20 per cent solution of methanol in the solvent. The solution thus obtained was centrifuged to remove all traces of adsorbent and evaporated on a steam bath under a stream of helium to remove the methanol. The isolate was then dissolved in solvent and adsorbed on the next column of the series.

Table 1. Data for adsorption columns

Column no.	Column diameter (mm)	Column length (cm)	Adsorbent*	Solvent
1	34	78	Activated aluminium oxide†	*cyclo*Hexane
2	34	80	Activated aluminium oxide†	*cyclo*Hexane
3	16	75	Activated aluminium oxide†	*cyclo*Hexane
4	12	85	Activated aluminium oxide†	*cyclo*Hexane
5	12	70	Ignited aluminium oxide‡	*n*-Heptane
6	12	64	Florisil§	*n*-Heptane
7	9	30	Silica gel‖	*n*-Heptane
8	9	30	Silica gel‖	*n*-Heptane
9	12	75	Silica gel‖	*n*-Heptane

* In each column adsorbent was mixed with equal parts by weight of Celite-545 (Johns–Manville Corp.).
† Alcoa F-20, 80–200 mesh, Aluminum Co. of America.
‡ Merck and Co., Inc.
§ 100–200 mesh, Floridin Co.
‖ 60–200 mesh, Davison Chemical Co.

The final isolate was obtained after passing the sample through a series of nine columns. Table 1 shows the column dimensions, adsorbents and solvents used during the separations. Changes in adsorbents and solvents were made in an effort to improve the resolution of the sample on the column. When *n*-heptane was used, the column was first filled with solvent and then the dry adsorbent mixture was sifted into it and allowed to settle by gravity. Pressure was then applied as when *cyclo*hexane was used.

Fractions of eluant (5 or 10 ml) were taken from the columns during the separations. These fractions were evaporated on a steam bath under a stream of helium and infra-red spectra were determined on the residues to detect any possible loss of colourless or non-fluorescent material.

A Perkin–Elmer infrared spectrophotometer, Model 21, was used to obtain all of the infra-red spectra in this laboratory. Samples were prepared as films on sodium chloride plates. Spectra obtained from other sources are noted on Fig. 1.

The weight of the isolate from the final column was 0·610 g representing 0·15 per cent by weight of the original oil. The isolate was quite viscous and very dark red in colour. Its infra-red spectrum (Fig. 1, curve 1), when compared with card 98 of the National Research Council–National Bureau of Standards punched card series of infra-red spectra (Fig. 1, curve 4), indicated it to be a

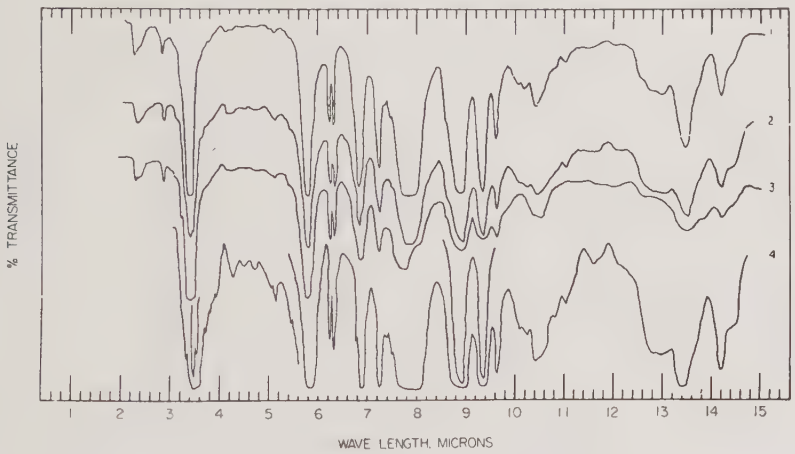

Fig. 1. Infra-red absorption spectra. Curve 1, final column isolate; curve 2, distillate from final column isolate; curve 3, di-*n*-octylphthalate (Product P6479, Eastman Kodak Co.); curve 4, dioctylphthalate, copy of Card 98 furnished the National Research Council–National Bureau of Standards punched card series of infra-red spectra by the U.S. Rubber Co.

dioctylphthalate. Inasmuch as phthalic esters are colourless, the dark colour of the material indicated the presence of an impurity.*

Micro vacuum distillation. The final chromatographic isolate was purified by dissolving it in a few millilitres of *n*-heptane and transferring it to a micro vacuum distillation apparatus similar to that designed by Soltys (1936) but without the thermometer and capillary inlet. The distilling flask was placed in a copper heating block equipped with a thermometer; transferring solvent was removed from the sample by raising the block temperature to 65°C while passing a stream of nitrogen over the surface of the sample. The top of the flask was closed, the vacuum line connected, and the flask was then evacuated. The temperature of the block was raised slowly and a very pale yellow distillate was collected at a pressure of 0·03–0·05 mm Hg. It was thought likely that a small amount of the coloured impurity was carried over imparting the slight colour to the distillate.

The infra-red spectrum of the distillate (Fig. 1, curve 2) was almost identical

* The authors are indebted to Dr. Douglas Montgomery of the Canadian Bureau of Mines for pointing out the difficulty in separating porphyrins from oxygenated compounds by chromatography.

to that for the impure, dark red, chromatographic isolate (Fig. 1, curve 1). Removal of the highly coloured impurity from the isolate had no visible effect on the spectrum, indicating the material to have been present in very small percentage. Analytical data for the distilled isolate are shown in Table 2.

Table 2. Analytical data for distilled isolate

	Isolate	Di-*n*-octylphthalate	Di*iso*octylphthalate	Di-(2 ethylhexyl)-phthalate
Carbon, (%)	74·07*	73·80†	73·80†	73·80†
Hydrogen (%)	9·96*	9·81†	9·81†	9·81†
n_D^{20}	1·4876	1·4845‡		
n_D^{25}	1·4857	1·4826‡		
n^{20}				1·4859§
n^{25}		1·482§	1·486§	1·484–1·485§

* Analysis by Edward B. Brittin, U.S. Geological Survey.
† Calculated.
‡ Product P6479, Eastman Kodak Co.
§ *Modern Plastics Encyclopedia and Engineers Handbook* pp. 702–3, Plastics Catalogue Corp., New York, 1952.

Saponification. In an attempt to identify the dioctylphthalate further, the distilled ester was saponified using the micro method of Schneider (1946). The ester (10 mm^3) was absorbed on a small amount of ignited asbestos. This, with about 30 mm^3 of a solution of 0·1N KOH in diethylene glycol, was heated in a small distillation tube and the condensed ring of alcohol was collected in a capillary for identification. The small quantity of alcohol obtained (1–2 mg)

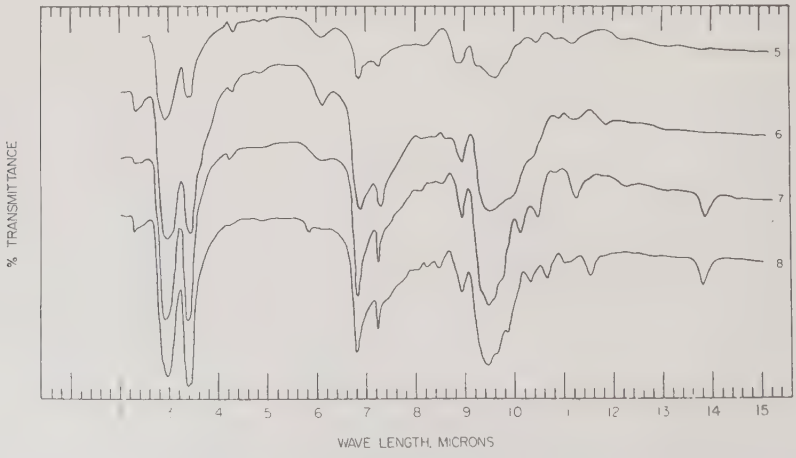

Fig. 2. Infra-red absorption spectra. Curve 5, alcohol recovered by saponification of the isolated ester; curve 6, *iso*octyl alcohol (Gulf Oil Corp.); curve 7, *n*-octyl alcohol (Product 871, Eastman Kodak Co.); curve 8, *n*-heptyl alcohol (Product 381, Eastman Kodak Co.).

made it desirable to attempt identification by means of infra-red absorption spectra. The spectrum for the alcohol so isolated is shown in Fig. 2.

Discussion

Comparison of the infra-red spectra of Fig. 1 shows the isolate to be a dioctylphthalate. The triplet at 7·8, 8·95, and 9·35 μ is especially useful for this identification (Barnes *et al.*, 1944). R. R. Hampton of the U.S. Rubber Co. has noted (personal communication) that curve 4 represents the 2-ethylhexyl isomer of dioctylphthalate. Further examination of the curves of Fig. 1, especially in the regions of 8·0–8·1, 9·85, 10·0–10·4, 11·05, and 11·9 μ, indicates the isolate to be more nearly similar in structure to the branched chain isomer (curve 4) than to the straight chain isomer (curve 3).

The spectra of Fig. 2 are for the alcohol recovered by saponification of the isolated ester (curve 5), *iso*octyl alcohol (curve 6), *n*-octyl alcohol (curve 7), and *n*-heptyl alcohol (curve 8). Curves 7 and 8 are for Eastman Kodak Co. products 871 and 381, respectively; the *iso*octyl alcohol, with the distribution of isomers shown below (A. Lewis, Jr., personal communication), was obtained through the courtesy of the Gulf Oil Corp.

Isomer	Percentage by weight
4:5-dimethyl hexanol-1	30
3:5-dimethyl hexanol-1	30
5-methyl heptanol-1	15
3:4-dimethyl hexanol-1	15
5:5-dimethyl hexanol-1	5
Miscellaneous isomers	5

Curve 5, of Fig. 2, for the saponification product, is similar to the other spectra of Fig. 2, but appears to be more nearly similar to the spectra of the C_8 alcohols (curves 6 and 7) than to the spectrum for the C_7 alcohol (curve 8), especially at 5·8, 6·1, 10·85, 11·0, 11·2, and 11·5 μ. Examination of curves 5, 6, and 7, moreover, shows variations at 10·0, 10·1, and 13·85 μ that indicate the alcohol isolated by saponification to be more nearly similar to the *iso*octyl alcohol than to the *n*-octyl alcohol.

Summary

The ester isolated from the crude oil has been identified as a dioctylphthalate by means of elemental analysis, refractive index, and infra-red absorption curves.

Consideration of infrared curves for various dioctylphthalates leads to the conclusion that the isolate is a branched chain dioctylphthalate. This conclusion has been supported by a comparison of infra-red spectra for the alcohol recovered by saponification of the ester with other alcohols in the C_7–C_8 range.

Although the evidence supports the conclusion that the ester is a dioctylphthalate, the structure of the alcohol cannot be determined absolutely from

the infra-red spectra, nor can it be determined whether the compound is one of the following structures where R and R′ are different *iso*octyl alcohol chains:

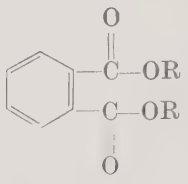

(I)

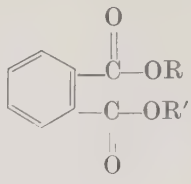

(II)

The origin of the ester is unknown: it may be a preserved metabolic product or may have been formed during formation of the oil.

Acknowledgements—The authors wish to thank R. G. Milkey of the U.S. Geological Survey for obtaining the infra-red spectra. Mr. Milkey's assistance in interpretation of the spectra was most helpful. K. G. Bell, also of the U.S. Geological Survey, directed the attention of the authors to this unusual oil and assisted in its collection. This work is part of a programme being conducted by the U.S. Geological Survey on behalf of the Division of Research of the U.S. Atomic Energy Commission.

References

Barnes R. B., Gore R. C., Liddel U. and Williams V. Z. (1944) *Infrared Spectroscopy, Industrial Applications and Bibliography* pp. 23, 76, 77. Reinhold, New York.

Hunt J. M., Stewart F. and Dickey P. A. (1954) Origin of hydrocarbons of the Uinta Basin, Utah. *Bull. Amer. Ass. Pet. Geol.* **38,** 1671–1698.

Schneider F. (1946) *Qualitative Organic Microanalysis* p. 160. John Wiley, New York.

Soltys A. (1936) Preparative treatment of small quantities of substance. *Mikrochemie, Festschr. von Hans Molisch* 393–404; also see Schneider, F. (1946) Qualitative Organic Microanalysis p. 36. John Wiley, New York.

Geochimica et Cosmochimica Acta, 1958, Vol. 15, pp. 57 to 72. Pergamon Press Ltd., London

Mechanism of gypsification*

R. F. Conley† and W. M. Bundy†

(*Received* 1 *April* 1957; *in revised form* 24 *February* 1958)

Abstract—Petrographic studies have shown that many gypsum deposits have been formed by the hydration of anhydrite, but the mechanism for hydration has not been fully explained. Gypsum has been produced experimentally by the agitation of anhydrite in pure water, a reaction that is accelerated by certain acids, bases, and salts, particularly alkali sulphates.

Phase investigations and reaction velocity studies indicate that accelerated hydration of anhydrite takes place through the medium of transient surface complexes in dilute solution. Concentrated solutions may precipitate double salts.

Contrary to recent hypotheses of gypsum dehydration by concentrated salt solutions, double salts and/or gypsum are stable phases below a temperature of 42°C. Above 42°C double salts may replace anhydrite as the stable phase. Gypsum, however, may remain a metastable phase indefinitely in its saturated solution below the hemihydrate transition temperature (98°C).

Experimental data indicate that precipitation of anhydrite from sea water is unlikely.

Introduction

Hydration of the mineral anhydrite ($CaSO_4$) to gypsum ($CaSO_4 \cdot 2H_2O$) has been a well-known phenomenon for many years. Although the hydration of anhydrite by pure water is extremely slow, it is accelerated in the presence of certain salts, alkalis and acids. The mechanism whereby this acceleration takes place has never been fully understood. This paper attempts to shed new light on the mechanism by which activation of anhydrite takes place.

Previous Work

Farnsworth (1925) carried out hydration experiments using very finely ground anhydrite agitated in pure water. Several weeks were required for complete conversion. This reaction has been demonstrated by Posnjak (1940) to take place via solution phase. His results are based on solubility data for calcium sulphate phases in water which show gypsum to be the least soluble phase below 42°C.

Thermodynamic studies by MacDonald (1953) show that hydrostatic pressure assists hydration by driving the components of the following reaction to a state of lesser volume.

(A) $$CaSO_4 \text{ (anhydrite)} + 2H_2O \longrightarrow CaSO_4 \cdot 2H_2O \text{ (gypsum)}$$

However, when the lithostatic pressure exceeds the hydrostatic pressure, and confined water is allowed to escape, the equilibrium temperature for the above reaction is lowered. MacDonald theorized that when pressure differential exists, gypsum in pure water could exist only at depths less than about 2500 ft.

Several investigators have also postulated that certain salt solutions decrease the solubility of anhydrite relative to gypsum to the point that anhydrite is the stable phase at temperatures well below 42°C. This change in solubility is based

* Published with the permission of the State Geologist, Indiana Department of Conservation, Geological Survey, Bloomington, Indiana.

† Present address: Georgia Kaolin Company, 433 North Broad, Elizabeth, New Jersey, U.S.A.

on the thermodynamic considerations of vapour pressure relationships by MacDonald and Posnjak and also Kelley, Southard and Anderson (1941). MacDonald proposed that concentrated saline solutions, as evaporating bodies of sea water, precipitate anhydrite at temperatures as low as 7°C.

Posnjak (1940) demonstrated the persistence of gypsum as a metastable phase up to 98°C (hemihydrate transition temperature) and this has been substantiated in the present investigation. Finely ground gypsum in contact with saturated NaCl solution remained unchanged at room temperature over a period of 6 months. Anhydrite nuclei added to this mixture were subsequently transformed to gypsum. Upon elevation of the solution temperature to 60°C, no alteration to anhydrite took place after 3 weeks. Other similar experiments with saturated solutions of sea water, $MgCl_2$, $CaCl_2$ and Na_2SO_4 over more extended periods of time gave the same results. Precipitated calcium sulphate formed by the following reaction occurs as gypsum up to about 70°C:

$$\text{(B)} \qquad CaCO_3 + 2H^+ + SO_4^{=} \xrightarrow{H_2O} CO_2\uparrow + Ca^{++}\,SO_4^{=} \longrightarrow \text{ppt.}$$

At higher temperatures hemihydrate precipitates and readily reverts to gypsum in water below 70°C. Hence, it may be concluded that the following reaction under standard conditions of temperature and pressure proceeds with extreme slowness, if at all:

$$\text{(C)} \qquad CaSO_4{\cdot}2H_2O(G) \xrightarrow[\text{soln.}]{\text{satd. salt}} CaSO_4(A) + 2H_2O$$

In contrast to the work of Posnjak and MacDonald showing that in certain salt solutions the gypsum–anhydrite transition temperature is lowered, several workers have demonstrated that these salts activate rather than inhibit hydration. This activation occurs even under conditions theoretically favouring anhydrite.

Hennicke (1923) introduced in Germany a mortar-forming process which utilized solutions of "alkali salts, acids and bases" with ground anhydrite. These solutions accelerated the hydration process. Further investigations of acceleration processes have been carried out by Randel (1933), Otteman (1950), and Gelmroth (1953).

Recent experiments (Leininger, Conley and Bundy, 1957) conducted to determine the relative effectiveness of activators yielded the following qualitative series:

$$K^+ \geqslant Na^+ \geqslant NH_4^+ > Mg^{++} > Fe^{++} > H^+ > Al^{+++} > Ca^{++}$$

$$\text{and } SO_4^{=} \geqslant Cl^- > OH^-$$

Although other ions may promote conversion, only these were studied because of their industrial and geochemical application. Potassium and sodium sulphate were investigated in detail because of their efficiency in activation and presence in natural waters.

Double Salt Formation

The reaction for the conversion of anhydrite to gypsum with activator solutions:

$$\text{(D)} \qquad CaSO_4\,(A) \xrightarrow[H_2O]{\text{act.}} Ca^{++} + SO_4^{=} \xrightarrow{H_2O} CaSO_4{\cdot}2H_2O\ (G)$$

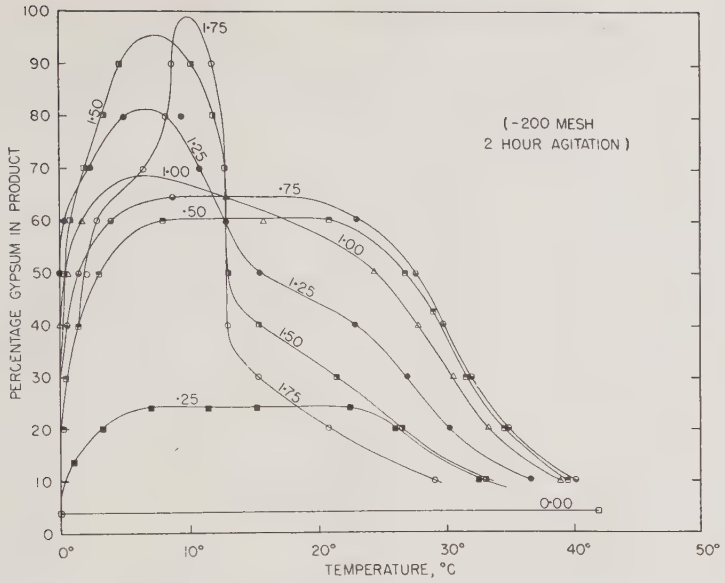

Fig. 1. Sodium sulphate isomolarity curves.

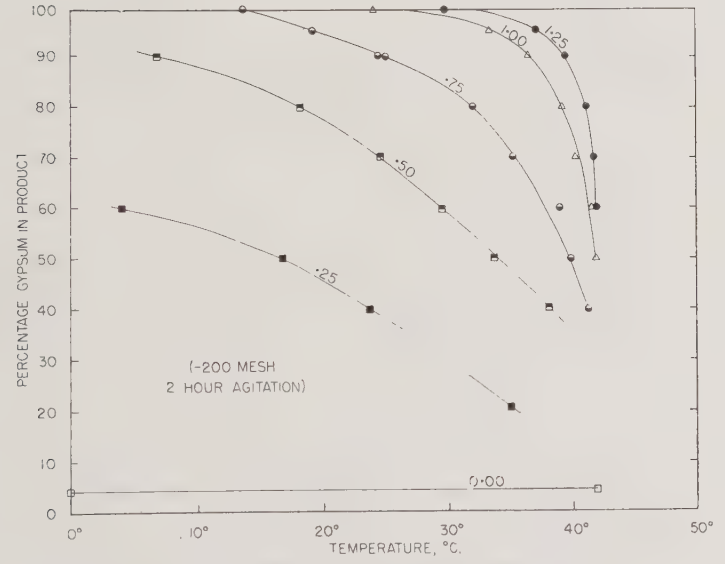

Fig. 2. Potassium sulphate isomolarity curves.

is primarily dependent upon solution temperature and concentration. Figs. 1 and 2 illustrate the effects of these parameters when sodium sulphate and potassium sulphate are used as activators and the product is removed and washed free of activator.* In this process gypsum results from decomposition of any double salt that has been formed. In Fig. 1 it is apparent that anomalous conversion to gypsum occurs at temperatures below 13°C and concentrations above 0·75M

* Gypsum content determined by standard A.S.T.M. gravimetric method.

Na_2SO_4. Experiments conducted within this field give rise to the formation of a stable double salt which subsequently decomposes upon washing. This double salt appears identical in composition with the sodium hemicalcium sulphate salt, $2Na_2SO_4 \cdot CaSO_4 \cdot 2H_2O$, designated as labile salt, and synthesized by Hill and Wills (1938) by the following method:

> A slight excess of gypsum is placed in a solution of sodium sulphate, 24·2 to 29·0 per cent by weight. The mixture is maintained in a sealed container at 75°C for 72 hr.

Table 1. Chemical analyses of labile salt

Component	Labile salt (theory)	Synthetic (Hill and Wills)	Synthetic (Conley and Bundy)
Na_2SO_4	62·27	61·6	69·4*
$CaSO_4$	29·83	29·7	23·8
H_2O	7·90	8·7	7·7
	100·00	100·0	100·9

* High sodium content due to activator contamination.

Table 1 includes chemical analyses of the double salt obtained from a solution at 6·5°C, the salt synthesized by Hill and Wills, and the stoichiometric composition of labile salt. X-ray spectrometer data of the synthesized salts are shown in Fig. 3.

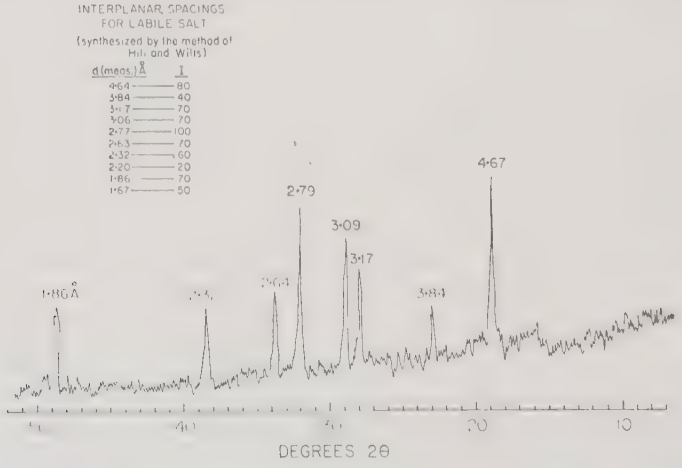

Fig. 3. X-ray spectrometer trace and interplane spacings for labile salt.

Fig. 2 shows that conversion is largely dependent upon K_2SO_4 concentration, and no critical temperature is observed below 42°C. Throughout the operating range 0–42°C and 0·25–1·25 M K_2SO_4 a double salt which corresponds to the mineral syngenite, $K_2SO_4 \cdot CaSO_4 \cdot H_2O$, is obtained. Chemical analyses for the double salt obtained in these experiments and the stoichiometric composition of

syngenite are given in Table 2. An X-ray spectrometric trace of the double salt is shown in Fig. 4. Although this pattern is not in complete accord with the A.S.T.M. data listed for syngenite,* it is believed that chemical and X-ray data are adequate to conclude that syngenite is present.

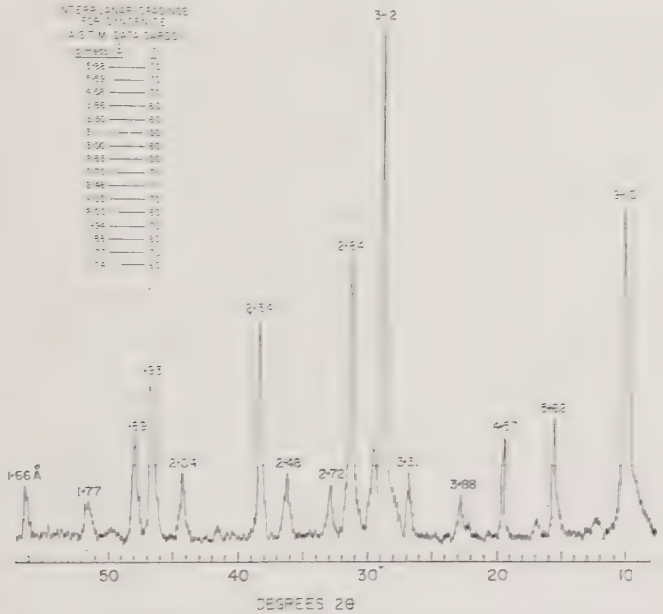

Fig. 4. X-ray spectrometer trace and interplane spacings for syngenite.

Phase Studies

Ternary phase diagrams for the systems $CaSO_4$–Na_2SO_4–H_2O and $CaSO_4$–K_2SO_4–H_2O have been constructed in order to obtain a better understanding of phase equilibria. Hill and Wills (1938) collected data for the former in the range 25°–100°C and Hill (1934) for the latter from 40°–100°C. These workers

Table 2. Chemical analyses of syngenite

Component	Syngenite (theory)	Synthetic (Conley and Bundy)
$CaSO_4$	41·46	41·0
K_2SO_4	53·06	53·5
H_2O	5·48	5·5
	100·00	100·0

* All the lines on the diagram that are within the range of those recorded on the A.S.T.M. card check to within 0·02 Å. The one line on the card that does not show up on the diagram, 6·88 Å, is also missing from the syngenite pattern on file at the U.S. Geological Survey, so it is possible that it was due to an impurity in the material from which the pattern summarized on the A.S.T.M. card was made. Ed.

have demonstrated the stability of various double salts above 42°C. It was necessary to supplement these data with information obtained in the range 0–25°C.

For this purpose a warming-curve method modified after Tammann cooling-curves (1903) was employed. Fig. 5(a) shows the temperature change with time

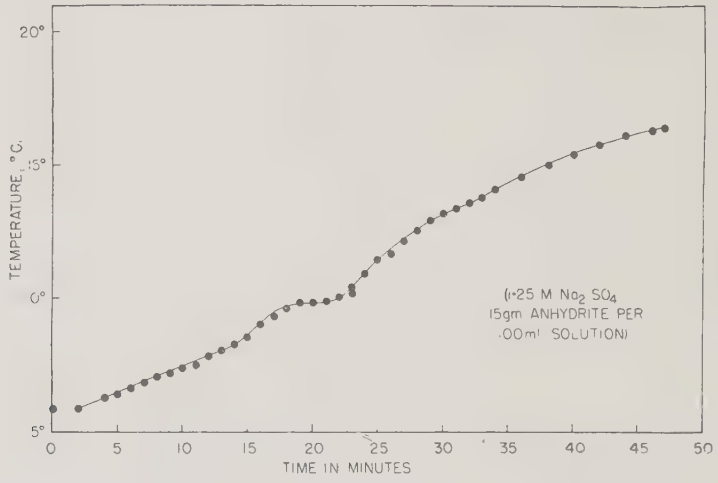

Fig. 5(a) Warming curve for the system Na_2SO_4–$CaSO_4$–H_2O.

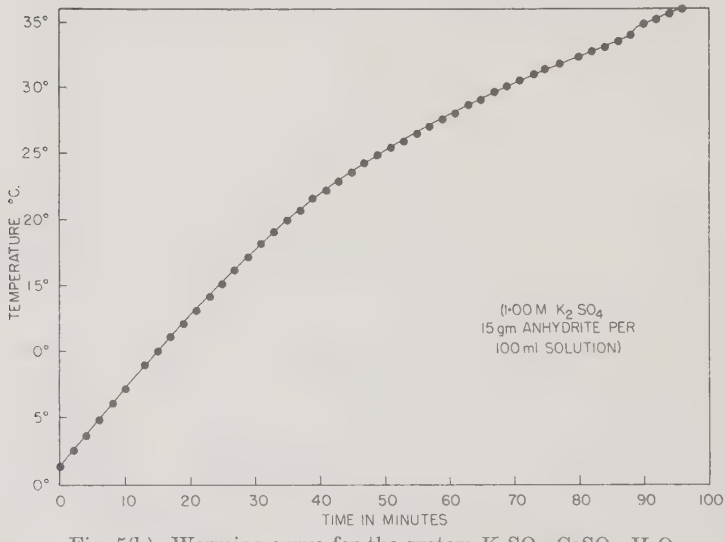

Fig. 5(b). Warming curve for the system K_2SO_4–$CaSO_4$–H_2O.

of a Na_2SO_4 activated suspension of anhydrite. The composition of this mixture was selected from the field of complex salt stability in Fig. 1. The mixture was agitated for 6 hr in a 2°C bath to obtain maximum double salt formation. The resulting mixture was removed from the bath and allowed to warm in air at room temperature. Temperature measurements of the warming solution were determined periodically with an N.B.S. calibrated thermometer graduated in 0·1°C.

A well-defined plateau in Fig. 5(a), originating from an endothermic reaction, is observed at 9·8°C. The change of slope above this temperature indicates the formation of a new phase. Results of X-ray analysis show that below 9·8°C labile

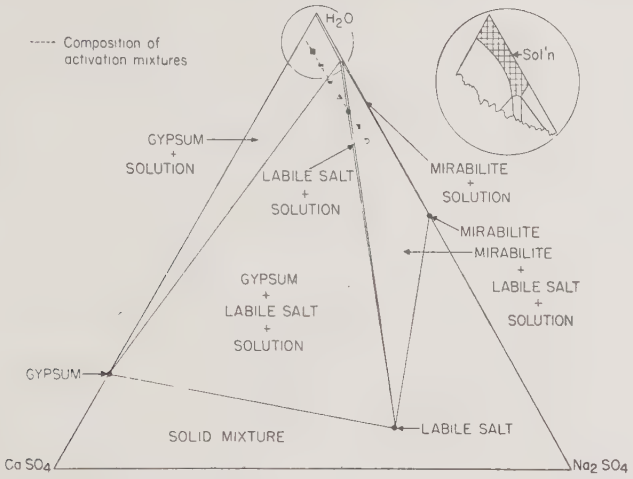

Fig. 6(a). Weight (%) ternary diagram of Na_2SO_4–$CaSO_4$–H_2O at 9°C.

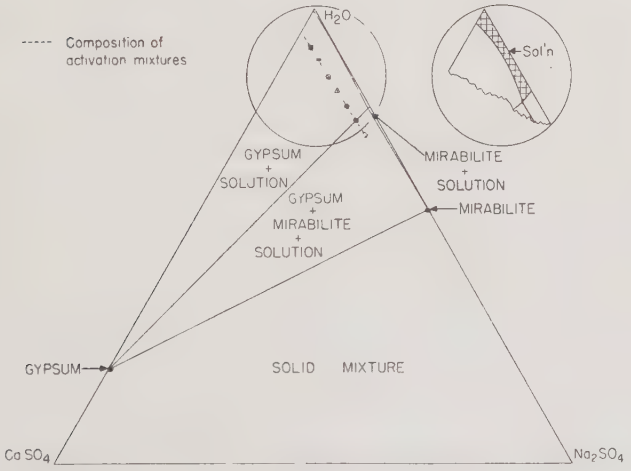

Fig. 6(b). Weight (%) ternary diagram of Na_2SO_4–$CaSO_4$–H_2O at 25°C.

salt and small quantities of gypsum exist as stable phases but above this temperature gypsum and mirabilite, $Na_2SO_4 \cdot 10H_2O$, are stable. Therefore, 9·8°C is the temperature at which labile salt begins to dissociate into gypsum and mirabilite (the solubility of labile salt equals the solubility of gypsum). It should be noted that the transition temperature 13°C apparent in Fig. 1, probably represents

equilibrium between the solubilities of the two metastable phases, labile salt and anhydrite. In Fig. 5(a) a very small break occurs at about 13°C. At this point equilibrium is believed to exist between metastable labile salt and the very small

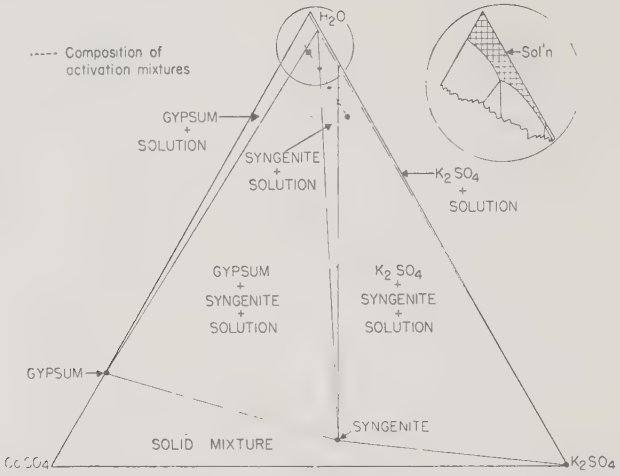

Fig. 6(c). Weight (%) ternary diagram of K_2SO_4–$CaSO_4$–H_2O at 25°C.

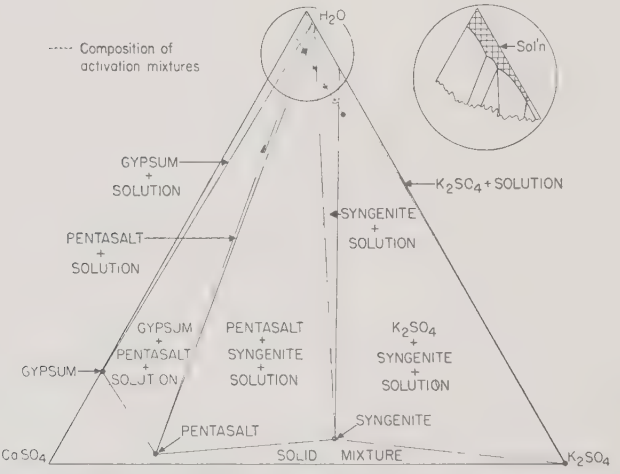

Fig. 6(d). Weight (%) ternary diagram of K_2SO_4–$CaSO_4$–H_2O at 40°C.

quantity of anhydrite remaining in the mixture. Other warming-curve data taken from an automatic recorder and plotted as the second derivative, d^2T/dt^2, support this interpretation.

The discontinuity occurring at a temperature lower than 9°C could not be interpreted with present phase information. A new phase region may be indicated by this break.

From the above determinations, along with $CaSO_4 \cdot 2H_2O$ and $Na_2SO_4 \cdot 10H_2O$ solubility data, the ternary diagram [Fig. 6(a)] was constructed. The extreme narrowness of the field, labile salt + solution, inhibits precise determination of the phase boundary, labile salt + solution/solution. The diagram was drawn in accordance with the general principles reviewed by Marsh (1935) and Rivett (1923). A similar ternary phase diagram [Fig. 6(b)] was constructed from 25°C data to show the shift of the various stability fields.

A second warming curve [Fig. 5(b)] was obtained by using a K_2SO_4 activated suspension of anhydrite. The methods employed were similar to those used in obtaining the Na_2SO_4 warming curve. An exothermic reaction was obtained at about 34·5°C. This represents the equilibrium temperature between the fields of syngenite + gypsum and syngenite + pentasalt [$(CaSO_4)_5K_2SO_4 \cdot H_2O$]. No other phase changes were observed up to the terminal temperature, 60°C. These phases are substantiated by X-ray analysis, and the results are in agreement with conclusions of Hill (1934). Figs. 6(c) and 6(d) are two ternary phase diagrams constructed from 25°C and 40°C data. The greater efficiency of K_2SO_4 over Na_2SO_4 activation may be expected to result from the greater stability range of the K–Ca double salts. X-ray determinations and warming-curve data show syngenite to be stable throughout the temperature range in Fig. 5(b).

Mechanism of Double Salt Formation

The transition from anhydrite to a double salt and the decomposition of the double salt to gypsum by washing were observed to be relatively rapid processes. Transformation of anhydrite to gypsum by means of stable double salt formation and decomposition can therefore be readily understood. Comparison of Fig. 1 with Figs. 6(a) and (b) and Fig. 2 with Figs. 6(c) and (d) indicates that relatively rapid conversion also occurs outside the double salt stability fields. The reactions within these areas of complex salt instability require a more thorough explanation.

Otteman suggested the formation of transient double salts as a possible mechanism of transformation. He further postulated that the increased solubility of anhydrite in concentrated Na_2SO_4 solution is a primary factor in this transformation process. Results of the present investigation are in agreement with Otteman's "transient double salt" postulation; however, the writers do not believe that the slight increase in anhydrite solubility contributes significantly to the conversion process. The negligible effect of this solubility increase is shown in Fig. 7. Fig. 8 shows that after 2 hr of agitation in pure water 0·2 per cent of anhydrite is converted to gypsum, whereas under the same conditions with 0·75 M Na_2SO_4 in saturated $CaSO_4$ solution about 60 per cent of anhydrite is converted. The reaction rate is increased 300-fold, but the solubility-differential between anhydrite and gypsum for these two solutions shows only a slight increase.

This relation is further demonstrated by an analysis of the effects produced by NaCl activation. The solubility of calcium sulphate in 0·5 M sodium chloride solution is approximately three times greater than in an equivalent sodium sulphate solution (Comey and Hahn, 1921). Conversely, the activating efficiency of the Na_2SO_4 is about fifty times greater than that of NaCl. It is concluded that both the cation and anion enter into an activation complex.

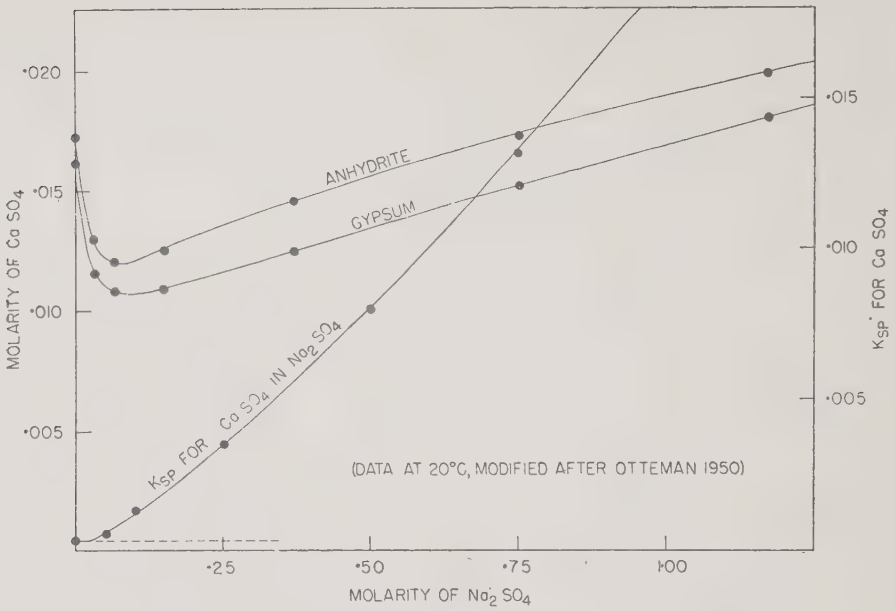

Fig. 7. Solubility and solubility product relationship of $CaSO_4$ in Na_2SO_4 solutions.

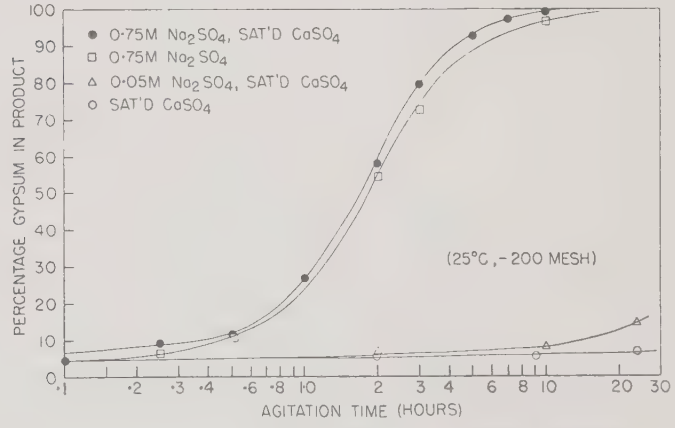

Fig. 8. Rate of gypsum formation in activating solutions.

Experimental work (Leininger, Conley and Bundy, 1957) indicates that sulphate salts are more effective activators than foreign anion salts. To comprehend better the effect of the anion upon activation, the following theoretical treatment is given. The surface of anhydrite* is considered as a network of alternating Ca^{++} and SO_4^{--} ions. When this surface is in contact with a saturated

* Microscopic observations of anhydrite undergoing hydration by an activating solution show that the 100 plane is most susceptible to this attack (Otteman, 1950).

calcium sulphate solution, the following transitions take place and approach equilibrium:

	Interfacial ion		Solvated ion
(E)	(Ca^{++})	⟷	Ca^{++}
(F)	$(SO_4^{=})$	⟷	$SO_4^{=}$

This exchange process is shifted slightly to the solution phase below 42°C and results in very slow rate of gypsum precipitation.

If the anhydrite surface is in contact with a calcium sulphate solution which contains a dissolved salt $M^{+a}X^{-b}$ of a given concentration, the following transitions can occur:

	Interfacial ion		Solvated ion
(E)	$1(Ca^{++})$	⟷	$1Ca^{++}$
(F)	$1(SO_4^{=})$	⟷	$1SO_4^{=}$
(G)	$1(Ca^{++})$	⟷	$2/aM^{+a}$
(H)	$1(SO_4^{=})$	⟷	$2/bX^{-b}$
(I)	$1(Ca^{++}SO_4^{=})$	⟷	$1M^{+a} + X^{-b}$

Only these ionic transitions permit the net surface charge to remain electrostatically unaltered. If the molar concentration of the salt $M^{+a}X^{-b}$ is large with respect to the concentration of calcium sulphate, transitions (G), (H) and I predominate.

It is apparent that when X^{-b} is the sulphate ion, the statistical probability of a surface transient complex formation is considerably higher than when X^{-b} is Cl^{-}, etc. Many investigators have reported double sulphate salts of Ca^{++} and cation M^{+a}, but relatively few complex salts which have a composition of the general type MX·NY (different cations and different anions) are known. The increased quantity of $SO_4^{=}$ ions in solution also increases the precipitation rate of gypsum by virtue of a greater number of Ca^{++}–$SO_4^{=}$ collisions in the solution phase.

The formation of surface transient complexes may then be considered as a statistical replacement process whereby M^{+a} ions are substituted randomly for Ca^{++} ions or adsorbed on the calcium sulphate surface. The adsorption of these foreign ions in localized areas produces surface deformities and reduces the surface energy. Because of surface energy reduction, more Ca^{++} and $SO_4^{=}$ ions are released per unit time. These, in turn, precipitate as gypsum from the already saturated calcium sulphate solution. The increased rate of gypsum formation is produced, therefore, by making the anhydrite more readily soluble.

If a double salt is the least soluble species under the conditions of the system, a double salt crystallite will be formed. Growth will occur upon the crystallite surface by depletion of Ca^{++}, M^{+a} and $SO_4^{=}$ ions from the surrounding solution. The solution is replenished by dissolution of the more soluble anhydrite and, if present, solid phase $M_{2/a}SO_4$. This process of precipitation may result in the inclusion of the anhydrite grain by peripheral double salt growth. Microscopic observations show this type of inclusion to occur.

Nuclei for double salt formation also may be provided by direct precipitation from solution. This type of nuclei formation can be observed during the interaction of saturated calcium sulphate solution with potassium sulphate solutions above approximately 0·2 M and concentrated $NaSO_4$ solutions below 9·8°C.

If the solubility of the double salt is greater than that of gypsum (the double salt is unstable under the conditions of the system), dissolution of the crystallite surface will occur and supersaturate the solution with resepct to $CaSO_4 \cdot 2H_2O$. Precipitation of $CaSO_4 \cdot 2H_2O$ then will occur either on the surface of existing nuclei or by spontaneous nucleation. Depletion of the solid phase anhydrite will be most rapid when the ratio of anhydrite to gypsum is large. As greater quantities of gypsum form, a competing reaction due to foreign cation adsorption on the gypsum surface will then decrease the anhydrite dissolution rate and, consequently, the gypsum formation rate. Therefore, an inflexion in the hydration rate curve would theoretically be obtained when the surface area (or surface activity) of calcium sulphate in the anhydrite phase is equal to that of the calcium sulphate in the gypsum phase. It is apparent from Fig. 8 that the data show a maximum for the rate change at about 50 per cent yield.

The precipitation of gypsum from a saturated calcium sulphate solution may then be considered as a two-stage process: (1) formation of incipient nuclei, and (2) crystal growth of these nuclei. The overall reaction may be represented by the following equation:

$$\text{(J)} \qquad n\text{Ca}^{++} + n\text{SO}_4^{=} + 2n\text{H}_2\text{O} \longrightarrow n\text{CaSO}_4 \cdot 2\text{H}_2\text{O}.$$

If the mole fraction of water is large relative to the concentration of calcium and sulphate ions, the precipitation of gypsum will be limited primarily by the Ca^{++} and $SO_4^{=}$ ion concentrations. Crystallite formation is dependent upon the total number of anion–cation collisions which in turn are a function of the anion and cation concentrations. The rate of formation of nuclei is proportional to $[(Ca^{++})(SO_4^{=})]^{p/2}$ where p is the number of monomers, or ion members of a nucleus, required to sustain the crystalloid (O'Rourke and Johnson, 1955). With regard to nucleation, it must be pointed out that natural anhydrite may contain intrinsic gypsum and also may provide simultaneous growth planes (Spangenberg and Neuhaus, 1930; Turnbull and Vonnegut, 1952) for gypsum. Both of these processes would circumvent the necessity of incipient nuclei formation.

The precipitation rate of gypsum by crystal growth of nuclei is represented by the following solution equation:

$$\text{(K)} \qquad -\frac{dC}{dt} = k(C - C_s)^q$$

where C = concentration of monomers

C_s = concentration at saturation

q = number of monomers in the growth nucleus

Simply stated, the driving force for precipitation is a function of the concentration

of calcium and sulphate ions above the saturation concentration. The equation can be transformed to:

$$(L) \qquad -\frac{dC}{dt} = k\{\sqrt{([Ca^{++}]\,[SO_4^{=}])} - \sqrt{([Ca^{++}]_s[SO_4^{=}]_s)}\}^q.$$

The value $\sqrt{([Ca^{++}]_s[SO_4^{=}]_s)}$ can be equilibrated with the $(K_{sp})^{1/2}$ for calcium sulphate. As Fig. 7 shows, the K_{sp} varies strongly with $SO_4^{=}$ concentration. The growth order, q, and nucleation order, p, for the reactions are assigned the value of 4 based on the similar barium sulphate kinetic study by Johnson and O'Rourke (1954). Hence, it is concluded that the rate of precipitation is $\alpha([Ca^{++}][SO_4^{=}])^2$ for nucleation and $\alpha\{\sqrt{([Ca^{++}][SO_4^{=}])} - \sqrt{K_{sp}}\}^4$ for growth.

The above treatment of solution kinetics has been incorporated to show that a sulphate activator provides greater precipitation rate for gypsum than other anion activators do. These kinetics also indicate that very dilute activator solutions, even in the range where calcium sulphate solubility is sharply depressed, are more efficient in producing hydration (as $[M_{2/a}SO_4] \rightarrow 0$) than water alone. This is substantiated by the 0·05M Na_2SO_4 data appearing in Fig. 8.

Geological Application

Gypsification of secondary anhydrite is believed to take place primarily by the action of activating cations. This concept of natural activation is supported both by the prevalence of saline solutions associated with gypsum–anhydrite deposits and by laboratory evidence.

The salinity of ground water associated with evaporite deposits is largely dependent upon beds of the more soluble K, Mg and Na salts. The prevalence of these salts in the Stassfurt evaporite deposits of Germany should result in the formation of concentrated salt solutions. It can be assumed, therefore, that activation of anhydrite through the formation of both stable and unstable double salts is a significant process in these deposits. Some of the complex salts which occur in the Stassfurt deposits and which may be related to activation processes (Clarke, 1924) are:

Glauberite	$CaSO_4 \cdot Na_2SO_4$
Polyhalite	$2CaSO_4 \cdot MgSO_4 \cdot K_2SO_4 \cdot 2H_2O$
Krugite	$4CaSO_4 \cdot MgSO_4 \cdot K_2SO_4 \cdot 2H_2O$ (polyhalite admixed with anhydrite (Ford, 1947))
Syngenite	$CaSO_4 \cdot K_2SO_4 \cdot H_2O$

Obviously, the stable double salts persist only as long as their environments lie within their fields of stability. Dilution of the salt solutions and, with some salts, change of temperature result in their decomposition and subsequent precipitation of calcium sulphate as gypsum.

In contrast to the Stassfurt deposits the evaporites occurring in south-western Indiana (McGregor, 1954) are limited to anhydrite and gypsum. The ground water associated with these deposits contains relatively little solute. Chemical

analyses of water samples from the National Gypsum Co. and United States Gypsum Co. mines near Shoals, Ind., show a salinity of less than 20 parts per thousand. The following analysis (Table 3) of a sample taken from the National Gypsum Co. mine indicates the dilute character of the subsurface water:

Table 3. Analysis of mine water (National Gypsum Co., Shoals, Ind.)

Constituent	Concentration (%)
Na	0·56
$Ca^{+}Mg$	<0·1
Cl	0·59
SO_4	0·43
B	trace
Fe	trace
K	trace
Li	trace
Sr	trace
S (as sulphide)	trace
Total dissolved solids	1·78
pH	8·0

The constituents of these subsurface waters may have been derived from any of the following sources:

(1) Connate water. Occurs as liquid inclusions in mineral grains and pore fluids within rock strata.

(2) Disseminated salts. Minute crystals included in the anhydrite–gypsum beds.

(3) Adsorbed ions. On clay structures by ion exchange.

(4) Previous salt deposits. Although petrographic evidence does not indicate the presence of soluble K, Na and Mg salts, these may have been removed by the action of ground water.

The relative rate of hydration produced by dilute solutions is illustrated in Fig. 8. The amount of conversion obtained by using a 0·75M Na_2SO_4 activator solution is shown by the upper two curves. The time lag between these two curves indicates the necessity of calcium sulphate saturation before gypsum precipitation can occur. At 0·75M sodium sulphate concentration the anhydrite solubility is noticeably increased with respect to dilute Na_2SO_4 solutions (see Fig. 7). The curve obtained with 0·05M Na_2SO_4, where anhydrite solubility is depressed, shows that activation occurs even in very dilute solutions. Although dilute solutions do not greatly accelerate hydration, the slight rate increase over pure water is significant when geologic time is considered. This observation becomes important when applied to geologic conditions in which the number of nuclei and amount of reaction surface are comparatively small.

On the assumption that crystallites of anhydrite form in sea water, as postulated by earlier workers, the present investigation indicates that activating constituents

contained therein would bring about almost immediate conversion to gypsum and/or double salts. Gypsum formation requires that temperatures during precipitation do not greatly exceed 42°C. The activating effect of sea water is shown in Fig. 9.* A second curve of activation by NaCl is included for comparison. The greater efficiency of sea water activation can be accounted for by the presence of small quantities of sulphate ion in sea water. It can be seen that above 214 parts per thousand salinity for sea water and 196 parts per thousand for NaCl, anhydrite is still converted to gypsum. Above these concentrations, theoretical vapour

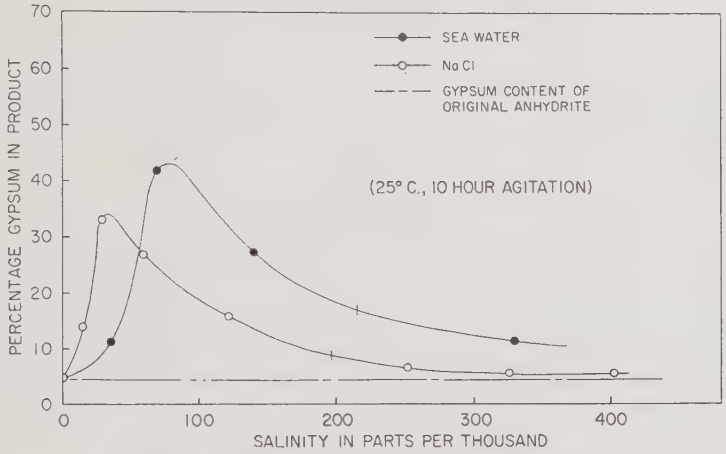

Fig. 9. Activation effect of sea water and NaCl.

pressure calculations indicate that at 25°C only anhydrite can be precipitated from solution. It must be concluded, therefore, that former thermodynamic applications based on vapour pressure relationships, which predict the formation of anhydrite from gypsum in concentrated salt solutions are incomplete. These applications do not incorporate the lattice alterations and intermediate calcium sulphate–activator complexes which influence the reaction kinetics.

It appears more reasonable to assume that anhydrite is formed, given sufficient time, only after burial when gypsum is subjected to directed stresses and increased temperatures.

Summary

(1) The hydration of anhydrite is accelerated by certain acids, bases, and salts. Alkali sulphates are the most effective of these activators.

(2) In dilute activating solutions hydration proceeds via transient complexes. Depending upon temperature, double salts can be stable in concentrated activator media. The formation of complexes is believed to be a surface ionic transfer process and is a function of probability.

(3) Hydration of anhydrite in nature is believed to take place primarily by action of the activating cations occurring in ground water.

(4) Primary precipitation of anhydrite from sea water is improbable. The

* Robert F. Conley (1957) Unpublished manuscript.

relative ease of crystallization of metastable gypsum within the anhydrite stability field prevents sufficient supersaturation for nucleation of anhydrite. Abundant activating cations present in sea water further inhibit the formation of anhydrite.

Acknowledgement—The authors are indebted to Dr. Ralph L. Seifert, Indiana University, for his assistance and suggestions in the construction of the phase diagrams.

References

Clarke F. W. (1924) *U.S. Geol. Surv. Bull.* 770.
Comey A. M. and Hahn D. A. (1921) *A Dictionary of Chemical Solubilities, Inorganic* (2nd Ed.). Macmillan, New York.
Farnsworth M. (1925) *Amer. Pat.* 1566186.
Ford W. E. (1947) *A Textbook of Mineralogy.* John Wiley, New York.
Gelmroth W. *Silikattechnik* **4,** 21–24.
Hennicke R. (1923) *Amer. Pat.* 1442406.
Hill A. E. (1934) *J. Amer. Chem. Soc.* **56,** 1071–1078.
Hill A. E. and Wills J. H. (1938) *J. Amer. Chem. Soc.* **60,** 1647–1655.
Johnson R. A. and O'Rourke J. D. (1954) *J. Amer. Chem. Soc.* **76,** 2124–2126.
Kelley K. K., Southard J. C. and Anderson C. F. (1941) *U.S. Bur. Mines Tech. Paper* 625.
Leininger R. K., Conley R. F. and Bundy W. M. (1957) *Indust. Engng. Chem.* **49,** 818–821.
MacDonald G. J. (1953) *Amer. J. Sci.* **251,** 883–898.
McGregor D. J. (1954) *Indiana Geol. Survey, Rept. Progress* 8.
Marsh J. S. (1935) *Principles of Phase Diagrams* pp. 99–170. McGraw-Hill, New York.
O'Rourke J. D. and Johnson R. A. (1955) *Analyt. Chem.* **26,** 1699–1704.
Otteman J. (1950) *der Geol. Landesanstalt,* No. 219.
Posnjak E. (1940) *Amer. J. Sci.* **238,** 559–568.
Randel W. S. (1933) *Amer. Pat.* 1941188 (to U.S. Gypsum Co.).
Rivett A. C. (1923) *The Phase Rule* pp. 93–125. Oxford University Press, London.
Spangenberg K. and Neuhaus A. (1930) *Chemie Der Erde* **5,** 437–529.
Tammann G. (1903) *Z. anorg. Chem.* **37,** 303–313.
Turnbull D. and Vonnegut B. (1952) *Industr. Engng. Chem.* **44,** 1292–1297.

Geochimica et Cosmochimica Acta, 1958, Vol. 15, pp. 73 to 79. Pergamon Press Ltd., London

Natural and synthetic ferroselite

A roentgenographic mimesis of rammelsbergite

G. Kullerud and G. Donnay
Geophysical Laboratory, Carnegie Institution of Washington, Washington 8, D.C.

(*Received* 9 *April* 1958)

Abstract—Iron diselenide ($FeSe_2$) has been synthesized in sealed, evacuated silica-glass tubes at temperatures between 450 and 550°C. Its powder pattern is identical with that of ferroselite described by Buryanova and Komkov (1955). The first fifteen lines of the pattern are indistinguishable from those of rammelsbergite ($NiAs_2$). Single crystals of ferroselite from Temple Mountain, Utah, were studied on the precession camera. Their diffraction patterns are also deceivingly similar to those of rammelsbergite.

Introduction

In 1955 and 1956 Buryanova and Komkov described a new mineral, ferroselite $FeSe_2$, which they had found in the Middle Devonian deposits of the Tuvinsk Tuva Autonomous Territory. Since 1956 about ten ferroselite localities have been found on the Colorado plateau alone (Coleman, 1958). Special interest is attached to these finds because ferroselite is commonly associated with uranium minerals and also because the increasing importance of selenium in industry has focused attention on the modes of occurrence of this element.

Synthesis of $FeSe_2$

History. Little (1859) reported that he had synthesized a compound of composition Fe_2Se_3 by heating a mixture of iron and selenium. Fonces-Diacon (1900) thought that he had synthesized not only Fe_2Se_3 but also Fe_3Se_4, Fe_7Se_8, FeSe and $FeSe_2$, but, except for FeSe, failed to establish the existence of such compounds. Moser and Doctor (1921) synthesized FeSe by heating Fe and Se together. They mention no other compounds in the Fe-FeSe join. De Jong and Willems (1928) reported unsuccessful attempts to obtain $FeSe_2$ by heating FeSe and Se together *in vacuo* at 230°C and by passing H_2Se over FeSe at 200°C. Hägg and Kindström (1933), in a study of the Fe Se system, working at 600°C, also failed to obtain $FeSe_2$. Hansen (1936) surveyed the literature and concluded that no intermediate compound exists between FeSe and Se. Two years later, however, Tengnér (1938), by heating finely powdered iron and selenium in the atomic ratio 1 : 2 for 4 months at 250°C, succeeded in growing $FeSe_2$. He published a crystallographic description of this compound, including cell dimensions and space group (Table 1) determined from powder patterns. He found the structure to be of the marcasite type with the two parameters, the x- and y-co-ordinates of selenium, very similar to those found by Buerger (1937) for marcasite.

Present experiments. One of us (G. K.) synthesized $FeSe_2$ in evacuated and sealed silica-glass tubes. The iron used in these experiments was open-hearth iron (National Bureau of Standards, Standard sample 55d) containing 99·84 per cent Fe and the following impurities: 0·010 per cent C, 0·030 per cent Mn, 0·005

Table 1. X-ray data on $FeSe_2$ (ferroselite). Space group *Pnnm*

Origin of sample	Fe + Se synth. at 250°C, 4 months, by Tengnér	FeSe + Se synth. at 450°C, 24 days, by Kullerud	Ferroselite Tuvinsk Autonomous Territory	Ferroselite Temple Mountain, collected by Coleman
Data obtained by	Tengnér	Donnay	Buryanova and Komkov	Donnay
X-ray method used	Powder photograph. Cr$K\bar{\lambda}$ (λ not given	Powder photographs. Fe$K\alpha$ (λ = 1·9373 Å)	Laue, rotation and oscillation photographs. Radiation not given	Precession photographs Mo$K\alpha$ (λ = 0·7107)
a (Å)	*4·801 (from kX)	$4{\cdot}79_9 \pm 0{\cdot}015$	4·79 ± 0·02 (from kX)	4·80 ± 0·02
b	5·727	$5{\cdot}71_4 \pm 0{\cdot}017$	5·74 ± 0·02	5·80 ± 0·02
c	3·582	$3{\cdot}55_7 \pm 0{\cdot}011$	3·58 ± 0·02	3·59 ± 0·01
V (Å^3)	98·5	97·5	98·4	99·9
ρcalc (g/cm^3)	7·21	7·28	7·21	7·11
ρobs (g/cm^3)	—		—	7·20 ± 0·02 26°C

* Reoriented to conform with setting of other authors.

per cent P, 0·014 per cent S, <0·001 per cent Si, 0·056 per cent Cu, 0·010 per cent Ni, 0·005 per cent Cr, <0·001 per cent V, 0·001 per cent Mo, 0·007 per cent Co, 0·005 per cent Sn, 0·002 per cent Al, 0·009 per cent As and 0·004 per cent N. Ultra-pure selenium (T-623, from the Mallinckrodt Chemical Works) was used. Analysis of this material shows 99·96 per cent Se and the following impurities: <0·0001 per cent Ag, 0·005 per cent Al, 0·0005 per cent B, 0·0005 per cent Ba, <0·0001 per cent Bi, 0·0005 per cent Ca, 0·0005 per cent Fe, <0·0001 per cent Li, <0·0001 per cent Mg, 0·005 per cent Si.

We find that $FeSe_2$ does not form easily from stoichiometric mixtures of iron and selenium. It grows readily, however, when FeSe and Se are mixed in the ratio given by the $FeSe_2$ formula. Iron monoselenide, therefore, was synthesized first. $FeSe_2$ was synthesized from the 1 : 1 mixture of iron monoselenide and selenium, which was kept at 450°C for 24 days. After quenching, 99 per cent of the material in the tube appeared, under the binocular microscope, as a homogeneous fine-grained phase of a medium-grey colour. The rest of the material occurred in tiny drop-shaped aggregates having the dark brown colour of selenium. These drop-shaped aggregates could readily be separated from the grey material. X-ray diffraction powder patterns showed the aggregates to consist of selenium; the grey substance gave a pattern identical with that of synthetic $FeSe_2$ published by Tengnér (1938). Polished sections, however, showed the grey material to consist of two phases: the diselenide, which amounts to 99 per cent, and the monoselenide, about 1 per cent.* The monoselenide is ferromagnetic, like FeS and NiS, and was separated by means of a magnet from the diselenide, which is not magnetic.

Separation and weighing showed that only 0·6 weight per cent free selenium

* The monoselenide was found to occur as tiny cores coated by diselenide. The diselenide, thus, prevented some of the selenium from reacting with FeSe to form homogeneous $FeSe_2$.

was present in the tube at the termination of this experiment. The amount of monoselenide present, estimated from polished sections, was about 1 per cent by volume. The composition of the diselenide, if the presence of monoselenide were not taken into consideration, would, by calculation of the free selenium in the tube, be $FeSe_{1\cdot982}$. However, if we adjust for the 1 per cent of monoselenide, the composition of the diselenide is very close to that of $FeSe_2$ and within the limit of $FeSe_{2\cdot00\pm0\cdot005}$.

On heating above 700°C in sealed evacuated silica-glass tubes, synthetic $FeSe_2$ decomposes into $Fe_{1-x}Se$ and vapour. The cell dimensions of this iron-deficient

Table 2. Data on ferroselite and rammelsbergite

Locality of sample	Ferroselite, Temple Mt.	Ferroselite, Tuvinsk Autonomous Territory	Rammelsbergite,* Eisleben and Schneeberg
Observations made by	Donnay	Buryanova and Komkov	Peacock
Length of crystals (mm)	0·1 to 0·3	0·2 to 0·5	1·00
Lustre	metallic	metallic	metallic
Colour on freshly broken surface	brass yellow	steel-grey to tin-white with pink shade	tin-white
Brittleness		very brittle	
Colour of powder	black	black	black
Habit	{110} dominant, striated // *c*; occasional narrow faces of {100}	{110} dominant, striated, // *c* with vicinal faces {450}; occasional narrow pinacoidal faces	compact, fibrous to bladed; elongated along *b*[010]; spherulitic
Goniometry	(110) $\wedge$ ($\bar{1}$10) $\approx$ 80° 40′ $a : b \sim 0{\cdot}849$	— —	— —
Morphological point group	*mmm*	*mm*2 or *mmm*	*mm*2 or *mmm*
Cleavage	—		{101}
Twinning	not observed	penetration, marked	on (101); index 3; obl. 2° 20½′; always present. Also complex, lamellar, on undetermined law.

* Reoriented to conform with setting of other authors.

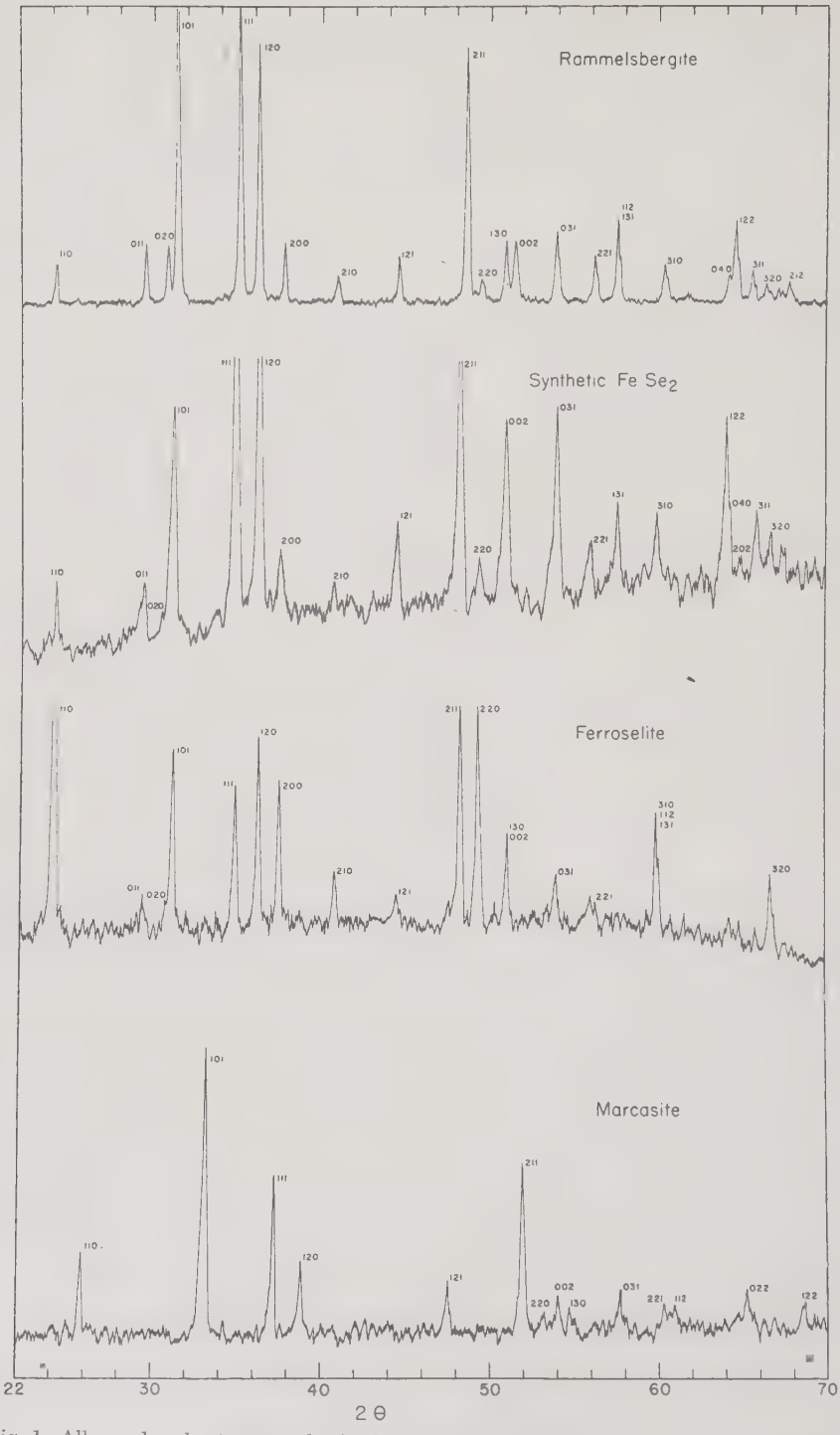

Fig. 1. All powder charts were obtained on Norelco diffractometer with Cu$K\alpha$ radiation. (a) Rammelsbergite, $NiAs_2$, synthesized by Roseboom (1957); (b) ferroselite, $FeSe_2$, synthesized by Kullerud; (c) ferroselite, $FeSe_2$, Temple Mountain; (d) marcasite, FeS_2, Joplin, Mo.

compound, in agreement with the results of Hägg and Kindström (1933), are smaller than those of stoichiometric FeSe.

No single crystal of $FeSe_2$ large enough for X-ray work was obtained, so that cell dimensions were determined from powder patterns. The values obtained (Table 1) agree well with those reported by Tengnér.

Natural $FeSe_2$

Crystallography. Single crystals from Temple Mountain were collected and kindly given to us by Dr. Coleman, who will describe their occurrence in this journal. The crystals are very similar in appearance to the Russian ones (Table 2) and, what is more surprising, to the crystals of rammelsbergite ($NiAs_2$) described by Peacock and Dadson (1940). One would, offhand, assume that X-ray study of single crystals or powder samples must be resorted to for reliable identification of either species. But, amazingly enough, even X-ray diffraction data will not tell these minerals apart. Powder charts obtained with Cu$K\alpha$ radiation on the Norelco diffractometer [Figs. 1(a), 1(b), 1(c)] illustrate this statement. A chemical test is thus absolutely indispensable for identification. The a and b cell dimensions of $FeSe_2$ from different origins (Table 1) cover ranges that include the a and b values of $NiAs_2$ (Table 3); the c dimensions of $FeSe_2$ and $NiAs_2$ differ by less than

Table 3. X-ray data on rammelsbergite and marcasite

	Rammelsbergite $NiAs_2$	Marcasite FeS_2
Origin of sample	Eisleben	Joplin, Missouri
Data obtained by	Peacock and Dadson	Donnay
X-ray method used	Weissenberg	Diffraction pattern
	Cu$K\alpha$ (λ not given)	Cu$K\alpha$ (λ = 1·5405)
a (Å)	4·79 (from kX)	4·59 ± 0·02
b	5·79	5·34 ± 0·02
c	3·54	3·34 ± 0·01
V (Å^3)	98·2	81·9
Space group	*Pnnm*	*Pnnm*
ρ_{calc} (g/cm^3)	7·05	4·86
ρ_{obs} (g/cm^3)	6·97*	4·887

* Higher values such as 7·20 also reported for material from Schneeberg.

0·2 per cent (Table 1). The measured d spacings of the first fifteen lines on a powder pattern obtained with synthetic $FeSe_2$ agree within 0·02 Å with those of rammelsbergite reported by Peacock and Dadson.* We are therefore not publishing the detailed powder pattern; it would be a duplication of data already in the literature (Peacock and Dadson, 1940, pp. 570–571). The intensities too are strikingly similar. Both compounds have the marcasite-type structure, space group *Pnnm*, with Fe or Ni at (a) 000, $\frac{1}{2}\frac{1}{2}\frac{1}{2}$, and Se or As at ($g$) ± ($xy0$, $\frac{1}{2} + x$,

* The transformation of axes from Peacock and Dadson's setting to the present one is 001/100/010/.

$\frac{1}{2} - y$, $\frac{1}{2}$), where $x = 0{\cdot}21$ and $y = 0{\cdot}37$ for $FeSe_2$ as determined by Tengnér. The parameters of As in rammelsbergite were determined by Kaiman (1947) and found to be $x = 0{\cdot}215$, $y = 0{\cdot}370$, so that we may set them equal to the Se parameters in $FeSe_2$. The structure factor can thus be written as:

$$(F_{hkl})_{FeSe_2} = f_{Fe}[1 + \cos \pi(h + k + l)] + 2f_{Se}[\cos 2\pi(hx + ky) + \cos \pi(h + k + l + 2hx - 2ky)]$$

and letting $A(a)$ and $A(g)$ stand for the trigonometric contributions of atoms in positions (a) and (g) we have:

$$(F_{hkl})_{FeSe_2} = f_{Fe}A(a) + 2f_{Se}A(g)$$

and

$$(F_{hkl})_{NiAs_2} = f_{Ni}A(a) + 2f_{As}A(g)$$

For all reflections for which $h + k + l = 2n + 1$, $A(a) = 0$ and

$$\frac{(F_{hkl})_{FeSe_2}}{(F_{hkl})_{NiAs_2}} = \frac{f_{Se}}{f_{As}} = 1{\cdot}03 \approx 1$$

When $h + k + l = 2n$, $A(a) = 2$ and

$$\frac{(F_{hkl})_{FeSe_2}}{(F_{hkl})_{NiAs_2}} = \frac{f_{Se}}{f_{As}} \frac{(f_{Fe}/f_{Se}) + A(g)}{(f_{Ni}/f_{As}) + A(g)} \approx 1$$

since the ratios f_{Fe}/f_{Se} and f_{Ni}/f_{As} differ from one another by only 14 per cent over a range of $(\sin \theta)/\lambda$ from 0·0 to 1·2 (*International Tables*, 1935, p. 572).

Both Peacock and Dadson, in their description of rammelsbergite, and Buryanova and Komkov, in their paper on ferroselite, draw attention to the "close similarity" of the compound they describe to marcasite, and Buryanova and Komkov point out that without a microchemical test for selenium, ferroselite might be mistaken for marcasite. Yet marcasite differs from the other two minerals as to density, cell dimensions (Table 3), and diffraction patterns [Fig. 1(d)]. The latter are not comparable, even though the x and y parameters of S in marcasite as determined by Buerger (1937), $x = 0{\cdot}200 \pm 0{\cdot}003$, $y = 0{\cdot}378 \pm 0{\cdot}003$, are similar to those of Se in $FeSe_2$, because the ratios f_{Fe}/f_S and f_{Fe}/f_{Se} differ by 72 per cent. If, then, a danger exists that ferroselite *may be* mistaken for marcasite, it is almost certain that ferroselite *has been* mistaken for rammelsbergite in the past.

Acknowledgements We wish to express our gratitude to Dr. R. G. Coleman, who kindly offered us his hand specimens to work on. We are indebted to Professor J. D. H. Donnay for reading the manuscript and making many helpful suggestions. We also wish to thank Dr. M. Fleischer of the U.S. Geological Survey for letting us see his translations of the Russian papers by Buryanova and Komkov and by Buryanova.

References

Buerger M. J. (1937) Interatomic distances in marcasite and notes on the bonding in crystals of löllingite, arsenopyrite and marcasite types. *Z. Kristallogr.* **97,** 504–513.

Buryanova E. Z. (1956) Ferroselite. *Zap. Vsesoyuz. mineral. obshch.* **85,** 286–291; *Chem. Abstr.* (1957) **51,** 2477.

Buryanova E. Z. and Komkov A. I. (1955) A mineral—ferroselite. *Dokl. Akad. Nauk SSSR* **105,** 812–813.

Coleman R. G. (1958) In preparation

Fonzes-Diacon H. (1900) Sur les séléniures de fer. *C.R. Acad. Sci., Paris* **130,** 1710–1712.

Hägg G. and Kindström A. (1933) Röntgenuntersuchung am System Eisen-Selen. *Z. Phys. Chem.* B **22,** 453–464.

Hansen M. (1936) *Fe-Se. Eisen-Selen. Der Aufbau der Zweistofflegierungen* p. 731. Springer, Berlin.

Jong W. F., De and Willems H. W. V. (1928) Die Verbindungen $FeSe_2$, $CoSe_2$ und $NiSe_2$. *Z. anorg. Chem.* **170,** 241–245.

Kaiman S. (1947) The crystal structure of rammelsbergite, $NiAs_2$. *Univ. Toronto Stud. Geol.* **51,** 49–58.

Little G. (1859) Über einige Selenmetalle. *Ann. Chem. Pharm.* **112,** 211–214.

Moser L. and Doctor E. (1921) Die Darstellung des Selenwasserstoffes aus Metallseleniden. *Z. anorg. Chem.* **118,** 284–292.

Peacock M. A. and Dadson A. S. (1940) On rammelsbergite and pararammelsbergite: Distinct forms of nickel diarsenide. *Amer. Min.* **25,** 561–577.

Roseboom E. H., Jr. (1957) The $CoAs_2$–$NiAs_2$–$FeAs_2$–As system. Annual Report of the Director of the Geophysical Laboratory, 1956–57. *Carnegie Instn. Wash. Year Book* **56,** 201.

Tengnér S. (1938) Über Diselenide und Ditelluride von Eisen, Kobalt und Nickel. *Z. anorg. Chem.* **239,** 126–132.

Geochimica et Cosmochimica Acta, 1958, Vol. 15, pp. 80 to 90. Pergamon Press Ltd., London

The isotopic composition of rocks of the earth and of meteorites*

A. P. Vinogradov

In the overwhelming majority of cases, the chemical elements represent a mechanical mixture of isotopes. And, as we know, the same chemical elements, and the same isotopes, are to be found throughout the cosmos. With a certain degree of probability and proceeding from certain theoretical arguments and empirical data concerning the composition of the earth, meteorites and stars, one might construct a curve of the abundance of atomic nuclei in the cosmos as a function of their mass numbers. This curve would show (among other things) that there is a predominance in the cosmos of light elements, of light atomic nuclei. Despite the fact that our knowledge of the composition of cosmic bodies is today far from perfection, we must take into account an undoubtedly varying distribution of the chemical elements even within the planets of our solar system. With still greater definiteness one may speak of a varying relative content of the isotopes of light elements on planets and in stars. The discovery of the so-called carbon-nitrogen and proton proton cycles not only explained the possibility of variation in the isotopic composition of H, C, N, O and other light elements in certain stars, but also was an impetus for searches in this direction. And as you know, as a result of these searches there have been found isotopic displacements for H, C, O and other light elements in different types of stars.

We are obviously far from the truth when we repeat that in the Galaxy there takes place a continuous evolution of the nuclear composition of cosmic bodies. The cause of these disturbances in the isotopic ratio in different stars is thermonuclear processes, stellar nucleogenesis. But the question arises: Is this primary process the sole explanation for all possible variations in the isotopic relations that we now observe in cosmic bodies? It is precisely and only this aspect of the problem to which I should like to direct your attention. The isotopic alterations that proceed in cold cosmic bodies are incommensurably small in regard to their productivity and their ultimate effect, if compared with stellar nucleogenesis. And maybe it would not be worth speaking of them if the minutest changes in the isotopic composition, for example of igneous rock of the earth's crust and in the meteorites, did not, in some degree, point to definite processes that led to the formation of the earth's crust, its rocks and of different classes of meteorites. This is why I have agreed to tell about the results of a comparative study of the isotopic composition of the only cosmic materials accessible today to direct investigation that of the deep igneous rocks of the earth and of the substance of meteorites.

Before doing this I must remind you what the earth's crust and various classes of meteorites are. The earth consists of a number of concentric shells—the atmosphere, hydrosphere, biosphere, lithosphere, and the earth's mantle.

* Presented at the International Conference on Radio-isotopes in Scientific Research. Held under the auspices of the United Nations Educational Scientific and Cultural Organization, Paris, 9–20 Sept. 1957.

The lithosphere is a hard surface shell, which in turn consists of a granite layer and a basaltic layer. The basaltic layer covers the entire earth, while the granite layer covers about half the surface of the earth. It is absent on the bottom of the Pacific Ocean and, apparently, in the deep depressions of the other oceans. The basaltic layer is on the average about 15–25 km thick; under the ocean it is noticeably less. On the continents, the granitic layer reaches a maximum of 15–20 km. Structurally, the earth's crust is distinguished not only by its chemical compositions, but also by its seismic properties. At a depth of about 40 km it is separated from the lower-lying rocks of the mantle by a so-called Mohorovicic layer. The rocks of the earth's mantle, for example dunites, which in composition approach the molecules of olivine, sometimes reach the surface of the earth in the form of deeper breaks of the crust. From above, the crust of the earth is covered with a "cover" of sedimentary rocks.

It is most probable that the earth's crust and its igneous rocks were formed during geologic time as a result of a partial melting of the substance of the earth's mantle. In this process, apparently, a considerable thickness of the mantle material was mobilized to create the high concentrations of a number of chemical elements in the igneous rocks of the earth's crust. The rock composition of the mantle, as is accepted (with different insignificant modifications) by the majority of scientists, is chemically identical with stony meteorites, namely, chondrites. Apparently, this idea of identity in the composition of iron meteorites and the core of the earth, of stony meteorites (chondrites) and the deeper ultrabasic rocks of the earth's mantle, etc., was first expressed over a hundred years ago by the French mineralogist, G. O. Daubrée, member of the French Academy of Sciences and corresponding member of the Russian Academy of Sciences.

All meteorites are divided into three principal classes: (a) stony, (b) iron–nickel, and (c) iron. The dominant among the stony ones are the so-called chondrites. In chemical composition they are closest to the ultrabasic rocks of the earth. The most interesting peculiarity that distinguishes them from the igneous rocks of the earth is their structure. They are composed of so-called chondrules of silicate composition.

These chondrules are cemented together by fragments or crushed particles of the destroyed chondrules themselves. In the chondrite cement there is found an iron–nickel alloy in the form of a metallic sponge (about 12 per cent by weight on an average), and troilite (FeS). Iron stony meteorites, for example, the so-called pallasites, are in the form of a sponge of metallic iron (FeNi), with inclusions of chondrules of the silicate substance (chiefly olivine and enstatite).

Iron meteorites contain an average of about 8 per cent Ni. Their more ordinary inclusions are troilite, FeS, and schreibersite, $(Fe, Ni)_3P$, and others. This chief mass of iron in meteorites is in two phases, kamacite and taenite, which determine the character of the structure and the composition of iron meteorites.

Table 1, compiled at one time by Watson, gives an idea about the relations between stony and other classes of meteorites and their stability under conditions on the earth.

Now permit me to return to the isotopic composition of a number of elements which we observe in the igneous rocks of the earth and in meteorites. We may

Table 1. Statistics of observed falls and finds of different classes of meteorites

Type of meteorite	Finds	Observed falls
Iron meteorites	409	29
Iron–stony meteorites	46	6
Stony meteorites	165	547
Total	620	582

speak of three principal processes which compete in disturbing the isotopic relations in the rocks of the earth and in meteorites. These are:

(1) The disintegration of radioactive elements, the spontaneous fission of U and Th caused by α-, β- and γ-radiation of U and Th, and other nuclear transformations on light nuclei, and the like. All these processes lead to the formation of new stable isotopes.

(2) Nuclear reactions under the influence of cosmic radiation.

(3) Disturbances in the relations of stable isotopes either as a result of isotopic exchange and other similar processes of division, or as a result of the mixing of stable isotopes of radiogenic and other origin.

As regards naturally radioactive substances, there are among all chemical elements (with very few exceptions) radioactive isotopes; or some part of the stable isotopes forms the end products of radioactive decay of neighbouring radioactive isotopes. An essential role in changing the isotopic composition is played primarily by the end products of radioactive decay of the series of uranium, actino-uranium, thorium, and possibly of the neptunium series, namely Pb, He, and also the transformation $K^{40} \rightarrow E \rightarrow A^{40}$ and about twenty more similar such pairs: Rb^{87}-β-Sr^{87}; Sm^{147}-α-Nd^{143}, Bi^{209}-α-Tl^{205}, etc. But, as is now sufficiently well known, the influence of the radioactive elements on the composition of rocks and meteorites is not restricted to the primary processes of radioactive decay. Under the influence of their radiations (the α-, β-, and γ-rays of naturally radioactive elements) there arise in rocks and minerals in suitable geochemical associations diverse secondary nuclear processes, of the type (α, n) and $(\alpha, 2n)$ on light nuclei of Be, Li, B, etc. Khlopin observed, for example, a rather high content of He in pegmatite minerals rich in either Be, or Li, B, etc. The formation of a natural source of neutrons, such as Be–Ra or Be–Po, is not excluded in rare-earth pegmatites that contain uraninite or thorium minerals. In its turn, the appearance of neutrons in the material of rocks and minerals causes a reaction of neutron capture. At present, the natural nuclear reactions (n, α), (n, p), (n) and others have been discovered for a number of elements such as $U^{235} + n_0$, which leads to fission. And, as we shall soon see, this reaction of the fission of $U^{235} + n_0$ competes (as to productivity) in nature with the reaction of the spontaneous fission of U or Th. In their turn, they form in natural conditions a big range of fission fragments. The production, in rocks and minerals, of inert gases as a result of the spontaneous fission of U^{238} and $U^{235} + n_0$ is discussed below. Secondary reactions

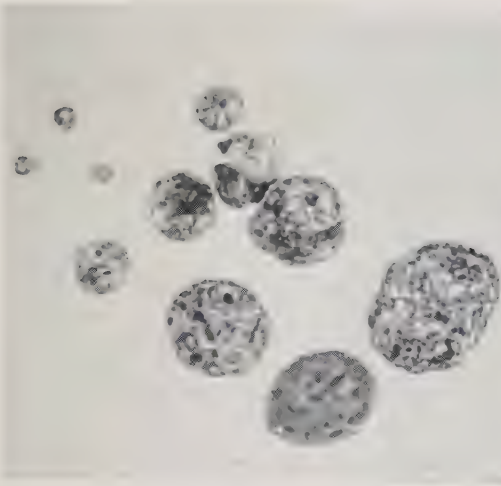

Fig. 1. Chondrules from a meteorite (Nikolskoye). ×4·5.

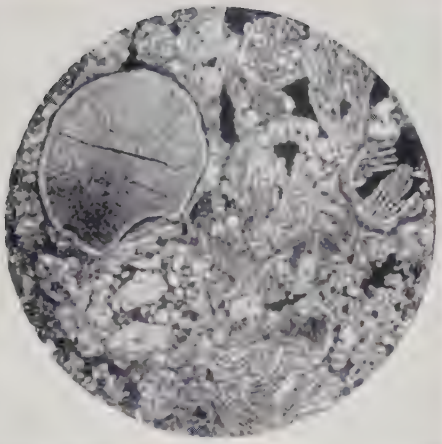

Fig. 2. Chondrules. Appearance under the microscope, in transmitting light. ×20.

Fig. 3. A piece of iron meteorite (Sikhote–Alin). Appearance from the surface.

of the type (γ, n), $(\gamma, 2n)$ or (γ, np) with Be or other nuclei also arise in the very same manner.

Certain of this broad range of radioactive transformations were actually utilized for geological purposes, for example, for determining the absolute geologic age of minerals, rocks, the earth's crust, the age of the earth or the age of meteorites. Many other series still require a detailed study. For this reason, I should like to dwell here in slightly more detail only on one or two illustrations concerning the significance of variations in the isotopic composition of Pb and inert gases in rocks and meteorites. Pb has four stable isotopes, 204, the cosmic non-radiogenic variety, the quantity of which does not increase, 206, 207, and, apparently, the partially radiogenic and partially cosmic 208. A study of the isotopic composition of Pb in iron meteorites has enabled us to give a most trustworthy determination of the age of the matter of meteorites, since Pb in meteorites is not lost, and the processes which might disturb its isotopic composition are absent. Further, on the basis of several hundred determinations of the isotopic composition of ore lead of different geologic age, it has been possible for the first time to evaluate experimentally, so to speak, the age of the earth. But the most considerable achievement obtained by means of an isotopic analysis of the ores and rocks of Pb is the proof that there is no layer of constant isotopic composition of ore lead either in the earth's crust or in the mantle. Any ore lead is torn away from the magma or rocks of the earth during geologic time and retains in its isotopic composition the tag of time. And what is more, the isotopic composition of Pb, which is always to be found in traces in any other ores, as those of iron, copper, etc., also turns out to be a tag of time of the processes of tearing away this ore from the rock or magma. It is interesting to note that the large quantity of data now available on the isotopic composition of ore lead of different geologic age and from different places is an indication of the consolidation of the ore process in time within the limits of a limited number of tectonomagmatic cycles of the earth's crust. In this connexion, the early ideas of the metallogenic epochs of the earth cannot help but come to mind. This is still only the beginning in the sense of utilizing the isotopic relations of Pb to reveal the ore process in the earth's crust. It seems to me that a study of the distribution of radioactive elements and their products in basalts and granites on the basis of the laws of radioactive transformations will, without a doubt, lead logically to an answer to the question about the relations of basalts to granites, this complex and constantly topical geologic problem.

In this connexion I should like to call your attention to one particular aspect of the behaviour of leads in stony meteorites, basalts and granites.

If we proceed from the present-day isotopic composition of lead in stony meteorites, basalts or granites of any geologic age and if we extrapolate the possible isotopic relations for each pair of isotopes of lead, for example, Pb^{207}_{204} into the past, we shall obtain the curves depicted in Fig. 4. The curves for stony meteorites and basalts proceed parallel (along the curve of the "age of the earth"). The Pb^{207}_{204} curves for granites break off very soon. Their further extrapolation becomes absurd. We believe that these curves are an indication that the material of basalts and of stony meteorites is an older material that has undergone but slight changes and has a but slightly disturbed isotopic relation of lead. The material of granites

underwent numerous alterations that disturbed the normal isotopic composition as compared with the "primary" composition. This in general is but a detail, but to some extent it is an indication of the character of the relations of the substance of basalts to that of granites.

Let us now return to the isotopic composition of inert gases in rocks and meteorites, He, Ne, A, Kr and Xe. In their formation there participate not only the radioactive decay of U, Th, K^{40} and the fission of U and Th; at least for meteorites, a considerable contribution of inert gases is made by nuclear transformations which develop under the influence of cosmic radiation. For this reason it seems to me convenient to consider them together. New radioactive and non-radioactive nuclei appear (chiefly in the atmosphere) due to the impacts of cosmic particles,

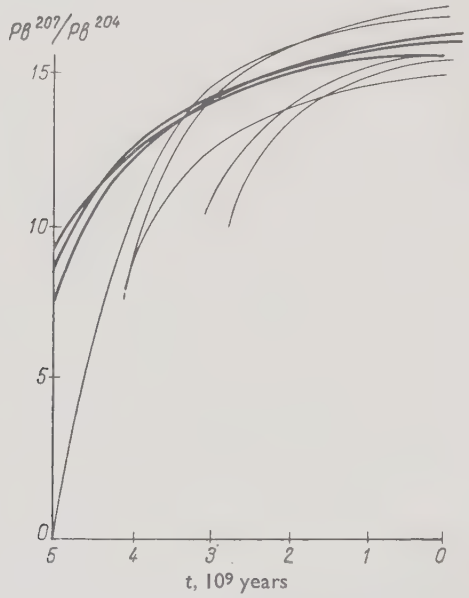

Fig. 4. Change of Pb^{207}/Pb^{204} with time.
Thick lines—in ultrabasic rocks, basic rocks and in stony meteorites; thin lines—in acid rocks and granites.

protons, etc., and also under the influence of secondary neutrons and mesons in the matter of meteorites and on the earth's surface. The chemical composition of the atmosphere and in particular the isotopic composition of its inert gases as we shall see presently, reflects the composition of the gases of igneous rocks. We believe that many gases in the atmosphere are the result of degasing of the earth during geologic time. Therefore, if we know the portion of inert gases brought into the atmosphere as a result of the action of cosmic radiation, we can get an idea of the composition of these gases from the deep-seated rocks of the earth. As for the action of cosmic radiation and the isotopic composition, for instance, of the inert gases of meteorites, it depends primarily on its dimensions; the smaller a meteorite is, the more it is affected by cosmic rays. Thus the accumulation of inert gases and other products of nuclear reactions with cosmic particles depends on the depth,

that is, the position of the material of the meteorite, whether on its surface or in the depth of the primary meteorite. It is also a function of the duration of irradiation of the meteorite; to a certain degree it depends on its age, on the intensity of irradiation, and on the chemical composition of the meteorite.

Helium, the most prevalent of the inert gases, is formed both radiogenically and under the action of cosmic particles on matter. It has two isotopes; He^3 and He^4. The quantity of He^4 in the gases of the earth's atmosphere and in rocks (where it was formed radiogenically) exceeds that of He^3 by a factor of 10^6. He^3 originates in the atmosphere by the reactions $N^{14} + n^0 \rightarrow 3He^4 + T^3(He^3)$ and similar ones, and is noticeably not carried off by rocks. In stony meteorites He^4 originates as a result of the radioactive decay of U and Th, and together with He^3 as a result of the action of cosmic radiation on the material of the meteorite.

The relation He^3/He^4 in stony meteorites is rather dispersive and oscillates about 0·02. And finally, in iron meteorites, where due to the impact of a cosmic particle Fe nuclei transform, He^3 and He^4 are also formed. But the content of U and Th in iron meteorites is negligibly small and, as PANETH and others have shown, we have the relation $H^3/He^4 = \sim 0{\cdot}3$. The quantity of He falls off with depth in the meteorite and the relation He^3/He^4 is slightly altered. Thus, the rocks of the earth, stony meteorites, and iron meteorites differ according to He^3/He^4 both qualitatively and quantitatively. Slightly different is the behaviour of isotopes of Ne and A.

Table 2. The isotopic composition of certain inert gases of the atmosphere, igneous rocks, and meteorites

Type of material	A^{40}/A^{36}	A^{38}/A^{36}	Ne^{21}/Ne^{20}	Ne^{22}/Ne^{20}	He^3/He^4
Earth's atmosphere	296	0·187	0·00283	0·097	10^{-6}
Igneous rocks	—	0·5	—	—	$\sim 10^{-7}$
Stony meteorites	—	0·6	0·6	0·6	0·02
Iron meteorites	—	1·6	0·89	0·98	0·3

The origin of the isotopic composition of Ne of the atmosphere and hence of igneous rocks has been sufficiently studied. The reactions which lead to the isotopic composition of Ne of the atmosphere are still obscure. In the atmosphere there is a sharp predominance of Ne^{20} (90·9 per cent). Since many investigators have shown that Ne/A for the atmosphere ($1{\cdot}9 \times 10^{-3}$) for igneous rocks ($3{\cdot}8 \times 10^{-3}$) and for natural gases ($2{\cdot}5 \times 10^{-3}$) have practically identical values, and, as we also note that Ne/A in stony meteorites is of the same order, it may be assumed that the isotopic composition of the Ne of the earth is the result partially of fission of U, partially of neutron reactions with fluorine and oxygen. In the iron meteorite of Sikhote-Alin we found the relations of the isotopes of Ne absolutely different. Here, the isotopes of Ne are likewise the residual nuclei of the spallation of Fe nuclei. The relation between these three isotopes is close to unity. In the iron Sikhote-Alin meteorite, the quantity of Ne diminishes with depth without changing the isotopic ratio. We have found nearly the same ratio of isotopes of Ne for stony meteorites. In stony meteorites, it is principally nuclei lighter than Fe that react

with cosmic particles, and therefore it is possible that this is the reason for the slight modification in the isotopic composition of Ne (and likewise A).

A^{40} predominates in rocks (and hence in the atmosphere) and its chief source is the process $K^{40} \rightarrow E \rightarrow A^{40}$. In the atmosphere the relation A^{38}/A^{36} is very close to A^{38}/A^{36} in radioactive minerals (neutron reactions). These two chief sources of isotopes of A are the ones that form the A of the atmosphere. But in rocks A^{38}/A^{36} approaches 0·5. Gerling supposes that the isomer K^{38} can likewise be a source of A^{38}. The accumulation in stony meteorites of A^{40} depends on their age and is a result of the decay of K^{40}, A^{36} and A^{38} nuclei originate as a result of the spallation of Fe nuclei and of still lighter nuclei of stony meteorites. Therefore, the ratio of A^{38}/A^{36} should be close in iron and stony meteorites. In iron meteorites, there is clearly observed a reduced content of A^{36} and A^{38} (and also A^{40}) with depth.

A few words about the heavy inert gases. Thode and others have shown that on earth the sources of a number of isotopes of Xe and Kr are two competing processes: the spontaneous fission of U^{238} and the fission of U^{235} by neutrons. The isotopic composition of Xe + Kr of radioactive minerals lies between the value of these two processes. And in natural processes there is observed a shift in the yields of these gases towards the heavy isotopes. For this reason, the gases of the uranium and other minerals have an Xe/Kr = 5. Though the gases of igneous rocks and the atmosphere have practically an identical (Xe + Kr)/A ($1{\cdot}9 \times 10^{-4}$ and $1{\cdot}2 \times 10^{-4}$), the isotopic composition of Xe and Kr of the atmosphere differ sharply; Xe/Kr = 0·08 is also different.

And, finally, about the constancy of isotopic relations of stable isotopes in igneous rocks and meteorites. As is to be expected from thermodynamical reasoning, the greatest effect in the division of isotopes in natural conditions is observed in the case of light elements. In the rocks of the lithosphere there are locally observed sufficiently noticeable variations in the isotopic relations for S, O, C, H, N, B, and others.

It may be supposed that as the sensitivity and precision of our instruments increase, the separation effect will be noticeable also for the heavier nuclei. It is easy to suppose that various physico-chemical processes that proceed in the earth's crust (and are well-known in the laboratory), for example, evaporation, diffusion, etc., are responsible for the disturbance in the isotopic relations in natural conditions. However, observation and experiment have shown that the most common reason for changes in isotopic relations and for changes of stable isotopes in nature is isotopic exchange. It proceeds in vapours, liquids and melts. As is well known, the constant of equilibrium in this exchange approaches unity with increase in temperature, that is, as the temperature increases the separation of isotopes becomes less and less probable, with certain exceptions. The geologic time scale is amply sufficient for this isotopic exchange to arrive at a state of equilibrium, for example, in the cooling of magma. Thus, the isotopic relation for different stable isotopes of rocks is actually a local geologic thermometer of the process if it is not spoiled later by an isotopic exchange of the cooled rock and the surrounding medium. I shall confine myself to a limited number of examples.

For instance, without at all expecting it, we found that the sulphur of iron meteorites and that of stony meteorites is absolutely identical as to isotopic

composition. The isotopic composition of the sulphur of igneous rocks of high-temperature sulphide ores produced a considerable dispersion.

Table 3. Mean data for the isotopic composition of sulphur, igneous rocks, ores and meteorites

Type of material	No. of cases	S^{32}/S^{34}
Stony meteorites	13	22·20
Iron meteorites	10	22·20
Volcanic sulphur	15	22·21
Ultrabasic rocks (dunites)	4	22·20
Basalts	2	22·178
Granites	2	21·780
Magmatogene sulphides	7	22·138
Hydrothermal sulphides	32	22·148
High-temperature sulphates		21·885
Marine sulphates	13	21·75

This spread is observed even in the most high-temperature magmatogene-liquation sulphides that originally separated from the magma. This spread in the isotopic composition of sulphur is still greater in the hydrothermal sulphides. At the same time, the isotopic composition of the sulphur of the igneous rocks of basalts and granites is also different from that of the sulphur of meteorites. Only ultrabasic rocks, which chemically are close to stony meteorites (as witness the sulphur of dunites), correspond to the isotopic composition of the sulphur of meteorites. And, finally, the sulphur of volcanoes. Its isotopic composition is close to, if not identical with, the isotopic composition of the sulphur of meteorites. In a word, then, the isotopic composition of the sulphur of iron, iron–stony, and stony meteorites, the rocks of the earth's mantle, and the sulphur of volcanoes is close and has a definite constant composition. The rocks of the lithosphere and ores contain sulphur of a considerably modified isotopic composition. Still greater dispersion in the isotopic composition of sulphur is attained in the biosphere.

It is possible, in part, to calculate the equilibrium which originate in the system Fe–S–O_2 at the instant the ore is torn away from the magma. In this process there is already a separation of the isotopes of sulphur.

Obviously nothing of the sort happened during the formation of different classes of meteorites, since they all have an identical sulphur composition. Consequently, their substance did not undergo processes comparable to the magmatic liquation or fractional differentiation which are observed in the case of rocks of the earth's crust.

The very same tendency of a growth in the effect of isotope separation for the rocks of the earth's crust from the deeper-lying rocks to the surface is observed with respect to the isotopes of oxygen. The isotopic composition of O_2 of stony meteorites is closest to O_2 of ultrabasic rocks. The maximum dispersion of isotopic composition of O_2 in the case of granites, as compared with the dispersion of the

isotopic composition of O_2 in the case of other igneous rocks was noted not only by us. Indeed, for granites this spread has $\Delta 7{\cdot}7$–$12{\cdot}2$ per cent, whereas for the basic rocks (basalts) $\Delta 6{\cdot}7$–7 per cent. Thus, the greatest difference in the isotopic composition of O_2 may be found between granites and stony meteorites.

Table 4. Mean data on the isotopic composition of oxygen in rocks and stony meteorites

Type of material	No. of cases	O^{18}/O^{16}
Granites	11	$4{\cdot}5 \times 10^{-2}$
Basic and ultrabasic rocks	8	$7{\cdot}0$
Stony meteorites	3	$7{\cdot}0$

The increase in the content of O^{18} in acid rocks, such as granites, is due to the high content of O^{18} on a molecule of quartz $SiO_2{}^{18}$, just as a molecule of CO_2 accumulates the greatest possible quantity of O^{18}. The influence of O^{18} in SiO_2 on the isotopic composition of O_2 of the rock is especially noticeable for rocks of the sedimentary cycle which are enriched with colloidal SiO_2.

Hence it is easy to understand that a still greater dispersion of the isotopic composition of O_2 is found in the biosphere.

Despite the tremendous amount of data on the isotopic composition of C^{12}/C^{13}, it is very difficult to compare the latter. For this reason, I am compelled to proceed mainly from the data of my laboratory. On the average, the isotopic composition of the carbon of iron meteorites and of different classes of stony meteorites is the same. However, the dispersion in the isotopic composition of carbon is considerably higher in the case of iron meteorites than in the case of stony meteorites. Aside from scattered carbon in the mass of iron of iron meteorites, the latter contain (rarely), it is true inclusions of the carbide Fe_3C, cohenite. According to Craig, in the Canyon Diablo meteorite the carbon of the iron had $C^{12}/C^{13} = 89{\cdot}45$, and the carbon of cohenite $90{\cdot}51$. The observed dispersion may possibly be explained by a difference in the relation of cohenite to scattered carbon in the iron of different meteorites.

Table 5. Mean data on the isotopic composition of the carbon of limestones, meteorites, and igneous rocks

Type of material	No. of cases	Dispersion C^{12}/C^{13}	Mean C^{12}/C^{13}
Limestones	92	$88{\cdot}1$–$89{\cdot}5$	$89{\cdot}0$
Iron meteorites	13	$89{\cdot}6$–$91{\cdot}8$	$90{\cdot}6$
Stony meteorites	26	$89{\cdot}6$–$91{\cdot}2$	$90{\cdot}6$
Igneous rocks	13	$90{\cdot}3$–$91{\cdot}2$	$91{\cdot}8$

The isotopic composition of C^{12}/C^{13} of igneous rocks is very close to the C^{12}/C^{13} of meteorites and, as far as may be noticed from the limited number of data in this

direction, has a tendency to a reduction in the content of C^{13}. The logic of this conclusion is that in the lithosphere and in the biosphere there takes place a more considerable separation of C^{12}/C^{13} in rocks, due in part to the deposition of great masses of $CaCO_3$ and the like, the molecules of which have a maximum accumulation of C^{13}.

I am coming to the end. In this brief lecture I have hardly touched on what appears to me the most important thing, the diversity of processes that proceed in the matter of the rock of the earth's crust and of meteorites under the influence of radioactive elements and cosmic radiation which constantly alter their isotopic composition.

I am sure you understand me correctly, that each of the processes considered that disturb the isotopic composition of the substance makes a different contribution. For the rocks of the earth, radioactive decay is of primary importance. The reaction on α-particles or on neutrons as a derivative of radioactive decay makes a fundamentally smaller contribution. For meteorites a considerable role is played by cosmic radiation.

As we have seen, alterations in the isotopic relations chiefly for light atomic nuclei in igneous rocks and meteorites are of a systematic nature, but they rarely attain differences of large magnitude.

However, at the present time we cannot speak of constancy in their isotopic composition. These small alterations in isotopic relations for lead, the inert gases, a number of light elements, etc., are of exceptional importance in geochemistry and cosmochemistry, being indicators of the genesis of rocks and meteorites. We are now convinced of the difference of isotopic relations: (1) on the one hand for different igneous rocks, and (2) on the other, as a comparison of their isotopic composition with the isotopic composition of meteorites. We are also convinced that the isotopic composition of the stable light elements varies in a definite manner as one passes from the depth of the earth's crust to the surface. At the same time, there is not observed any such alteration in the isotopic composition of meteorites. The isotopic composition of light elements in different classes of meteorites has a considerably smaller dispersion than those same elements in the igneous rocks of the earth. The accumulation of inert gases and their isotopic composition in the rocks of the earth (and hence the composition of the gases of the atmosphere) and in meteorites differ and are determined in the first case chiefly by natural radioactivity, and in the second case, chiefly by cosmic radiation, etc.

It seems to me that this peculiarity of the isotopic composition of rocks and meteorites enables one to draw the conclusion that the processes too, which led to the formation of igneous rocks of the earth's crust and meteorites must be different. The isotopic composition of lead and of other stable isotopes, for the rocks of the mantle and the earth's crust does not contradict the hypothesis of the melting of rocks in the earth's crust and of the formation of the atmosphere by degasing of the material of the mantle in geologic time.

But it seems to me that the isotopic composition of meteorites, namely, the identity in the composition of the stable isotopes of the light elements for all classes of meteorites, stony and iron, the presence of inert gases of an isotopic composition that differs from that on earth, etc., indicate an absence, in the process

of the formation of different meteorites, of the processes of melting, liquation of hydrothermal processes, and other analogous processes of the fractional differentiation of material that resemble those in the earth's crust and on the earth. For example, I view the formation of iron and stony meteorites not as a process of the melting of iron from the primary meteorite Fe-silicate material (in which case, incidentally, chondrules would disappear in stony meteorites), but as a result of the mutual accumulation of cooled drops of silicate material with iron (in the case of the formation of iron-stone meteorites). Then, at these relatively high temperatures (ca. 2000°K) the isotopes of sulphur or carbon and others will distribute themselves uniformly in the substance matter of silicates and iron. Only the appearance, at these temperatures, of new phases, as for instance, the formation of carbides for carbon, can cause a certain division of isotopes, and so forth. The facts do not seem to contradict this. In a word then, the study of the isotopic composition of natural objects, and the findings of explanations for them raises the hopes of geochemists to penetrate deeper into the mighty processes of the formation of cosmic bodies. And if I, through the medium of my lecture, have attracted at least one enthusiast, then you must admit that the use of isotopes in geochemistry is a magnificent method.

Geochimica et Cosmochimica Acta, 1958, Vol. 15, pp. 91 to 112. Pergamon Press Ltd., London

Experimentelle Gesteinsmetamorphose—II

Bildung von anatektischen granitischen Schmelzen bei der Metamorphose von NaCl-führenden kalkfreien Tonen

Helmut G. F. Winkler und Hilmar von Platen
Mineralogisches Institut der Universität Marburg/Lahn, Germany

(*Received* 5 *June* 1958)

Abstract—Illite–quartz clays to which NaCl was added (to allow for saline solutions in the rock pores) were hydrothermally and isochemically treated between 350° and 800°C under 2000 atm of H_2O pressure. The results are compared with the experimental metamorphism and ultrametamorphism of the NaCl-free clay.

Below 390°C no reactions take place but at 390° illite + kaolinite + NaCl + H_2O + Ca give muscovite + chlorite + Ab-rich plagioclase + HCl + H_2O. The next reaction follows at about 550°C giving rise to the mineral assemblage cordierite, biotite, muscovite, plagioclase and quartz; chlorite is now absent. At this temperature the amphibolite facies is reached and at 600°, 625° or 665° (depending on the Na content) the pyroxen–hornfels facies is entered with the assemblage alkalifeldspar, cordierite, biotite ± sillimanite–mullite, plagioclase and quartz; muscovite is now absent.

At 670° and 720°C, respectively, the cordierite–gneisses derived from the NaCl-containing clays give rise to anatectic melts of granitic composition and calc–alkaline character. Since these melts comprise up to two-thirds of the previous cordierite–gneisses they are believed to have a fundamental bearing on the genesis of granites.

Einleitung

Bei der experimentell unter 2000 atm H_2O-Druck durchgeführten isochemischen Metamorphose von kalkfreien Kaolinit–Illit–Quarz–Tonen bzw. von Illit–Quarz–Tonen wurde festgestellt (Winkler, 1957), dass sich bei 665°C ein Gestein (Gneis) bildet, welches aus Sillimanit (-Mullit) + Quarz + Alkalifeldspat und etwas Biotit bzw. aus Cordierit + Sillimanit + Quarz + Alkalifeldspat und etwas Plagioklas besteht. Von diesen Gesteinen schmilzt bei 700°–725°C ein sehr erheblicher Teil, nämlich 45–65 Prozent ihres Gewichts, wobei Sillimanit, Cordierit und—wenn relativ viel Quarz vorhanden war—Reste von Quarz übrig bleiben. Trotzdem verschiedene Tone als Ausgangsgesteine für die experimentelle Metamorphose verwendet wurden, sind die Zusammensetzungen der anatektisch gebildeten Schmelzen fast gleich in bezug auf das Verhältnis der Komponenten Quarz: K-Feldspat: Albit $\approx$ 43 : 49 : 8. Es ist also die erwartete selektive Aufschmelzung nachgewiesen, welche in jenen Fällen zu leukogranitischen Schmelzen geführt hat. Die Schmelzen liegen sehr nahe der von Bowen und Tuttle (Bowen, 1954) für das System Qz–Or–Ab bei 2000 atm H_2O-Druck bestimmten kotektischen Linie, und zwar nahe der Qz–Or–Seite des Systems (siehe Lage des Kreuzes in Abb. 6).

Da bei den kalkfreien Tonen der Gehalt an CaO sehr gering war, konnte sich kein oder nur wenig Anorthit–Anteil bilden, so dass auch die Schmelzen ihn nicht oder nur in wenigen Prozenten enthalten. Da ferner der Na_2O-Gehalt der Tone sehr gering ist, ist es offensichtlich, dass nur sehr wenig Albit-Komponente (die im Alkalifeldspat und im Plagioklas steckt) in den Schmelzen vorhanden sein

kann, so dass die anatektischen Schmelzen zwar sehr nahe der kotektischen Linie des Systems Qz-Or-Ab H_2O liegen, aber nahe der Qz–Or–Seite und nicht im Zentrum des Komponentendreiecks, um das sich die Zusammensetzungen von Graniten scharen. Es wurde nun vermutet, dass Na in Form von zugesetztem NaCl eine zusätzliche Menge an Albit-Komponente bilden könnte, welche in die Schmelze gehen und so ihre Zusammensetzung derjenigen der Granite weiter annähern würde. Diese Vermutung wird durch die im folgenden dargestellten Experimente bestätigt.

Da in der Tiefe das Porenvolumen der Gesteine von salinaren Lösungen ausgefüllt ist,* ist es notwendig, sie zu berücksichtigen, damit die Experimente wirklich die Vorgänge bei der natürlichen Metamorphose unter H_2O-Druck erfassen. Die Porenwässer sind hinsichtlich Zusammensetzung und Konzentration sehr variabel, aber es wurden gesetzmässige Änderungen mit der Tiefe festgestellt, derart, dass in grossen Tiefen (um 1000 m) die Konzentration am grössten und die Zusammensetzung überwiegend NaCl ist (Afanas'ev, 1947). Wenn nun etwas NaCl den Tonen, die ja aus Gruben von der Erdoberfläche stammen, zugesetzt wird, dann wird damit der chemische Zustand angenähert, der in grösseren Tiefen herrscht. Ausser NaCl sind noch andere Salze zu berücksichtigen, worüber Untersuchungen laufen. Zunächst wird hier nur der Einfluss von NaCl auf die Metamorphose behandelt.

Nach Hedberg (1936) können tektonisch nicht gestörte tonige Sedimente z.B. in 3000 m Tiefe ein Porenvolumen von fast 10% haben. Wenn eine konzentrierte NaCl-Lösung in den Poren angenommen würde, dann ergäbe sich, dass der getrocknete Ton eine Menge von ca. 1,5 Gew-% NaCl enthielte. Ausserdem muss noch etwas Na an den Tonmineralen adsorbiert sein. Es wurde nun unserem Ton so viel NaCl zugesetzt, dass er für die eine Versuchsreihe 1,77% enthielt. Für die andere Versuchsreihe wurde der Anteil des zugesetzten NaCl im Ton bewusst etwas höher gehalten, damit ein in Reaktionen nicht verbrauchter Rest von NaCl besser nachgewiesen werden konnte. Die Menge des NaCl im Ton betrug für die zweite Versuchsreihe 4,76 Gew-%.

Ausgangsgestein und experimentelle Durchführung

Als Ausgangsgestein für die Experimente diente der Blaue Ton von Heppenheim/Bergstrasse, der aus etwas 55-60% Illit, 24–25% Quarz, etwa 5% Kaolinit, jeweils etwa 2% von Plagioklas, Chlorit, Montmorillonit und Eisenhydroxyd und Spuren von Rutil, Apatit und Pyrit besteht; ausserdem enthält der Ton etwa 3% organische Substanz. Dieser Ton wurde als Beispiel für die sehr weit verbreiteten hauptsächlich aus Illit und Quarz bestehenden Tone gewählt. Seine Metamorphose wurde bereits dargestellt (Winkler, 1957). Eine neue chemische Analyse† zeigt Tab. 1, Spalten 1 und 2; die zuverlässigeren Analysenwerte weichen nur wenig von den früher (Winkler, 1957, Tab. 1, Ton C) angegebenen ab. Für die neuen Versuche wurden nun diesem bei 105°C getrockneten Ton 5%

* Für diesen Hinweis danken wir Herrn Prof. Dr. von Engelhardt und Herrn Prof. Dr. C. W. Correns.

† Herrn Dr. von Gaertner, Amt für Bodenforschung, Hannover, sind wir für die Analyse sehr dankbar.

bzw. 1,8% NaCl zugesetzt, so dass er 4,76% bzw. 1,77% NaCl enthält, Tab. 1 Spalte 3 bzw. 4.

Die Experimente wurden wie bisher isochemisch unter 2000 atm H_2O-Druck ausgeführt. Die Fehlergrenze bei den Temperaturangaben beträgt etwa ±5°C. Die Dauer der hier ausgewerteten Versuche betrug stets 21 Tage. Nach dieser

Tab. 1. Chemische Zusammensetzung des Tons ohne und mit Zusätzen von NaCl

	1 Chemische Analyse (Gew-%)	2 Analyse ohne H_2O^- (Gew-%)	3 Analyse +1,8% NaCl ohne H_2O^- (Gew-%)	4 Analyse +5% NaCl ohne H_2O^- (Gew-%)
SiO_2	56,11	58,62	57,58	55,83
Al_2O_3	19,38	20,25	19,89	19,29
Fe_2O_3	3,29	3,44	3,38	3,28
FeO	0,99	1,03	1,01	0,98
MnO	0,02	0,02	0,02	0,02
MgO	2,36	2,47	2,43	2,35
CaO	1,23	1,29	1,27	1,23
Na_2O	0,41	0,43	0,42*	0,41†
K_2O	2,93	3,06	3,01	2,91
TiO_2	0,73	0,76	0,75	0,72
V_2O_5	0,08	0,08	0,08	0,08
P_2O_5	0,15	0,16	0,15	0,15
S	0,13	0,14	0,13	0,13
CO_2	Spuren	Spuren	Spuren	Spuren
H_2O^-	4,56	—	—	—
H_2O^+	4,80	5,02	4,93	4,78
org. Substanz	3,10	3,24	3,18	3,09
NaCl	—	—	1,77	4,76
	100,27	100,01	100,00	100,01

* Die Versuche ergaben, dass bei Temperaturen oberhalb 625° die 1,77% NaCl in den Reaktionen verbraucht worden sind, wobei HCl entstand. Das Na ist für die Bildung von Albit verbraucht worden. $2NaCl + H_2O$ haben also die Komponenten $Na_2O + 2HCl$ gebildet. Für 1,77% NaCl sind dann 0,94% Na_2O anzusetzen, so dass die Gesamtmenge 0,42 + 0,94 = 1,36% NaCl beträgt.

† Die Versuche mit 4,76% NaCl ergaben, dass bei Temperaturen oberhalb 600°C stets 1,6 ± 0,1% NaCl nachgewiesen werden konnten, während die restlichen 3,2% NaCl in Reaktionen verbraucht worden sind. Daraus berechnen sich analog 1,70% Na_2O, so dass die Gesamtmenge an Na_2O, die in Reaktionen bis 600° verbraucht wurde, 0,41 + 1,70 = 2,11% beträgt.

Zeit, aber noch nicht nach 6 Tagen, hatten sich die Reaktionsgleichgewichte eingestellt. Die erfolgte Gleichgewichtseinstellung konnte in einigen Fällen überzeugend nachgewiesen werden: Die Mineralmengen, die sich bei der Metamorphose des Tons mit 4,8% NaCl, z.B. bei 670° nach 21 Tagen gebildet hatten, wurden verglichen mit denjenigen, die sich ergaben, nachdem der Ton zunächst über 1 Woche der höheren Temperatur von 740°C ausgesetzt und dann (ohne Unterbrechung des Versuchs) 21 Tage lang bei 670°C gehalten worden war. Im ersten Fall handelt es sich um eine aufsteigende Metamorphose, im zweiten um eine

fallende, denn bei 740°C hatte sich zunächst eine Teilschmelze gebildet, so dass also andere Phasen vorlagen als bei 670°C. Da in beiden Fällen bei 670°C die gleichen Mineralmengen festgestellt wurden, ist der Nachweis der Gleichgewichtseinstellung erbracht. Die hier geschilderten Versuche sind ein Beispiel für mehrere gleichartige aber bei anderen Temperaturen durchgeführte Versuche.

Die Mineralmengen von Quarz, Cordierit, Alkalifeldspat und NaCl wurden mittels des Zählrohrgoniometers (Cu$K\alpha$-Strahlung) und Vergleichspräparaten bestimmt. Die quantitative Bestimmung des Muskovits und Plagioklases war auf diese Weise nicht befriedigend.

Beim Plagioklas wurde folgendermassen vorgegangen: Der untersuchte Ton mit 4,8% NaCl enthält auf Grund der chemischen Analyse 0,4% Na_2O, hierzu kommen weitere 1,7%, die sich aus der oberhalb von 600° verbrauchten NaCl-Menge von 3,2% errechnen. Das Na_2O wird nur in der Albitkomponente des Plagioklases und des Alkalifeldspates gebunden, und zwar entsprechen der verbrauchten Na_2O-Menge von 2,1% 17,9 Gew-% Albit-Komponente. Davon sind 3,4% im Alkalifeldspat gebunden (es bilden sich 19 Gew-% Alkalifeldspat) der sich auf Grund der Lage der (20$\bar{1}$)-Interferenz aus 18% Ab und 82% Orthoklas zusammensetzt (siehe Seite 100), so dass noch 14,5% Albit-Komponente für den Plagioklas zur Verfügung stehen. Die auf Grund des CaO-Gehaltes der Analyse bildbare Anorthitmenge beträgt 5,1 Gew-% bei Berücksichtigung des vorhandenen Apatits. Die rechnerisch ermittelte maximale Plagioklasmenge beträgt also 14,5 + 5,1 = 19,6 Gew-%; als Zusammensetzung des Plagioklases ergibt sich ein Oligoklas mit An 26.

Die quantitative Plagioklasbestimmung erfolgte nun in der Weise, dass bei den Proben oberhalb 600° der Mittelwert für die Höhe der mit dem Zählrohrgoniometer vermessenen Plagioklasinterferenz bei $2\vartheta = 22°$ (20$\bar{1}$) gleich 20% gesetzt wurde. Durch Vergleich mit diesem Wert wurde die Plagioklasmenge in den einzelnen Proben bestimmt.

Röntgenographische Messungen mit einem Tiefoligoklas als Vergleichssubstanz ergaben zu hohe Plagioklaswerte, was auf eine Intensitätszunahme der (20$\bar{1}$)-Interferenz vom Tief-zum Hocholigoklas zurückgeführt werden muss. Untersuchungen über die Abhängigkeit der Intensitäten von Zusammensetzung und thermischen Zustand der Plagioklase werden am hiesigen Institut durchgeführt. Wegen der relativ geringen Plagioklasmenge und der Koinzidenz einiger Plagioklasinterferenzen mit Interferenzen anderer Minerale können bis jetzt keine sicheren Aussagen über den thermischen Zustand des gebildeten Plagioklases gemacht werden. Wegen der geringen Grösse der Kristalle war eine optische Untersuchung und damit eine Kontrolle der berechneten Plagioklaszusammensetzung leider nicht möglich.

Auf Grund der Intensitäten der Muskovit-Interferenzen bei $2\vartheta = 19{,}8°$ (110, 11$\bar{1}$) und $2\vartheta = 35{,}0°$ (20$\bar{2}$) konnte die im Laufe der Metamorphose erfolgte relative Mengenabnahme gut beobachtet werden. Die quantitative Bestimmung der jeweiligen Mengen jedoch stiess auf Schwierigkeiten: Die Intensitäten der beiden erwähnten Interferenzen des in unseren Versuchen gebildeten Muskovits stimmen in ihrem Verhältnis nicht mit demjenigen Verhältnis überein, welches man bei Mischungen von Quarz mit Muskovit erhält. Die Intensität der Interferenz bei $2\vartheta = 19{,}8°$ spricht für höhere Muskovitmengen, die bei $2\vartheta = 35°$ für niedrigere Mengen als sich auf Grund der chemischen Analyse errechnen. Der Mittelwert der Muskovitmengen aus den Intensitäten stimmt jedoch recht gut mit der berechneten Muskovitmenge überein. In den graphischen Darstellungen und der Abb. 1 und 2 sind die Muskovitmengen auf Grund der Berechnung unter Berücksichtigung der beobachteten relativen Mengenänderung und der Mineralreaktionen eingetragen worden. Dies gilt ebenfalls für die eingezeichneten Mengen von Chlorit, Biotit und Sillimanit-Mullit. Lediglich auf Grund von Berechnungen erfolgte die Darstellung der Mengen an freigewordenem H_2O.

Experimentelle Metamorphose des Illit–Quarz–Tons mit und ohne NaCl-*Zusatz*

Wie bei der Metamorphose des NaCl-freien Tons (Winkler, 1957, S. 54 ff.) wird bei den NaCl-führenden Tonen etwas unterhalb 400°C die Reaktion Illit +

Muskovit + Chlorit + Quarz + H_2O beobachtet, welche bei 400° innerhalb 21 Tagen vollständig abgelaufen ist. Elektronenmikroskopische Aufnahmen zeigen die idiomorphe Gestalt der neugebildeten sehr kleinen Muskovitblättchen, so wie es bereits vorher (Winkler, 1957, Abb. 3) abgebildet worden ist; ausserdem wurden röntgenographisch alle für den 2M-Muskovit charakteristischen Linien beobachtet, die beim Illit z.T. nicht vorhanden oder diffus waren. Die Gegenwart von NaCl verschiebt die Temperatur der Reaktion nicht.

Bei den beiden NaCl-führenden Tonen wird jedoch jene Reaktion von einer zweiten Reaktion, bei der 12–14 Gew-% Plagioklas gebildet werden, überlagert. Hier wird das Natrium des NaCl für die Bildung von Albit-Komponente herangezogen, wobei 1,5% NaCl verbraucht werden und 1% HCl entsteht. Der Nachweis von HCl gelang, indem die verschweisste Probe nach dem Versuch in einem Destillierkölbchen unter H_2O mit einer Nadel geöffnet und nach Destillation HCl festgestellt wurde. Die für die Bildung von Albit-Komponente notwendige Menge von Al_2O_3 und SiO_2 entstammt dem etwas unterhalb 400°C abgebauten Kaolinit und dem im Mineralgemenge reichlich vorhandenen Quarz.

Röntgenographisch wurde festgestellt, dass bei den Reaktionen um 400°C in den beiden Versuchsreihen mit verschieden grossem Zusatz von NaCl jeweils die gleiche Menge von 1,5% NaCl verbraucht worden ist. Diese NaCl-Menge entspricht 0,8% Na_2O, die zusammen mit den 0,4% Na_2O der Analyse des Ausgangstons in maximal 10 Gew-% Albit enthalten sind. Beobachtet wurde jedoch eine Plagioklasmenge von 12–14%, die durch eine zusätzliche Anorthitkomponente zu erklären ist. Es können sich aus dem CaO-Gehalt der Analyse (abzüglich der für Apatit benötigten Menge) maximal 5% Anorthitkomponente bilden. Rechnerisch ergibt sich demnach eine maximale Plagioklasmenge von 15%, die kaum von der gemessenen Menge abweicht.

Die in den NaCl-führenden Tonen etwas unterhalb 400°C und bei 2000° atm H_2O-Druck ablaufende Reaktion kann also folgendermassen zusammengefasst werden:

$$\text{Kaolinit} + \text{Quarz} + \text{NaCl} + H_2O + \text{CaO} \rightarrow \text{Albit–Anorthit} + \text{HCl} + H_2O$$

Diese Reaktion läuft nur dann ab, wenn eine relativ geringe Menge von Kaolinit und NaCl zur Verfügung stehen. Bei grösseren Mengen bildet sich in der Reaktion mehr HCl, der pH-Wert wird zu sauer, und statt Albit bildet sich Paragonit. Dies wird in einer späteren Mitteilung ausführlicher belegt werden.

Bei den Versuchsreihen mit 4,8 bzw. 1,8% NaCl ist die für die Bildung von Plagioklas benötigte Quarzmenge fast gleich derjenigen Quarzmenge, die beim Illitzerfall frei wird. Da beide Reaktionen bei gleicher Temperatur ablaufen, ist in den Abb. 1 und 2 unterhalb und oberhalb von 400°C eine gleichbleibende Quarzmenge vorhanden.

Biotit- und Cordieritbildung

Von 400°C bis etwa 550°C ist die Mineralassoziation Muskovit + Chlorit + Plagioklas + Quarz stabil, aber bei etwa 550°C setzt die folgende bereits bei NaCl-freien Illit–Quarz–Tonen erkannte Reaktion ein:

$$\text{Chlorit} + \text{Muskovit} \rightarrow \text{Biotit} + \text{Cordierit} + H_2O$$

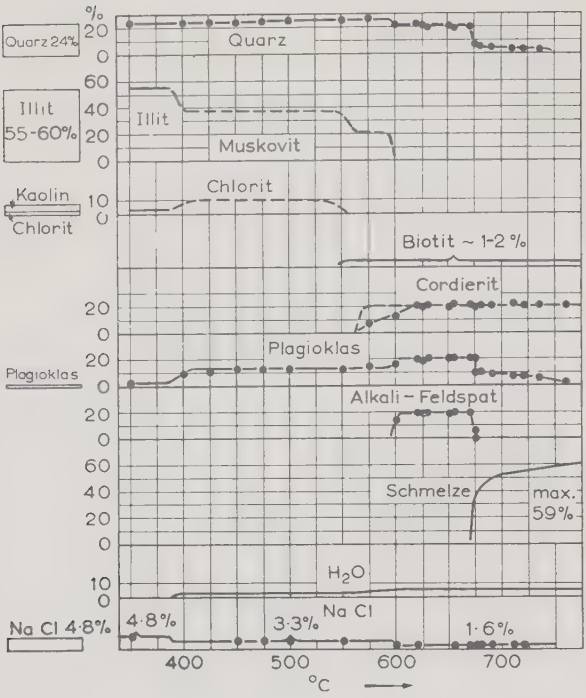

Abb. 1. Mineralumwandlungen bei der Metamorphose des Illit–Quarz-Tons mit Zusatz von 5% NaCl unter 2000 atm H_2O-Druck. Nicht dargestellt worden sind etwa 10 Gew-% und zwar: Organische Substanz (3%), die bis etwa 600 C erhalten zu bleiben scheint; Hämatit–Ilmenit–Mischkristalle (max. 5%); Spuren von Apatit. Ausserdem ist HCl (max. 2%), welches sich bei den Reaktionen bildet, nicht dargestellt.

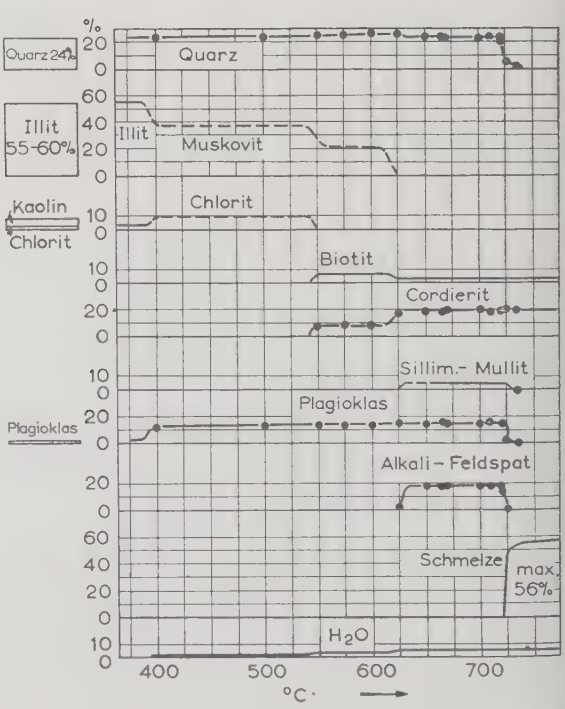

Abb. 2. Mineralumwandlungen bei der Metamorphose des Illit–Quarz-Tons mit Zusatz von 1,8% NaCl unter 2000 atm H_2O-Druck. Siehe ausserdem Anmerkung unter Abb. 1.

Nur ein Teil der in unseren Versuchen vorhandenen Muskovitmenge wird für die Reaktion benötigt, so dass neben Biotit und Cordierit auch Muskovit, Quarz und der vorher bereits gebildete Plagioklas als Mineralassoziation zwischen 550°C bis 600–620°C vorliegt. Die Reaktionstemperatur ist bei Illit–Tonen ohne und mit NaCl praktisch gleich, aber das Mengenverhältnis Cordierit zu Biotit ist unterschiedlich. Ohne NaCl und mit 1,8% NaCl beträgt es fast 1, während es bei der Metamorphose des Tons mit 4,8% NaCl wesentlich grösser, etwa 10 ist. Es ist noch nicht klar, wodurch die Interrelation Cordierit–Biotit kontrolliert wird. Wenn viel Cordierit und wenig Biotit gebildet werden, dann wird sehr wenig Quarz verbraucht und K_2O-Komponente wird frei, die erst bei 50°C bis 70°C höherer Temperatur in eine Phase (Alkalifeldspat) eingebaut wird. Wenn dagegen viel Biotit und wenig Cordierit gebildet werden, dann werden etwas SiO_2 und Al_2O_3 frei. Bei den Versuchen mit dem 1,8 prozentigen NaCl-Ton wird relativ wenig Cordierit bei 550°C gebildet, wobei eine geringe Erhöhung der Quarzmenge um etwa 2% nachgewiesen werden konnte. (Die Änderung ist so gering, dass sie in Abb. 2 kaum erkannt werden kann.) Bei dem in diesem Fall vorliegenden Mengenverhältnis von Cordierit zu Biotit wird noch kein Al_2O_3 frei.

Im Ton mit 4,8% NaCl bildet sich bei 550° nur sehr wenig Biotit (etwa 1–2%); die Cordieritbildung erfolgt erst 10–20° höher, und die bei dieser Temperatur röntgenographisch nachweisbare Menge ist geringer als man erwarten sollte; erst bei 620° wird die maximale Menge nachgewiesen. Wir vermuten, dass bei 550°C noch alle Cordieritkristalle in Sub-X-Ray-Grösse vorliegen und dass selbst bei 600°C ein Teil der Kristalle diese Grössenordnung noch nicht überschritten hat, sondern erst bei etwa 615°C. Dies ist in Abb. 1 durch den strichlierten Teil der Mengenkurve des Cordierits angedeutet worden.

Durch den Abbau des Chlorits und die Bildung von Cordierit ist bei etwa 550°C die Amphibolit-Fazies erreicht. Diese untere Temperaturgrenze der Amphibolit-Fazies (bei 2000 atm H_2O-Druck) ist für das Ausgangsgestein von Illit–Quarz–Tonen ohne und mit NaCl bei der gleichen Temperatur von 550°C bestimmt worden, während sie für Kaolinit–Illit–Quarz–Tone etwas niedriger bei 525° liegt (siehe Winkler, 1957, S. 68). Kennzeichnend für diese Fazies ist unter anderem, dass noch kein K-Feldspat vorliegt, und für den hochtemperierten Teil dieser Fazies, dass, wenn K-Feldspat anwesend ist, auch Muskovit auftritt. Bei der hydrothermalen Metamorphose des hier untersuchten Illit-Quarz–Tons *ohne* Zusatz von NaCl (Ton C in Winkler, 1957) trat bei 620° erstmals K-Feldspat auf, aber bis 665° war Muskovit damit vergesellschaftet, so dass die Obergrenze der Amphibolit-Fazies bei 665° gezogen werden konnte. Die gleiche Temperatur ergab sich auch aus Versuchen mit anderen kalkfreien Tonen ohne NaCl-Zusatz. Die jetzigen Experimente mit NaCl-führenden Tonen zeigen jedoch, dass bei diesen Ausgangsgesteinen die Obergrenze der Amphibolit-Fazies etwas tiefer liegt, nämlich bei 620° bzw. 600°C.

Abbau des Muskovits und Bildung von Feldspat

Bei der Metamorphose des Blauen Tons von Heppenheim, dem kein NaCl zugesetzt worden ist, ist Muskovit neben anderen Phasen bis 665°C beständig. Von 625°C bis 665°C liegt K-Feldspat neben Muskovit vor; denn bei 625°C ist nur ein Teil des Muskovits für die Bildung von K-Feldspat verbraucht worden.

Wenn der Ton jedoch NaCl enthält, dann ist beim Auftreten von K-Feldspat (genauer gesagt von Alkalifeldspat) die gesamte Muskovitmenge abgebaut. Beim Ton mit 1,8% NaCl beträgt jene Temperatur 620°C, und beim Ton mit 4,8% NaCl liegt sie sogar etwas unterhalb 600°C. Bei diesen Temperaturen und darüber laufen komplexe Reaktionen ab, die man in folgende Einzelreaktionen unterteilen kann:

$$\text{Muskovit} \rightarrow \text{K-Feldspat} + H_2O + Al_2O_3 \qquad (1)$$

Wenn genügend Na zur Bildung von Albit-Komponente zur Verfügung steht dann (2a), anderenfalls (2b):

$$Al_2O_3\,[\text{aus 1}] + \text{Quarz} + \text{NaCl} + H_2O \rightarrow \text{Albit-Komponente} + \text{HCl} \qquad (2a)$$

$$Al_2O_3\,[\text{aus 1}] + \text{Quarz} \rightarrow \text{Sillimanit–Mullit} \qquad (2b)$$

$$\text{Muskovit} + \text{Biotit} + \text{Quarz} \rightarrow \text{Cordierit} + \text{K-Feldspat} + H_2O \qquad (3)$$

Im Falle des Tons mit 4,8% NaCl liegt die Kombination (1) + (2a) vor; denn es werden bei und oberhalb 600°C etwa 19 Gew-% Alkalifeldspat der Zusammensetzung Ab 18, Or 82 und ausserdem eine Erhöhung der Plagioklasmenge von etwa 13 auf 20% ermittelt, während Muskovit vollständig abgebaut und ca. 5% Quarz verbraucht worden sind. Nach dieser Reaktion haben sich insgesamt 2 Gew-% HCl gebildet, und ferner ist (fast) das gesamte als Hydroxyl gebundene H_2O von 5% freigeworden. Wenn der Plagioklas oberhalb 600°C homogen ist (was wohl zutrifft), dann enthält er etwas mehr Ab-Komponente als unterhalb 600°C; rechnerisch Ab 74 gegenüber Ab 67. Für die bei 600°C erfolgte Bildung der Ab-Komponente, die im Alkalifeldspat und im Plagioklas enthalten ist, sind 1,7% NaCl verbraucht worden. Die gesamte Reaktion ist also folgende:

$$\text{Muskovit} + \text{Quarz} + \text{NaCl} + H_2O \rightarrow$$
$$\text{Alkalifeldspat} + \text{Ab-Komponente im Plagioklas} + \text{HCl} + H_2O \qquad (4)$$

Bei der Reaktion um 400°C waren bereits 1,5% NaCl verbraucht worden, für die Reaktion bei 600°C werden nochmals 1,7% NaCl benötigt, so dass insgesamt, 3,2% NaCl von den 4,8% des Ausgangstons in Reaktionen umgesetzt worden sind. Die maximal verbrauchte NaCl-Menge ist 3,2%, die restlichen 1,6% NaCl werden in allen Proben oberhalb 600°C neben den anderen Phasen röntgenographisch nachgewiesen. Zum vollen Ablauf der Reaktion (4) sind also nicht mehr als etwa 3% NaCl nötig. Die Phasenbildungen bei Gegenwart einer geringeren NaCl-Menge erkennen wir aus den anderen Versuchen.

Im Falle der Metamorphose des Tons mit nur 1,8% NaCl war nicht genügend Na vorhanden, um die ganze Menge des beim Abbau des Muskovits freiwerdenden Al in der Albit-Komponente zu binden. Nur 0,3% NaCl standen bei 600° noch zur Verfügung, so dass nur 1,4% Albit-Komponente gebildet werden konnten, die im Alkalifeldspat stecken. Es sind 18 Gew-% Alkalifeldspat der Zusammensetzung Ab 8–9, Or 92–91 gebildet worden. Eine merkliche Zunahme der Plagioklasmenge erfolgte nicht, weil kein NaCl mehr zur Verfügung stand; ab 600°C

war also die gesamte NaCl-Menge verbraucht. Das bei der Reaktion übriggebliebene Al_2O_3 hat dann mit Quarz nach (2b) etwas Sillimanit–Mullit gebildet; die Menge ist so gering, dass sie nur mikroskopisch, nicht röntgenographisch bestimmt werden konnte. Eine grössere Menge von Sillimanit–Mullit hat sich natürlich bei der Metamorphose des NaCl-freien Tones gebildet, weil bei den Reaktionen sich kaum eine Albit-Komponente bilden konnte und daher mehr Al für die Bildung von Sillimanit zur Verfügung stand. (Vergleiche Abb. 2 mit Abb. 5 in Winkler, 1957.) Bei der Metamorphose des Tons ohne und mit 1,8% NaCl überlagert sich den Reaktionen (1), (2a) und (2b) noch die Reaktion (3); denn bei 620° (beim Ton mit 1,8% NaCl) und bei 660°C (beim Ton ohne NaCl) wird auch die Biotitmenge deutlich vermindert zu Gunsten einer Bildung von Cordierit. Für den Ton mit 1,8% NaCl ergibt sich also bei 620°C der Ablauf folgender Reaktion:

$$\text{Muskovit} + \text{Biotit} + \text{Quarz} + \text{NaCl} + H_2O \rightarrow$$
$$\text{Alkalifeldspat} + \text{Cordierit} + \text{Sillimanit} + \text{HCl} + H_2O \qquad (5)$$

Muskovit und die 1,8% NaCl sind völlig verbraucht worden. Quarz hat nur um etwa 2% abgenommen und nur Reste von Biotit (ca. 2%) sind noch vorhanden; andererseits sind 18% Alkalifeldspat und wenige Prozente Sillimanit–Mullit gebildet worden, und die Menge des Cordierits hat sich von 8% (unterhalb 600°) auf 20% erhöht. Nach Ablauf dieser Reaktion ist ausserdem (fast) das gesamte Hydroxyl der Minerale des Ausgangstons als 5% H_2O freigeworden und ferner haben sich insgesamt 1,1% HCl gebildet.

Verteilung der Ab-*Komponente auf die Feldspäte*

Die Versuche ohne und mit NaCl zeigen sehr deutlich an der Lage der $(20\bar{1})$-Interferenz, dass der Alkalifeldspat umso mehr Ab-Komponente enthält, je reicher an Na der Ausgangston ist. Ab 600°C bzw. 625°C tritt Alkalifeldspat zusammen mit Plagioklas auf, der mit steigendem NaCl-Gehalt des Ausgangstons ebenfalls reicher an Ab-Komponente ist.

Um zu prüfen, ob in den Feldspäten, die bei der aufsteigenden Metamorphose ab etwa 600°C nebeneinander auftreten, die Verteilung der Ab-Komponente auf Alkalifeldspat und Plagioklas sich im Gleichgewicht befindet, wurden folgende Versuche angestellt: die Proben wurden unter 2000 atm H_2O-Druck 7 Tage lang bei so hoher Temperatur gehalten, dass Feldspäte und Quarz eine anatektische Schmelze bildeten (siehe S. 103ff.); ohne Unterbrechung des Versuchs wurde dann eine tiefere Temperatur eingestellt, bei der nach den Ergebnissen der aufsteigenden Metamorphose keine Schmelze sondern Plagioklas und Alkalifeldspat gemeinsam vorkommen. Nachdem während 21 Tagen die Schmelze wieder vollständig kristallisiert war, waren Menge und Zusammensetzung der Phasen identisch mit denjenigen, die sich bei aufsteigender Metamorphose gebildet hatten. Dadurch ist nachgewiesen, dass speziell die Zusammensetzung des Alkalifeldspats, so wie sie bei der aufsteigenden Metamorphose ermittelt wurde, sich im Gleichgewicht befindet. Der Alkalifeldspat ist homogen; denn die Kristalle, welche aus der anatektischen Schmelze im Falle der 5-prozentigen NaCl-Zugabe bei 670°, 650° und selbst bei 620°C (im Falle 1,8-prozentiger NaCl-Zugabe bei 700°, 665° und

650°C) kristallisieren, haben stets dieselbe Zusammensetzung, so dass also keine Entmischung auftritt. Dies ist bei den vorliegenden Or-reichen Zusammensetzungen auch mit den Arbeiten von Bowen und Tuttle (1950) und von Yoder, Stewart und Smith (1957) in Übereinstimmung. Die Ab-Komponente wurde aus der Lage der $(20\bar{1})$-Interferenz an Hand des von Bowen und Tuttle (1950) abgebildeten Diagramms ermittelt;* Die Zusammensetzung des Plagioklases wurde (siehe S. 94) aus dem Na_2O der Analyse, abzüglich des im Alkalifeldspat gebundenen Na_2O, und aus dem CaO der Analyse, abzüglich des im Apatit gebundenen CaO, berechnet. Die prozentualen Mengen der nebeneinander auftretenden Feldspäte sind in Tab. 2 in Abhängigkeit vom Na-Gehalt der Ausgangstone angegeben. Besonders betont sei, dass bei gleicher Ausgangszusammensetzung die Verteilung der Ab-Komponente auf die Feldspäte in dem untersuchten Temperaturbereich von etwa 50°–70° *unverändert* ist. Der Anteil der Ab-Komponente des Alkalifeldspats mit 2,5% Ab ergab sich als Mittelwert dreier verschiedener Proben, die übrigen Zusammensetzungen mit 8,5 bzw. 18% Ab wurden als Mittelwert von jeweils 10 verschiedenen Proben erhalten; die in Tab. 2 angegebenen geringen Schwankungen von z.B. $\pm$ 1% Ab liegen innerhalb der Messgenauigkeit.

Tab. 2. Albit-Komponente im Alkalifeldspat und in dem damit vergesellschafteten Plagioklas

Ausgangsgestein	Albit-Komponente Gew-%, (bzw. Mol-%) im Alkalifeldspat	im Plagioklas	Temperatur (°C)	Na_2O Gew-%, (bzw. Mol-%)	k nach Barth
Ton ohne NaCl	2,5 $\pm$ 1 (2,5)	41 (42)	670, 675, 700	0,43 (0,42)	0,06 $\pm$ 0,02
Ton mit 1,8% NaCl	8,5 $\pm$ 1,5 (8,5)	67 (68)	650, 670, 700, 710, 720	1,36 (1,32)	0,13 $\pm$ 0,02
Ton mit 4,8% NaCl (nur 3,2% NaCl sind verbraucht worden)	18 $\pm$ 1 (19)	74 (75)	620, 630, 650 670	2,11 (2,07)	0,25 $\pm$ 0,02

Aus Tab. 2 sieht man, dass mit zunehmendem prozentualen Gehalt des Tons an Na_2O sowohl Alkalifeldspat als Plagioklas reicher an Ab werden, was zu erwarten ist. Barth (1956) hat nun das Nernst'sche Verteilungsgesetz auf die Feldspäte angewendet. Wenn dieses gültig wäre, dann müsste im Gleichgewicht die Ab-Komponente sich im Alkalifeldspat und im Plagioklas derart verteilt haben, dass das Verhältnis k = Mol-% Ab im Alkalifeldspat zu Mol-% Ab im Plagioklas konstant ist, wenn Druck und Temperatur konstant sind. Die Konstante ist "unabhängig von der Gesamtmenge des zur Verteilung gelangenden Stoffes (Albit) bzw. von der Menge des ersten und zweiten Lösungsmittels (Anorthit

* Für die genaue Messung des Glanzwinkels diente als innerer Standard die $(10\bar{1}0)$—Interferenz des in den Proben vorhandenen Quarzes. Verwendet wurden Guinier–Kamera (114,6 mm ϕ) und Zählrohr-Goniometer.

und K-Feldspat), welches für den Versuch benützt wird."* Dies gilt, so lange die Konzentrationen von Ab in den Feldspäten gering sind.

Da in unseren Versuchen (durch hydrothermales Auskristallisieren der anatektischen Schmelzen, was bei jeweils gleicher chemischer Zusammensetzung zum gleichen Ergebnis wie bei der aufsteigenden Metamorphose führte) Plagioklas und Alkalifeldspat bei gleicher Temperatur von z.B. 670°C und gleichem Druck von 2000 atm im Gleichgewicht kristallisiert sind, sollte—bei Gültigkeit des

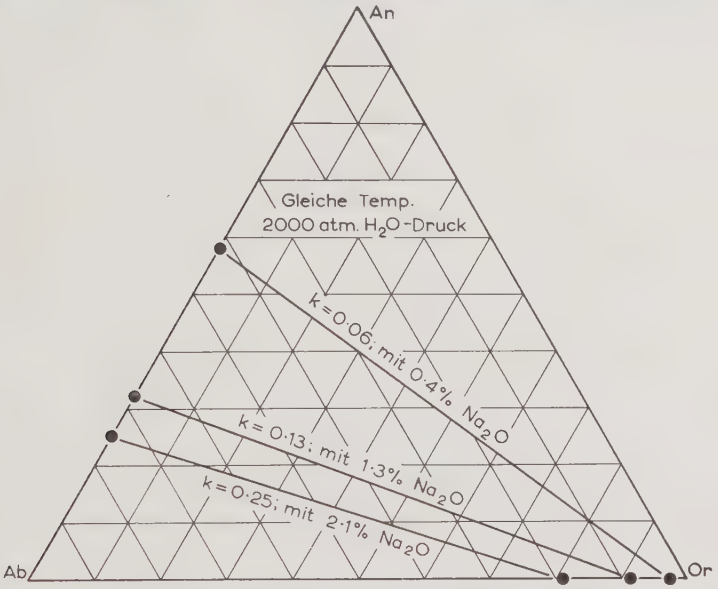

Abb. 3. Zusammensetzung der koexistierenden Plagioklase und Alkalifeldspäte bei gleicher Temperatur und 2000 atm H_2O-Druck. Die beiden jeweils zusammen vorkommenden Zusammensetzungen sind durch eine Gerade verbunden. Die jeweiligen Na_2O-Mengen, die bei der Bildung der Feldspäte verbraucht worden sind, sind angegeben. Ausserdem ist das k-Verhältnis, nämlich Mol-% Ab im Alkalifeldspat zu Mol-% Ab im Plagioklas (nach Barth) angeführt. k ist also nicht konstant.

Verteilungsgesetzes—ein gleiches k-Verhältnis vorliegen, unabhängig von dem prozentualen Na_2O-Gehalt der Ausgangsgesteine. Tab. 2 und Abb. 3 zeigen für die experimentellen Metamorphite, die sich chemisch allein durch ihren Na-Gehalt unterscheiden, die koexistierenden Feldspatphasen. Der Verteilungsquotient k ist keineswegs konstant sondern trotz gleicher Temperatur- und Druckbedingungen sehr unterschiedlich, so dass das Verteilungsgesetz hier nicht anwendbar ist. Der Verteilungsquotient ist z.B. im Bereich von 650–720°C, also in einem Temperaturbereich von 70°C, auch nicht von der Temperatur abhängig, vielmehr hängt er in *linearer* Weise von der prozentualen Na_2O-Menge ab (Abb. 4), wobei in unseren drei Gesteinen das Verhältnis K_2O/CaO gleich und die jeweiligen Mengen von K_2O und CaO fast gleich sind; denn unserem Ausgangston wurden ja nur jeweils verschiedene Mengen an NaCl zugesetzt.

Unsere Versuche sprechen also dafür, dass die Zusammensetzungen der

* K. Kuhn, *Physikalische Chemie*, Heidelberg 1948, S. 153.

vergesellschafteten Feldspäte durch die chemische Zusammensetzung des Magmas bzw. des Gesteins bedingt sind, was auch von Niggli (1941) vermutet wurde.

Barth (1956) räumt zwar auch der chemischen Zusammensetzung einen gewissen Einfluss auf die Grösse des Verteilungsquotienten ein, aber "the ratio of distribution of soda between alkalifeldspar and plagioclases is in its first approximation governed by the temperature." Er meint daher, dass "for practical work an average curve (seihe Abb. 9) can be constructed giving temperature indications of the greatest value for the study of the thermal history of rocks." Unsere experimentellen Ergebnisse bestätigen die Barth'schen Vorstellungen

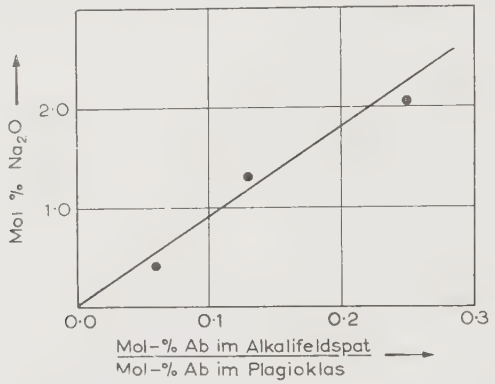

Abb. 4. Lineare Abhängigkeit des Verhältnisses Mol-% Ab im Alkalifeldspat zu Mol-% Ab im Plagioklas von der Na_2O-Menge (Mol-%), die für die Feldspatbildung verbraucht worden ist.

leider nicht; denn wenn man die k-Werte für die vergesellschafteten Feldspäte $Or_{81}Ab_{19}/An_{25}Ab_{75}$ mit $k = 0{,}25$ bzw. $Or_{91}Ab_9/An_{32}Ab_{68}$ mit $k = 0{,}13$ in Abb. 9 von Barth einträgt, dann betragen die Abweichungen von der Kurve 100–150° für $k = 0{,}25$ und sogar 230°–300°C für $k = 0{,}13$. Ausserdem sei noch einmal darauf hingewiesen, dass über dem untersuchten Temperaturbereich von 50–70°C *keine* Änderung der Zusammensetzung des Alkalifeldspats erfolgt war, so dass die sehr temperaturempfindliche Barth'sche Kurve schon allein aus diesem Grunde nicht mit den experimentellen Ergebnissen im Einklang steht. Ferner sei erwähnt, dass sich aus den neuen Untersuchungen von Yoder, Stewart und Smith (1957) im Vergleich mit den Ergebnissen von Bowen und Tuttle (1950) eine beträchtliche Druckabhängigkeit des Verteilungsverhältnisses ergibt, die nicht vernachlässigt werden darf.

Bildung von HCl, H_2S *oder* Na_2S

Bei der Metamorphose von NaCl-führenden Tonen entsteht HCl. Diese Tatsache sei besonders betont, weil sie petrogenetisch, insbesondere für hydrothermale Erzbildungen wichtig sein dürfte. Bei der hydrothermalen Metamorphose der beiden Tone mit 1,8 und mit 4,8% NaCl hat sich bei 400°C 1% HCl gebildet; bei 600°C sind es insgesamt 1,1% HCl im Falle des Tons mit 1,8% NaCl und 2% HCl im Falle des Tons mit 4.8% NaCl. Im letzteren Falle sind nur 3,2%

NaCl in Reaktionen verbraucht worden; mit anderen Worten, die bei der Metamorphose bei 600°C gebildete Menge an HCl beträgt ebenfalls 2%, wenn nur etwa 3% NaCl in Tom als Porenlösung vorhanden sind.

Im Ausgangston sind Spuren von FeS_2 vorhanden, die entsprechend den 0,13% S der chemischen Analyse 0,24 Gew-% betragen. Bei dem NaCl-freien Ton wurde nun bei allen Temperaturen die Bildung von H_2S festgestellt; rechnerisch sind es etwa 0,14%. Bei den NaCl-führenden Tonen bildete sich kein H_2S sondern ab 575°C ist auf den Proben ein gelber Anflug von Na_2S (0,32 Gew-%) beobachtet worden.

Bildung anatektischer granitischer Schmelzen

Verschiedene Tone und auch der hier untersuchte Ton ohne Zusatz von NaCl bilden oberhalb etwa 720°C unter 2000 atm H_2O-Druck eine anatektische Schmelze

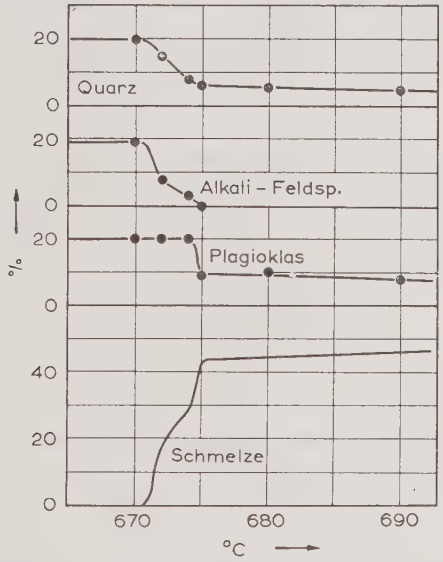

Abb. 5. Detailierter Ausschnitt aus Abb. 1, welcher die schrittweise Bildung der anatektischen Schmelzen zeigt.

von leukogranitischer Zusammensetzung (Winkler, 1957). Die Bildung und Zusammensetzung der anatektischen Schmelzen, die bei der Ultrametamorphose der Tone mit NaCl-Zusatz entstehen, seien nun dargestellt.

Aus dem Illit–Quarz–Ton mit 4,8% NaCl ist bei 60°C die Mineralassoziation Alkalifeldspat (19 Gew-%), Oligoklas (20%), Cordierit (20%), Quarz (20%), Biotit (etwa 1–2%), wenige Prozente von Hämatit–Ilmenit-Mischkristallen und Spuren von Apatit gebildet worden; freigeworden sind 5% H_2O, 2% HCl, 3% organische Substanz dürften sich verflüchtigt haben, und ein Rest von 1,6% NaCl ist in Reaktionen nicht verbraucht worden. Diese Mineralvergesellschaftung eines Cordierit–Gneises ist bis 670°C stabil, unmittelbar oberhalb 670°C beginnt sich eine Teilschmelze zu bilden. Durch vier Versuche zwischen 670° und 675°C konnte die schrittweise Bildung der Schmelze erkannt werden, siehe Abb. 5. Die

angegebenen Temperaturen sind absolut betrachtet nur auf etwa ±5° genau, aber trotzdem konnten die relativen Temperaturen der Schmelzschritte wesentlich genauer ermittelt werden.

Bei 671°C begann die Schmelzbildung, wobei bis 674°C *nur* Alkalifeldspat (16–17%) und Quarz (12%) in die Schmelze gehen. Bei 674°C hatten sich etwa 28 Gew-% (bezogen auf den Ausgangston bzw. 31% bezogen auf den Cordierit–Gneis) einer Alkalifeldspat–Quarz–Schmelze gebildet, deren Komponenten-Zusammensetzung folgende ist: 42 Qz, 47,5 Or, 10,5 Ab. Diese Zusammensetzung ist leukogranitisch und fast identisch mit den anatektischen Schmelzen, die sich bei der Ultrametamorphose aus NaCl-freien Tonen, jedoch erst oberhalb 700–725°C, bilden. (Vergleiche die Lage des Kreuzes und des mit 1 bezeichneten Kreises in Abb. 6.) Aber bei dem NaCl-führenden Ausgangston stellt diese Schmelzzusammensetzung nicht den Endzustand sondern nur den ersten Schmelzschritt dar; denn unmittelbar oberhalb 674°C gehen 11% des Oligoklases (An 26) zusammen mit 1,5% Quarz und dem Rest von 2–3% Alkalifeldspat in die Schmelze. Insgesamt hat sich bei 675°C eine Schmelzmenge von etwa 44% (bzw. 49%, bezogen auf den Cordierit-Gneis) gebildet, deren Zusammensetzung in Tab. 3 angegeben ist. Mit dieser Zusammensetzung ist der Endzustand fast, aber noch nicht ganz erreicht; denn mit zunehmender Temperatur gehen ab 675°C nur allmählich weitere Quarz- und Oligoklasmengen in die Schmelze (siehe Abb. 5). Erst bei 765°C ist der Endzustand erreicht, bei dem sämtlicher Oligoklas, Alkalifeldspat und Quarz sich in der Schmelze befinden, siehe Abb. 1. (Wenn mehr Quarz im Cordierit–Gneis vorhanden gewesen wäre, dann würde die zusätzliche Menge bei 765°C nicht in die Schmelze gehen.) Die Menge der bei 765°C vorliegenden Schmelze beträgt 59% (bzw. 66%), und ihre Zusammensetzung ist in Tab. 3 angegeben.

Tab. 3. Verhältnis der Komponenten in den Schmelzen in Gew-%

Komponenten	Schmelze bei 674°C	Schmelze bei 675°C	Schmelze bei 765°C
Qz	42	32	34
Or	47,5	36	26,5
Ab	10,5	26	31
An	—	6	8,5
Anteil der Schmelze in Gew-%, bezogen auf den Cordierit-Gneis	31	49	66

Wenn die relativ geringen Mengen der An-Komponente zum Zwecke der graphischen Darstellung der Zusammensetzungen in dem Qz–Or–Ab–System unberücksichtigt bleiben, dann erhält man die folgenden Verhältnisse jener Komponenten, Tab. 4.

Die Werte der Tab. 4 sind in Abb. 6 im Konzentrationsdreieck Qz–Or–Ab eingetragen. Die Kreise mit einer Zahl geben die Schmelzzusammensetzungen an nach dem (1), (2) und nach dem (3) Schmelzschritt bei 674°, 675° und 765°C.

Tab. 4

Komponenten	Schmelze bei 674°C	Schmelze bei 675°C	Schmelze bei 765°C
Qz	42	34	37
Or	47,5	38	29
Ab	10,5	28	34

(Die Dreiecke mit ihren Zahlen beziehen sich auf die Schmelzen, die bei der Ultrametamorphose des Tons mit 1,8% NaCl entstehen.) Die Linie, welche den Quarzraum vom Alkalifeldspatraum trennt, ist die von Tuttle und Bowen (Bowen,

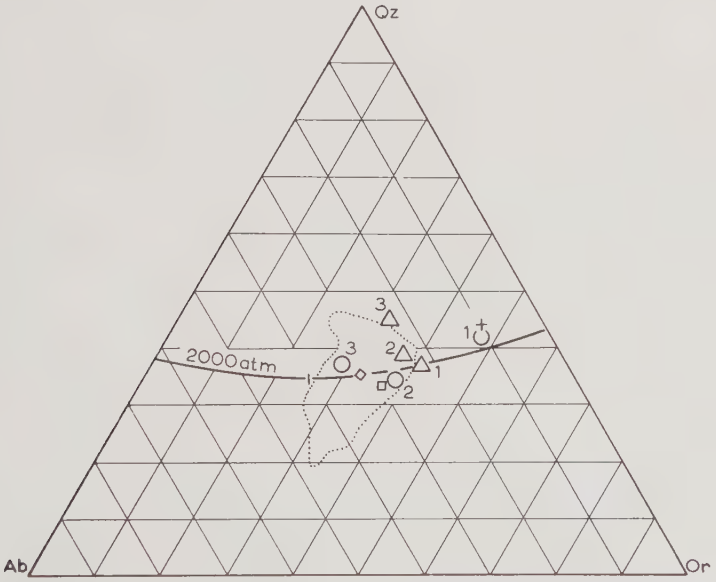

Abb. 6. Darstellung der Komponenten Qz, Ab und Or, der bei der Ultrametamorphose von NaCl-führenden Illit–Quarz–Tonen gebildeten anatektischen Schmelzen.

Die Dreiecke beziehen sich auf den Ausgangston mit 1,8% NaCl; (1) bezeichnet die Zusammensetzung der Schmelze bei 722°C, (2) bei 725°C. (3) bei 745°C.

Die Kreise beziehen sich auf diejenigen Schmelzen, die sich bei der Ultrametamorphose des Tons unter Verbrauch von 3,2% NaCl gebildet haben; (1) gibt die Zusammensetzung bei 674°C, (2) bei 675°C und (3) bei 765°C an. Das Quadrat bezeichnet die mittlere Zusammensetzung von Kalkalkali-Graniten, und das auf der Ecke stehende Quadrat bezeichnet die mittlere Zusammensetzung von Alkali-Graniten (nach Nockolds, 1954). Das Kreuz gibt die mittlere Zusammensetzung der anatektischen Schmelzen verschiedener NaCl-freier Tone an (Winkler, 1957).

1954) für einen H_2O-Druck von 2000 atm bestimmte kotektische Linie; der punktiert, umrandete Bereich gibt nach Bowen den Bereich an, in dem das Verhältnis des normativen Gehalts an Qz, Or und Ab der meisten Granite liegt.

Weiterhin ist noch das Verhältnis jener normativen Minerale für die von Nockolds (1954) berechnete mittlere Zusammensetzung von Kalkalkali–Graniten und von Alkali–Graniten dargestellt.

Man erkennt nun aus Abb. 6 sehr deutlich, dass alle Schmelzen sehr nahe der kotektischen Linie liegen, obgleich sie fast alle einige Prozente An-Komponente enthalten. Während jedoch im reinen System Qz–Or–Ab–H_2O die Phasengrenzlinie sich von der Seite Qz–Or bis zu dem auf ihr eingezeichneten Querstrich um etwa 40°C einsenkt, d.h. die niedrigst schmelzende Zusammensetzung liegt weit von der Qz–Or–Seite entfernt, sind bei Gegenwart von Plagioklas die Verhältnisse gerade umgekehrt. Hier bildet sich, wie die Experimente eindeutig gezeigt haben, bei der niedrigsten Temperatur eine Schmelze aus Quarz und K-reichem Alkalifeldspat, deren Zusammensetzung in der Nähe der Qz–Or–Seite liegt (Kreis 1 in Abb. 6), während erst bei etwas höherer Temperatur die Ab-Komponente stärker vertreten ist, weil dann Oligoklas auch mit in die Schmelze geht (Kreis 2 in Abb. 6).

Petrogenetisch wichtig sind folgende Feststellungen: Es bedarf nur einer ganz geringen Temperaturerhöhung um wenige Grade, damit sich bei Gegenwart von NaCl statt einer leukogranitischen Schmelze (Kreis 1 in Abb. 6) eine granitische Schmelze (Kreis 2 in Abb. 6) bildet. Bei weiterer starker Temperaturerhöhung um 90°C, nämlich von 675° auf 765°C, ändert sich dann die Zusammensetzung nur wenig und sie bleibt granitisch. Kreis 3 in Abb. 6 zeigt die Schmelzzusammensetzung, die bei 765°C und darüber vorliegt. Da in der Natur niemals eine bestimmte Temperatur genau eingestellt wird, müssen auf Grund unserer Experimente leukogranitische Zusammensetzungen wesentlich seltener sein als granitische. Da das auch in der Natur der Fall ist, und granitische Schmelzen bei der Ultrametamorphose NaCl-führender Tone, nicht aber NaCl-freier Tone, entstehen können, ergibt sich ausserdem eine starke Stütze für unsere Ansicht, dass NaCl als Porenlösung von entscheidender petrogenetischer Bedeutung für das Granitproblem ist. Dies ist schon von v. Gaertner (1951) und Nieuwenkamp (1956) vermutet worden.

Dass die Schmelzzusammensetzungen bei 675° und 765°C granitisch sind, sieht man aus der Lage ihrer darstellenden Punkte (Kreise 2 und 3) im punktiert umgrenzten Bereich der Abb. 6 und im Vergleich zur Lage der darstellenden Punkte der mittleren Zusammensetzung von Kalkalkali–Graniten und Alkali–Graniten. Berücksichtigt man nun auch die An-Komponente in den anatektischen Schmelzen, dann sind sie nicht alkaligranitisch sondern kalkalkaligranitisch; letztere sind wiederum in der Natur wesentlich häufiger als erstere. Tab. 5 zeigt den Vergleich zwischen der mittleren Zusammensetzung von Kalkalkaligraniten (Nockolds, 1954) und unseren Schmelzen.

In Tab. 5 sind auch noch aufgeführt die Bereiche der Zusammensetzungen von Eskolas (1956) "idealen" Graniten und "eutektoiden" Graniten, welche unseren anatektischen granitischen Schmelzen gegenübergestellt sind. Ausser denjenigen Schmelzen, die bei der Ultrametamorphose des Tons mit 3,2% NaCl erhalten werden, sind auch diejenigen des Tons mit 1,8% angegeben, welche noch näher besprochen werden.

In den Graniten bestreiten die Komponenten der Tab. 5 im Mittel 93%, der

Rest sind mafische Gemengteile, welche u.a. Mg und Fe enthalten. Bis jetzt konnte noch nicht mit Sicherheit nachgewiesen werden. dass in unseren Schmelzen sich auch jene Elemente gelöst befinden, bzw. dass mafische Minerale aus den anatektischen Schmelzen auskristallisieren. Ihr Nachweis wird wohl nicht leicht sein, da nur geringe Mengen zu erwarten sind.

Tab. 5

Normative Komponenten	Nockolds Mittelwert	Eskolas ideale Granite	Anatektische Schmelzen			Eskolas eutektoide Granite	Anatektische Schmelze
			(1)	(2)	(3)		(4)
Qz	31,5	33,5–34	32	34	35	30–32	34
Or	34,5	40 –37	36	38	34	28–31,5	26,5
Ab	28	21,5–20,5	26	20	22	38–31,5	31
An	6	5 –8,5	6	8	9	4–5	8,5

(1) Bei 675°C aus Ton mit 3,2% NaCl.
(2) Bei 722°C aus Ton mit 1,8% NaCl.
(3) Bei 725°C aus Ton mit 1,8% NaCl.
(4) Bei und oberhalb 765°C aus Ton mit 3,2% NaCl.

Granitische anatektische Schmelzen werden nicht nur bei der Ultrametamorphose des Illit–Quarz–Tons gebildet, wenn 3% NaCl bei der Metamorphose für die Cordierit–Gneis–Bildung verbraucht worden sind, sondern auch wenn nur 1,8% NaCl vorhanden waren. Vor Beginn der Schmelzbildung liegt ebenfalls ein Cordierit–Gneis vor, der aber etwas Sillimanit führt und etwas weniger Plagioklas, dafür aber etwas mehr Quarz enthält, als derjenige Gneis, der sich aus dem Ton mit grösserem NaCl-Gehalt bildet (vergl. Abb. 2 und 1). Alkalifeldspat und Plagioklas sind etwas ärmer an Ab. Dies allein kann nur der Grund dafür sein, dass sich noch nicht bei 671°C sondern erst bei 720°C (wie bei dem Ton ohne NaCl) eine Schmelze zu bilden beginnt. Die erste Teilschmelze ist auch hier, wie bei dem NaCl-reicheren Ausgangston, eine Alkalifeldspat–Quarz–Schmelze, und bei nur ganz geringer Temperaturerhöhung um wenige Grade geht auch Plagioklas zusammen mit weiteren Mengen an Alkalifeldspat und Quarz in die Schmelze. Diese Schmelze nimmt auch, wie beim NaCl-freien Ausgangston, die wenigen Prozente an Sillimanit–Mullit mit auf. Bei 725°C ist schon fast der Endzustand der Schmelzzusammensetzung erreicht, denn von 725°C bis etwa 745°C gehen nur noch die restlichen Quarz- und Plagioklasmengen von jeweils etwa 2% in die Schmelze, Abb. 2. Tab. 6 zeigt die Komponentenzusammensetzung der Schmelzen bei 722°C (kurz nach Beginn der Schmelzbildung), bei 725°C und 745°C, wo der Endzustand erreicht ist. Die gebildeten Schmelzmengen betragen, bezogen auf den Ausgangston (bzw. den Gneis) bei 722°C = 41 (46) %, bei 725°C = 49 (55) % und bei 745°C = 56 (63) %.

In Abb. 6 sind die Schmelz-Zusammensetzungen der Tab. 6 als Dreiecke eingezeichnet, wobei die Zahlen 1, 2 bzw. 3 die Schmelze bei 722°C, 725°C bzw.

Tab. 6

Komponenten	Schmelze bei			Komponenten	Schmelze bei		
	722°C	725°C	745°C		722°C	725°C	745°C
Qz	34	35	41	Qz	37	38,5	45
Or	38	34	29	Or	41	37	32
Ab	20	22	21	Ab	22	24,5	23
An	8	9	9				
Schmelzanteil bezogen auf den Gneis; in Gew-%	46	55	63				

745°C kennzeichnen. Man erkennt aus der Abb., dass auch dann, wenn der Ton nur 1,8% NaCl enthält, granitische Schmelzen gebildet werden. Die Zusammensetzungen bei 722°C und 725°C sind übrigens bezüglich des dargestellten Verhältnisses der Komponenten fast dieselben wie beim "Ideal-Granit" Eskolas (1956), vergl. Tab. 5.

Zusammenfassend ergibt sich also, dass bei der Metamorphose von NaCl-freien Tonen (Illit + Kaolinit + Quarz- und Illit + Quarz–Tone) leukogranitische anatektische Schmelzen bei 700°–725°C unter 2000 atm H_2O-Druck entstehen. Wenn aber NaCl in Illit–Quarz-Tonen vorhanden ist, dann entstehen granitische anatektische Schmelzen. Der Beginn der Schmelzbildung variiert bei 2000 atm H_2O-Druck zwischen 670°C und 720°C und schon bei 675°C bzw. 725°C liegen granitische Schmelzen kalkalkalischen Charakters vor.

Zusammenfassung und petrogenetische Folgerungen

Einem Illit–Quarz–Ton, der beispielhaft für diese weit verbreitete Gruppe von Tonen ist, wurden einige Prozente NaCl zugemischt, weil angenommen werden darf, dass in Porenlösungen vor allem NaCl in Tiefen von einigen Kilometern vorhanden ist. Die Metamorphose und Ultrametamorphose des gleichen, aber NaCl-freien Tones ist bereits mitgeteilt (Winkler, 1957), während diejenige der NaCl-führenden Tone hier dargestellt ist. In dem einen Falle sind 1,8% NaCl in Reaktionen verbraucht worden, in dem anderen sind es maximal 3,2% NaCl. Die erkannten Mineralreaktionen sind in Tab. 7 aufgeführt.

Da nicht die gesamte Menge eines Minerals in einer Reaktion benötigt zu werden braucht, sind folgende Mineralvergesellschaftungen beobachtet worden, Tab. 8.

Zwischen 480°C bis 530°C liegen Chlorit + Muskovit + Plagioklas + Quarz vor, die in der Grünschiefer–Fazies angetroffen werden, aber auch noch in der Albit–Epidot–Amphibolit–Fazies bei der vorliegenden Gesamtzusammensetzung auftreten können. Es kann also nicht entschieden werden, ob bei 550°C die

Tab. 7

	Reagierende Minerale	Temp. (°C)	Reaktionsprodukte + H_2O	Bemerkungen
(1)	Illit	ca. 390	Muskovit + Chlorit + Quarz	Wie beim Ton ohne NaCl, aber Überlagert von (2)
(2)	Kaolinit + Quarz + NaCl + H_2O + CaO		Plagioklas + HCl	
(3)	Chlorit + Muskovit ± Quarz	545–570	Cordierit + Biotit	wie beim Ton ohne NaCl
(4)	Muskovit + Quarz + NaCl + H_2O	600	Alkalifeldspat + Ab im Plagioklas + HCl	beim Ton mit 3% NaCl
(5)	Muskovit + Biotit + Quarz + NaCl + H_2O	620	Alkalifeldspat + Cordierit + Sillimanit + HCl	beim Ton mit 1,8 NaCl, und ohne NaCl, aber dort bei 665°
(6)	Alkalifeldspat + Plagioklas + Quarz	670–720	Schmelze	670° beim Ton mit 3% NaCl 720° beim Ton mit 1,8% NaCl, wie beim Ton ohne NaCl

Tab. 8

Temperaturbereich (°C)	Mineralassoziation	Bemerkung*
390–550	Muskovit + Chlorit + Plagioklas + Quarz	(1), (2), (3); bei (1) ab 525°C Spuren von Biotit
550–610 ± 15	Muskovit + Biotit + Cordierit + Plagioklas + Quarz. Kein Chlorit.	(1), (2), (3)
620–665	Muskovit + Alkalifeldspat + Plagioklas + Cordierit + Biotit + Sillimanit + Quarz	nur (1)
600–670	Alkalifeldspat + Plagioklas + Cordierit + Biotit + Quarz. Kein Muskovit	nur (3)
625–720	Alkalifeldspat + Plagioklas + Cordierit + Biotit + Sillimanit + Quarz. Kein Muskovit	(2); (1) hat erst ab 665°C keinen Muskovit mehr
670	Schmelze + Cordierit + Hämatit–Ilmenit	(3)
720		(1), (2)

* Hier ist der Ausgangston angegeben: (1) bedeutet Ton ohne NaCl;
(2) ist der Ton mit 1,8% NaCl
(3) ist der Ton mit 3,2% NaCl

Obergrenze der Grünschiefer- oder der Albit–Epidot-Amphibolit–Fazies erreicht ist. Die vollständige Abwesenheit von Chlorit bei 550°C spricht aber dafür, dass bei 550°C die Amphibolit–Fazies mit der Mineralvergesellschaftung Cordierit + Biotit + Muskovit + Plagioklas + Quarz erreicht ist. Der Temperaturbereich von 525°–560°C wurde auch aus Untersuchungen an anderen Tonen als Untergrenze der Amphibolitfazies ermittelt (Winkler, 1957, S. 68). Die Temperatur der Obergrenze der Amphibolitfazies ist verschieden: Wenn 3% NaCl vorliegen,

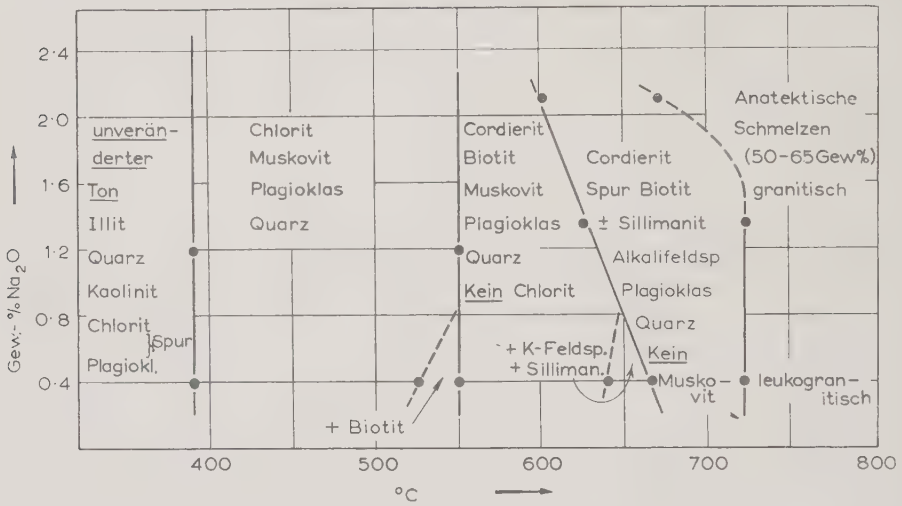

Abb. 7. Temperaturbereich der Mineralassoziationen in Abhängigkeit von der Na_2O-Menge (Gew-%), die in Reaktionen bei der Metamorphose der Ausgangstone verbraucht worden ist. Die Tone unterscheiden sich nur in der Menge des zugesetzen NaCl. Alle Komponenten mit Ausnahme des Na_2O sind konstant.

dann ist sie bereits bei 600°C erreicht, wenn 1,8% NaCl vorliegen bei 625°C und, wenn der Ton kein NaCl enthält, dann liegt die Obergrenze erst bei 665°C, wie bei anderen NaCl-freien Illit-Quarz- und Illit-Kaolinit-Quarz Tonen. Der Ton mit 3% NaCl erreicht also bei 600°C die Pyroxen–Hornfelsfazies (gekennzeichnet durch die Gegenwart von Alkalifeldspat bei Abwesenheit von Muskovit) und gelangt schon bei 670°C in das Gebiet der Ultrametamorphose. Beim Ton mit 1,8% NaCl umfasst die Amphibolit–Fazies den Temperaturbereich von 625° bis 720°C, und wenn kein NaCl vorhanden ist, dann erstreckt sich der Temperaturbereich nur von 665°–720°C.

Die auf Grund der Mineralassoziationen festgelegten Temperaturgrenzen für die Amphibolit–Pyroxen–Hornfels Fazies und für den Beginn der Ultrametamorphose sind (bei gleichem Druck) recht unterschiedlich. Das ist bei verschiedenem Chemismus durchaus zu erwarten, aber unsere Versuche zeigen deutlich, dass jene Unterschiede allein schon auf die unterschiedliche Na-Menge zurückzuführen sind; denn Na ist die einzige chemische Komponente, deren Menge sich bei den beiden NaCl-führenden und dem NaCl-freien Ton ändert. Die Abb. 7 zeigt dies graphisch; als Ordinate ist die Menge des in Silikaten gebundenen Na_2O (in Gew-%) aufgetragen, die Abszisse gibt die Temperaturen an, die bei 2000 atm H_2O-Druck gelten.

Als petrogenetisch besonders wichtiges Ergebnis wurde festgestellt, dass NaCl-führende Illit–Quarz–Tone granitische anatektische Schmelzen bilden, vergl. Abb. 6 und Tab. 5. Die Schmelzbildung beginnt unter 2000 atm H_2O-Druck bereits ab 670°C beim Ton mit 3,2% NaCl und ab 720°C beim Ton mit 1,8% NaCl. Wichtig ist, dass in jedem Falle sich eine granitische Schmelze bildet, unabhängig davon, ob 3,2 oder 1,8% NaCl benötigt worden sind. Wenn kein NaCl vorhanden ist, dann bildet sich zwar auch bei 700°–725°C eine anatektische Schmelze aber von leukogranitischem Charakter. Die granitische Schmelze macht etwa die Hälfte bis Zweidrittel des vor der Schmelzbildung entstandenen Cordierit–Gneises aus, daher dürfte ihre petrogenetische Bedeutung ausser Zweifel stehen. Wenn das Ausgangsgestein ärmer an Mg, Fe ist, dann muss ein noch grösser Teil des Metamorphits verflüssigt werden. Somit sind Vorstellungen wie die Migmatisierung und Granitisation nunmehr experimentell unterbaut, sofern sie ein granitisches Porenmagma, den Ichor Eskolas, als granitisierendes Agenz in Anspruch nehmen. Auch die Palingenese von Graniten ist nun verständlich, denn es dürfte tektonische Vorgänge geben, die ein Abpressen eines erheblichen Teils der granitischen anatektischen Schmelze von dem Kristallbrei ermöglichen. Dass ein derartiger Vorgang nicht immer eine saubere Trennung zwischen den festen und der flüssiger Phase zustande zu bringen braucht, dafür scheinen uns die cordieritführenden Granite des Schwarzwaldes, der Schweiz und an anderen Stellen zu sprechen. Die weite Verbreitung von Illit–Quarz–Tonen und die durch Ultrametamorphose aus ihnen gebildete grosse Menge an granitischen Schmelzen würde wesentlich besser als die fraktionierte Kristallisationsdifferentiation erklären, warum Granit das bei weitem häufigste Tiefengestein ist. Zur Frage der metasomatischen Entstehung von Graniten ohne Beteiligung einer Schmelzphase liegen bis jetzt leider noch keine Experimente vor.

Die Deutsche Forschungsgemeinschaft, Bad Godesberg, hat durch die Bewilligung einer Assistentenstelle (H.v.P.) und durch apparative Leihgaben die Arbeit sehr gefördert, wofür wir ihr unseren verbindlichsten Dank aussprechen. Gedankt sei auch Herrn Feinmechanikermeister Friebertshäuser, der in unserem Institut die Hydrothermalanlage apparativ betreut.

Literatur

Afanas'ev T. P. (1947) Über die chemische Zusammensetzung und zonale Verbreitung des Grundwassers im mittleren Wolga-Gebiet. *Dokl. Akad. Nauk SSSR* **56,** 621.

Barth T. F. W. (1956) Studies on gneiss and granite. *Norsk. Vid. Akad. I. Nat.-Naturv. Klasse* No. 1.

Bowen N. L. (1954) Experiment as an aid to the understanding of the natural world. *Proc. Acad. Nat. Sci. Philad.* **106,** 1.

Bowen N. L. and Tuttle O. F. (1950) The system $NaAlSi_3O_8$ $KAlSi_3O_8$ $-H_2O$. *J. Geol.* **58,** 489.

Eskola P. (1956) Postmagmatic potash metasomatism of granite. *C. R. Soc. géol. Finlande* **29,** 85.

Gaertner von H. R. (1951) Über die Alkali-Quelle der Granitisierung. *Z. Dtsche Geol. Ges.* **103,** 7.

Hedberg H. D. (1936) Gravitational compaction of clays and shales. *Amer. J. Sci.* Ser. 5. **31,** 241.

Nieuwenkamp W. (1956) Géochimie classique et transformiste. *Bull. Soc. géol. Fr.* Ser. 6. **6,** 407.

Niggli P. (1941) Das Problem der Koexistenz der Feldspäte in den Eruptivgesteinen. *Schweiz. Min. Petrogr. Mitt.* **21,** 193.

Nockolds S. R. (1954) Average chemical compositions of some igneous rocks. *Bull. Geol. Soc. Amer.* **66,** 1007.

Winkler H. G. F. (1957) Experimentelle Gesteinsmetamorphose I. Hydrothermale Metamorphose karbonatfreier Tone. *Geochim. et Cosmochim. Acta* **13,** 42.

Yoder H., Stewart D. B. and Smith J. R. (1957) Ternary feldspars. *Annual Report of the Director of the Geophysical Laboratory* 1956–1957, p. 206.

Geochimica et Cosmochimica Acta, 1958, Vol. 15, pp. 113 to 130. Pergamon Press Ltd., London

Equilibrium distribution of dissolved sulphur species in water at 25°C and 1 atm total pressure*

R. M. Garrels† and C. R. Naeser
U.S. Geological Survey, Washington 25, D.C.

(*Received* 12 *May* 1958)

Abstract—The E_h-pH diagrams for the equilibrium concentrations in aqueous solution at 25°C of native sulphur and all the various sulphur-containing ions and acids from which the ions are produced have been constructed for systems having a total sulphur concentration of 0·1 molar. The composite of these diagrams indicates that elemental sulphur, H_2S, HS^- HSO_4^- and $SO_4^=$ are the species that predominate in the environments that might be found in nature. This indication is in agreement with the composition of all sulphur-containing minerals.

Introduction

The importance of sulphur in many fields of geology has long been recognized, but the complexity of its chemistry has retarded understanding of its role in natural processes. A considerable step forward was made in 1950 by Valensi, who calculated fields of stability of the known ionic and molecular species of sulphur in aqueous solution at 25°C and 1 atm total pressure as functions of pH and oxidation potential (E_h). He also discussed at some length the general behaviour of sulphur in solution, with particular attention to the relations between stable and metastable species.

It is of interest to geologists that of the more than thirty ionic and molecular species of sulphur that are of sufficient importance in the laboratory to have permitted determination of their properties in detail, only those few that are familiar in nature are thermodynamically stable in appreciable quantity at room temperature. Valensi's diagram showing major species includes only sulphate ion, bisulphate ion, native sulphur, hydrogen sulphide, bisulphide ion and sulphide ion.

Our chief purpose is to present a series of diagrams showing the distribution of various individual species at equilibrium. We certainly cannot improve on Valensi's discussion of metastable relations, but because so many geologic processes seem to occur near equilibrium it seemed worthwhile to show stable distribution patterns of many species, if only as a guide to their behaviour under more favourable conditions for their existence.

The work is part of a programme being conducted by the U.S. Geological Survey on behalf of the Division of Research of the U.S. Atomic Energy Commission.

Equations and Calculations

The first step in determining stability relations is to write the reactions from one sulphur-bearing species to another in such a way that only water, hydrogen ions and electrons are involved. The reactions are given in Table 1.

* Publication authorized by the Director, U.S. Geological Survey.
† Present address: Dept. Geology, Harvard University, Cambridge, Mass.

Activities as Functions of Oxidation Potential and pH

The relative activities (thermodynamic concentrations) of the various dissolved sulphur species can be expressed as functions of the oxidation potential (E_h) and pH of the system under consideration. By arbitrarily selecting a pair of values for these variables it is possible to calculate the ratio of the activities of any given pair of ions, or the activity of a given ion in equilibrium with a solid (the only solid in the system considered is elemental sulphur). The equations necessary for the calculations are derived from the reactions given in Table 1. In the following discussion no distinction will be made between thermodynamic concentration (activity) and stoichiometric concentration (molality). Instead of writing $a_{s^=}$ or $m_{s^=}$ to indicate activity or molality we will write $[S^=]$ to indicate either or both. An error is thus introduced, but it is small at the concentrations considered ($a = 0{\cdot}05$ m), and is essentially a proportional error throughout. Because of the large range in ratios involved, the difference between a and m does not affect the nature of the diagrams appreciably.

The hydrogen ion dissociation reactions (Group B of Table 1) are said to be E_h-independent, inasmuch as no change in valence state is involved. At equilibrium we can write, for the general case:

$$HA = H^+ + A^-$$

and

$$\frac{[H^+][A^-]}{[HA]} = K$$

where A represents any sulphur-bearing ion.

In logarithmic form:

$$\log \frac{[A^-]}{[HA]} = \log K - \log [H^+]$$

But $$-\log [H^+] = pH$$

therefore $$\log \frac{[A^-]}{[HA]} = \log K + pH$$

Thus the ratios of the sulphur species at equilibrium can be expressed in terms of a constant K and the pH. K-values were obtained directly from Latimer (1952), or calculated from the relation:

$$\Delta F_r^\circ = -RT \ln K$$

where ΔF_r° is the standard free energy of the reaction, R is the gas constant, and T the absolute temperature.

Using reaction (12) of Table 1 as a specific example:

$$H_2S = H^+ + HS^-; \quad \Delta F_r^\circ = 9{\cdot}55 \text{ kilocalories (kcal)}$$

$$\Delta F_r^\circ = -RT \ln K$$

which at 25°C reduces to:

$$\Delta F_r^\circ = -1{\cdot}364 \log K$$

then:

$$9{\cdot}55 = -1{\cdot}364 \log K$$

$$\log K = -7{\cdot}00$$

and

$$\log \frac{[HS^-]}{[H_2S]} = -7 + pH$$

Just as these reactions involve only H^+, others can be expressed in terms of constants and E_h. For example, where

$$aA^{=} = bB^- + ne^-$$

then, since $E = E^\circ + \frac{RT}{nf} \ln \frac{[B^-]^b}{[A^{=}]^a}$, and $E_h = -E$

$$E_h = -E^\circ + \frac{RT}{nf} \ln \frac{[B^-]^b}{[A^{=}]^a}$$

where E° is a constant obtained directly from LATIMER's compilation or from the relation $E^\circ = -\Delta F_r^\circ / nf$; R and T are defined as before; n is the number of electrons involved in the transfer; and f is the Faraday. At 25°C the term:

$$\frac{RT}{nf} \ln \frac{[B^-]^b}{[A^{=}]^a} \quad \text{reduces to} \quad \frac{0{\cdot}06}{n} \log \frac{[B^-]^b}{[A^{=}]^a}$$

As a specific example we can write for reaction (8) of Table 1:

$$2SO_3^{=} = S_2O_6^{=} + 2e$$

$$E_h = -E^\circ + \frac{0{\cdot}06}{2} \log \frac{[S_2O_6^{=}]}{[SO_3^{=}]^2}$$

$$E_h = 0{\cdot}026 + 0{\cdot}03 \log \frac{[S_2O_6^{=}]}{[SO_3^{=}]^2}$$

Still other reactions are dependent both on E_h and pH, and are handled similarly. For reaction (7) of Table 1:

$$S_2O_4^{=} + 2H_2O = 2SO_3^{=} + 4H^+ + 2e$$

$$E_h = -E^\circ + \frac{0{\cdot}06}{2} \log \frac{[SO_3^{=}]^2[H^+]^4}{[S_2O_4^{=}][H_2O]^2}$$

In these dilute solutions (total molality of sulphur species = 0·1), the activity of water is very nearly unity; as before $-$pH can be substituted for log $[H^+]$, and a numerical value for E°, so:

$$E_h = 0{\cdot}535 + 0{\cdot}03 \log \frac{[SO_3^{=}]^2}{[S_2O_4^{=}]} - 0{\cdot}12 \text{ pH}$$

The complete list of equations from which the molalities of the various species

were calculated as functions of E_h and pH are given in Table 2. The equations in Table 2 are numbered to correspond with the reactions listed in Table 1.

Table 1. Reactions among sulphur species

A. Oxidation reactions

Reaction	Formal change in oxidation state of sulphur
(1) $H_2S = S^\circ + 2H^+ + 2e$	$-2 \leftrightharpoons 0$
(2) $S^= + S^= = S_2^= + 2e$	$-2 \leftrightharpoons -1$
(3) $S_2^= + S^= = S_3^= + 2e$	$-1 + -2 \leftrightharpoons -\frac{2}{3}$
(4) $2S^\circ + 3H_2O = S_2O_3^= + 6H^+ + 4e$	$0 \leftrightharpoons 2$
(5) $2S_2O_3^= = S_4O_6^= + 2e$	$2 \leftrightharpoons 2\frac{1}{2}$
(6) $S_4O_6^= + 2H_2O = 2S_2O_4^= + 4H^+ + 2e$	$2\frac{1}{2} \leftrightharpoons 3$
(7) $S_2O_4^= + 2H_2O = 2SO_3^= + 4H^+ + 2e$	$3 \leftrightharpoons 4$
(8) $2SO_3^= = S_2O_6^= + 2e$	$4 \leftrightharpoons 5$
(9) $S_2O_6^= + 2H_2O = 2SO_4^= + 4H^+ + 2e$	$5 \leftrightharpoons 6$
(10) $S^= + 4H_2O = SO_4^= + 8H^+ + 8e$	$-2 \leftrightharpoons 6$
(11) $S_2O_3^= + 5H_2O = 2SO_4^= + 10H^+ + 8e$	$+2 \leftrightharpoons 6$

B. Hydrogen ion dissociation reactions

Reaction	Remarks*
(12) $H_2S = H^+ + HS^-$	K_{obs} 10^{-7} (a) K_{calc} 10^{-7}
(13) $HS^- = H^+ + S^=$	K_{obs} $10^{-12.9}$ (b) K_{calc} 10^{-14}
(14) $H_2S_2O_4 = H^+ + HS_2O_4^-$	A strong acid K_{calc} $10^{-0.346}$
(15) $HS_2O_4^- = H^+ + S_2O_4^=$	K_{obs} $10^{-2.46}$ (c) K_{calc} $10^{-2.46}$
(16) $H_2SO_3 = H^+ + HSO_3^-$	K_{obs} $10^{-1.77}$ (d) K_{calc} $10^{-1.9}$
(17) $HSO_3^- = H^+ + SO_3^=$	K_{obs} $10^{-7.2}$ (d) K_{calc} $10^{-7.25}$
(18) $H_2S_2O_6 = 2H^+ + S_2O_6^=$	No data for intermediate step
(19) $H_2SO_4 = H^+ + HSO_4^-$	A strong acid K_{calc} 10^2
(20) $HSO_4^- = H^+ + SO_4^=$	K_{obs} $10^{-1.9}$ (e) K_{calc} $10^{-1.9}$
(21) $2S_5O_6^= + 3H_2O = 5S_2O_3^= + 6H^+$	K_{obs} no data K_{calc} 10^{-6}

* K_{obs} are the experimentally determined values for the dissociation constants.
K_{calc} are the values for the dissociation constants as calculated from thermodynamic data.
(a) Kubli (1946); (b) Kury (1953); (c) Jelinch (1911); (d) Tarter and Garretson (1941); (e) Hamer (1934).

To solve these equations simultaneously for a given pair of E_h–pH values it is necessary to stipulate the sum of the concentrations of the sulphur species. For convenience we chose 0·1 molar; at this value the solubility of gases such as H_2S or SO_2 is not exceeded. This concentration is comparable to that in many mine waters and of the same order of magnitude as that for the ocean ($10^{-1.5}$). Also, the difference between activity of a given ion and its molality is not great and interaction among species to form unknown complexes probably is not important. Thus a defining equation can be written:

$$[H_2S] + [HS^-] + [S^=] + [S_2^=] + [S_3^=] + [S_2O_3^=] + [S_4O_6^=] + [SO_3^=] + [H_2S_2O_6] + [S_2O_6^=] + [SO_4^=] + [HSO_4^-] + [H_2SO_4] + [HSO_3^-] + [H_2SO_3] + [S_5O_6^=] + [S_2O_4^=] + [HS_2O_4^-] + [H_2S_2O_4] = 0{\cdot}1m \quad (22)$$

Table 2. Equations relating E_h, pH, and other ratios of sulphur species

(1) $E_h = 0{\cdot}141 + 0{\cdot}03 \log \frac{[S^0]}{[H_2S]} - 0{\cdot}06\ pH$

(2) $E_h = -0{\cdot}48 + 0{\cdot}03 \log \frac{[S_2^{=}]}{[S^{=}]^2}$

(3) $E_h = -0{\cdot}49 + 0{\cdot}03 \log \frac{[S_3^{=}]}{[S_2^{=}][S^{=}]}$

(4) $E_h = 0{\cdot}50 + 0{\cdot}015 \log \frac{[S_2O_3^{=}]}{[S^0]^2} - 0{\cdot}09\ pH$

(5) $E_h = 0{\cdot}082 + 0{\cdot}03 \log \frac{[S_4O_6^{=}]}{[S_2O_3^{=}]^2}$

(6) $E_h = 1{\cdot}53 + 0{\cdot}03 \log \frac{[S_2O_4^{=}]^2}{S_4O_6^{=}]} - 0{\cdot}12\ pH$

(7) $E_h = 0{\cdot}535 + 0{\cdot}03 \log \frac{[SO_3^{=}]^2}{[S_2O_4^{=}]} - 0{\cdot}12\ pH$

(8) $E_h = 0{\cdot}026 + 0{\cdot}03 \log \frac{[S_2O_6^{=}]}{[SO_3^{=}]^2}$

(9) $E_h = -0{\cdot}226 + 0{\cdot}03 \log \frac{[SO_4^{=}]^2}{[S_2O_6^{=}]} - 0{\cdot}12\ pH$

(10) $E_h = 0{\cdot}142 + 0{\cdot}0075 \log \frac{[SO_4^{=}]}{[S^{=}]} - 0{\cdot}06\ pH$

(11) $E_h = 0{\cdot}28 + 0{\cdot}0075 \log \frac{[SO_4^{=}]^2}{[S_2O_3^{=}]} - 0{\cdot}075\ pH$

(12) $\log \frac{[HS^-]}{[H_2S]} = -7 + pH$

(13) $\log \frac{[S^{=}]}{[HS^-]} = -14 + pH$

(14) $\log \frac{[HS_2O_4^-]}{[H_2S_2O_4]} = -0{\cdot}346 + pH$

(15) $\log \frac{[S_2O_4^{=}]}{[HS_2O_4^{=}]} = -2{\cdot}46 + pH$

(16) $\log \frac{[HSO_3^-]}{[H_2SO_3]} = -1{\cdot}90 + pH$

(17) $\log \frac{[SO_3^{=}]}{[HSO_3^-]} = -7{\cdot}25 + pH$

(18) No data

(19) $\log \frac{[HSO_4^-]}{[H_2SO_4]} = 2 + pH$

(20) $\log \frac{[SO_4^{=}]}{[HSO_4^-]} = 1{\cdot}9 + pH$

(21) $\log \frac{[S_5O_6^{=}]^2}{[S_2O_3^{=}]^5} = 5{\cdot}2 - 6\ pH$

In setting up the above equation it was assumed that any polysulphide present was completely dissociated as $S_x^=$, because H_2S_x and HS_x^- are unstable with respect to decomposition into H_2S and S or HS^- and S at temperatures above 0°C.

A typical set of calculations for determining the activities at an arbitrarily chosen pH and E_h is as follows. Instead of making successive substitutions into equation (22) so that the entire expression could be solved for a single species, which would be a satisfactory but laborious method, we made a guess concerning the single dominant species under the conditions chosen, and proceeded to calculate all the others successively, hoping that our first guess was correct. For the specific values pH = 12, E_h = 0·4 which are rather strongly oxidizing and alkaline, we chose $SO_4^=$ as the predominant species, and further assumed that all others would be quantitatively unimportant. Then from equation (9) of Table 2:

$$E_h = -0{\cdot}226 + 0{\cdot}03 \log \frac{[SO_4^=]^2}{[S_2O_6^=]} - 0{\cdot}12 \text{ pH}$$

Substituting the chosen values:

$$0{\cdot}4 = -0{\cdot}226 + 0{\cdot}03 \log \frac{[10^{-1}]^2}{[S_2O_6^=]} - 0{\cdot}12 \times 12$$

Solving for $[S_2O_6^=]$ yields:

$$[S_2O_6^=] = 10^{-70{\cdot}9}$$

Thus for this first attempt the original assumption of the vast excess of $SO_4^=$ over other species holds. Next the value of $[S_2O_6^=]$ can be substituted in another equation, such as (8) of Table 2:

$$0{\cdot}4 = 0{\cdot}026 + 0{\cdot}03 \log \frac{10^{-70{\cdot}9}}{[SO_3^=]^2}$$

which in turn gives $[SO_3^=] = 10^{-41{\cdot}7}$.

Successive substitution of such calculated values into the equations of Table 2 gives molalities for all the species listed. If the sum of all species except $[SO_4^=]$ is much less than 10^{-1}, then the original assumption of its predominance is justified, and the requirements set by equation (22) are satisfied. By working "lines of equal pH", and making calculations for decreasing or increasing E_h-values, we could watch the change in various species and predict the conditions under which a different species would become predominant. Fortunately only a few occur, so that the calculations although tedious are not difficult.

The calculated molalities of the various species at numerous E_h pH points were plotted on diagrams of E_h vs. pH, and the values contoured. These diagrams are shown in Figs. 1–17 inclusive. From these diagrams that species showing maximum molality at a given E_h–pH combination was chosen to construct the composite "major species" diagram shown in Fig. 18. This figure checks well with Valensi's (1950) diagram labelled "Stable Species." Fig. 19 is a composite showing contours of maximum molality of some of the lesser species of interest.

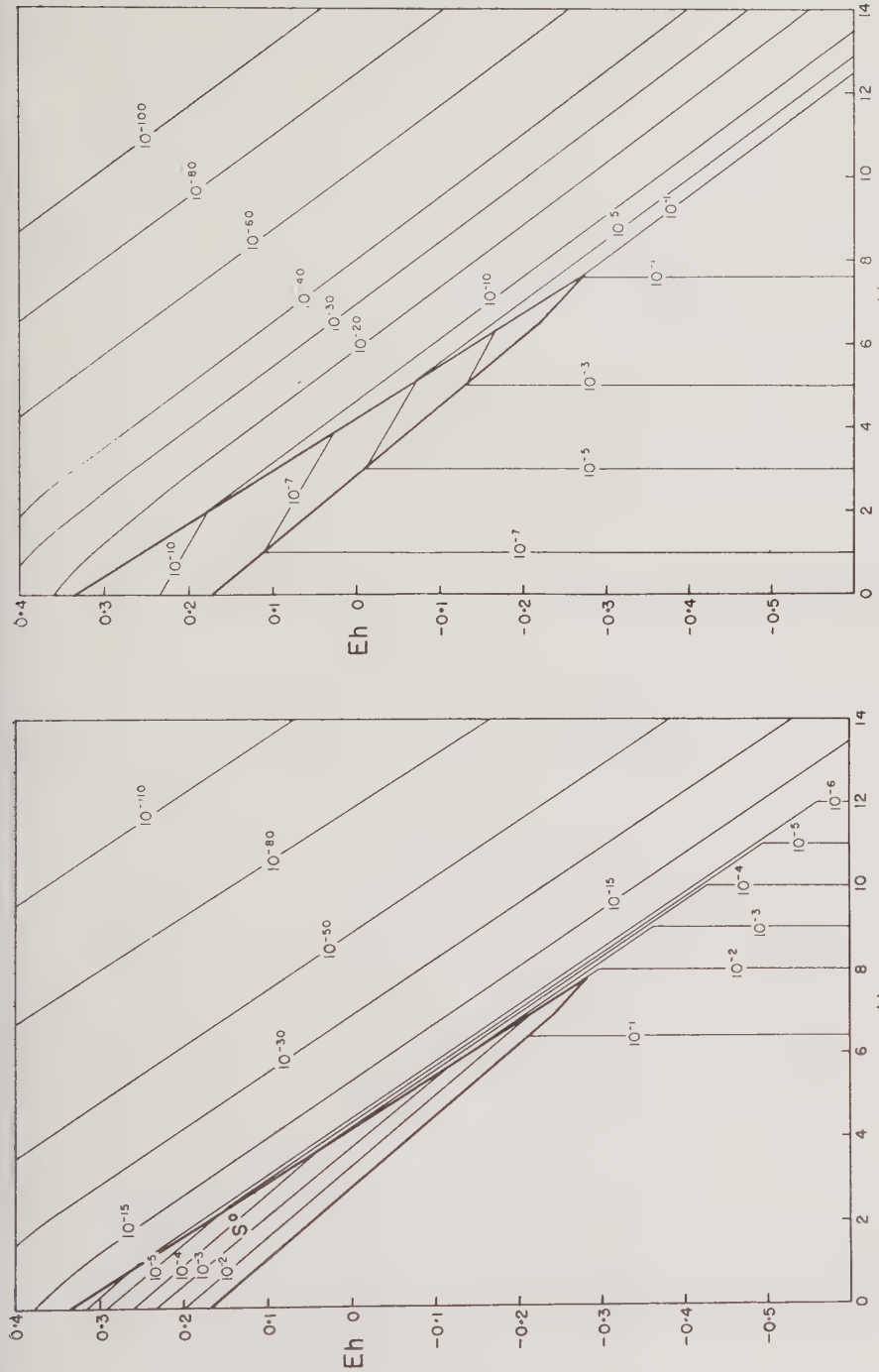

Fig. 1. H_2S.

Fig. 2. HS^-.

Figs. 1–17. Concentration contours, as determined by E_h and pH, of the respective sulphur-containing species in equilibrium with all other sulphur-containing species in aqueous solution at 25°C, 1 atm total pressure, and total sulphur concentration of 0·1 molar.

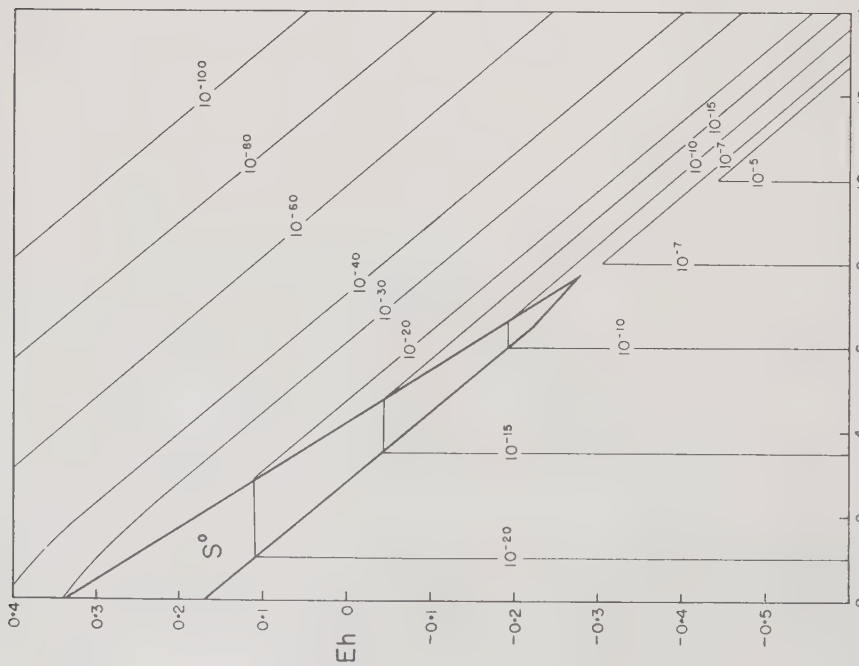

Fig. 3. $S^=$.

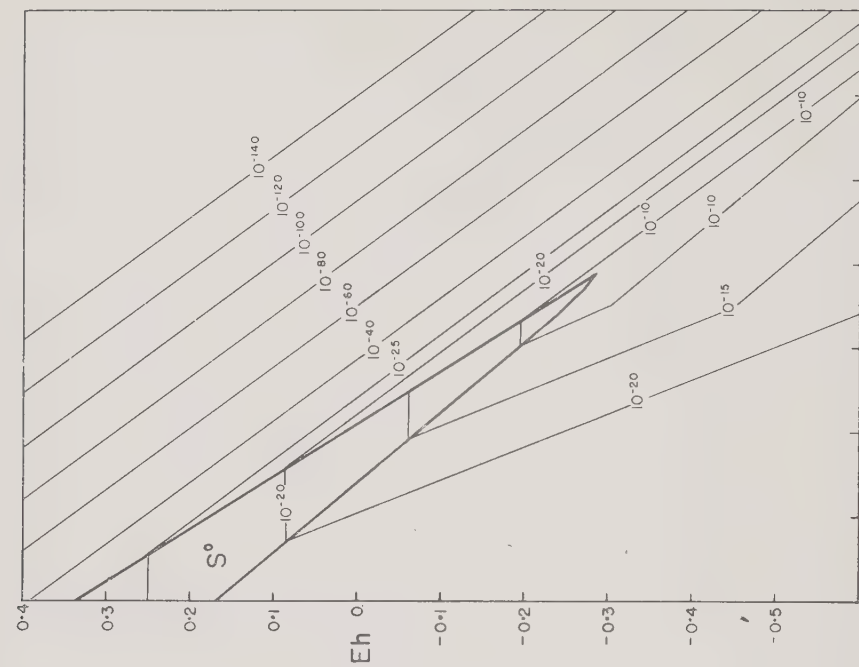

Fig. 4. $S_2^=$.

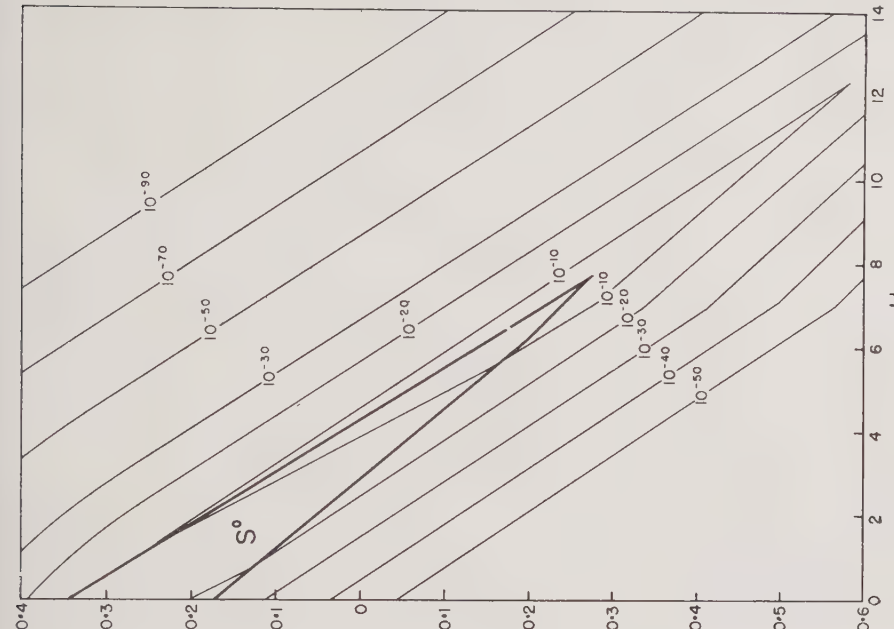

Fig. 6. $S_2O_3^=$.

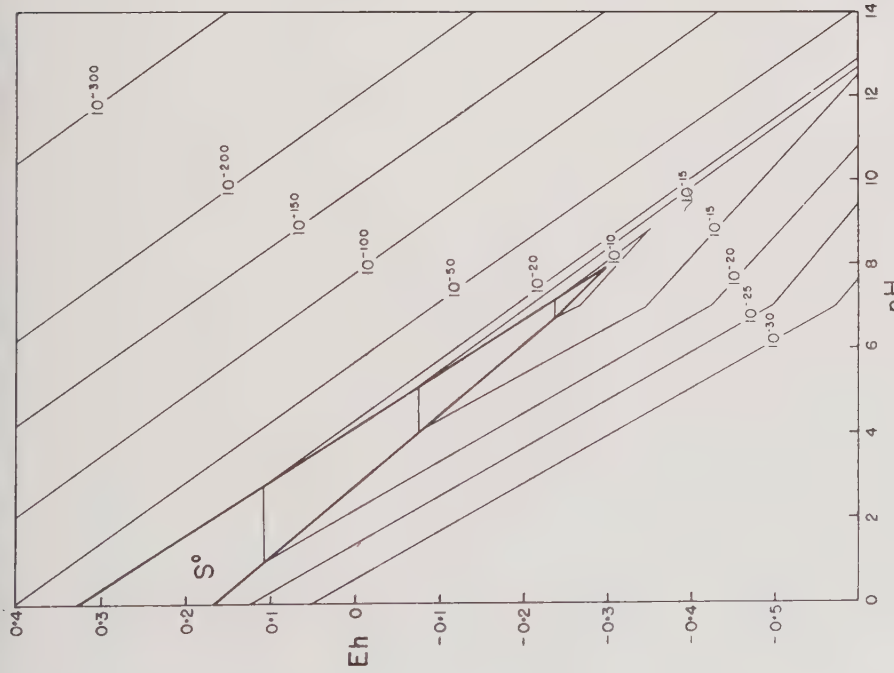

Fig. 5. $S_3^=$.

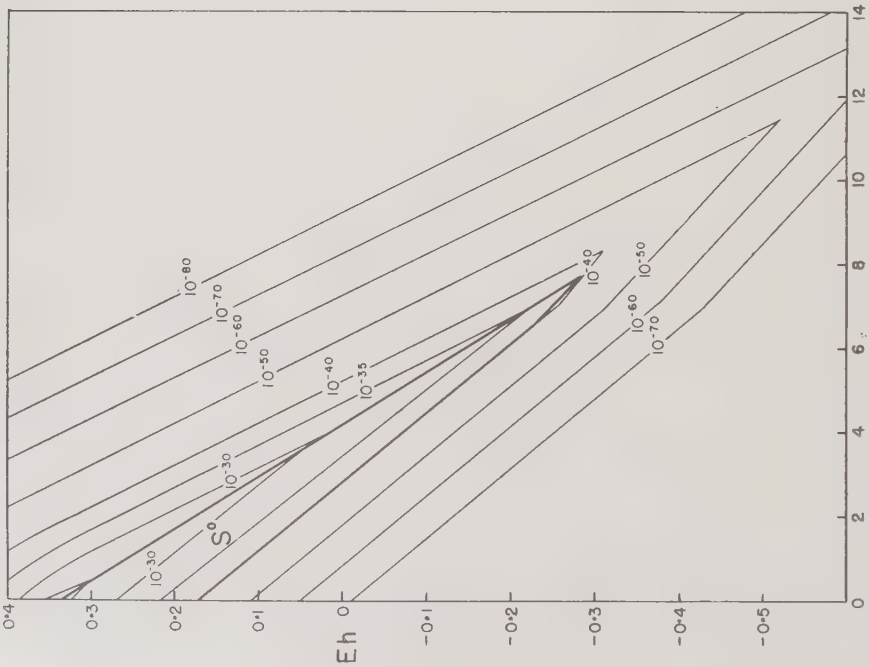

Fig. 7. $H_2S_2O_4$.

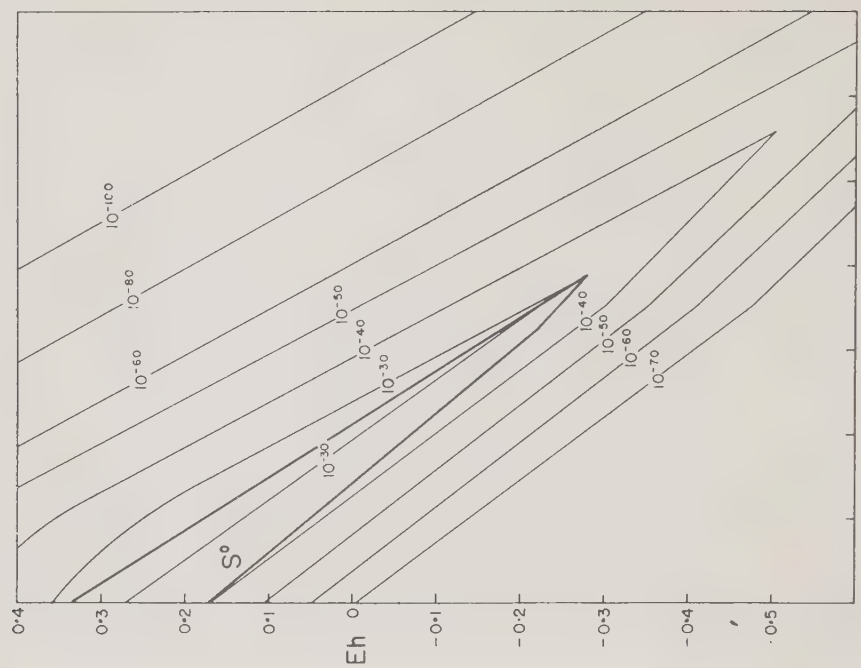

Fig. 8. $HS_2O_4^-$.

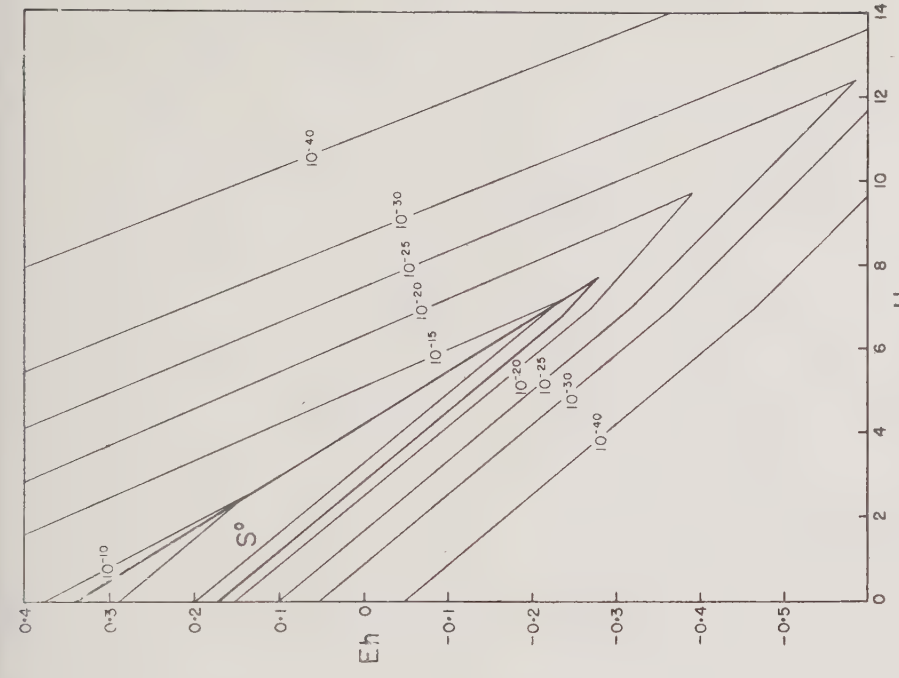

Fig. 10 H_2SO_3.

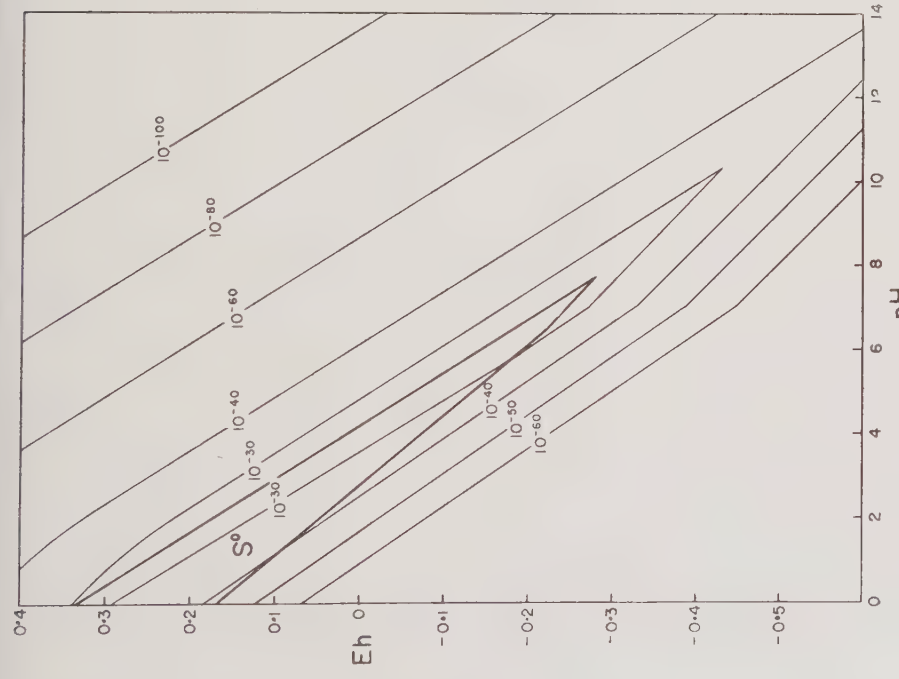

Fig. 9. $S_2O_4^{=}$.

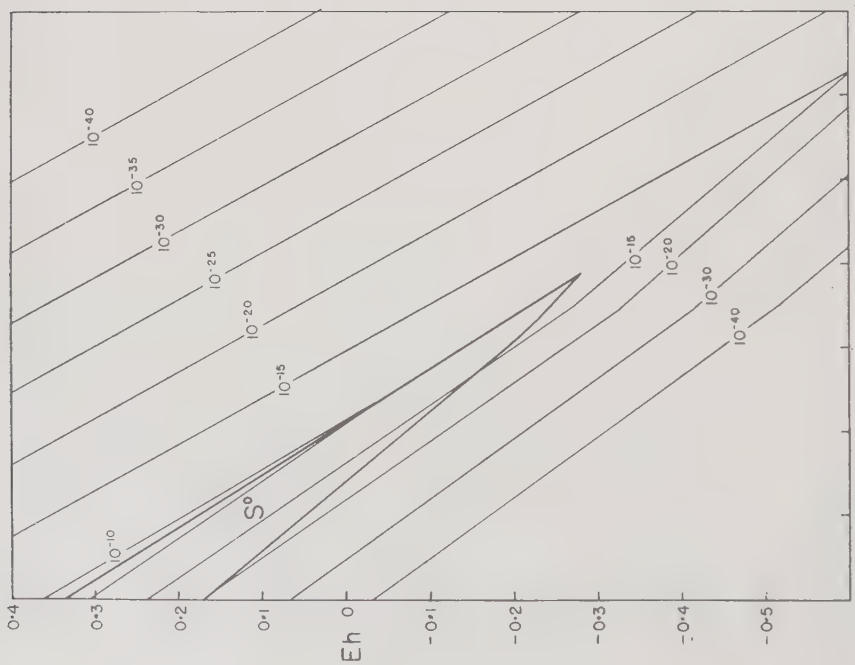

Fig. 11. HSO_3^-.

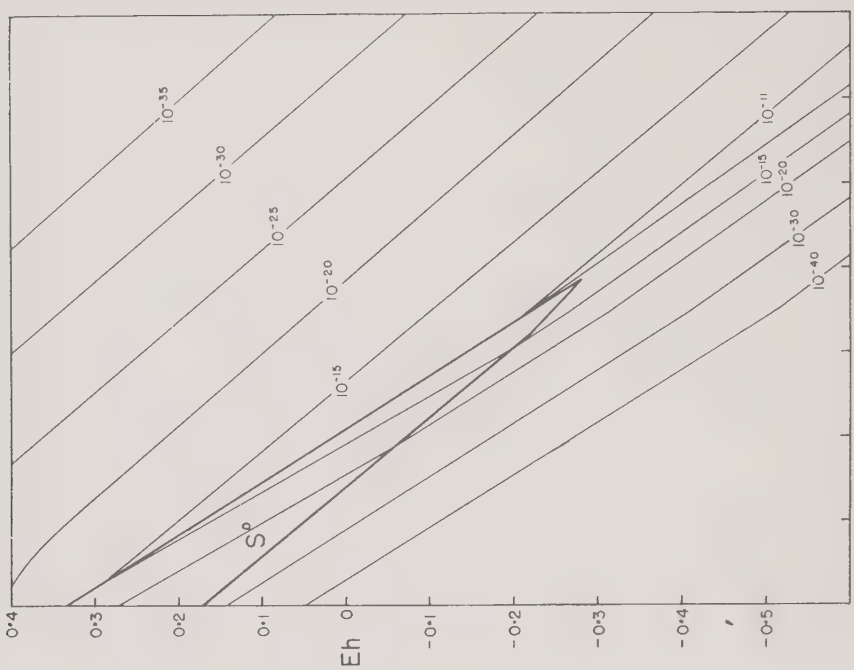

Fig. 12. $SO_3^=$.

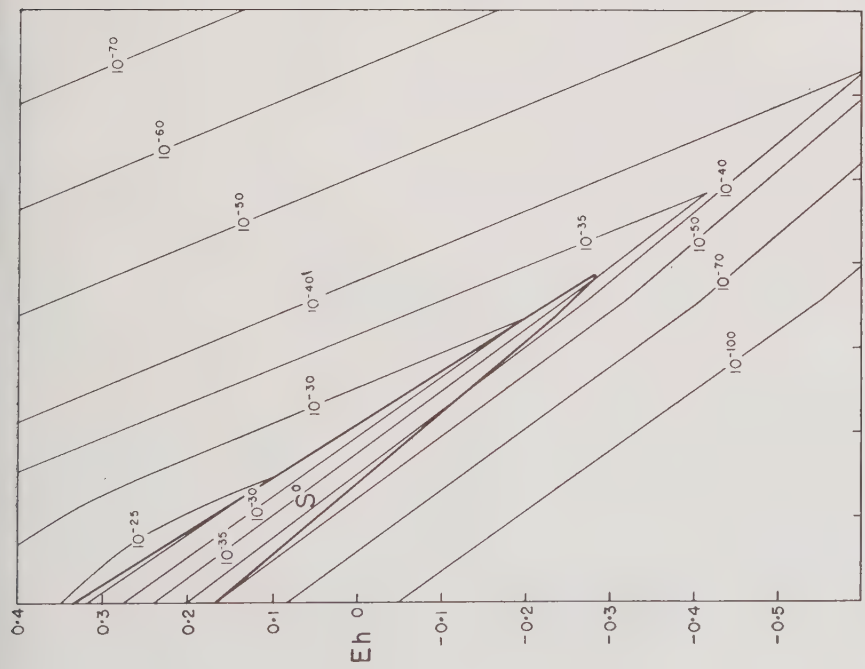

Fig. 13. $S_2O_6^=$.

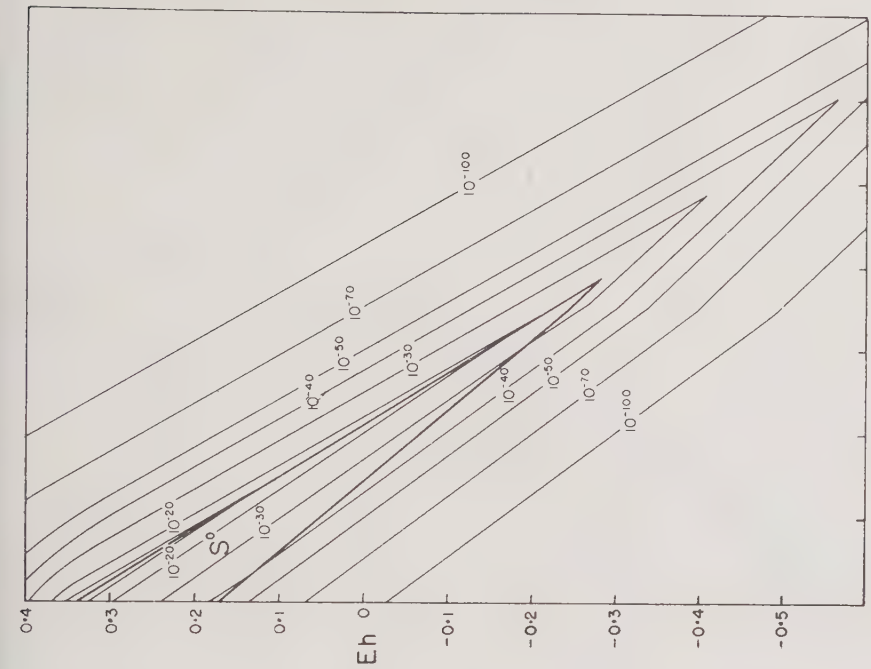

Fig. 14. $S_4O_6^=$.

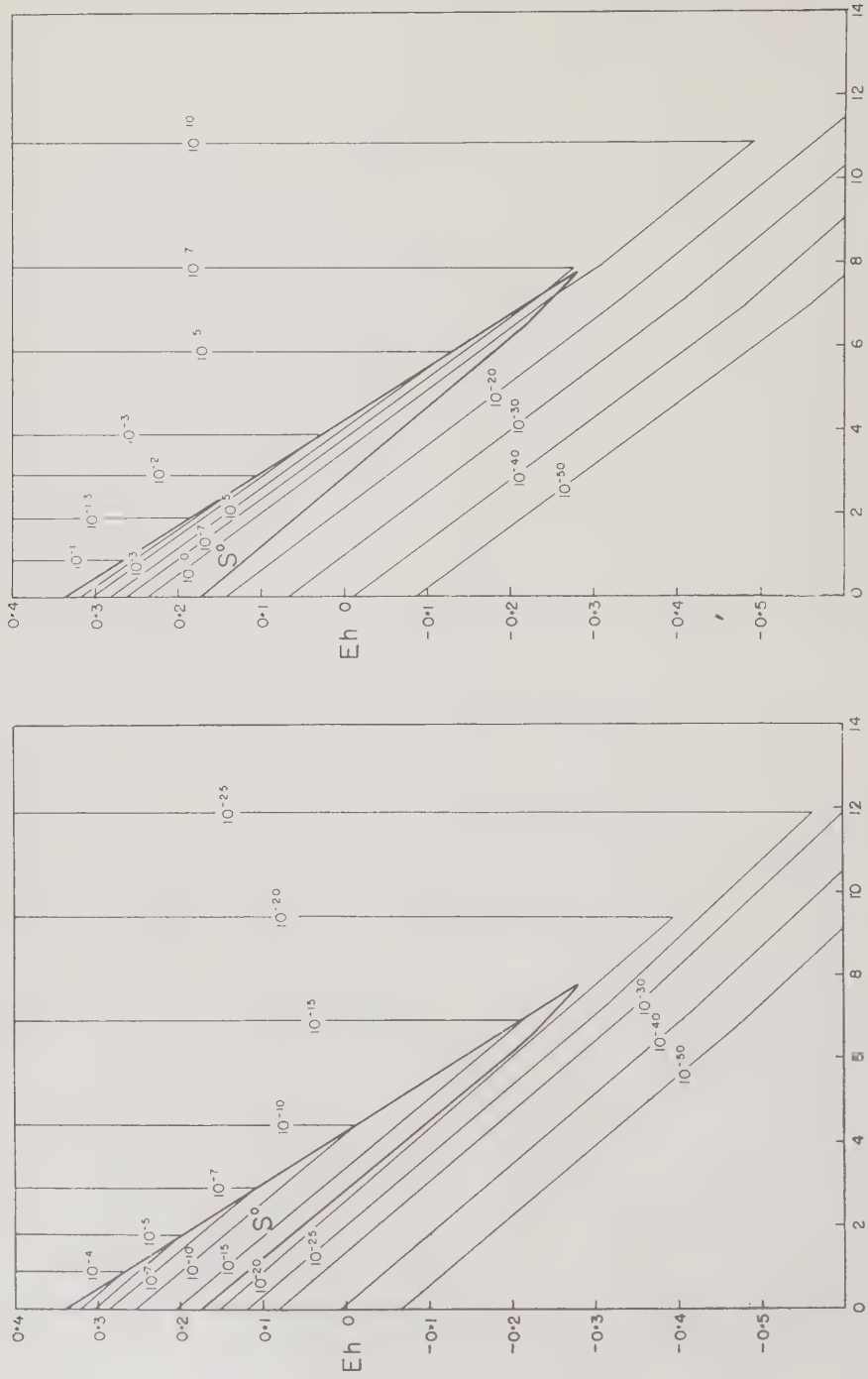

Fig. 16. HSO_4^-.

Fig. 15. H_2SO_4.

Discussion and Interpretation

The most striking aspect of the equilibrium distribution of sulphur species is the near-absence of all but HSO_4^-, $SO_4^=$, S°, H_2S and HS^- under the range of conditions expected in aqueous solutions at the earth's surface. Most of the others, however, are well known in the laboratory as major species in solution under these

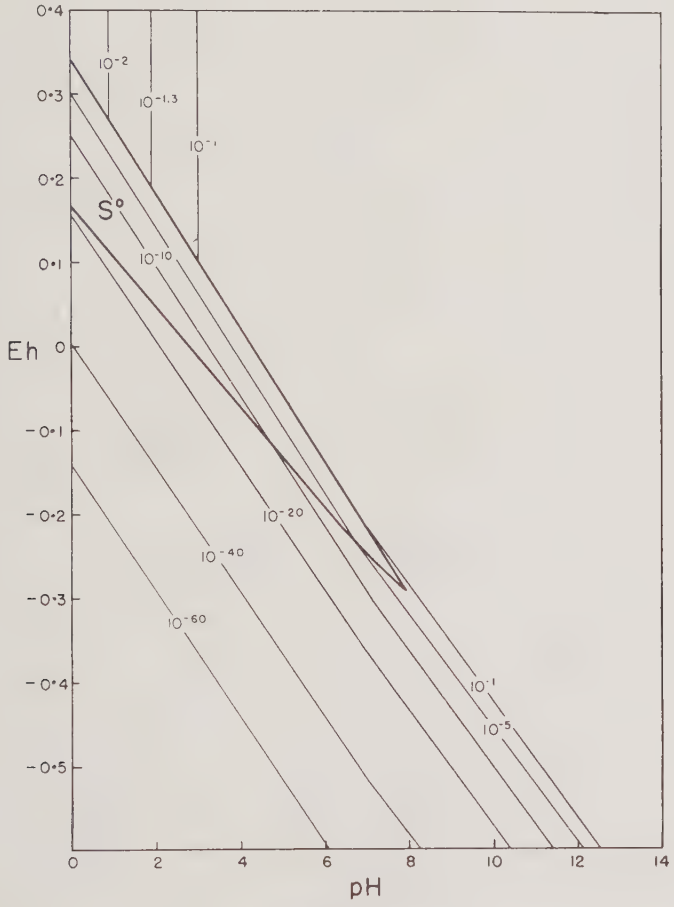

Fig. 17. $SO_4^=$.

same conditions, so the system is notable for the great variety of these metastable ons. Except for $S^=$, which becomes a dominant species under reducing conditions ust above the pH range studied, none of the others studied exceeds 10^{-6} molal nder equilibrium conditions; most are far less.

The occurrence of minerals containing sulphur fits into the picture of formation of minerals generally representing close approach to equilibrium. The chief minerals are sulphides, sulphates and basic sulphates. The disulphides, pyrite nd marcasite, are important minerals, and $S_2^=$ is among the most important of he minor equilibrium species. Minerals containing any other species of combined

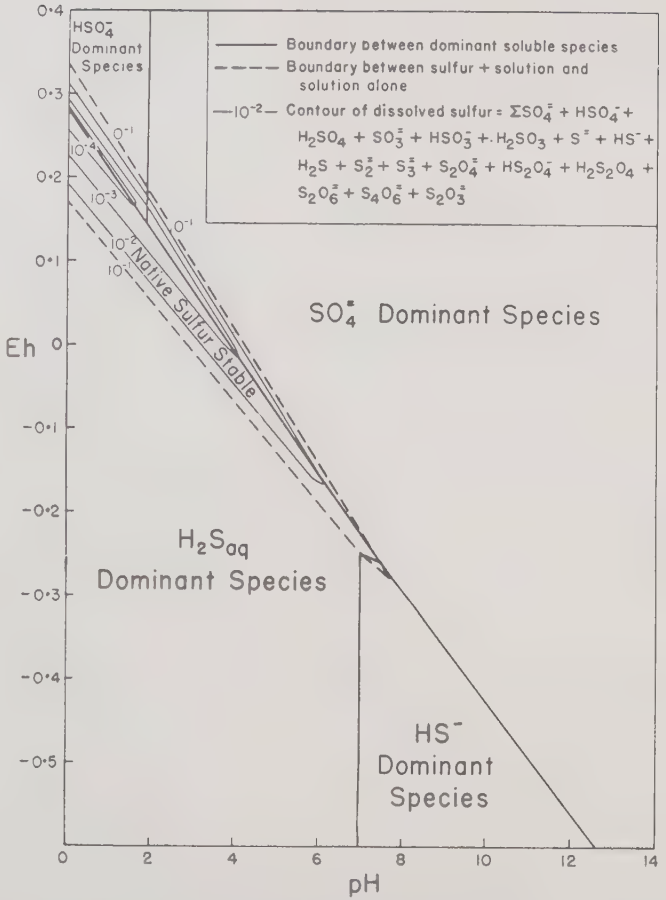
HSO4⁻ Dominant Species
Boundary between dominant soluble species
Boundary between sulfur + solution and solution alone
10⁻²— Contour of dissolved sulfur = ΣSO4⁼ + HSO4⁻ + H2SO4 + SO3⁼ + HSO3⁻ + H2SO3 + S⁼ + HS⁻ + H2S + S2⁼ + S3⁼ + S2O4⁼ + HS2O4⁻ + H2S2O4 + S2O6⁼ + S4O6⁼ + S2O3⁼
Native Sulfur Stable
SO4⁼ Dominant Species
H2Saq Dominant Species
HS⁻ Dominant Species
Eh
pH

Fig. 18. Distribution of major ionic species of sulphur at equilibrium at 25°C and 1 atm pressure. Total sulphur in system = 0·1 M, except in field of native sulphur, where contours show total dissolved sulphur in equilibrium with solid.

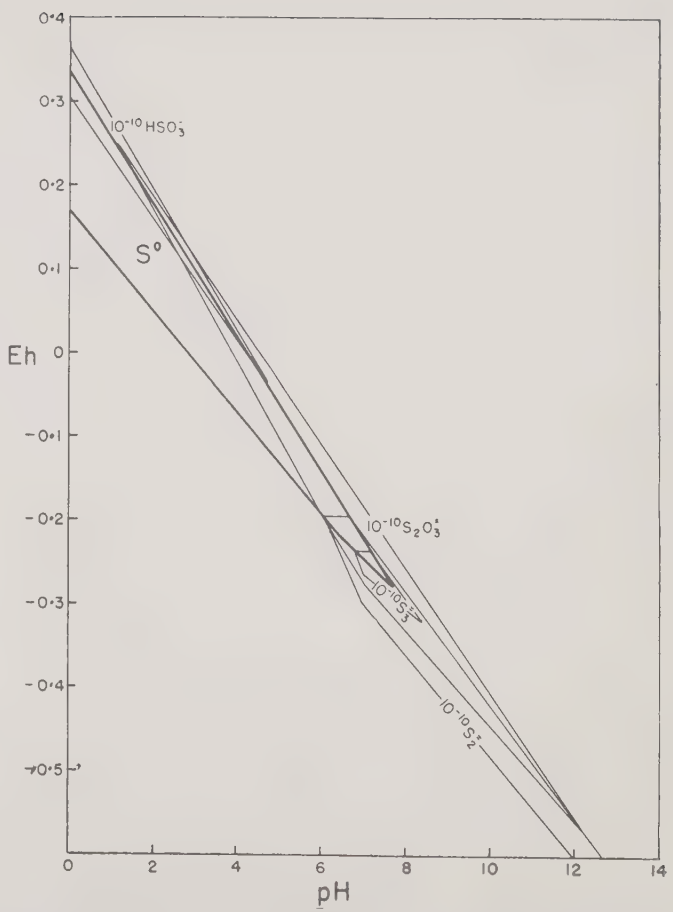

Fig. 19. Distribution of 10^{-10} contour of some minor sulphur species in equilibrium with total sulphur = 0·1 M. Approximate maxima are as follows: $S_2^{=} = 10^{-8}$, $S_3^{=} = 10^{-9}$, $S_2O_3^{=} = 10^{-6}$, $HSO_3^{=} = 10^{-9}$. Note maxima tend to lie on upper boundary of S° stability field and its extension.

sulphur are unknown, and such species have not been reported in solution except in hot springs, in which both thiosulphate and pentathionate have been reported by Allen and Day (1927) and Day and Allen (1925).

The restriction of the stability field of elemental sulphur to acid or very weakly alkaline solutions as portrayed points up some geochemical relations of interest. Sulphur in sea water occurs as sulphate at about pH 8·2. Under euxinic conditions bacteria can reduce sulphate to sulphide (actually HS^-), but the concentration of sulphur in sea water (0·03 M) is not sufficient to enter the field of elemental sulphur stability during reduction. Native sulphur formation would require an environment either lower in pH or higher in total sulphur than ordinary sea water. It seems that native sulphur might best be produced from oceanic water by reduction of sulphate to bisulphide, and perhaps organic production of H_2S, with concomitant lowering of pH, followed by either bacterial oxidation or air oxidation up into the native sulphur field. This path fits that deduced from isotope studies by Thode *et al.* (1953).

Another feature that might be emphasized is the steepness of the boundary between sulphate and H_2S, HS^- and $S^=$. The pH–E_h line running from about E_h 0·3 at pH 0 and E_h −0·6 at pH 12 can be considered as the middle of a narrow zone of rapid change from −2 valent sulphur below to +6 valent sulphur above. Because this boundary is so sharp, it marks a general limit between the stable region for sulphide minerals below and sulphate minerals above. It also indicates that sulphides are stable only in environments with oxygen concentration of less than 10^{-70} atm to less than 10^{-15} atm in the pH range of from zero to 12, whereas sulphates are stable in the presence of any concentration from mere traces on up. This "sulphate cliff" is best shown by Fig. 3 which illustrates $[S^=]$ and which is the fundamental control on metal sulphide stability. This same line (Fig. 18) is a major axis for almost all sulphur species. The intermediate species tend to be distributed roughly symmetrically above and below it, with a maximum for any given pH falling on the line.

Although the gross picture of sulphur species in nature seems to fit equilibrium relations fairly well, some of the metastable relations summarized by Valensi (1950) have important geologic effects, and others may also be important in geochemistry. Chief among these relations is the generalization that among the sulphur–oxygen combinations, the most stable are slowest to form and also hardest to get rid of. Outstanding among the offenders is the sulphate group—H_2SO_4, HSO_4^-, and $SO_4^=$. Oxidizing agents sufficient to form sulphate from less oxidized species commonly will not do so at a measurable laboratory rate; instead the reaction appears to stop at an intermediate species or not go at all. Once sulphate is formed, it is practically impossible to remove it by inorganic reduction. Even metallic zinc, which releases hydrogen from acid solution, will not reduce sulphate in dilute acid. Micro-organisms can do the job with apparent ease, so that in environments rich in organisms reduction takes place, but where an ore deposit is oxidizing and sulphate-bearing solutions move down into water-saturated rocks where conditions are sufficient to reduce sulphate to a −2 valent sulphur species, no reduction occurs. Thus the accompanying metal ions must encounter primary unoxidized −2 valent sulphur species if they are to precipitate and much zinc and

iron may move entirely away from the vicinity of the ore deposit although they are accompanied by more than enough of metastable sulphate if it were reducible.

The sulphide ion diagram (Fig. 3) should be useful to anyone interested in calculating the equilibrium activity of metal ions in equilibrium with a metal sulphide at any given E_h–pH conditions and at any given total sulphur in the system. For example, what is the activity of lead ion in a solution saturated with PbS and H_2S and pH 1? In this case total sulphur is 0·1, the condition for which the diagrams were calculated. From Latimer (1952, p. 153):

$$[Pb^{++}][S^{=}] = 10^{-28.15}$$

From Fig. 3, $$[S^{=}] = 10^{-20}$$

Then: $$[Pb^{++}] = \frac{10^{-28.15}}{10^{-20}} = 10^{-8.15}$$

For a lower sulphur total, such as 10^{-3} M, all contours are reduced proportionately, so $[S^{=}] = 10^{-28}$, and $[Pb^{++}] = 10^{-6.15}$.

Fig. 4, which shows $[S_2^{=}]$, can be used similarly for determining $[Me^{++}]$ for disulphides.

It must be emphasized that the data and diagrams in this paper are valid for the particular conditions indicated in the title, not for all conditions of temperature, pressure and total sulphur concentration.

Summary

The distribution of dissolved sulphur species in aqueous solution at 25°C and 1 atm total pressure has been calculated as a function of E_h and pH for a solution containing 0·1 molal total sulphur, and the results presented as stability diagrams showing the distribution of individual molecular and ionic species. The only species that predominate, that is, that contain essentially all the sulphur at various environments that might be found in nature, are H_2S, HS^-, HSO_4, $SO_4^{=}$, and elemental sulphur.

Of the other species only $S^{=}$ exceeds 10^{-6} under earth surface conditions.

References

Allen E. T. and Day A. L. (1927) Steam wells and other thermal activity at The Geysers, California. *Carnegie Inst. Washington* **378,** 33.

Day A. L. and Allen E. T. (1925) The volcanic activity and hot springs of Lassen Peak. *Carnegie Inst. Washington* **360,** 115–117.

Hamer W. J. (1934) The ionization constant and heat of ionization of the bisulphate ion from electromotive force measurements. *J. Amer. Chem. Soc.* **56,** 860–864.

Jellinek K. (1911) Uber die Herstellung von reinens Hydrosulfit und über das System Hydrosulfit–Wasser. *Z. anorg. Chem.* **70,** 93–134.

Kubli H. (1946) The dissociation of hydrogen sulfide. *Helv. Chim. Acta* **29,** 1962–1973.

Kury J. W., Zielen A. J. and Latimer W. L. (1953) Heats of formation and entropies of HS^- and S^{--}. *Potential of the Sulphur–Sulphide Couple.* UCRL-2108, Univ. Calif. Radiat. Lat.

Latimer W. M. (1952) *Oxidation Potentials* (2nd Ed.). Prentice-Hall, New York.

Tartar H. V. and Garretson H. H. (1941) The thermodynamic ionization constants of sulfurous acid at 25°. *J. Amer. Chem. Soc.* **63,** 808–816.

Thode H. G., MacNamara J. and Fleming W. H. (1953) Sulphur isotope fractionation in nature and geological and biological time scales. *Geochim. et Cosmochim. Acta* **3,** 235–243.

Valensi G. (1950) Contribution au diagramme potential-pH du soufre. *Comptes Rendus Deuxéme Réunion, Comité Thermodynamique et Cinétique Electrochimie, Milan,* p. 51–68.

Geochimica et Cosmochimica Acta, 1958, Vol. 15, pp. 131 to 149. Pergamon Press Ltd., London

Thermodynamic equilibria of vanadium in aqueous systems as applied to the interpretation of the Colorado Plateau ore deposits*

H. T. Evans, Jr. and R. M. Garrels†
U.S. Geological Survey, Washington, D.C.

(*Received* 6 *March* 1958)

Abstract—All available chemical and thermodynamic information is utilized to construct a diagram showing the stability relationships of the known vanadium compounds in aqueous equilibrium in terms of oxidation potential and pH. The disparity between the observed precipitation conditions and those calculated from the published free energies of the oxides is used to estimate the free energy of hydration of the hydrated forms found in nature. The well-established vanadium mineral species (not including silicates) are assigned regions of stability on the equilibrium diagram on the basis of chemical constitution, crystal structure and observed petrologic associations. It is found that a completely self-consistent alteration sequence appears on the mineral diagram, showing the changes that occur in the vanadium ores under weathering conditions. Montroseite, VO(OH), is evidently the primary mineral source of vanadium. Two distinct branches appear in the alteration sequence: one is confined to acid conditions characteristic of zones of primary vanadium oxide concentration in the sandstone in the presence of pyrite; and the other occurs in more basic conditions where calcite is common. The equilibrium diagram is used to draw tentative conclusions regarding the conditions under which the original montroseite was deposited in the sandstones, presumably through the action of mineralizing solutions.

Introduction

An outstanding feature of the uranium ores in the Colorado Plateau sandstones is their high vanadium content. Vanadium has a maximum at the eastern bounds of the Plateau and tends to decrease toward the west, whereas the uranium content tends to decrease toward the east. Thus, at Rifle, on the flank of the Park Range in Colorado, uranium is virtually absent from the vanadium ore, while in the White Canyon, Green River and San Rafael areas of Utah, vanadium is usually absent from the uranium ore. In the intermediate regions of western Colorado, known appropriately as the Uravan mineral belt (Fisher and Hilpert, 1952), the ores are mainly vanadium ores with a uranium content corresponding to a V : U ratio ranging from 20 : 1 to 4 : 1. It is apparent that vanadium is the predominant extrinsic element in most of these ores and that our knowledge of their deposition, transportation, and properties will depend to a large extent on our understanding of this element. Consequently, in recent years considerable effort has been devoted to the study of the geochemistry of vanadium in sandstones.

Up to 1953, the state of knowledge concerning vanadium geochemistry had not materially advanced since a review of the subject was written by Hess (1933). At that time, the Plateau ores were generally considered to have been syngenetic with the sandstones of Jurassic age, having been deposited largely in the oxidized state. Hess was one of the first to recognize the possibility that the primary ores may have been deposited in a reduced form. As a result of the intensive programme of study and development in the Colorado Plateau area sponsored by the Atomic Energy Commission and the U.S. Geological Survey, a large mass of new data and

* Publication authorized by the Director, U.S. Geological Survey.
† Present address: Department of Geology, Harvard University, Cambridge, Massachusetts, U.S.A.

information has accumulated since 1950. As a consequence, the syngenetic view has been significantly altered. It is now generally held that the ores were deposited in the reduced state from aqueous fluids in the Late Cretaceous or Early Tertiary epoch and subsequently subjected to weathering by meteoric waters and exposure to the atmosphere. An extensive summary of these geochemical investigations is in preparation by the U.S. Geological Survey. Meanwhile, the new interpretation of the geologic history of the Colorado Plateau ore deposits has been reviewed and evaluated by McKelvey *et al.* (1955).

One of the major sources of information for the geochemical studies has been the description and characterization of new mineral species and redefinition of old species. The mineralogy of vanadium is exceedingly complex because of its sensitivity to oxidation potential, its strong amphoteric behaviour in the higher valence states, and its sensitivity to degree of acidity in the higher valence states in the formation of complex polyions of high molecular weight. Mineralogical studies have been further complicated by the fact that most of the secondary minerals involved were formed at low temperatures (probably less than 40°C) and therefore, since grain growth is slow and effective nucleation more frequent than at higher temperatures, they occur in a finely divided state, and in intimate mixtures. Nevertheless, great progress has been made, particularly as a result of the work of Weeks and Gruner and their colleagues (Weeks and Thompson, 1954; Gruner *et al.* 1953). The elucidation of the geochemical behaviour of vanadium has depended finally on the comprehensive definition and compilation of the mineral species that form in the sandstone horizons.

With the geologic and mineralogic background now fairly well filled in, it has been found possible to relate the geochemical properties of vanadium with those that can be predicted from thermodynamic studies which have appeared intermittently over the years in the chemical literature. In the study described in this paper, these thermodynamic properties have been used to evolve an equilibrium diagram which shows the stability of the various vanadium compounds and minerals in the presence of water with respect to the prevailing oxidation potential and acidity at 25°C. As a result, the weathering process and alteration sequence of minerals are clarified. Further, it is also possible to place severe restrictions on the conditions that obtained during the deposition of the original ores.

The validity of the application of thermodynamic principles in this way to the geochemical environment under consideration depends on the rapidity with which equilibrium conditions are achieved. In a weathering environment, the ultimate equilibrium state obtains when all elements are in a fully oxidized state and present in the most stable form, a condition in which there is no tendency for further changes in the mineral suite. The presence of minerals in a lower valence state indicates either a gradient in the oxidation potential or a lack of equilibrium, or both. Local equilibrium conditions may change rapidly in the buried deposits and the thermodynamic studies have proved extremely useful to determine what changes are to be expected as the fully oxidized state is approached: that is, what the mineral alteration sequences should be.

The studies described in this paper have been greatly aided by the work and generous co-operation of many other people in this laboratory. Especial mention

should be made of the mineralogical studies of WEEKS and her associates, the chemical studies of synthetic vanadates by MARVIN, and the thermodynamic and physical chemical studies of BARTON and POMMER. The work has been supported by the Divisions of Raw Materials and Research of the U.S. Atomic Energy Commission.

EQUILIBRIUM DIAGRAM

The value of diagrams showing the stability of phases in aqueous systems in terms of oxidation potential E_h and hydrogen ion concentration (pH) has been most effectively demonstrated by POURBAIX (1949) in the field of metal corrosion, and KRUMBEIN and GARRELS (1952) in geochemistry. As pointed out by the latter authors, these two variables can be used to characterize almost all geochemical changes in sedimentary environments.

For a known set of solid or solution phases for a given element, for which all the standard free energies are known, it is possible to calculate the solubility of the element or its solution phase for any combination of E_h and pH. It is sometimes of interest to plot such values and draw iso-solubility contours, but more often it is convenient simply to demarcate the areas in which certain solution species predominate, or in which the solubility falls below a certain value. The boundary between a soluble and insoluble area on the E_h–pH diagram may be determined from the change of free energy with solution. For example, for the reaction:

$$2VO^{+2} + 2H_2O \rightarrow V_2O_4(s) + 4H^+$$

$$\Delta F^\circ = 13{\cdot}4 \text{ kcal/mole}$$

The equilibrium constant

$$K = \frac{[H^+]^4}{[VO^{+2}]^2}$$

is calculated from the relation

$$\Delta F^\circ = -RT \ln K = -1{\cdot}364 \log K$$

Thus the solubility of vanadium falls to 10^{-2} moles/l. at pH 3·5, and the vertical line on the E_h–pH diagram may serve as a boundary between the vanadyl solution and the V_2O_4 solid stability fields. The equilibrium oxidation potential with respect to the H_2/H^+ couple, E_h, between oxidized and reduced species can also be estimated from free energy changes according to:

$$E_h = E^0 - \frac{0{\cdot}05916}{n} \log K$$

where E^0 is the potential at pH 0 and n the number of Faradays involved in the reaction. If H^+ ions are consumed or produced in the reaction, E_h varies with pH, and the lines separating fields where the oxidized and reduced phases predominate slope, usually toward lower E_h at higher pH values. The convention with respect to the sign of E_h used in this paper is that of LATIMER (1952), according to which reducing potentials are more negative than oxidizing potentials.

A preliminary study of the thermodynamic stability of the vanadium oxides was

made by Garrels (1953), and the results subsequently correlated with the uranium oxide system and the Colorado Plateau ores (Garrels, 1955). It is now possible to expand Garrels' preliminary diagram to include many more vanadium-bearing species. Fig. 1 shows the key relations among the various ions in solution and stable solids in the vanadium–water system. Shaded areas are fields of stability of solids, and are defined as areas in which the solubility of the solid is less than approximately 0·01 mole/l. of the major vanadium species in equilibrium. Unshaded areas are fields in which the predominant dissolved vanadium species exceeds 0·01 mole/l., and are labelled with these species. Boundaries between dissolved species are drawn where

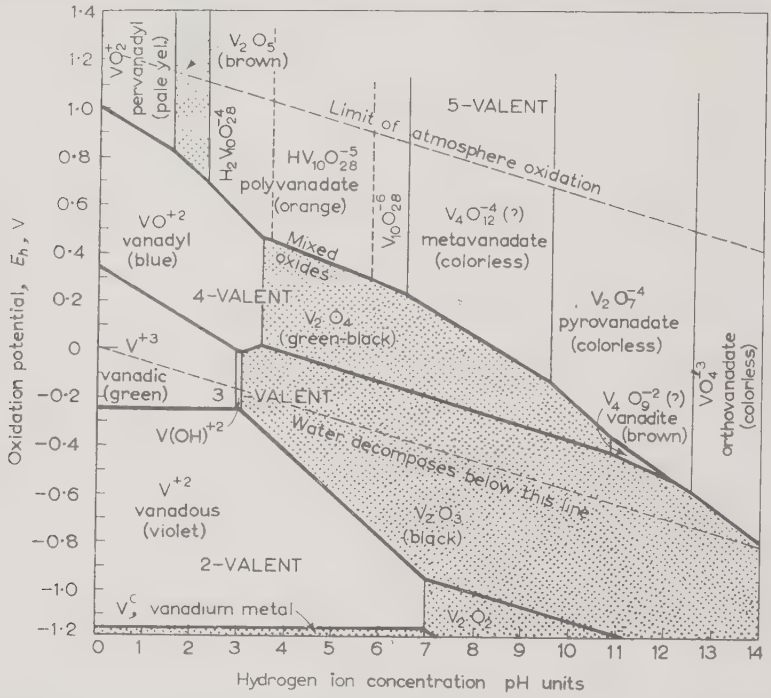

Fig. 1. Aqueous equilibrium diagram showing stability ranges of various solid and solution phases as explained in the text. In stippled areas, the solubility of vanadium is less than about 0·01 moles/l.

the molar concentration ratio of the two major ions is unity. The only solids considered are those resulting from interaction of vanadium and water. A diagram very similar to the theoretical one portrayed would be achieved by controlling pH with $HClO_4$ and NaOH, and oxidation potential with H_2O_2. None of these reagents would yield solids involving Na^+ or ClO_4^-—they would be essentially inert diluents, and would serve chiefly to maintain electrical neutrality.

The dashed lines on the diagram indicate the range of stability of water and hence by inference the general limits of a natural system. Above the upper dashed line water is in equilibrium with more than 1 atm of oxygen; below the lower dashed line with more than 1 atm of hydrogen.

An independent study of the vanadium–water system has recently been reported by Deltombe, Zoubov and Pourbaix (1956). Detailed information is available in

their paper on the concentration distribution of individual ions, as well as a variety of diagrams somewhat similar to our Fig. 1. Their paper has provided us with valuable checks on our work, even though we have felt it necessary to place a different interpretation on the chemistry of vanadium in some instances, particularly in the quinquevalent vanadium fields.

Fig. 1 is drawn on the basis of thermodynamic data for anhydrous oxides. Actually, these oxides are normally precipitated from aqueous solutions in hydrated forms which have slightly but significantly different free energy contents. It is not surprising to find discrepancies between various precipitation pH values experimentally determined (i.e. the pH determined at which the solubility of vanadium

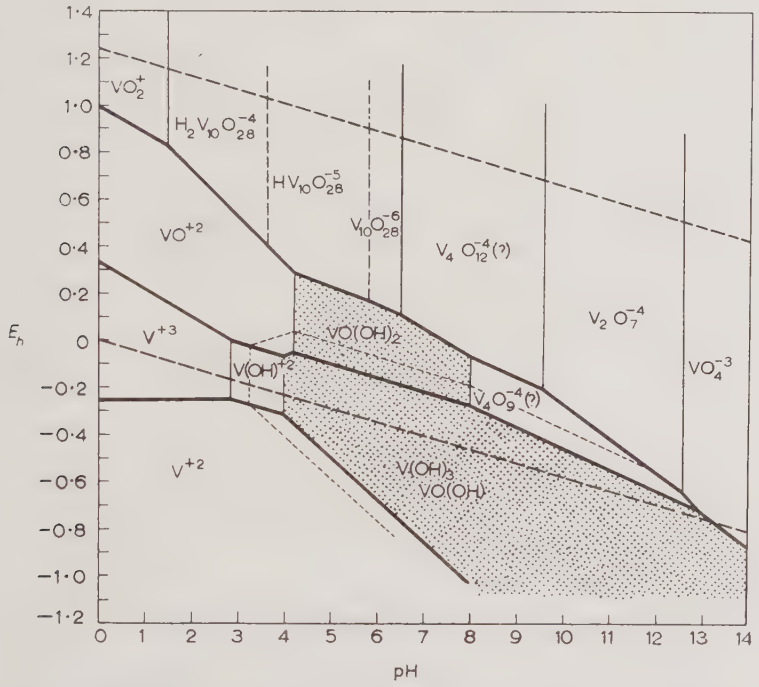

Fig. 2. The diagram of Fig. 1 modified according to the estimated free energies of hydration of the oxides. The dotted boundary indicates the estimated region of stability of montroseite, VO(OH).

falls below about 0·01 mole/l.) and those predicted by Fig. 1. These discrepancies are utilized in a later section to estimate the energies of hydration of V_2O_3, V_2O_4 and V_2O_5. On the basis of these estimates, the equilibrium diagram has been modified and redrawn in Fig. 2. Presumably, since all of the mineral vanadium oxides (except the metastable paramontroseite) are hydrated, the diagram of Fig. 2 will have significant bearing on the natural system.

Perhaps the most satisfactory scheme in developing the interrelations of the diagram is to discuss them sequentially in terms of the various valences of vanadium, to work from the top of the diagram to the bottom, considering first the behaviour

of vanadium (V), then that of (IV), (III), and (II). Free energy data basic to the discussion are given in Table 1.

Quinquevalent vanadium

In water solutions in equilibrium with air at room temperatures, only solids and dissolved species containing quinquevalent vanadium are quantitatively important.

Table 1. Free energies of vanadium compounds and ions

Phase	State(a)	Valence	Latimer(b)	Deltombe *et al.*(c)	This paper
V	cr	0	0	0	0
V^{+2}	aq	2	−54·7	−54·2	−54·2
V^{+3}	aq	3	−60·6	−60·1	−60·1
VO^{+2}	aq	4	-109	−109·0	−109·0
VO_2^+	aq	5	−143(d)	−142·6	−142·6
V_2O_2	cr	2	−189	−189·0	−189·0
V_2O_3	cr	3	−271	−271·0	−271·0
V_2O_4	cr	4	−318	−318·0	−318·0
V_2O_5 (aged)	s	5	−344	−344·0	−344·0
V_2O_5 (fresh)	s	5		−342·0	−342·0
$V(OH)_3$	s	3			−218·0(e)
$V(OH)^{+2}$	aq	3		−112·8	−112·8
$VO(OH)_2$	s	4			−213·6(f)
NH_4VO_3	cr	5	−221·8		−221·8
$V_4O_9^{-2}$	aq	4		−665·3(g)	−665·3
$H_2V_{10}O_{28}^{-4}$	aq	5	−1867(h)		−1875·2(j)
$HV_{10}O_{28}^{-5}$	aq	5			−1870·3(j)
$V_{10}O_{28}^{-6}$	aq	5	−1863(h)	−1856(k)	−1862·4(j)

Notes:

(a) Symbols: cr, crystalline; s, solid; aq, aqueous solution.

(b) Latimer (1952).

(c) Deltombe, de Zoubov and Pourbaix (1956).

(d) Latimer (1952) gives for $V(OH)_4^+$, $\Delta F^\circ = -256$ kcal/mole; $V(OH)_4^+ = VO_2^+ + 2H_2O$.

(e) From $E^\circ = 0{\cdot}10$ volt observed for reaction $V(OH)_3(s) \rightarrow VO(OH)_2(s) + H^+ + e^-$ (A. M. Pommer, personal communication).

(f) From precipitation pH of 4·1 observed by Ducret (1951), and free energy of VO^{+2}.

(g) Deltombe *et al.* (1956) give for $HV_2O_5^-$, $\Delta F^\circ = -361$ kcal/mole; $2HV_2O_5^- = V_4O_9^{-2} + H_2O$

(h) Latimer (1952) gives for $HV_6O_{17}^{-3}$, $\Delta F^\circ = -1132$ kcal/mole, and for $H_2V_6O_{17}^{-2}$, $\Delta F^\circ = -1135$ kcal/mole; $5HV_6O_{17}^{-3} = 3V_{10}O_{28}^{-6} + 3H^+ + H_2O$, and $5H_2V_6O_{17}^{-2} = 3H_2V_{10}O_{28}^{-4} + 2H^+ + H_2O$.

(j) Calculated from solubility of V_2O_5 (fresh) (Ducret, 1951) and dissociation constants of Rossotti and Rossotti (1956).

(k) Deltombe *et al.* (1956) give for $H_3V_2O_7^-$, $\Delta F^\circ = -451$ kcal/mole; $5H_3V_2O_7^- = V_{10}O_{28}^{-6} + H^+ + 7H_2O$.

Vanadium forms a pervanadyl cation VO_2^+ only at low pH; the isoelectric point is between pH 1 and 2, above which the vanadium is converted to complex anions. At this point, the solubility of vanadium falls to a minimum, as is evidenced by the stability field of the solid hydrated V_2O_5. At higher pH values a variety of anions occurs; in general they range from deeply coloured, highly polymerized species at lower pH values to colourless, less condensed ions at high pH values.

The most direct information concerning the fields of stability of vanadates in

solutions is provided by the diffusion rate studies of JANDER and JAHR (1933). According to their technique, vanadium in a solution at a specified pH is allowed to diffuse upward into a vanadium-free solution of equal ionic strength and pH for a period of days, after which time the solution is separated and analysed by layers. Several sharp breaks were found in their diffusion rate–pH curve, which is redrawn from their data in Fig. 3(b). They also attempted to approximate values of the molecular weights of the diffusing ions by assuming that the molecular weight is proportional to the inverse square of the diffusion rate, but this assumption is subject to gross errors. The most careful titration experiments have been made by

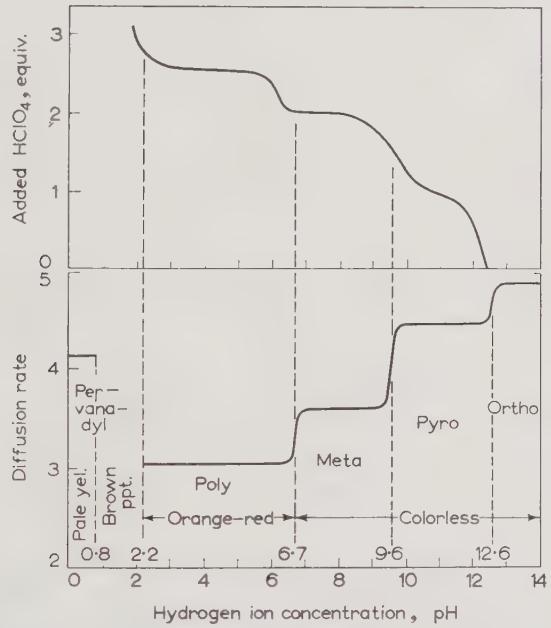

Fig. 3. Diagrams showing the behaviour of quinquevalent vanadium in solution. Upper curve (a) shows the titration curve of DUCRET (1951); lower curve (b) shows the results of diffusion experiments of JANDER and JAHR (1933).

DUCRET (1951), and his final titration curve (pH vs. added $HClO_4$) is shown redrawn in Fig. 3(a). It is very similar to a curve determined by JANDER and JAHR (1933). DUCRET also attempted to determine the formula of the reacting vanadate ions by careful interpretation of the shapes of the curves. Such an interpretation is very uncertain, and his conclusion that the largest vanadate ion produced is $H_3V_2O_7^-$ (corresponding to the orange polyvanadate) is not supported by any other evidence that has been accumulated for this system.

Crystallographic data on the vanadate system are meagre. BAKER (1885) has described a series of very soluble crystalline orthovanadates which are isomorphous with the corresponding phosphates and arsenates thus indicating the existence of the VO_4^{-3} ion in solution. A series of compounds has been shown by crystallographic study to be salts of the ion $V_{10}O_{28}^{-6}$, which corresponds to the orange polyvanadate ion (EVANS *et al.*, 1955), but its structure is still unknown.

Crystal structures of two metavanadates (NH_4VO_3, Syneček and Hanic, 1954; $KVO_3 \cdot H_2O$, Christ *et al.*, 1954) reveal chain structures, which do not indicate directly the nature of the species in solution.

The best expression of the condensation reactions involved that can be written at present is as follows:

$$2VO_4^{-3} + 2H^+ \rightleftharpoons V_2O_7^{-4} + H_2O$$
$$[VO_4^{-3}] = [V_2O_7^{-4}] \text{ at pH12·6}$$

$$2V_2O_7^{-4} + 4H^+ \rightleftharpoons V_4O_{12}^{-4} + 2H_2O$$
$$[V_2O_7^{-4}] = [V_4O_{12}^{-4}] \text{ at pH 9·6}$$

$$5V_4O_{12}^{-4} + 8H^+ \rightleftharpoons 2V_{10}O_{28}^{-6} + 4H_2O$$
$$[V_4O_{12}^{-4}] = [V_{10}O_{28}^{-6}] \text{ at pH 6·7}$$

$$V_{10}O_{28}^{-6} + H^+ \rightleftharpoons HV_{10}O_{28}^{-5}$$
$$K = 10^{5·8}$$

$$HV_{10}O_{28}^{-5} + H^+ \rightleftharpoons H_2V_{10}O_{28}^{-4}$$
$$K = 10^{3·6}$$

$$H_2V_{10}O_{28}^{-4} + 4H^+ \rightleftharpoons 5V_2O_5 \cdot nH_2O(s) + (3 - n)H_2O$$
$$[H_2V_{10}O_{28}^{-4}] = 0·01 \text{ mole at pH 2·2}$$

$$V_2O_5 \cdot nH_2O(s) + (5 - n)H_2O + 2H^+ \rightleftharpoons 2VO_2^+ + 6H_2O$$
$$[VO_2^+] = 0·01 \text{ mole at pH 0·8}$$

The pH data for the condensation and precipitation reactions are taken from Jander and Jahr (1933). In all of their experiments, the ionic strength was held constant, corresponding to 1 molar KNO_3 or $NaNO_3$ and the concentration of V was 0·112 mole/l. The equilibrium constants for the acidification of the polyvanadate ion are given by Rossotti and Rossotti (1956).

The boundaries in Fig.1 are drawn approximately where the two reacting ions are in equal molar concentration. They may shift slightly with variation of concentration of ions indicated, or changes in ionic strength of the solutions.

The pH boundaries of $V_2O_5 \cdot nH_2O$ as drawn are based upon "aged" material, rather than upon freshly precipitated oxide. Aged material is more stable than that newly precipitated, as indicated by the difference of 2 kcal in the standard free energies of formation (Table 1). Rapid neutralization of an acid solution 0·01 molar in VO_2^+, in fact, permits passage from VO_2^+ to the orange polyvanadates without precipitation of the hydrated pentoxide, whereas the same titration, if done slowly, results in formation of the yellow-brown oxide. The increase in stability with time may be correlated with a decrease in hydration as well as with a change in crystalline state.

The striking behaviour of the vanadates, that of forming higher and higher molecular weight complexes with increasing acidity, strongly suggests that, unlike

the phosphates and arsenates, the acidified ions are inherently unstable and immediately split out water through condensation reactions. Only the acidified polyvanadate ions $HV_{10}O_{28}^{-5}$ and $H_2V_{10}O_{28}^{-4}$ persist as predominant species in solution, but even these may actually be metastable. Below pH 5·5, polyvanadate solutions on heating or long standing precipitate insoluble products such as $K_2V_6O_{16}$ and $CaV_6O_{16}{\cdot}9H_2O$ (hewettite) (Marvin, unpublished data). The tendency of vanadates to form high molecular weight complexes in acid solutions is very similar to that of the molybdates and tungstates. These form isopoly ions in solutions of pH 3 to 6 such as $Mo_7O_{24}^{-6}$, $Mo_8O_{20}^{-4}$ and $H_{10}W_{12}O_{46}^{-20}$. The structures of these complexes are known, but no relation has been found between the structure of the polyvanadate ion and the polymolybdate and polytungstate compounds. Laboratory investigations of compounds of this type are hampered by the sluggishness with which the condensation and decomposition reactions occur in solution. Sometimes, many hours are required for a freshly prepared solution of a poly-ion to reach a stable condition.

Quadrivalent vanadium

Ducret (1951) gives acid–base titration curves for quadrivalent vanadium. At low pH the ion in the blue solution is vanadyl, VO^{+2}, which behaves like a simple metallic cation. It hydrolyses to form $VO(OH)^+$ according to the reaction (Rossotti and Rossotti, 1955):

$$VO^{+2} + H_2O \rightarrow VO(OH)^+ + H^+$$

Further hydrolysis results in precipitation of the hydroxide:

$$VO(OH)^+ + H_2O \rightarrow VO(OH)_2(s) + H^+$$

At a $VO(OH)^-$ content of 0·01 molar, the precipitation pH calculated from the free energy of formation (as illustrated earlier) of the anhydrous oxide is 3·5 (Fig. 1, Table 1). This difference in precipitation pH may be ascribed to the hydration free energy of V_2O_4:

$$V_2O_4(s) + 2H_2O \rightarrow 2VO(OH)_2(s) \qquad \Delta F^\circ = 4{\cdot}1 \text{ kcal}$$

Garrels (1953) estimated that the free energy of hydration would be 2 kcal or less: the new data show an energy difference of more than twice this amount. It is not known whether the rate of conversion of hydroxide to anhydrous oxide is finite; the hydroxide is always produced experimentally, and the stable anhydrous oxide has not been found in nature.

As pH is further increased, the hydroxide dissolves to form an anion, and the solution turns brown-red:

$$4VO(OH)_2(s) \rightarrow V_4O_9^{-2} + 3H_2O + 2H^+$$

The free energy of the vanadite ion (written tentatively as $V_4O_9^{-2}$) is derived from that of $VO(OH)_2$ and the precipitation point of pH 8·0 observed by Ducret.

Trivalent vanadium

Trivalent vanadium dissolves in acid to form V^{+3} in blue-green solution. It hydrolyses to $V(OH)^{+2}$ before the grey-black hydroxide precipitates from 0·01 molar

solution at pH 4; according to free energy relations, the anhydrous oxide should precipitate at equilibrium at pH 3. No extensive experiments have been made to see if a solution held in the pH 3–4 interval will eventually precipitate the anhydrous oxide. The free energy of hydration, based on the precipitation pH of the hydroxide and the published free energy of the anhydrous oxide, is:

$$V_2O_3(s) + 3H_2O \rightarrow 2V(OH)_3(s) \qquad \Delta F^\circ = 5{\cdot}1 \text{ kcal}$$

Thus, V_2O_3 is more stable than $V(OH)_3$, and is analogous in this respect to Fe_2O_3 and Mn_2O_3. The apparent difficulty in obtaining artificially the anhydrous oxide, or perhaps a compound such as $V_2O(OH)_4$ or VO(OH), is not surprising in view of the fairly small free energy change on hydration. The free energy of montroseite, VO(OH), is unknown, but its prevalence in the Colorado Plateau sandstones, and the absence of V_2O_3, suggests that it is the most stable hydrated phase at the temperature of formation. At present, we can only assume that the energy of formation of montroseite from V_2O_3 is quite small, without predicting whether at the lower temperatures it is positive or negative. An estimated stability field for VO(OH) is indicated by the dotted lines in Fig. 2, and is used in interpreting the mineral system in Fig. 4, described in later sections.

The hydroxide shows no amphoteric behaviour in the pH range up to 14. Trivalent vanadium ions and compounds are notably unstable with respect to the atmosphere: even the natural oxide montroseite alters at an appreciable rate in the laboratory.

Bivalent vanadium

Bivalent vanadium will decompose water at 25°C under all pH conditions, and therefore, as Garrels (1955) has pointed out, it is not likely to occur in nature.

The preceding paragraphs have discussed pH boundaries for vanadium within its several valence states; it remains to be shown how the sloping boundaries between these valence domains are obtained.

Boundaries between ions

In the case where the solubility of the ionic species of vanadium in different valence states exceeds 0·01 molar, so that only dissolved species are represented, the boundary is calculated from equations exemplified by the V^{+2}–V^{+3} relation:

$$V^{+2} \rightarrow V^{+3} + e^-$$

$$\Delta F^0 = nE^0\mathbf{F}$$

where E^0 is the standard electrode potential, **F** is the Faraday, and n the number of electrons involved. Thus E^0 is obtained from ΔF^0, and E_h is obtained from:

$$E_h = E^0 + \frac{0{\cdot}059}{n} \log \frac{(V^{+3})}{(V^{+2})} \qquad (25°C)$$

The further condition is imposed that (V^{+3}) and (V^{+2}) (activities) are equal. As can be determined from the equation, or from Fig. 1, the boundary between these two species is simply E^0, and extends parallel to the pH axis.

The slope of the V^{+3}–VO^{+2} boundary results from the necessity of including water and hydrogen ion in the half-cell reaction:

$$V^{+3} + H_2O \rightarrow VO^{+2} + 2H^+ + e^-$$

The E_h equation becomes:

$$E_h = E^0 + 0{\cdot}059 \log \frac{(VO^{+2})}{(V^{+3})} - 2 \times 0{\cdot}059 \text{ pH}$$

The pH term causes a downward slope of the boundary from left to right, with an intercept of E^0 at pH 0.

Boundaries between solids

Where two solids containing vanadium in different valence states are juxtaposed, the boundary is determined by equations such as that relating V_2O_3 and V_2O_4:

$$V_2O_3(s) + H_2O \rightarrow V_2O_4(s) + 2H^+ + 2e^-$$

$$E_h = E^0 + \frac{0{\cdot}059}{2} \log (H^+)^2$$

or:

$$E_h = E^0 - 0{\cdot}059 \text{ pH}$$

Boundaries between a solid and an ion

Several cases occur involving a solid containing vanadium in one valence and solution containing dissolved vanadium in a species of higher or lower valence. For example. V_2O_3 dissolves to form $V_4O_9^{-2}$ as the oxidation potential is increased in alkaline solution. The equation is:

$$2V_2O_3(s) + 3H_2O \rightarrow V_4O_9^{-2} + 6H^+ + 4e^-$$

$$E_h = E^0 + \frac{0{\cdot}059}{4} \log [V_4O_9^{-2}] - \frac{6}{4} \times 0{\cdot}059 \text{ pH}$$

The specific position of the line thus is fixed by knowledge of E^0, pH, and the stipulation that $[V_4O_9^{-2}]$ is 0·01 molar.

Considerable uncertainty attends the boundaries drawn between V_2O_4 and the vanadates. As shown on Fig. 1, mixed oxides containing both quadrivalent and quinquevalent vanadium occur in this position. The possibility presents itself that these mixed oxides may be regarded as "vanadyl vanadates", but the few structures of these compounds that have been published indicate that they have no saltlike character (e.g. NaV_6O_{15}, Wadsley, 1955). No thermodynamic data are available for them, but there is no evidence to indicate that their appearance will appreciably shift the precipitation boundary from that shown.

Effect of temperature

The effect of temperature on the field boundaries shown in Fig. 1 cannot be calculated with assurance in the absence of data on heat capacities of the species involved. However, the temperature coefficient at 25°C can be found and used to

determine the trend and probable change of boundaries over a limited temperature change. Changes in boundaries can be calculated in terms of $\partial E^\circ/\partial T$ or $\partial \Delta F^\circ/\partial T$:

$$\frac{\partial E^\circ}{\partial T} = -\frac{1}{\mathbf{F}n}\Delta S^\circ$$

$$\frac{\partial \Delta F^\circ}{\partial T} = -\Delta S^\circ$$

In general, a temperature change of a few tens of degrees would appear to have little effect on the general fields of stability. For example, for the reaction:

$$V_2O_3 + H_2O \rightarrow V_2O_4 + 2H^+ + 2e^-$$

using entropy data given by Latimer (1952) for V_2O_3 and V_2O_4, the change in entropy is:

$$\Delta S^\circ = -15{\cdot}65 \text{ cal/mole/°C}$$

whence

$$\frac{\partial E^\circ}{\partial T} = \frac{15{\cdot}65}{2 \times 23{,}060} = 0{\cdot}00034 \text{ volt/°C}$$

Thus, for a 30°C rise in temperature, assuming ΔS° constant, E° would be raised only 0·01 volt, giving rise to a corresponding change in the phase boundary. Such changes are fairly typical of the oxidation reactions.

For the precipitation-pH boundaries, changes are of the order of −0·01 to −0·02 pH units/°C, using estimated entropies for the ions involved. In other words, the precipitation boundaries of the oxides move to lower pH values with rising temperature, and with approximately the same coefficient as for the change of pH of pure water alone. Unfortunately, neither ΔH nor ΔS values can be obtained at present to determine the direction of migration of the boundary between V_2O_4 and $V_4O_9^{-2}$.

Regions of Thermodynamic Stability for the Vanadium Minerals

The first oxide of vanadium which was recognized as a distinct mineral species was montroseite, VO(OH) or $V_2O_3 \cdot H_2O$ (Weeks *et al.*, 1953). Its discovery showed that, the vanadium minerals of the Colorado Plateau span the whole range of oxidation states of vanadium consistent with an aqueous environment. Since montroseite was described, many new mineral species have been discovered and characterized representing vanadium in all valence states from (III) to (V). When each species is examined with respect to its probable thermodynamic properties, it is found that it can be assigned to a particular field of the equilibrium diagram with little ambiguity. In the following paragraphs, a number of vanadium minerals are reviewed from the point of view of their stability properties. Fig. 4 shows the basic equilibrium diagram of Fig. 2, with these minerals indicated on it, each in its appropriate range of stability.

Montroseite: $V_2O_3 \cdot H_2O$ or VO(OH) (Weeks *et al.*, 1953). As shown in Fig. 2, there is an extended portion of the hydrated V_2O_3 stability field above the water

decomposition boundary between pH 4 and pH 10. As has been noted earlier, this region probably expands slightly upward and to the left at higher temperatures. Montroseite is formed in this region.

Paramontroseite: V_2O_4 or VO_2 (Evans and Mrose, 1955). This mineral is derived by solid state oxidation from montroseite; it is probably metastable and has no place on the aqueous equilibrium diagram. Nevertheless, it is important in the weathering process, because it provides a path for the breakdown of the chemically resistant montroseite. It probably always forms an intermediate first step in the weathering of montroseite.

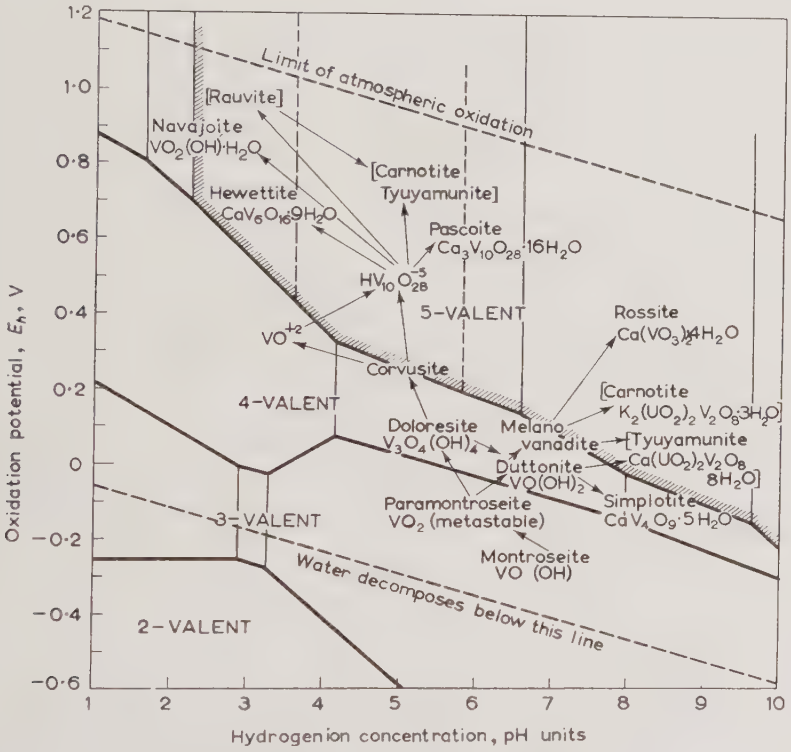

Fig. 4. Aqueous equilibrium diagram for vanadium with the stability regions of various vanadium minerals indicated. Arrows show expected and observed alteration sequences under weathering conditions. Shaded boundary indicates stability region of carnotite and tyuyamunite, which supersede all other vanadium species in the presence of sexivalent uranium.

Doloresite: $3V_2O_4\cdot 4H_2O$ or $V_3O_4(OH)_4$ (Stern *et al.*, 1957). This species is common replacing montroseite in partially oxidized ores. Its mode of occurrence indicates that it results from solid state alteration of montroseite (or paramontroseite) under conditions in which vanadium is not dissolved.

Duttonite: $V_2O_4\cdot 2H_2O$ or $VO(OH)_2$ (Thompson *et al.*, 1957). This species is a hydrated quadrivalent phase, occurring as crystalline crusts lining cavities. It evidently forms from solution in ground waters carrying vanadium not yet oxidized beyond the quadrivalent state.

Simplotite: $CaO{\cdot}2V_2O_4{\cdot}5H_2O$ (Thompson *et al.*, 1958). Though its formula may be written $CaV_4O_9{\cdot}5H_2O$, simplotite is green in colour and does not represent fixation of the soluble brown-red vanadite ion. Its structure appears to be a complex sheet related to that of autunite, and as yet has no synthetic analogue. It is commonly associated with duttonite but appears to indicate a relatively alkaline environment.

Corvusite: $CaO{\cdot}xV_2O_4{\cdot}yV_2O_5{\cdot}nH_2O$. This mineral has distinct physical properties but has not been defined chemically within the above general formula. The valence apparently can vary without appreciable alteration of the structure so that it may be either inherently non-stoichiometric or an intimate mixture of two or more closely related phases. The ratio $x : y$ is usually about 1 : 5 or 1 : 6. It is associated with acid environments and evidently hovers near the top of the V_2O_4 field.

Melanovanadite: $2CaO{\cdot}2V_2O_4{\cdot}3V_2O_5{\cdot}nH_2O$. Although this species also has not been clearly defined chemically, it is entirely distinct from corvusite. It is found in alkaline environments and appears to be associated with the metavanadate field, while corvusite is associated with the polyvanadate field.

Navajoite: $V_2O_5{\cdot}3H_2O$ or $VO_2(OH){\cdot}H_2O$ (Weeks *et al.*, 1955). Navajoite has not been synthesized, but it apparently corresponds to the hydrated V_2O_5 field. It has a crystal structure closely related to that of corvusite and hewettite.

Hewettite: $CaO{\cdot}3V_2O_5{\cdot}9H_2O$ or $CaV_6O_{16}{\cdot}9H_2O$. Hewettite is an insoluble product of the more acid side of the polyvanadate field, forming below pH 5·5. Its structure consists of a sheet arrangement closely similar to that of navajoite and corvusite.

Pascoite: $3CaO{\cdot}5V_2O_5{\cdot}16H_2O$. This mineral has formerly been incorrectly described as $2CaO{\cdot}3V_2O_5{\cdot}11H_2O$ (Palache *et al.*, 1951, p. 1055) but actually is a soluble salt of the orange polyvanadate complex, $Ca_3V_{10}O_{28}{\cdot}16H_2O$ (Evans *et al.*, 1955).

Hummerite: $K_2Mg_2V_{10}O_{28}{\cdot}16H_2O$ (Weeks *et al.*, 1953), also is a soluble polyvanadate.

Rossite: $Ca(VO_3)_2{\cdot}4H_2O$. Rossite is a metavanadate, and is easily synthesized from neutral solutions.

Metarossite: $Ca(VO_3)_2{\cdot}2H_2O$ is the dehydration product of rossite.

Carnotite: $K_2(UO_2)_2V_2O_8{\cdot}3H_2O$. The least soluble vanadium complex (except possibly montroseite and the silicates) is carnotite and its analogues. It decomposes below pH 2·2 but is stable at the expense of all other quinquevalent vanadium minerals at higher pH values. The crystal structure does not contain orthovanadate groups as proposed by Sundberg and Sillén (1949), but has been found by recent work (Barton and Appleman, 1957; Appleman and Evans, 1958) to have structural and chemical properties of a metavanadate. The structure contains $V_2O_8^{\ 6}$ groups with vanadium in five-fold co-ordination (as in $KVO_3{\cdot}H_2O$).

Tyuyamunite: $Ca(UO_2)_2V_2O_8{\cdot}8H_2O$ is the calcium chemical analog of carnotite.

Rauvite: $xUO_3{\cdot}yV_2O_5{\cdot}zH_2O$. In acid solutions deficient in metal cations, rauvite is formed as an insoluble colloidal product of variable composition with y usually somewhat greater than x. It is believed to have a structural relationship to the sheet structure of carnotite, and may be a precursor to the formation of carnotite in very acid environments.

Vanadium Mineral Paragenesis under Weathering

A typical partially oxidized ore body in the central Colorado Plateau region consists of bluish-black vanadium oxide disseminated through the sandstone in bands. Locally, sometimes in conjunction with woody debris, the vanadium oxide ore is concentrated into pods or blue-black "eyes". In the centre of these pods, in fresh openings, jet-black montroseite is often still preserved. Outward from these cores the vanadium mineral assemblage changes continuously to a more oxidized state. This change in state of oxidation is accompanied by characteristic colour changes. Generally speaking, the trivalent and trivalent–quadrivalent minerals are black, the quadrivalent–quinquevalent minerals are dark blue, green or brown, and the fully oxidized minerals are lighter brown, yellow or red-orange. Sometimes these three zones are separated by sharp boundaries. Pyrite is usually present, creating locally rather strongly acid conditions under weathering. Good examples of these relations can be seen at the Bitter Creek Mine and the J. J. Mine in Montrose County, Colorado, and the Monument No. 2 Mine in the Monument Valley district of Arizona.

More rarely, the environment of oxidation is slightly alkaline, in regions where pyrite is absent and calcite is abundant. The most notable example of this situation is the Peanut Mine in Bull Canyon, Montrose County, Colorado. In this case, a wholly different series of minerals is found in the oxidation sequence.

Petrologic and paragenetic studies almost always indicate that the primary vanadium minerals are silicates and the oxide, montroseite. It is very likely that all of the other vanadium minerals in the sandstones, including carnotite, were derived from montroseite. Vanadium bound in silicates apparently is not released by weathering and therefore these minerals, although important commercially, are incidental to the present discussion.

The first stage in the oxidation of montroseite under any conditions is the formation of paramontroseite. The conversion is brought about by a solid state reaction in the presence of oxygen either in the air or in groundwater as explained by Evans and Mrose (1955). Reaction is very rapid, and fresh montroseite specimens alter quickly in the open air. Evans and Mrose have concluded that paramontroseite itself is metastable, owing its existence purely to the crystal structural control of the original montroseite. In the presence of water, paramontroseite is quickly decomposed and new hydrated oxides of quadrivalent and quinquevalent vanadium are formed. This process gives rise to an interesting sequence in which one anhydrous variety of V_2O_4 (paramontroseite) is apparently less stable than various hydrated hydroxides (e.g. duttonite, $V_2O_4 \cdot 2H_2O$), which in turn are thermodynamically less stable than the normal anhydrous oxide having a distorted rutile structure. No trace of the stable anhydrous oxide has yet been found in nature; therefore, the rate of conversion of the hydrated oxides is apparently neglible, even in terms of earth processes.

If further oxidation is retarded (especially if the ore is kept submerged below the water table where the supply of oxygen is limited), two other quadrivalent minerals may form in place of the paramontroseite—doloresite or duttonite. Doloresite is observed as a paramorphic replacement of the paramontroseite, with remnants of the latter usually remaining (Stern *et al.*, 1957). Duttonite forms as drusy crystals

in fissures in the sandstone and therefore apparently represents quadrivalent vanadium transported a short distance at least from the site of the paramontroseite source. Duttonite and paramontroseite are the starting points of two branches in the vanadium oxidation sequence, one acid and the other alkaline.

The sequence of vanadium minerals is easily followed in the acid suite. Adjacent to the doloresite–paramontroseite crystalline aggregates are usually found fibrous brown or bluish-black seams of corvusite. Commonly, the intermediate quadrivalent–quinquevalent vanadium oxides form earthy bluish or greenish masses of indeterminate constitution ("blue-black ore"). These oxides are dissolved through leaching of the concentrated ores by acid waters, and the vanadium is washed into the adjacent sandstone. The oxide "eyes" are thus often coated with bright orange crusts of pascoite. Occasionally, dark green "pascoite" is found, isostructural with the ordinary orange variety, indicating that the polyvanadate complexes may form with quadrivalent vanadium at least partly replacing quinquevalent vanadium. The leaching solutions are evidently sufficiently acid to carry appreciable amounts of vanadyl ion (VO^{+2}), but this ion is quickly oxidized by air if the pH is raised, as when it passes into the surrounding rock and reacts with calcite. Pascoite is metastable with respect to hewettite below about pH 5·5 and probably has only a transitory existence.

In the alkaline environment typified by the Peanut Mine, duttonite and simplotite are found. Since duttonite has been found abundantly only at the Peanut Mine where the ores are largely submerged below the water table, it is likely that it will form only when the quadrivalent vanadium is protected from active oxidation by the atmosphere. When further oxidation does occur, melanovanadite is likely to result. In the presence of high calcium concentrations, simplotite is formed, and at the end of the oxidation sequence, rossite.

The two branches in the oxidation sequence, acid and alkaline, may be evident in fairly close proximity, especially in the vicinity of sulphide-bearing oxide ore pods. As soon as the original montroseite is oxidized to paramontroseite, the resulting quadrivalent vanadium becomes appreciably soluble. At the original site, the oxidized minerals follow the pattern of the acid branch described above, but at the same time much of the vanadium will be transported into the surrounding sandstone where neutral or slightly alkaline conditions prevail as a result of the calcite cement. In these adjacent regions, therefore, melanovanadite, simplotite, and in the fully oxidized state, rossite, all characteristic of the alkaline branch, are frequently found. In the quinquevalent state vanadium does not form silicates and, being soluble, is washed away rapidly, except in the presence of uranium.

As Garrels (1955) has shown, by the time the oxidation of quadrivalent vanadium begins, the uranium, which was originally present as uraninite and coffinite (Stieff *et al.*, 1956), is completely oxidized to the sexivalent state. No synthetic or natural compounds of uranium and trivalent or quadrivalent vanadium have ever been found, and apparently the properties of the two elements in reducing conditions are independent of each other as far as solubilities and mineral formation are concerned. When vanadium reaches the quinquevalent state in the presence of uranyl ion (UO_2^{+2}), the insoluble carnotite or slightly soluble tyuyamunite becomes the stable phase at pH values above 2·2 (Marvin, private communication). Their

stability range is indicated by the shaded boundary in Fig. 4, and all other vanadium minerals in this range become metastable with respect to the uranium complex. The ready formation of carnotite from acid solutions has been a puzzle in view of the crystal structure determination of Sundberg and Sillén (1949), which indicated that the vanadium is bound in it as orthovanadate groups (VO_4^{-3}), because in such solutions the orthovanadate concentration is exceedingly small (less than 10^{-12} moles/l. at pH 6). New studies (Appleman and Evans, 1958) have shown that the proposed structure is incorrect, and that vanadium is in five-fold co-ordination in the carnotite structure in $V_2O_8^{-6}$ groups. Also, it is found (Barton and Appleman, 1957) that carnotite behaves chemically like a metavanadate, so that its association with neutral or slightly acid environments is fully explained.

When the environment is strongly acid, rauvite may be formed. The role of this unusual mineral in the paragenetic sequence is uncertain, but it may have an intermediate position between the formation of the polyvanadate complex and carnotite under very acid conditions. The structure of rauvite cannot be directly determined since it is characteristically non-crystalline, at least in three dimensions; but it is felt that it probably consists of a random stacking of a sheet type of structure, which is related in some way to the sheet structure of carnotite.

In concluding this survey of the weathering paragenesis of vanadium minerals, it may be said that all field or microscopic observations of petrology and mineral associations studied, without any significant exceptions, support the weathering scheme derived herein from the thermodynamic properties of vanadium.

Implications of the Equilibrium Diagram on the Problem of Ore Deposition

While the paragenesis of the vanadium and uranium minerals under weathering conditions on the Colorado Plateau now seems fairly well defined, the manner of deposition of the primary montreseite–uraninite–coffinite ore is still an unsolved problem. Accepting the current hypothesis that the ores were brought in by mineralizing solutions at 55–110°C (Coleman, 1957), it appears probable from the thermodynamic considerations that they could not have been carried in solution in the reduced state in which they were deposited. Trivalent vanadium is too insoluble for transport except at pH values considerably below those expected for such solutions; a similar situation holds for quadrivalent uranium. Consequently, the vanadium and uranium must have been carried in more oxidized state, and deposited under the action of reducing agents, such as divalent sulphur or the wood debris commonly enclosed in the sandstone. On the other hand the E_h could not have been sufficiently high to permit all vanadium to be in the quinquevalent state, as the small solubility of carnotite would prevent transport. Therefore the best estimate is that vanadium was carried as the quadrivalent $V_4O_9^{-2}$, which, so far as is known, does not interact with sexivalent uranium. These considerations suggest, referring to Fig. 2, that the mineralizing solutions had a pH of about 9 and an oxidation potential of about −0·1 volt. Even if the transport and deposit of vanadium and uranium can be accounted for under the conditions, the presence of pyrite or marcasite, which petrologically appears to be contemporary with montroseite,

poses a problem because of the presumably low solubility of iron in this thermodynamic range.

The only certain conclusion that can be made now is that the problem of ore deposition on the Colorado Plateau will be solved at least partly through the further study and refinement of the thermodynamic equilibrium properties, especially in the region suggested above.

Summary

(1) The published thermodynamic and chemical data for vanadium have been used to construct an equilibrium diagram showing the stability ranges of the various solution and solid phases on the pH-oxidation potential field. The effects of heat of hydration and elevated temperatures on the relations determined at 25°C are estimated and found to be minor.

(2) The conditions of stability on the equilibrium diagram of the various vanadium minerals of the Colorado Plateau have been determined from mineral association and analogy to artificial compounds.

(3) The mineralogy of vanadium on the Colorado Plateau, interpreted in the light of the equilibrium diagram, indicates that nearly all the vanadium minerals (except some silicates) were derived from the primary mineral montroseite by weathering processes.

(4) The weathering process has been shown to follow two sequences, an acid branch and an alkaline branch. The acid branch occurs in primary oxide concentrations where pyrite is present and follows the sequence: montroseite, paramontroseite, doloresite, corvusite, pascoite, hewettite, carnotite. The alkaline branch obtains in regions where pyrite is absent and follows the sequence: montroseite, paramontroseite, duttonite, simplotite, melanovanadite, rossite, carnotite.

(5) The hydrothermal deposition of the primary montroseite–coffinite–uraninite ore has been considered briefly in the light of the equilibrium diagram.

References

Appleman D. E. and Evans H. T., Jr. (1958) Crystal structure of carnotite. *Acta Cryst. Camb.* **10,** 765.

Baker H. (1885) The orthovanadates of sodium and their analogs. *J. Chem. Soc.* **47,** 353–361.

Barton P. B., Jr. and Appleman D. E. (1957) Crystal chemistry of carnotite. *Advances in Nuclear Engineering,* Vol. II: *Proceedings of the Second Nuclear Engineering and Science Congress. Philadelphia* (Edited by Dunning J. R. and Prentice B. R.), Pt. 2, pp. 294–299. Pergamon Press, New York.

Christ C. L., Clark J. R. and Evans H. T., Jr. (1954) The crystal structure of potassium metavanadate monohydrate, $KVO_3.H_2O$. *Acta Cryst. Camb.* **7,** 801–807.

Coleman R. G. (1957) Mineralogical evidence on the temperature of formation of the Colorado Plateau uranium deposits. *Econ. Geol.* **52,** 1–4.

Deltombe E., de Zoubov N. and Pourbaix M. (1956) Comportement electrochimique du vanadium. Diagramme d'équilibre tension–pH du système V–H_2O a 25°C. *Rapport technique No.* 29 Centre Belge d'Etude de la Corrosion, Bruxelles.

Ducret L. P. (1951) Contribution a l'étude des ions des valence quatre et cinq du vanadium. *Ann. Chim.* **6,** 705–776.

Evans H. T., Jr. and Mrose M. E. (1955) A crystal chemical study of montroseite and paramontroseite. *Amer. Min.* **40,** 861–875.

Evans H. T., Jr., Mrose M. E. and Marvin R. (1955) Constitution of the natural and artificial decavanadates. *Amer. Min.* **40,** 314–315 (Abstract).

Fischer R. P. and Hilpert L. S. (1952) Geology of the Uravan mineral belt. *U.S. Geol. Survey Bull.* 988-A.

Garrels R. M. (1953) Some thermodynamic relations among the vanadium oxides, and their relation to the oxidation state of the uranium ores of the Colorado Plateaus. *Amer. Min.* **38,** 1251–1265.

Garrels R. M. (1955) Some thermodynamic relations among the uranium oxides and their relation to the oxidation states of the uranium ores of the Colorado Plateaus. *Amer. Min.* **40,** 1004–1021.

Gruner J. W., Gardiner L. and Smith D. K., Jr. (1953) *Annual report for July* 1, 1952 *to March* 31, 1953. U.S. Atomic Energy Comm. RME–3044, Tech. Inf. Service, Oak Ridge, Tenn.

Hess F. L. (1933) Uranium, vanadium, radium, gold, silver, and molybdenum sedimentary deposits. *Ore Deposits of the Western States, Lindgren Memorial Volume,* pp. 450–481. Amer. Inst. of Mining and Metallurgical Engineers, New York.

Jander G. and Jahr K. F. (1933) Aufbau und Abbau Höhermolekularer anorganischer Verbindungen in Lösung an Beispiel der Vanadinsäure, Polyvanadate und Vanadansalze. *Z. Anorg. Chem.* **212,** 1–20.

Krumbein W. C. and Garrels R. M. (1952) Origin and classification of chemical sediments in terms of pH and oxidation-reduction potentials. *J. Geol.* **60,** 1–33.

Latimer W. M. (1952) *Oxidation Potentials* (2nd Ed.). Prentice-Hall, New York.

McKelvey V. E., Everhart D. L. and Garrels R. M. (1955) Origin of uranium deposits. *Econ. Geol., Fiftieth Anniversary Volume* Pt. I, pp. 464–533.

Palache C., Berman H. and Frondel C. (1951) *Dana's System of Mineralogy* (7th Ed.) Vol. II. Wiley, New York.

Pourbaix M. J. N. (1949) *Thermodynamics of Dilute Aqueous Solutions.* Arnold, London.

Rossotti F. J. C. and Rossotti H. (1955) Studies on the hydrolysis of metal ions. XII: The hydrolysis of vanadium (IV) ion. *Acta Chem. Scand.* **9,** 1177–1192.

Rossotti F. J. C. and Rossotti H. (1956) Equilibrium studies of polyanions. I: Isopolyvanadates in acidic media. *Acta Chem. Scand.* **10,** 957–984.

Stern T. W., Stieff L. R., Evans H. T., Jr. and Sherwood A. M. (1957) Doloresite, a new vanadium oxide mineral from the Colorado Plateau. *Amer. Min.* **42,** 587–593.

Stieff L. R., Stern T. W. and Sherwood A. M. (1956) Coffinite, a uranous silicate with hydroxyl substitution: A new mineral. *Amer. Min.* **41,** 675–688.

Sundberg I. and Sillén L. G. (1949) On the crystal structure of KUO_2VO_4 (synthetic anhydrous carnotite). *Ark. Kemi* **1,** 337–351.

Syneček V. and Hanic F. (1954) The crystal structure of ammonium metavanadate. *Phys. J. Czech.* **4,** 120–130.

Thompson M. E., Roach C. H. and Meyrowitz R. (1957) Duttonite, a new quadrivalent vanadium oxide from the Peanut mine, Montrose County, Colorado. *Amer. Min.* **42,** 455–460.

Thompson M. E., Roach C. H. and Meyrowitz R. (1958) Simplotite, a new quadrivalent vanadium mineral from the Colorado Plateau. *Amer. Min.* **43,** 16–24.

Wadsley A. D. (1955) The crystal structure of $Na_{2-x}V_6O_{15}$. *Acta Cryst. Camb.* **8,** 695–701.

Weeks A. D., Cisney E. and Sherwood A. M. (1953) Montroseite, a new vanadium oxide from the Colorado Plateaus. *Amer. Min.* **38,** 1235–1241.

Weeks A. D. and Thompson M. E. (1954) Identification and occurrence of uranium and vanadium minerals from the Colorado Plateaus. *U.S. Geol. Survey Bull.* 1009–B, 13–62.

Weeks A. D., Thompson M. E. and Sherwood A. M. (1955) Navajoite, a new vanadium oxide from Arizona. *Amer. Min.* **40,** 207–215.

Geochimica et Cosmochimica Acta, 1958, Vol. 15, pp. 150 to 152. Pergamon Press Ltd., London

GEOCHEMICAL NOTE

Caesium in chondrites

(*Received* 3 *May* 1958)

RECENTLY caesium has been determined in stony meteorites by two analytical methods. Neutron activation analyses made at Harwell (CABELL and SMALES, 1957) gave results for seven chondrites in the range 0·01–0·1 p.p.m., whereas the determinations made by GORDON, FRIEDMAN and EDWARDS (1957) by an isotope dilution method were significantly higher, the values being 0·5 and 0·9 p.p.m. for two chondrites and 0·3 p.p.m. for an achondrite. This discrepancy is unfortunate in attempting to define the cosmic abundance of caesium.

To resolve this problem, caesium has again been determined in seven chondrites, using the mass spectrometric isotope dilution method, but avoiding the large "blank" uncertainty of GORDON, FRIEDMAN and EDWARDS' method by replacing the initial distillation step for the alkali metal separation by a more conventional acid attack. The samples include two examined by CABELL and SMALES, and one by GORDON *et al.* These results are recorded in Table 1.

Table 1. The caesium contents of seven chondrites determined by the mass spectrometric isotope dilution method

Sample	Results (p.p.m. Cs)			Mean value and uncertainty*
Homestead	$0{\cdot}05_5$;	$0{\cdot}05_5$		$0{\cdot}05_5 \pm 0{\cdot}01$
Bluff	<0·01;	<0·01		<0·01
Holbrook	0·278;	0·284;	0·287	0·283 ± 0·009
Chandakapur	0·201;	0·202;	0·209	0·204 ± 0·008
Ochansk	0·114;	0·121;	0·124	0·120 ± 0·008
Bjurböle	0·101;	0·112;	0·112	0·109 ± 0·009
Château-Renard	0·009;	0·010;	0·010	$0{\cdot}009_5 \pm 0{\cdot}001_3$

* The uncertainty is in each case the sum of the standard deviations of the set of determinations, the calibration of the tracer, and the blank correction.

The values which were found for Homestead and Bluff by neutron activation analysis (CABELL and SMALES, 1957) are 0·07 p.p.m. and 0·01 p.p.m. respectively; the agreement between these and the results in Table 1 is satisfactory. The values found by Gordon *et al.* however, are Holbrook 0·49 p.p.m., Beardsley 0·91 p.p.m., Pasamonte 0·28 p.p.m., and for the olivine from Finmarken 0·20 p.p.m. They used a distillation process (EDWARDS and UREY, 1955) to extract the alkali metals and stated that the blank for this stage was uncertain, but the caesium found in the olivine from Finmarken could be taken as the upper limit for contamination. With this correction their value for Holbrook becomes

0·29 p.p.m., which agrees well with the value reported here, i.e. 0·283 ± 0·009 p.p.m. While this comparison is not rigorous, for the determinations were made with different samples of Holbrook, it does suggest that their table of results may be somewhat misleading, and that a better view of the distribution of caesium in chondrites would be given by a combination of the results reported in this note with those found by neutron activation analysis. Table 2 records these values, some sodium and potassium contents (Edwards and Urey, 1955; Edwards, 1955), and the rubidium concentrations. For each of samples 1, 2, 3, 4 and 11 the rubidium figure quoted is the result of a single new determination made by isotope dilution and should be accurate to at least 10 per cent; the rubidium values for the other samples have been published previously (Cabell and Smales, 1957; Webster, Morgan and Smales, 1957).

Table 2. Assembled results for alkali metals in chondrites

Sample	Cs by isotope dilution (p.p.m.)	Cs by neutron activation (p.p.m.)	Rb by isotope dilution (p.p.m.)	Rb by neutron activation (p.p.m.)	K (%)	Na (%)
1 Holbrook	0·28	—	2·3	—	0·088	0·73
2 Chandakapur	0·20	—	3·5	—	—	—
3 Ochansk	0·12	—	2·1	—	0·075	0·64
4 Bjurböle	0·11	—	2·9	—	0·086	0·70
5 Limerick	—	0·10	—	2·3	—	—
6 Forest City	—	0·10	2·9	3·0	0·084	0·69
7 Modoc	—	0·08	—	3·0	0·083	0·69
8 Homestead	$0·05_5$	0·07	—	3·1	0·090	0·72
9 Ness County	—	0·04	—	2·9	0·077	0·61
10 Long Island	—	0·01	—	2·1	—	—
11 Château-Renard	0·01	—	2·9	—	—	—
12 Bluff	<0·01	0·01	—	1·0	0·073	0·60

Ness County, Long Island and Bluff are *finds*, and one possible explanation of their low caesium contents is that they have been altered by leaching (Urey, 1957); Château-Renard however is a *fall*, but it also has a low caesium content. Also if leaching had caused the observed range of caesium concentrations, the rubidium values might be expected to show a similar variation. In fact, apart from Bluff, there is no systematic relation between rubidium and caesium contents.

Another explanation lies in the geochemical behaviour of caesium. The results listed for chondrites in Table 2 show that the potassium values are very nearly constant, but those for caesium are distributed over a wide range; those for rubidium show a much smaller variation and have little relation to those for caesium. In a recent paper Taylor and Heier (1958) give the concentrations of the alkali elements in over forty potash feldspars, and for caesium and rubidium their results show a very similar distribution to that reported here for chondrites. They point out that caesium shows little geochemical coherence with potassium and attribute this to the influence of its greater ionic radius.

It would seem that the results in Table 2 show a real range of caesium contents of from <0·01 p.p.m. to 0·3 p.p.m. The average for these twelve chondrites is 0·09 p.p.m., and if

a value of 0·7 p.p.m. is assumed for Beardsley, the average for thirteen chondrites is 0·14 p.p.m. These are significantly lower than the value of 0·4 p.p.m. interpolated by Suess and Urey (1956) for the cosmic abundance of caesium.

Acknowledgements—We would like to express our gratitude for the provision of meteorite specimens to Drs. W. H. Pinson and L. F. Herzog, Massachusetts Institute of Technology; Dr. B. H. Mason, New York American Museum of Natural History; and Dr. E. A. Vincent, Oxford University Museum.

Atomic Energy Research Establishment,
Harwell, Didcot, Berks.

R. K. Webster
J. W. Morgan
A. A. Smales

References

Cabell M. J. and Smales A. A. (1957) *Analyst* **82,** 390.
Edwards G. and Urey H. C. (1955) *Geochim. et Cosmochim. Acta* **7,** 154.
Edwards G. (1955) *Geochim. et Cosmochim. Acta* **8,** 285.
Gordon B. M., Friedman L. and Edwards G. (1957) *Geochim. et Cosmochim. Acta* **12,** 170.
Suess H. E. and Urey H. C. (1956) *Rev. Mod. Phys.* **28,** 53.
Taylor S. R. and Heier K. S. (1958) *Geochim. et Cosmochim. Acta* **13,** 293.
Urey H. C. (1957) Private communication.
Webster R. K., Morgan J. W. and Smales A. A. (1957) *Trans. Amer. Geophys. Un.* **38,** 543.

Geochimica et Cosmochimica Acta, 1958, Vol. 15, pp. 153 to 161. Pergamon Press Ltd., London

LETTERS TO THE EDITORS

On the isotopic composition of the ammonia and the nitrate ion in rain

(*Received* 3 *February* 1958)

In a recent issue of your journal Hoering (1957) reports data on the isotopic composition of ammonia-N and nitrate-N in nine rainwater samples collected in Arkansas. The importance of such studies can hardly be overemphasized as the atmosphere has a dominating role in the circulation of nitrogen compounds in nature. Hoering finds a considerable day-to-day variation in the enrichments δ of N^{15} relative to the inert nitrogen in the atmosphere but a strong positive correlation between δ_{H_3N} and $\delta_{NO_3^-}$. This fact leads him to suspect that the nitrate originates by oxidation of ammonia and postulating this process he calculates a kinetic isotope effect, β, which is simply the ratio of the rate constants in the oxidation of H_3N^{14} and H_3N^{15}. The β-values obtained vary from 1·002 to 1·008 with an average of 1·004. Hoering regards this as reasonably constant, which of course is a matter of opinion, and takes the constancy as an indication that the process suggested accounts for the presence of nitrate in rain. His data certainly do not seem to support the simple fixation process from molecular nitrogen, suggested so frequently in the past, because in this case as Hoering points out the enrichment in nitrate should be constant.

As the origin of the nitrate in the atmosphere is of considerable geochemical interest, Hoering's paper is of great concern, but before his hypothesis is accepted one should look for other possible processes that can cause the correlation between the enrichments of N^{15} in the ammonia and the nitrate. First, one should be aware of the fact that a rain does not remove all the nitrogen compounds from an air mass just as it does not remove all the water. The reason for this is simple. Both ammonia and nitrogen oxides occur in the gas phase in equilibrium with the liquid phase. If the liquid phase is removed by gravitational pull there is always the gaseous phase left. One may expect a fractionation effect in nitrogen isotopes between the gaseous and liquid phases, the heavier isotope being probably enriched in the liquid phase. The actual enrichment will depend upon how much of nitrogen compounds has been added and removed in the past history of the air mass and how much is being removed. So the problem is by no means simple. However, the fractionation effect would be expected to vary from day to day just as revealed in Hoering's data and as known to occur in the case of O^{18} in rain water (Dansgaard, 1953) and also deuterium in rain water (S. Epstein, California Institute of Technology, personal communication). Further, all factors causing an enrichment of N^{15} in ammonia by a certain magnitude can be expected to cause a proportional enrichment of N^{15} in nitrate, as well as effect the enrichment of any isotope to be considered. Therefore, the enrichments of N^{15} in ammonia and nitrate should be strongly correlated which in fact they are in Hoering's data. Considering such physical fractionation processes it does not seem feasible to get any indications on the origin of nitrate from isotope analyses of nitrogen compounds in rain. Probably isotope analyses on air samples—where all the nitrogen compounds are recovered—would be more decisive, especially if N_2O, which is fairly abundant, were included.

Erik Eriksson

Department of Meteorology, University of Chicago

References

Dansgaard W. (1953) The abundance of O^{18} in atmospheric water and water vapour. *Tellus* **5**, 461–469.

Hoering T. (1957) The isotopic composition of the ammonia and the nitrate ion in rain. *Geochim. et Cosmochim. Acta* **12**, 97–102.

A reply to the preceding note by E. Eriksson

(*Received* 2 *May* 1958)

An interesting alternate mechanism to account for the observed distribution of the stable isotopes of nitrogen between the ammonia and nitrate fractions of rain is proposed in the preceding note (Hoering, 1957; Eriksson, 1958). It is the purpose of this reply to discuss the possibility of this new mechanism and to propose a test of it.

In the original data, the constancy of the isotope effect that was calculated is somewhat impressive. The percentage deviation is large due to the small absolute value of the effect. The absolute value of the deviation is very respectable and, indeed, in many controlled laboratory experiments on kinetic isotope effects it is difficult to keep the value of the deviations to such a limit.

Eriksson's model for the slow step of the introduction of ammonia nitrogen and nitrate nitrogen into rain is apparently the partition of gaseous ammonia and nitric oxide between the liquid and gas phase.

$$NH_{3\,(gas)} = NH_{3\,(aqueous)} \tag{1}$$

$$NO_{(gas)} = NO_{(aqueous)} \xrightarrow{\text{oxidation}} NO_3^-{}_{(aqueous)}. \tag{2}$$

He postulates that the nitrogen isotope effect for (1) and (2) will be similar. The isotope effect for (1) has been measured (Kirschenbaum, 1947). The fractionation factor for the reaction

$$N^{15}H_{3\,(gas)} + N^{14}H_{3\,(aqueous)} = N^{14}H_{3\,(gas)} + N^{15}H_{3\,(aqueous)} \tag{3}$$

has the value 1·005 at 25°C. There have not been any isotope effects reported for the corresponding reaction of the oxides of nitrogen. Eriksson postulates that a partial extraction of the two compounds by rain would cause the strong correlation between the isotopic composition of the two.

There are several reasons for thinking that equation (1) does not describe the system well. Hutchinson (1954) has shown that the concentration of gaseous ammonia in the atmosphere is far too small to account for the amount of it found in rain. He concludes that the ammonia has entered into rain mainly in a solid form.

In an aqueous solution, the ratio of the concentrations of ammonium ion and dissolved ammonia is given by:

$$\frac{(NH_4^+)}{(NH_3)} = \frac{1{\cdot}8 \times 10^{-5}}{(OH^-)} \quad \text{at } 25°C \tag{4}$$

where the quantities in brackets are the molar concentrations. Since rain is usually slightly acidic (Hutchinson, 1954) most of the dissolved ammonia fraction would exist as ammonium ions.

The solubility of gaseous ammonia in water is much, much greater than for any other nitrogen compound. Thus, in such an equilibrium postulated by equation (1) and (2), the ammonia should be extracted by the rain much faster than other nitrogen compounds. However, the data of Angstrom and Hogberg (1952) show that the rate of appearance of the two into rain is of a similar order of magnitude.

These considerations lead to the suggestion that perhaps the two nitrogen compounds exist as ions adsorbed on solid surfaces in the air rather than as gaseous molecules. On this basis, Eriksson's model is expressed as

$$NH_4^+{}_{(adsorbed)} = NH_4^+{}_{(aqueous)} \tag{5}$$

$$NO_3^-{}_{(adsorbed)} = NO_3^-{}_{(aqueous)} \tag{6}$$

The nitrogen isotope effect in processes (5) and (6) is expected to be very small. The fractionation of the nitrogen isotopes between ammonium ions in solution and adsorbed on the ion

exchange resin, Dowex-50, has been studied in this laboratory (Ishimori, 1958). The fractionation factor for the reaction:

$$N^{14}H_4^{+}{}_{(\text{adsorbed})} + N^{15}H_4^{+}{}_{(\text{aqueous})} = N^{15}H_4^{+}{}_{(\text{adsorbed})} + N^{14}H_4^{+}{}_{(\text{aqueous})} \quad (7)$$

is 0·9998 ± 0·0005 at 30°C. Because of the structure of the nitrate ion a very small isotope effect for reaction (6) is expected also. Thus, this mechanism may not be effective enough to cause the observed isotope fractionation.

If, however, reactions (1) and (2) or reactions (5) and(6) are accompanied by similar isotope effects as proposed by Eriksson, then an experimental test may be made. Angstrom and Hogberg (1952) found that the amounts of ammonia nitrogen ($s_{NH_4^+}$) and nitrate nitrogen ($s_{NH_3^-}$) that have collected in accumulated samples of rain may be expressed as a function of the amount of rain (p) that has fallen as follows:

$$s_{NH_4^+} = a \ln (1 + p) \quad (8)$$

$$s_{NO_3^-} = b \ln (1 + p) \quad (9)$$

The coefficients a and b are constants for a particular fall of rain and a is usually about twice the value of b. Equations (8) and (9) show that NH_4^+ is accumulating at a faster rate (is being washed out more efficiently) than is NO_3^-. A test of Eriksson's mechanism would be to accumulate many samples of rain for different periods of a rapid rainfall and to compare the isotopic composition of the two nitrogen fractions in each as a function of time. If his mechanism is correct, the N^{15}/N^{14} ratio should increase as the rain progresses with the ratio increasing faster in the ammonia fraction. If the previous mechanism, based on the oxidation of ammonia to nitrate, is correct the difference in the isotopic composition of the two fractions should be constant with time.

The determination of the mechanism of a chemical reaction, this one included, is a difficult problem. An acceptable chemical mechanism is one that satisfies all the experimental data that is known about the reaction and is consistent with the chemical properties of the substances involved. The original reaction scheme, which is now written:

$$NH_4^+{}_{(\text{adsorbed})} \xrightarrow{\text{oxidation}} NO_3^-{}_{(\text{adsorbed})} \text{ (slow)} \quad (10)$$

followed by the much more rapid reactions

$$NH_4^+{}_{(\text{adsorbed})} = NH_4^+{}_{(\text{aqueous})} \quad (11)$$

$$NO_3^-{}_{(\text{adsorbed})} = NO_3^-{}_{(\text{aqueous})} \quad (12)$$

seem to be in accord with the chemistry of the system.

The work of Angstrom and Hogsberg shows that the appearance of ammonia nitrogen and nitrate nitrogen into rain is a continuous process. In the original discussion a "batch-wise" process was assumed. The fact that a constant kinetic isotope was obtained, without taking this continuous process into account, is an indication that a reaction such as (10) rather than (11) and (12) is the rate controlling process.

An attempt was made to isolate atmospheric N_2O, but preliminary experiments showed there were many experimental difficulties with the separation of this trace constituent of the atmosphere. If the problem of the relation of the ammonia and nitrate in rain is sufficiently important, more isotope work, as outlined here, would be profitable.

T. C. Hoering

Dept. of Chemistry, University of Arkansas,
Fayetteville, Ark., U.S.A.

References

Angstrom A. and Hogberg L. (1957). *Tellus* **4,** 31.
Eriksson E. (1958) *Geochim. et Cosmochim. Acta* **13,** 40.
Hoering T. C. (1957) *Geochim. et Cosmochim. Acta* **12,** 97.
Hutchinson G. E. (1954) *The Earth as a Planet* (Edited by Kuiper G. P.) Vol. II. University of Chicago Press.
Ishimori F. T. (1958) Ph.D. Thesis, University of Arkansas.
Kirschenbaum I. *et al.* (1947) *J. Chem. Phys.* **15,** 440.

Hydrothermale und röntgenographische Untersuchungen an gesteinsbildenden Mineralen—V

Über hydrothermal hergestellen Osumilith

(*Received* 25 *July* 1958)

In der Veröffentlichung II dieser Reihe (Euler und Hellner, 1958) wurde berichtet, dass sich bei hydrothermalen Untersuchungen in Druckbomben mit Temperaturgefälle ein "milaritähnliches Mineral" neu gebildet habe. Dieser Ausdruck wurde deshalb verwendet, weil bei dem Versuch, die Nuebildung zu identifizieren, die physikalischen Eigenschaften dem Milarit am nächsten kamen. Dreh-, Schwenk- und Weissenberg-Aufnahmen ergaben, dass die Raumgruppe der neu gebildeten Kriställchen mit der des Milarits übereinstimmt, dass aber die hexagonalen Gitterkonstanten nur ungefähr mit denen des Milarits zu vergleichen sind; a_0 ist

Tabelle 1. Vergleichstabelle für natürlichen und hydrothermal hergestellten Osumilith

Miyashiro (1956)	Eigene Messungen
aus Plagioliparit von Sakkabira, Kyusiu, Japan	hergestellt bei 1000 bar H_2O-Druck im Temperaturbereich 700–750°C
prismatisch oder tafelig mit {0001}{10$\bar{1}$0}{11$\bar{2}$0}{21$\bar{3}$0} {1011}{10$\bar{1}$2}{11$\bar{2}$2} (0001) : (10$\bar{1}$2) = 39°15′ c/a = 1,415 n_0 = 1,545 – 1,547 n_E = 1,549 – 1,551 (Na-Licht) $n_E - n_0$ = 0,004	blättchenförmig mit {0001}{10$\bar{1}$2}{10$\bar{1}$0}{11$\bar{2}$0} (0001) : (10$\bar{1}$2) = 39°18′, c/a = 1,417 n_0 = 1,537 (Na-Licht) $n_E - n_0$ = 0,006 (gemessen mit Berek-Kompensator)
beinahe oder vollständig einachsig positiv	einachsig positiv
a_0 = 10,17 Å c_0 = 14,34 Å c_0/a_0 = 1,410 $D_{6h}^2 - P6/ml$	a_0 = 10,11 ± 0,02 Å c_0 = 14,36 ± 0,03 Å c_0/a_0 = 1,420 $D_{6h}^2 - P6/ml$

kleiner und c_0 ist grösser als die entsprechenden Gitterkonstanten des Milarits. Die Intensitätsabfolge der Reflexe auf Einkristallaufnahmen ist ähnlich; wesentliche Unterschiede ergaben sich z.B. für den Reflex (80$\bar{8}$0), welcher bie Milarit nicht beobachtet wird, während er bei dieser Neubildung mit mittlerer bis starker Intensität auftritt.

Inzwischen wurden wir durch die 3. Auflage von Strunz (1957) auf das neue, der Milarit-Gruppe angehörende Mineral Osumilith,

$$(K, Na, Ca)(Mg, Fe^{2+})_2(Al, Fe^{2+}, Fe^{3+})_3[(Si, Al)_{12}O_{30}]\cdot H_2O$$

und auf die Arbeiten von Miyashiro (1953, 1956) aufmerksam; danach konnten die hydrothermal hergestellten Kristalle als Osumilith identifiziert werden. In der Tabelle 1 werden die an hydrothermal hergestelltem Osumilith erhaltenen Messergebnisse mit den von Miyashiro (1956) mitgeteilten Daten verglichen.

Es sei erwähnt, dass auch die Intensitäten der Röntgenreflexe des synthetischen Osumiliths gut mit den von MIYASHIRO (1956) angegebenen Intensitäten des natürlichen Osumiliths übereinstimmen.

Die beschriebenen synthetischen Osumilith-Kriställchen bildeten sich aus einer Leiste des Paragneises vom Gelbachtal (Schwarzwald), welche hydrothermal in einer Druckbombe mit einem Temperaturgefälle 800°/600°C bei 1000 bar H_2O-Druck behandelt wurde. Näheres über das Gestein und über die Versuchsanordnung ist bei EULER und HELLNER (1958) beschrieben. Insgesamt wurden funf blättchenförmige Osumilith-Kriställchen gefunden, die sich im Temperaturbereich zwischen 700° und 750° gebildet hatten. Sie haben einen Durchmesser von 0,2 mm und sind 0,02 mm dick. Die oben beschriebenen Flächenformen sind alle gut ausgebildet, aber Prismen- und Bipyramidenflächen sind wegen der geringen Dicke der Kristalle sehr klein. MIYASHIRO (1956) gibt an, dass der natürliche Osumilith mit blossem Auge betrachtet schwarz aussehe bemerkenswerten Pleochroismus zeige. Die hier beschriebenen seht dünnen (0,02 mm) Kriställchen sind sowohl im Auflicht als auch im Durchlicht klar durchsichtig; Pleochroismus konnte nicht beobachtet werden.

R. EULER
E. HELLNER

Mineralogisches Institut
der Universitat Marburg/Lahn

LITERATUR

EULER R. und HELLNER E. (1958) *Geochim. et Cosmochim. Acta* **13,** 220.
MIYASHIRO A. (1953) *Proc. Acad. Japan* **29,** 321.
MIYASHIRO A. (1956) *Amer. Min.* **41,** 104.
STRUNZ H. (1957) *Mineralogische Tabellen* (3rd. Ed.) p. 289. Akademische Verlagsgesellschaft Geest und Portig, Leipzig.

The A^{38} content of two potassium minerals

(*Received* 12 *May* 1958)

GERLING, LEVSKII and AFANASYEVA (1956) have presented evidence indicating the presence of A^{38} in potassium micas and feldspars. Their data indicate that the A^{38}/K ratio is constant for potassium minerals of a given age and that this ratio increases regularly with the age of the sample. They state that the observed data may be explained by assuming that K^{38} occurs in nature with an abundance of $K^{38}/K = 1 \times 10^{-10}$ and that the K^{38} has along lived isomeric state ($K^{38} \rightarrow A^{38} + \beta^+$; $t_{\frac{1}{2}} = 7{\cdot}70 \times 10^8$ yr). The only known isomers of K^{38} have half lives of the order of minutes. Because of the implications of their conclusion, we have investigated the A^{38} content of two minerals—MMl, a muscovite mica from Dickinson Co., Michigan, U.S.A., and N-45, a lepidolite from Bikita Quarry, So. Rhodesia.

According to the hypothesis of GERLING *et al.* the ratio of the radiogenic argon isotopes in a sample of age t should be:

$$(A^{40}/A^{38})_{rad} = \frac{K^{40}(R/1+R)}{K^{38}} \left\{\frac{e^{\lambda 40 t} - 1}{e^{\lambda 38 t} - 1}\right\}$$

where λ_{40}, λ_{38}, K^{40}, K^{38} are the decay constants and the present atomic abundance of potassium 40 and 38 respectively. R is the branching ratio of K^{40} and is approximately 0·126. Following GERLING we have $K^{40}/K^{38} = 1{\cdot}2 \times 10^6$, $\lambda_{38} = 0{\cdot}9 \times 10^{-9}$ yr^{-1} and $(A^{40}/A^{38})_{rad} = \left\{\frac{e^{0{\cdot}55t} - 1}{e^{0{\cdot}9t} - 1}\right\} \times 1{\cdot}3 \times 10^5$. Here t is the age of the sample in units of 10^9 years.

The radiogenic A^{40} and potassium contents of the samples investigated are presented in Table 1. Table 2 shows the isotopic composition of the argon as determined on a mass spectro-

meter with a 6 in. radius of curvature, in which no A^{38} tracer had ever been used. The machine was baked out prior to each experiment. A $10^{10}\ \Omega$ resistor was used in determining the A^{36} and A^{38} signals. The signal went to a vibrating reed electrometer. A fraction of the output of this instrument was sent into a 10 mV recorder. The A^{38} signal observed in sample MM1 corresponded to an ion current of about 5×10^{-15} A.

Sample MM1 was run at a time when the background was extremely low. There were very small peaks at masses 36, 38, 39. These were about one-fiftieth of the signal obtained at mass 36 from the sample. The ratios of A^{40}/A^{36} and A^{40}/A^{38} were obtained by two methods: (1) Dynamic—in which the sample was continuously introduced to the source while the mass spectrometer was continuously pumped. (2) Static—in which a sufficient fraction of the sample was introduced into the instrument and the system then isolated. In the static runs it was observed that the ratios decreased steadily with time, the A^{40}/A^{38} ratio changing more rapidly than the A^{40}/A^{36} ratio. The A^{40} intensity remained essentially constant. Data were obtained in static runs by extrapolating the ratios back to zero time. These results were in essential agreement with the dynamic data, although the static ratios were usually less by as much as 20 per cent. The data obtained on dynamic runs is presented in Table 2. No correction for background was made for any of the data listed in the first three data columns. The ratio of radiogenic A^{40} to A^{38} was computed assuming that all of the A^{36} was from air and that $(A^{38}/A^{36})_{air} = 0{\cdot}187$ (after Nier, 1950). The result for MM1 is presented in the penultimate column of Table 2. This is an order of magnitude greater than that calculated according to the Gerling hypothesis (last column, Table 2).

Table 1

Sample	K (%)	A^{40}_{rad} (cm^3 s.t.p./bm)	Age (yr)
MM1*	8·37	$9{\cdot}11 \times 10^{-4}$	$1{\cdot}74 \times 10^{9}$
N-45†	7·60	$1{\cdot}38 \times 10^{-3}$	$2{\cdot}65 \times 10^{9}$

* Wasserburg and Hayden (1956)
† After Aldrich *et al.* (private communication)

Table 2

Sample	$(A^{40}/A^{38}) \times 10^{4}$	$(A^{40}/A^{36}) \times 10^{-4}$	A^{36}/A^{38}	$(A^{40}/A^{38})_{rad.}$	
				Experimental	Calculated
MM1	10·1 ± 1·1	2·21 ± 0·07	4·4 ± 0·5	$5{\cdot}7 \times 10^{5}$	$0{\cdot}55 \times 10^{5}$
N-45	(1) 9·0 ± 0·9	4·06 ± 0·07	2·2 ± 0·24	$2{\cdot}8 \times 10^{5}$	$0{\cdot}43 \times 10^{5}$
	(2) 5·6 ± 0·3	4·26 ± 0·11	1·31 ± 0·10	$0{\cdot}95 \times 10^{5}$	$0{\cdot}43 \times 10^{5}$

Sample N-45 was run at a later time when the background level of the instrument had risen. Significant peaks were present at masses 36, 37, 38, 39. The ratio of the intensities of the background 36 peak to the sample 36 peak was about one-third. The ratio of the ion currents at masses 40 and 39 (I^{40}/I^{39}) steadily decreased during each run and the means of each run decreased in a series of eight separate determinations. These runs were made using the following procedure: the sample was introduced, data taken, the instrument pumped out, residual peaks measured and new sample or normal argon introduced and the procedure repeated. The mean ratios $I^{40}/I^{39} \times 10^{-4}$ obtained for each run were, in sequence, 6·94, 5·66, 2·9, 2·4, 1·57, 2·2, 1·9. The values of 1·57 and 1·9 were obtained from air argon. The presence and behaviour of the peak at mass 39 indicate clearly that the background increased during the introduction of the

sample. In all static runs the I^{40}/I^{38} and I^{40}/I^{36} ratios behaved in the same manner as described for sample MM1.

It was found that after 5 min of pumping the peak at mass 40 diminished by about a factor of 10^{-3} while masses 36 and 38 changed by about one-half. Prolonged pumping without bake-out did not alter the 36 and 38 residuals by a significant amount.

The highest ratios obtained for N-45 were taken on the first two runs. These data (1) are presented in Table 2. Data (2) represent the last run, the results of which were most favourable for the K^{38} hypothesis. Because of the considerable increase in background of N-45 over the MM1 experiment, it was necessary in computing $(A^{40}/A^{38})_{rad}$ to subtract from the I^{36} and I^{38} signals the residual peaks found after $\frac{1}{2}$ hr of pumping. The I^{38} residual was $1{\cdot}8 \pm 0{\cdot}2$ units, the I^{36} residual $2{\cdot}8 \pm 0{\cdot}3$ units. The largest I^{38} and smallest I^{36} peaks observed for runs (1) and (2) respectively were $I^{38} = 3{\cdot}8$ units, $I^{36} = 7{\cdot}1$ units, and $I^{38} = 6{\cdot}3$ units $I^{36} = 7{\cdot}0$ units. The radiogenic ratio was computed from the formula:

$$(A^{40}/A^{38})_{rad} = (A^{40}/A^{38})_{meas} \Big/ \left\{1 - \frac{(38)_{res}}{(38)_{tot}} - \frac{(38)_{air}}{(38)_{tot}}\right\}$$

where $(38)_{air} = [(36)_{tot} - (36)_{res}] \times 0{\cdot}187$). The smallest value obtained experimentally was 2·2 times larger than the calculated value. This result is from a run in which the background at mass 39 had risen considerably. Since the decrease in I^{40}/I^{38} follows the decrease in I^{40}/I^{39}, it is clear that a good part of the 38 signal came from rising background. The result (1) on N-45 would thus appear to be a more reasonable value for $(A^{40}/A^{38})_{rad}$.

Samples of normal argon were run during both experiments. The A^{36} signals were over fifty times larger than background. The data agreed with the accepted values determined by Nier (1950).

The preceding data would indicate that the value of $\lambda_{38}K^{38}$ given by Gerling *et al.* is too large by an order of magnitude. It would therefore appear that their hypothesis regarding K^{38} is open to question.

Acknowledgements—This work was supported by a grant from the National Science Foundation and in part by a Soan Foundation Fellowship. One of us (R. B.) would like to acknowledge the support of the joint O.N.A.–A.E.C. programme under contract. Nonr. 710 (18).

California Institute of Technology and
School of Physics, University of Minnesota

G. J. Wasserberg
R. Bieri

References

Gerling E. K., Leyskii L. K. and Afanasyeva L. I. (1956) On the discovery of A^{38} in potassium–containing minerals. *Dokl. Akad. Nauk SSSR*, **109,** No. 4, 813–815.

Nier A. O. (1950) A redetermination of the relative abundances of the isotopes of carbon, nitrogen, oxygen, argon and potassium. *Phys. Rev.* **77,** 789–793.

Wasserburg G. S., Hayden R. J. and Jensen K. J. (1956) A^{40} K^{40} dating of igneous rocks and sediments. *Geochim. et Cosmochim. Acta* **10,** 153–165.

* The data on sample MM1 were presented at the 1957 IUGG meeting in Toronto, Canada.

A vanadium–calcium spectral line coincidence at 3185 Å and its effect on vanadium abundance data

(*Received* 12 *April* 1958)

In a personal letter several years ago Mr. O. Joensuu, 3629 Premium Drive, Chattanooga, Tennessee, mentioned to the writer that V 3185 Å is subject to interference from an unlisted

Ca line. This has recently been confirmed in several laboratories and should be recorded, since some geochemical data based on this line may now be invalid.

During the d.c. analysis of calcium-bearing minerals the writer found a weak spectral line always to be present at 3185 Å. The spectrograph used was a JACO 21-ft Wadsworth grating instrument with first order dispersion of about 5·2 Å/mm: using a 30 μ slit, it is possible to discriminate between lines about 0·2 Å apart. The line was first interpreted as indicating the presence of low vanadium concentrations (about 10 p.p.m.) until it was found that Ca-rich minerals always showed apparently higher V and moreover the lines V 3183 Å, V 4379 Å and V 3102 Å were invariably absent. The absence appeared due to the fact that they were weaker lines, until it transpired that when using the Stallwood air-jet the sensitivity of V 3102 Å is adequate to indicate V concentrations down to about 3 p.p.m.

Ahrens (1950, p. 221) discusses the effect of Ca compounds in enhancing the sensitivity of V 3185: the effect is also discussed by Scott (1945). This recalled the letter of O. Joensuu mentioned above and simple tests with pure $CaCO_3$ and pure graphite confirmed that the so-called enhancement is spurious and is caused by Ca3185. There are in fact several Ca lines near this wavelength, none of which is recorded in the tables of Harrison (1939) or Saidel, Prokofjew and Raiski (1955). These results have been confirmed by spectrographic laboratories at the U.S. Geological Survey, Washington, the Geological Survey of Indiana, Bloomington, the Geology Department of Queen's University, Kingston, Ontario and by Mr. Joensuu. The three vanadium lines involved are as follows:

V (Å)	*Strength*
3183·408	200
3183·982	500
3185·396	500

The following estimates of Ca wavelengths and strengths were made by (a) G. MacDonald, Queen's University, (b) R. H. Filby, Bloomington, Indiana, and (c) the writer:

	Ca (Å)	Strength		Ca (Å)	Strength		Ca (Å)	Strength
(a)	3183·9	medium	(b)	3183·95	5	(c)	3184·0	5
	3184·4	strong		3184·34	15		3184·4	15
	3185·4	strong		3185·38	10		3185·4	10
	3186·4	strong		3186·37	8		3186·4	10

Weaker Ca lines were also recorded at 3182·5 Å (MacDonald) and 3183·58 Å (Filby). The Indiana results were made on the third-order of a JACO spectrograph, using Fe lines for reference, and are believed by R. H. Filby to be correct to within $\pm$0·05 Å.

The reason why these lines have so far been overlooked is hard to find. However, V is said to be a common contaminant in graphite electrodes and a line at 3185 Å in "pure" Ca-salts could perhaps have been blamed on impure graphite: also the commonly-used wavelength tables are so remarkably free of errors that they have perhaps come to be regarded as perfect, even against the spectral evidence.

From recent work it appears probable that V 3185 Å can only be used safely on samples containing less than about 2% CaO, if V concentrations as low as 10 p.p.m. are likely. Where CaO is higher it is possible to use V 3185 Å only if the intensity of Ca 3186·4 Å is subtracted: that is by applying a background correction measured at 3186·4 Å. This procedure is of doubtful value however. The line V 3102·299 is Å more reliable, provided that the background is measured

on the line Ca 3098·6 Å to compensate for the coincident line Ca 3102·359 Å. These conclusions are drawn from the following results of numerous replicate analyses on the well-known granite and diabase samples G1 and W1 (CaO values are taken from Fairbairn, 1953):

	G1	W1
CaO	1·41%	10·96%
	14 p.p.m.	
V. 3185 Å	14 p.p.m.	230 p.p.m.
V 3102 Å	11·5	120
V range	8–26	170–340

The figures for the range in V are taken from Ahrens (1954, Table 3–2), representing several analysts, some of whom used V 3185 Å. The V content of W1 is therefore at present quite uncertain. The writer's figure of 120 p.p.m. (V 3102 Å) may possibly be subject to a systematic error resulting from matrix effects, since the working-curve was established using granite-like standards. However, the Stallwood air-jet has been used in this laboratory for several years and minimizes such effects for other elements in W1.

The conclusion is that all V analyses which have been made by using the 3185 Å line on calcium-rich samples such as limestones, basic feldspars and calcic slags are likely to be erroneous.

D. M. Shaw

Department of Geology
McMaster University
Hamilton, Ontario, Canada

References

Ahrens L. H. (1950) *Spectrochemical Analysis.* Addison–Wesley, Cambridge, Mass.

Ahrens L. H. (1954) *Quantitative Spectrochemical Analysis of Silicates.* Pergamon Press, London.

Fairbairn H. W. (1953) Precision and accuracy of chemical analysis of silicate rocks. *Geochim. et Cosmochim. Acta* **4,** 143–156.

Harrison G. R. (1939) *Wavelength Tables.* John Wiley, New York.

Saidel A. N., Prokofjew W. K. and Raiski S. M. (1955) *Tables of Spectrum Lines.* VEB Verlag Technik, Berlin.

Scott R. O. (1945) The effect of extraneous elements on spectral line intensity in the cathode-layer arc. *J. Soc. Chem. Ind.* **64,** 189–194.

Book review

The Threshold of Space: The Proceedings of the Conference on Chemical Aeronomy. Edited by M. Zelikoff. Symposium Publications Division, Pergamon Press, London, 1957. 342 pp. 105s.

This collection of forty-five papers presented at the Conference on Chemical Aeronomy, held at Cambridge, Massachusetts, under the sponsorship of the Geophysics Research Directorate, summarizes our knowledge of the chemistry of the upper atmosphere at the time when we are ready to cross the threshold of space. The high scientific quality of the papers is proof of careful planning that must have preceded this conference; it has resulted in the presentation of profound ideas and in a thorough exploration of each subject.

The editor has successfully grouped the complex topics into four major categories, thus increasing not only the readability of the volume, but also its permanent usefulness as one of the standard reference books which it will become. Under the headings of "Atmospheric Photochemistry—Earth and Venus," "Spectroscopy and Photochemistry," "Rocket Probing of the Upper Atmosphere," and "Phenoma Produced by Hypersonic Flight," we find expressed the considered views and latest results obtained by the outstanding scientists in the field. To the individual reader, the value of the book is enhanced by the fact that the critical discussion that followed the presentation of each topic is printed after each paper.

The volume is profusely illustrated with tables, diagrams, and photographs, and its appearance in book form so soon after the conference adds greatly to its usefulness. This is probably the first time that such outstanding papers on upper atmosphere chemistry have been made available as an integrated collection rather than being spread through numerous periodicals. The author and subject indices will be helpful to those looking for exact up-to-date information in the field.

The first two sections deal with the processes of photochemistry and chemiluminescence, as well as with the reactions, emissions, and absorptions of atmospheric gases; the material is presented from the point of view of both the theorist and the ground-based experimentalist. The third part expands the vistas opened in the earlier chapters by discussing the results obtained from rocket flight attempts to study and measure the natural processes *in situ*. Yet it does not stop there; it includes the new experimental field opened by artificially enhancing and changing the natural processes.

The final part stresses the similarity and relations between problems encountered in hypersonic flight and those experienced in upper atmosphere research; and closes the gap between the engineer and designer of high-altitude and space vehicles and the scientist probing and exploring the atmosphere.

The volume also provides a fundamental answer to the question: Where does space begin?

In a sense, the scientist's exploration of the atmosphere shows us that there is no boundary or dividing line. From the moment we leave the surface of the earth we pass upward through a physical and chemical environment with gradually changing parameters and properties until, some day, we may look back to our planet from a distance and find: We have been in space all along, the physical threshold we passed when we stepped out of our laboratory into the open air.

G. F. Schilling

Geochimica et Cosmochimica Acta, 1958, Vol. 15, pp. 163 to 164. Pergamon Press Ltd., London

Papers to be published in future issues

R. J. W. McLaughlin: Geochemical partition in two illitic clays

James P. Forsman and John M. Hunt: Insoluble organic matter (kerogen) in sedimentary rocks

Edward C. Walker, Frank Cuttitta and Frank E. Senftle: Some natural variations in the relative abundance of copper isotopes

A. E. Ringwood: Constitution of the mantle—III. Consequences of the olivine–spinel transition

S. Ďurovič: Contribution to the lognormal distribution of elements

T. Isaacs and R. Roy: The α-β inversions in eucryptite and spodumene

Marjorie Hooker: Data of rock analyses—V. Australian periodical and serial literature

I. Friedman and R. L. Smith: The deuterium content of water in some volcanic glasses

M. D. Karkhanavala: On radioactive uraniferous iron oxides

A. E. Ringwood: On the chemical evolution and densities of the planets

Sayed A. El Wardani: Marine geochemistry of germanium and the origin of Pacific Pelagic clay minerals

A. Heydemann: Adsorption aus sehr verdünnten kupferlösungen an reinen tonmineralen

K. J. Murata, C. V. Dutra, M. Teixeira da Costa and J. R. Branco: Composition of monazites from pegmatites in eastern Minas Gerais, Brazil

K. S. Heier and S. R. Taylor: Distribution of Li, Na, K, Rb, Cs, Pb and Tl in southern Norwegian pre-Cambrian alkali feldspars

W. S. Brocker and Alan Walton: Geochemistry of C^{14} in the fresh water systems

R. A. Edge, R. R. Brooks, L. H. Ahrens and S. Amdurer: Some reconnaissance observations on the combined use of ion exchange enrichment and spectrochemical analysis for the determination of trace constituents in silicate rocks

D. Greenhalgh and P. M. Jeffery: A contribution to the pre-Cambrian chronology of Australia

N. Sen, S. R. Nockolds and R. Allen. Trace elements in minerals from rocks of the S. Californian Batholith

J. V. Jizba: Frequency distribution of elements in rocks

S. R. Taylor and L. H. Ahrens: The significance of K/Rb ratios for theories of tektite origins

D. Carroll and H. C. Starkey: Leaching of clay minerals in a limestone environment

R. E. Belin: Radon in the New Zealand geothermal regions

G. L. Bate, J. R. Huizenga and H. A. Potratz: Thorium in stone meteorites by neutron activation analysis

W. U. Ault and J. L. Kulp: Isotopic geochemistry of sulphur

H. H. Le Riche: The distribution of certain trace elements in the lower lies of southern England

J. F. G. Wilkinson: The geochemistry of a differentiated teschenite sill near Gunnedah, New South Wales

J. C. Vogel: Uber den Isotopengehalt des Kohlenstoffs in Süsswasser-Kalkablagerungen

INFORMATION FOR CONTRIBUTORS

I. GENERAL

1. Papers on geochemistry should be submitted to the appropriate Executive Editor. Papers submitted for publication will naturally be judged from the standpoint of scientific originality and novelty. Technical details of apparatus used in scientific investigation can, however, be presented in brief notes. Critical comments or preliminary results requiring early publication should be submitted as letters to the editors. Where possible, letters should be confined to 500 words. The preparation of progress reports and review articles will be invited by the editors from time to time. The journal appears as independent and complete numbers, which are combined into volumes of about 300 pages.

2. Only papers which have not been previously published can be accepted. Authors must agree not to publish elsewhere a paper submitted to and accepted by *Geochimica et Cosmochimica Acta*.

3. Fifty reprints of each paper are provided free. Additional copies can be purchased if ordered at the time the first proofs are returned. A reprint order form will accompany first proofs.

II. SCRIPT REQUIREMENTS

1. Scripts must be written in one of the three official languages—English, French, or German.

2. The script should be typed (not a carbon copy). The text must be ready for printing and should be carefully checked for errors. Authors will receive proofs for correction.

3. Illustrations should accompany the script, mounted on separate sheets. Line diagrams that require to be redrawn should include all relevant details. Half-tone illustrations should be restricted to the minimum necessary. Photographs should be enlarged sufficiently to permit their clear reproduction, and if words or numbers appear on them, two copies should be sent, one clearly printed and the other without inscription. All illustrations should be provided with descriptive legends, which should be given on a separate sheet. Any lettering on diagrams—other than Greek letters, symbols, etc.—should be stencilled and should be sufficiently large and bold to permit reproduction when the diagram has been reduced to a size suitable for inclusion in the journal.

4. References in the text should be given by quoting the author's name and year of publication, i.e. AHRENS (1952). **Full references should be listed at the end of each paper, in alphabetical order, in the following manner:**

AHRENS, L. H. (1952) The use of ionization potentials—I. Ionic radii of the elements. *Geochim. et Cosmochim. Acta* **2**, 155–169.

and should include the full title of the article, standard abbreviated title of the journal, year, volume number and inclusive page numbers. References to books should include the total number of pages.

5. The text of articles submitted should be concise and in a readily understandable style. The technical description of the methods used should only be given in detail when such methods are new. The essential contents of each paper should be briefly recapitulated in an abstract in English. Such an abstract may, however, be submitted by the author in the language of the original typescript for translation into English by the editorial staff.

6. To conserve space, authors are requested to mark less important portions of the paper (such as description of methods, record of experimental results, etc.) for printing in smaller type.

7. Indices of refraction should be denoted by the symbols α, β, γ, ω, ε, n, and vibration directions by X, Y, Z, O and E.

Pergamon Press are also publishers of the following Journals:

JOURNAL OF NUCLEAR ENERGY (*including* THE SOVIET JOURNAL OF ATOMIC ENERGY *on behalf of the Pergamon Institute, a non-profit-making foundation*)
REACTOR TECHNOLOGY (*Journal of Nuclear Energy, Part B*)
HEALTH PHYSICS (*The Official Journal of the Health Physics Society*)
JOURNAL OF INORGANIC AND NUCLEAR CHEMISTRY
TETRAHEDRON (*The International Journal of Organic Chemistry*)
TALANTA (*An International Journal of Analytical Chemistry*)
INTERNATIONAL JOURNAL OF APPLIED RADIATION AND ISOTOPES
BIOCHEMICAL PHARMACOLOGY
* BIOPHYSICS
* JOURNAL OF MICROBIOLOGY, EPIDEMOLOGY AND IMMUNOBIOLOGY
* PROBLEMS OF HEMATOLOGY AND BLOOD TRANSFUSION
* PROBLEMS OF VIROLOGY
* PROBLEMS OF ONCOLOGY
* SECHENOV PHYSIOLOGICAL JOURNAL OF THE U.S.S.R.
* BULLETIN OF THE ACADEMY OF SCIENCES OF THE U.S.S.R.; GEOPHYSICS SERIES
* ELECTRIC TECHNOLOGY, U.S.S.R.
* RADIO ENGINEERING
* RADIO ENGINEERING AND ELECTRONICS
* TELECOMMUNICATIONS
* PHYSICS OF METALS AND METALLOGRAPHY
* THE ABSTRACTS JOURNAL OF METALLURGY
* APPLIED MATHEMATICS AND MECHANICS
CHEMICAL ENGINEERING SCIENCE
JOURNAL OF ATMOSPHERIC AND TERRESTRIAL PHYSICS
PLANETARY AND SPACE PHYSICS
GEOCHIMICA ET COSMOCHIMICA ACTA
BULLETIN GÉODÉSIQUE
ANNALS OF THE INTERNATIONAL GEOPHYSICAL YEAR
SPECTROCHIMICA ACTA
JOURNAL OF THE MECHANICS AND PHYSICS OF SOLIDS
ACTA METALLURGICA (*for the Board of Governors of Acta Metallurgica*)
INTERNATIONAL JOURNAL OF THE PHYSICS AND CHEMISTRY OF SOLIDS
DEEP-SEA RESEARCH
JOURNAL OF NEUROCHEMISTRY
JOURNAL OF PSYCHOSOMATIC RESEARCH
JOURNAL OF INSECT PHYSIOLOGY
JOURNAL OF AIR POLLUTION
INTERNATIONAL ABSTRACTS OF BIOLOGICAL SCIENCES (*for Biological and Medical Abstracts Ltd.*)
RHEOLOGY ABSTRACTS
VACUUM
OPERATIONAL RESEARCH QUARTERLY
ANNALS OF OCCUPATIONAL HYGIENE

* *Translations of Russian journals published on behalf of the Pergamon Institute, a non-profit-making foundation*

Leaflets giving further details and subscription rates of each of these journals are available on request

6 Feb 1961R
7 Apr 61
3 Sep 64F
7 Dec 64F

THE GEOCHEMICAL SOCIETY

OFFICERS

FARRINGTON DANIELS, President
JOHN F. SCHAIRER, Vice-President
KONRAD B. KRAUSKOPF, Secretary
GEORGE T. FAUST, Treasurer

COUNCILLORS

WILLARD F. LIBBY, 1956–1958
HATTEN S. YODER, 1956–1958
JOHN A. S. ADAMS, 1957–1959
ALFRED O. NIER, 1957–1959
E. F. OSBORN, 1958–1960
H. G. THODE, 1958–1960

REGIONAL VICE-PRESIDENTS

LOUIS H. AHRENS
RUI RIBEIRO FRANCO
ING. GEORGES ORDOÑEZ
C. W. CORRENS
WILLIAM S. FYFE
KEN SUGAWARA

COMMITTEES

Auditing Committee:
JOSEPH J. TREGONING, Chairman
WILLIAM L. HILL
C. R. NASSER

Constitution and By-Laws Committee:
MICHAEL FLEISCHER, Chairman
JULIAN R. GOLDSMITH
DENIS M. SHAW

Education Committee:
H. D. HOLLAND, Chairman
J. A. S. ADAMS
D. M. HENDERSON
KURT E. LOWE
G. D. NICHOLLS

Membership Committee:
R. M. GARRELS, Chairman
HARVEY C. DIEBL
CHESTER B. SLAWSON
JAMES E. SLOSSON

Nominating Committee:
D. E. WHITE, Chairman
GEORGE EDWARDS
A. E. ENGEL
W. D. KELLER
T. G. SAHAMA
D. M. SHAW

Programme Committee:
H. T. EVANS, Chairman
GORDON J. F. MACDONALD
H. E. LOWENSTAM

Publications Committee:
E. W. HEINRICH, Chairman
JULIAN R. GOLDSMITH
JOHN C. MAXWELL
N. W. RAKESTRAW
S. C. ROBINSON
L. R. WAGER

Research Committee:
C. G. DODD, Chairman
LOUIS H. AHRENS
W. F. BRADLEY
C. W. CORRENS
RUI RIBEIRO FRANCO
WILLIAM S. FYFE
ING. GEORGES ORDOÑEZ
R. A. ROWLAND
KEN SUGAWARA
T. G. THOMPSON
G. W. WETHERILL

Russian Translations Committee:
EARL INGERSON

Seal Committee:
ALVIN VAN VALKENBURG, JR., Chairman
MARGARET D. FOSTER
JEWELL GLASS
EDWIN ROEDDER

Standards Committee:
HARRY A. BRIGHT, Chairman
FELIX CHAYES
ALBERT E. J. ENGEL
SAMUEL S. GOLDICH
KIGUMA J. MURATA
GEORGES S. SWITZER

Tellers Committee:
CHARLES MEYER, Chairman
HENRY R. CORNWALL
COLIN O. HUTTON